LEABHARLANN CHOLÁISTE NA TRÍONÓIDE, BAILE ÁTHA CLIATH | TRINITY COLLEGE LIBRARY DUBLIN
Ollscoil Átha Cliath | The University of Dublin

Terms and Conditions of Use of Digitised Theses from Trinity College Library Dublin

Copyright statement

All material supplied by Trinity College Library is protected by copyright (under the Copyright and Related Rights Act, 2000 as amended) and other relevant Intellectual Property Rights. By accessing and using a Digitised Thesis from Trinity College Library you acknowledge that all Intellectual Property Rights in any Works supplied are the sole and exclusive property of the copyright and/or other IPR holder. Specific copyright holders may not be explicitly identified. Use of materials from other sources within a thesis should not be construed as a claim over them.

A non-exclusive, non-transferable licence is hereby granted to those using or reproducing, in whole or in part, the material for valid purposes, providing the copyright owners are acknowledged using the normal conventions. Where specific permission to use material is required, this is identified and such permission must be sought from the copyright holder or agency cited.

Liability statement

By using a Digitised Thesis, I accept that Trinity College Dublin bears no legal responsibility for the accuracy, legality or comprehensiveness of materials contained within the thesis, and that Trinity College Dublin accepts no liability for indirect, consequential, or incidental, damages or losses arising from use of the thesis for whatever reason. Information located in a thesis may be subject to specific use constraints, details of which may not be explicitly described. It is the responsibility of potential and actual users to be aware of such constraints and to abide by them. By making use of material from a digitised thesis, you accept these copyright and disclaimer provisions. Where it is brought to the attention of Trinity College Library that there may be a breach of copyright or other restraint, it is the policy to withdraw or take down access to a thesis while the issue is being resolved.

Access Agreement

By using a Digitised Thesis from Trinity College Library you are bound by the following Terms & Conditions. Please read them carefully.

I have read and I understand the following statement: All material supplied via a Digitised Thesis from Trinity College Library is protected by copyright and other intellectual property rights, and duplication or sale of all or part of any of a thesis is not permitted, except that material may be duplicated by you for your research use or for educational purposes in electronic or print form providing the copyright owners are acknowledged using the normal conventions. You must obtain permission for any other use. Electronic or print copies may not be offered, whether for sale or otherwise to anyone. This copy has been supplied on the understanding that it is copyright material and that no quotation from the thesis may be published without proper acknowledgement.

The Mechanical Regulation of Skeletal Development:

Identification and characterisation of mechanosensitive genes that contribute to tissue differentiation in bone and joint development.

Rebecca A. Rolfe, B.A. (TCD), MRes (UCL)

A thesis submitted to the University of Dublin in partial fulfilment of the requirements for the degree of

Doctor in Philosophy

Trinity College Dublin

March 2015

Supervisor
Dr. Paula Murphy

Co-Supervisor
Dr. Daniel Kelly

TRINITY COLLEGE
2 9 JUL 2015
LIBRARY DUBLIN
Thesis 10596

Declaration

I declare that I am the sole author of this thesis and that the work presented in it, unless otherwise referenced, is entirely my own. I also declare that the work has not been submitted, in whole or in part, to any other university as an exercise for a degree of other qualification.

I agree that the library of Trinity College Dublin may lend this thesis upon request.



Rebecca Rolfe

March 2015

"Change is only possible through movement."

Aldous Huxley, *The Art of Seeing* (1982)

Summary

Mechanical stimulation has been implicated as an important regulator for the development of the skeleton. Decreased *in utero* foetal movement results in skeletal abnormalities including joint fusions and thin hypo-mineralised bones. Animal models that develop in the absence of mechanical stimulation show abnormal initiation and/or progression of ossification in long bones, loss of definition of tissue territories in the joint region and altered rudiment morphology (Kahn et al., 2009; Nowlan et al., 2010a; Roddy et al., 2011b). The skeletal system is a complex structure, and while we know much about the molecular mechanisms that guide the differentiation of progenitor cells into its individual elements; we know very little of the molecular mechanisms that sense and respond to mechanical stimulation to co-ordinate its correct development. The objective of this thesis was to uncover the molecular mechanisms underlying the response of developing skeletal cells to mechanical stimulation.

Using a mouse model (*Splotch-delayed*) that has altered mechanical stimulation due to the absence of limb musculature; the phenotypic abnormalities were confirmed and the hypothesis that mechanical stimulation of the embryonic skeletal system impacts expression levels of genes implicated in developmentally important signalling pathways, was tested. A comparative transcriptome profiling approach was utilised. Differentially expressed genes were analysed based on gene ontology annotations and were shown to be involved in development and differentiation, cytoskeletal architecture and cell signalling. Analysis of cell signalling pathways that were altered revealed that the Wnt signalling pathway was the most strongly disturbed. Differentially expressed Wnt signalling components were identified to show spatially restricted patterns in both the developing joint and in the ossification site, corresponding to the sites of the two most affected phenotypic disturbances in the muscle-less mutant. This led to the examination of the effect of altering Wnt signalling as a key point of integration for mechanical cues. *Ex ovo* electroporation targeting the developing limb allowed for the modulation of Wnt signalling, to assess whether manipulation of the pathway phenocopies what is seen following the removal of mechanical stimulation. Altering Wnt signalling was shown to have profound effects on chondrogenesis, however further refinement is required to target specific regions of the developing skeleton, to assess the localised response.

In parallel with the *in vivo* studies, chondrogenic differentiation was analysed in culture, examining the influence of mechanical stimulation in the form of applied dynamic hydrostatic pressure. Comparisons of adult stem cells and embryonic cell cultures exposed to hydrostatic

pressure revealed that the application of mechanical stimulation showed similar responses in gene expression that are indicative of maintenance of a stable cartilage phenotype in both cell types, similar to that displayed in joint articular cartilage, preventing maturation and hypertrophy. This revealed that embryonic and adult cell types respond in a similar manner to mechanical stimulation, at least in this respect, and thus the information gained from the developing embryo can be applied to adult derived cells used for regenerative therapies.

This thesis demonstrates that embryonic movement generated by muscle contractions regulates the expression of key developmental regulatory genes and that such genes are involved in the transduction of biophysical stimuli to elicit a response in cellular differentiation in the embryonic skeleton. In particular it highlights the Wnt signalling pathway as a potential point of integration of mechanical and molecular signalling and the cytoskeletal components as mediators of the response. A better understand of the molecular mechanisms that link mechanical stimuli to transcriptional control guiding cell differentiation will lead to new ideas about how to effectively prime stem cells for tissue engineering and regenerative therapies. This work sheds light on the molecular mechanisms that interpret mechanical stimulation during skeletal development and provides a valuable resource for further investigation of the mechanistic basis of mechanoregulation of skeletal development.

Acknowledgements

I want to start by expressing my most sincere gratitude to Dr. Paula Murphy, as my supervisor for my PhD, her enthusiasm, passion for research and guidance over the past four years has helped to shape me as a researcher. From her teaching me in the lab to chatting over coffee about our daily lives and our courgettes, I will forever be grateful. Her open-mindedness and constant support has allowed me to display freedom in my research and for that I will always be grateful. This has truly been a wonderful experience. I would also like to thank Dr. Daniel Kelly for his support and guidance during my project, and for introducing me to Bioengineering, even if I didn't always understand the engineering lingo.

I would like to thank all the staff in the Dept of Zoology for their assistance in making my research a success, in particular to Fiona Maloney, no matter the time of the day your door was always open for a chat, for that I will always be grateful, a true friend. I would also like to thank Peter Stafford and Dr. Martyn Linnie for all your help and assistance over the past few years. To all at Bioresources who helped with animals.

Thank you to all in the Lab and office over the years; Danielle, Claire, Anurati, Eoin, Reshma, Audrey, Aisha and Hanan, and also to the members past and present in the Bioengineering group for all your help along the way. To all the undergraduate, masters and international students that have been a part of this work, I have greatly enjoyed teaching you all, and learnt a lot from the experience. I would like to acknowledge and thank Pratik Singh and Dr. David Duffy for their contribution with Immunohistochemistry and Sequencing Data for this work.

Thanks also to fellow 2nd floor residents in the department, especially to Prof. Celia Holland, Joe and Karen, always a smile, a wave and a hello was much appreciated following the trek up those stairs for 4 years, a great way to keep active, the ground floorers don't know what they are missing.

To my friends, especially the 'grenades' and my extended cricket family, thank you for your support over my journey with this, you have been there throughout and for that I am truly grateful.

A very special thank you to my family, Mum, Dad, JJ and Will. Throughout my life you have always supported my choices, enabled me and encouraged me to participate, from bringing me to ballet and piano classes as a little girl, to helping me achieve success in my academic career. Even though none of you know what I actually do, (an "ology" is what Mum says) I am forever grateful for your support, I hope I have made you proud.

Finally I would like to thank Pete. You have given me so much support, encouragement and love over the past 4 years. From getting me up early to go to the gym and helping me achieve success in my cricket career. You have given me belief and motivation to complete this process. To our future together.

I would like to dedicate this thesis to my Mum, my Dad and Pete for their encouragement in every step of my life.

This work was supported by an Innovation Academy Bursary from Trinity College Dublin.

Publications resulting from this study

Rolfe R.A., Kenny E.M., Cormican P., Murphy P.: Transcriptome analysis of the mouse E14.5 (TS23) developing humerus and differential expression in muscle-less mutant embryos lacking mechanical stimulation. *Genomics Data*, December 2014, Vol 2 pages 32-36, doi: 10.1016/j.gdata.2014.03.003

Rolfe R.A., Nowlan N.C., Kenny E.M., Cormican P., Morris D.W., Prendergast P.J., Kelly D.J., Murphy P.: Identification of mechanosensitive genes during skeletal development: alteration of genes associated with cytoskeletal rearrangement and cell signalling pathways. *BMC Genomics* 2014 Vol 15 (1): 48, doi: 10.1186/1471-2164-15-48.

Rolfe R., Roddy K., Murphy P.: Mechanical Regulation of Skeletal Development. *Current Osteoporosis Reports*, 2013 Vol 11(2): pages 107-116, doi: 10.1007/s11914-013-0137-4.

Vinardell T., Rolfe R.A., Buckley C.T., Meyer E.G., Ahearne M., Murphy P., Kelly D.J.: Hydrostatic pressure acts to Stabilise a chondrogeneic phenotype in porcine joint tissue derived stem cells. *Journal of European Cells and Materials,* Vol 23; 2012; 23: pages 121-134

Presentations resulting from this study

Rolfe R.A., Shea C., Kelly D.J., Murphy P.: The impact of Mechanical Stimulation on ossification and joint formation during mouse development: Exploring developmental mechanisms disturbed in the absence of muscle contractions. *Joint Meeting of the British Societies of Developmental Biology and Matrix Biology.* Norwich, UK. [Oral presentation and Poster, 2nd September 2014].

Rolfe R.A., Kelly D.J. Murphy P.: Identification of Mechanosensitive Genes during Skeletal Development: Alteration of genes associated with Cell signalling pathways. Annual Conference of Irish Networks of Developmental Biologists (INDB), Cork, Ireland 2013. [Presented 12th February 2013].

Rolfe R.A., Kelly D.J. Murphy P.: Identification of Mechanosensitive Genes during Skeletal Development: Alteration of genes associated with Cell signalling pathways. *In Proceedings of the 19th Annual Conference of the Section of Bioengineering of the Royal Acadamy of Medicine in Ireland*, Meath, Ireland 2013. [Presented 18th January 2013, Meath, Ireland].

Rolfe R.A., Kelly D.J. Murphy P.: Identification of Mechanosensitive Genes during Skeletal Development: Alteration of genes associated with Cell signalling pathways. *Trinity Centre of Bioengineering Winter Symposium*, Dublin, Ireland 2012. [Poster, 18th December 2012, Dublin, Ireland].

Rolfe R.A., Kelly D.J. Murphy P.: The Mechanical Regulation of Bone Development: Identification of mechanically regulated genes *in vivo*. Annual Conference of Irish Networks of Developmental Biologists (INDB), Dublin, Ireland 2011. [Poster, 12th December 2011].

Rolfe R.A., Vinardell T., Kelly D.J. Murphy P.: Analysis of Chondrogeneic Gene Expression and Mechanosensitive Genes following Mechanical stimulation by Hydrostatic Pressure. *In Proceedings of the 17th Annual Conference of the Section of Bioengineering of the Royal Acadamy of Medicine in Ireland*, Galway, Ireland 2011. [Presented 29th January 2011, Galway, Ireland].

Table of Contents

Declaration i
Summary iii
Acknowledgements v
Publications resulting from this study vi
Presentations resulting from this study vii
Table of Contents ix
List of Figures xv
List of Tables xix
Nomenclature xxi
Chapter 1
1 Introduction 1
1.1 The Skeleton: Its Role and Importance 1
1.2 Skeletogenesis 2
1.2.1 Morphological development of the Limb 3
1.2.1.1 Development of Bone 4
1.2.1.2 Development of Articular Cartilage 7
1.3 Molecular Regulation of Skeletal Development 9
1.3.1 Transforming growth factor-Beta (TGF-β) signalling 11
1.3.2 Indian Hedgehog (Ihh) Signalling loop 13
1.3.3 Wnt Signalling 14
1.3.3.1 Wnt signalling regulation of mesenchymal condensation and chondrogenesis 16
1.3.3.2 Wnt signalling regulation of Hypertrophy 17
1.3.3.3 Wnt signalling regulation of Joint development 18
1.3.4 Fibroblast growth factor (FGF) signaling 20
1.3.5 Other signalling molecules involved in Joint Morphogenesis 21
1.3.6 Mechanosensory proteins: the potential link between mechanical stimulation and molecular regulation 22
1.4 Mechanical Influences on Developmental Processes 22
1.5 The Mechanical influence on Skeletal Development 24
1.5.1 Analysis of *In Ovo* Immobilisation 25
1.5.1.1 *In ovo* Immobilisation: Analysis of Ossification and skeletal rudiment length 26
1.5.1.2 *In ovo* Immobilisation: Analysis of Joint development 27
1.5.2 Analysis of the Role of Mechanical stimulation in Mammalian Mouse Models . 29

1.5.2.1 Analysis of Ossification in Muscle-less mutants 29
1.5.2.2 Analysis of Joint development in Muscle-less mutants 31
1.5.3 Response of Progenitor Cells *in vitro* to Mechanical Stimulation 33
1.6 Identification of Mechanosensitive Genes during embryonic skeletal development 37
1.7 Objectives of the Thesis 39

Chapter 2

2 Methods 43
2.1 Embryo Collection 43
2.2 Genotyping of Embryos 44
2.3 Histological Analysis 45
2.3.1 Safranin-O staining 46
2.4 Embedding and Sectioning of embryonic tissue for *in situ* hybridisation 47
2.4.1 Vibratome sectioning 47
2.4.2 Cryosectioning 47
2.4.3 Paraffin sectioning 48
2.5 *In Situ* Hybridisation 48
2.5.1 Probe Preparation 48
2.5.2 Fixation and pre-treatment of floating tissue sections 49
2.5.3 Fixation and pre-treatment of Frozen and Paraffin sections 50
2.5.4 Hybridisation, washing and detection of probe on vibratome sections 50
2.6 RNA Preparation for gene expression analysis 52
2.7 Quantitative Gene Expression 52
2.8 Microarray 53
2.9 RNA-sequencing: Alignment and Differential expression analysis 54
2.10 Immunohistochemistry 54
2.11 Laser capture Micro-dissection 55
2.12 Optical Projection Tomography 57

Chapter 3

3 Identification of Mechanosensitive genes during Skeletal Development 59
3.1 Introduction 60
3.2 Methods 64
3.2.1 Embyro Collection 64
3.2.2 Histology of TS23 limbs 64
3.2.3 RNA preparation 64
3.2.4 Microarray 64
3.2.5 RNA-sequencing: Alignment and Differential expression analysis 65
3.2.6 Quantitative real-time-polymerase chain reaction 65
3.2.7 Gene Ontology Annotation Analysis 66

3.2.8 Chromosome position of Differentially Expressed genes 67
3.3 Results 68
3.3.1 Establishment of the developmental defects in *Spd/Spd* muscle-less humeri and associated joints. 68
3.3.2 Transcriptome Profiling of the developing humerus and associated joints during early Ossification and Joint formation 71
3.3.3 Identification of differentially expressed genes in muscle-less versus control developing humeri and associated joints 75
3.3.4 Verification of differentially expressed genes 78
3.3.5 Biological Interpretation of Differentially expressed genes. 80
3.3.5.1 Up-regulated genes are associated with cell adhesion, cell signalling and development and differentiation. 83
3.3.6 Pathway Analysis of DE datasets 84
3.3.7 Genomic localisation of DE genes 86
3.4 Discussion 88
3.4.1 The transcriptome of a developing skeletal rudiment 88
3.4.2 Identification of Mechanoresponsive genes 93
3.4.3 Limitation of Approach 96
3.4.4 Technical Comparison 97
3.5 Conclusion 97

Chapter 4

4 Characterisation of Mechanosensitive genes: signalling pathways and developmental processes 99
4.1 Introduction 100
4.2 Methods 104
4.2.1 Bioinformatic analysis of associations with cell signaling pathways 104
4.2.2 Tissue Preparation 104
4.2.3 In Situ Hybridisation 105
4.2.4 Immunohistochemistry 105
4.2.5 Laser-Capture Microdissection 106
4.2.6 RNA preparation, amplification of laser capture micro-dissected tissue 107
4.2.7 Reverse transcription and quantitative Real Time PCR of LCM aRNA 108
4.3 Results 109
4.3.1 Signalling pathway analysis of differentially expressed genes 109
4.3.2 Expression analysis of signalling pathway component genes and proteins on tissue sections 112
4.3.2.1 BMP signalling pathway 113
4.3.2.2 Hedgehog signalling pathway 120
4.3.2.3 Wnt Signalling pathway 121
4.3.2.4 Other Signalling pathways identified as differentially expressed. 128

4.3.3 Distinguishing expression in the joint region and ossification site: exploring the use of Laser Capture Microdissection (LCM) 129
4.3.4 Differential expression in muscle-less humeri assayed by LCM 131
4.4 Discussion 135
4.4.1 Hedgehog pathway activation in muscle-less mutants 135
4.4.2 Reduced BMP signalling in the Joint line and Ossification Site 137
4.4.3 Complex cross interactions of Wnt signalling in the Joint and Ossification Site 140
4.4.4 Cd44 plays an important role in joint formation through interaction with Hyaluronic acid; Hyaluronan biosynthesis is also deregulated in muscle-less mutants. 143
4.4.5 Quantitative spatial detection of differentially expressed genes. 146
4.5 Conclusions 148
Chapter 5
5 Functional analysis of Wnt signalling: investigating a role in skeletal patterning.... 149
5.1 Introduction 150
5.2 Methods 156
5.2.1 *Ex ovo* cultivation setup 156
5.2.2 Alcian Blue staining of whole chick embryos 157
5.2.3 *Ex Ovo* electroporation Experimental Design 157
5.2.3.1 *Ex Ovo* electroporation 158
5.2.3.2 Expression Vectors 160
5.2.3.3 Analysis of transgenic embryos 160
5.2.3.4 Sectioning of electroporated specimens 160
5.2.3.5 Immunohistochemistry 161
5.2.3.6 In Situ Hybridisation 161
5.2.3.7 Optical Projection Tomography 162
5.3 Results 163
5.3.1 *Ex ovo*-cultivated chick embryos display normal morphological development and chondrogenesis 163
5.3.2 Viability of Electroporated chick embryos 164
5.3.3 Tissue Distribution of electroporated cells assessed through GFP transgene expression 165
5.3.4 The developing Cartilaginous Skeleton 168
5.3.5 Constitutive activation of Wnt signalling in the developing limb 170
5.3.5.1 Detection of Tcf-β-catenin fusion protein expression in electroporated limbs 170
5.3.5.2 Phenotypic Effects of activating the canonical Wnt pathway on skeletal development 171
5.3.5.3 Wnt target gene analysis following activation of Wnt signalling 179

5.3.6 The effect of overexpression of the Wnt antagonist Sfrp3 in the developing limb 182

5.3.6.1 Localisation of the electroporated Sfrp3 transgene expression 182

5.3.6.2 Phenotypic effect of Sfrp3 ectopic expression on skeletal development .. 183

5.3.6.3 Analysis of Wnt target gene expression following Sfrp3 ectopic expression 187

5.4 Discussion 190

5.4.1 The challenge of targeting ectopic expression to the developing limb during skeletogenesis 190

5.4.1.1 Tissue distribution of electroporated cells 192

5.4.2 Altering Wnt signalling in the developing limb has profound effects on chondrogenesis 194

5.4.2.1 Electroporation alone causes no changes in *Col2a1* or *Sfrp2* expression . 194

5.4.2.2 Activation of canonical Wnt signalling inhibits chondrogenesis 194

5.4.2.3 Suppression of Wnt signalling interferes with normal rudiment size and shape 197

5.4.3 Insight into Mechanoregulation of Skeletogenesis 199

5.5 Conclusion 201

Chapter 6

6 The influence of mechanical stimulation on chondrogenic differentiation from adult and embryonic cell sources 203

6.1 Introduction 204

6.2 Methods 208

6.2.1 Isolation of embryonic mouse progenitor cells: Micromass and pellet culture .. 208

6.2.2 Cell isolation and Expansion of Adult derived Mouse progenitor cells 208

6.2.3 Cell isolation and Expansion of Adult derived porcine progenitor cells 209

6.2.4 Tripotentiality differentiation assay of adult mouse derived MSCs 211

6.2.5 Application of Hydrostatic pressure 212

6.2.6 Histology 213

6.2.7 RNA Extraction 213

6.2.8 Quantitative Real-Time Polymerase Chain Reaction 214

6.2.9 Statistical Analysis 215

6.3 Results 216

6.3.1 Adult stem cells 216

6.3.1.1 Chondrogenic differentiation of porcine derived adult stems cells 216

6.3.1.2 The effect of HP on adult derived cell pellet cultures 218

6.3.1.3 Gene expression changes following HP and TGF-β3 supplementation on adult-derived pellets 219

6.3.2 Embryonic limb bud derived cells 222

6.3.2.1 Chondrogenic differentiation of mouse embryonic limb bud cells in pellet culture 222
6.3.3 Chondrogenic differentiation of mouse embryonic limb bud cells in micromass culture. 223
6.3.3.1 Influence of HP on morphology of cartilage nodules in embryonic micromass culture 225
6.3.3.2 Gene expression changes following HP on embryonic micromass cultures 226
6.3.4 Initial characterisation of cells derived from adult mouse cartilage and bone marrow 226
6.4 Discussion 229
6.4.1 Response of progenitor cells to Hydrostatic pressure 229
6.4.2 The effect of TGFβ on priming chondrogenic differentiation of adult derived stem cells 231
6.4.3 MSCs derived from adult mouse 233
6.5 Conclusion 235
Chapter 7
7 General Discussion 237
7.1 The developmental significance of the findings 238
7.1.1 Identification of mechanically regulated genes 238
7.1.2 Potential mechanisims of mechanotransduction 241
7.1.2.1 Cell membrane components responsible for sensing mechanical stimuli .241
7.1.2.2 Transmission of mechanical stimuli: The role of the Cytoskeleton 242
7.1.3 Molecular signalling is altered in the muscle-less mutant 244
7.1.4 The role of Wnt signalling in mechanotransduction 246
7.2 The Influence of mechanical stimulation on chondrogenesis 248
7.3 Other future Directions highlighted from this work 249
7.3.1 What is the role of Hippo signalling in mechanotransduction? 249
7.3.2 Potetinal role of microRNAs in mechanotransduction? 250
7.3.3 Investigation into the regulatory mechanisms impacted by mechanical stimulation? 252
7.4 Broader implications of understanding embryonic mechanobiology 254
Appendix A ..... A.I
Appendix B ..... B.XX
Appendix C ..... C.XXII

List of Figures

Figure 1.1 Schematic of limb bud initiation and patterning in the mouse forelimb across developmental time 4
Figure 1.2 Schematic of Endochondral Ossification and the zones in the growth plate. 6
Figure 1.3 The process of joint development. 8
Figure 1.4 Diagram of the canonical Wnt signalling pathway. 15
Figure 1.5: Lack of mechanical stimulation from muscle contractions impacts several aspects of skeletogenesis during embryonic development: the mouse forelimb and chick hindlimb are used here to summarise the effects on (✸) ossification, (▲) joint formation and (ᔓ) rudiment shape 33
Figure 3.1: Overview of gene expression profiling approach used. 65
Figure 3.2: Elbow joint line reduction and loss of interzone layer organisation in Spd/*Spd*$^{-/-}$ muscle-less mutants. 69
Figure 3.3: Loss of cellular organisation, and shoulder joint line reduction in Spd/*Spd*$^{-/-}$ muscle-less mutants. 69
Figure 3.4: Histological analysis of primary ossification centers in proximal humeri 71
Figure 3.5: Transcriptome Profiling of the developing humerus at TS23 by RNA-seq. 73
Figure 3.6: Transcriptome Profiling of the developing humerus at TS23 by RNA-seq. 74
Figure 3.7: Venn diagrams representing the overlap of independent genes detected as differentially expressed (up-regulated and down-regulated; cut off criteria $p \leq 0.05$, and fold change ≥ 2) from the Microarray and RNA seq analysis, as indicated. 76
Figure 3.8: Quantitative Real time PCR relative expression values of selected differentially expressed genes revealed by microarray and RNA-seq. 79
Figure 3.9: Ideogram of differentially expressed genes. 87
Figure 4.1: BMP cell signalling pathway genes, ... 117
Figure 4.2: Immunolocalisation of BMP signalling components Noggin (**a-l**) and pSMAD1/5/8 (**m-r**) in TS23 control 119
Figure 4.3: Analysis of the Hedgehog signalling pathway 121
Figure 4.4: Visual representation of Wnt signalling pathway components 122
Figure 4.5: Spatial analysis of Wnt signalling genes in the developing joints. 125
Figure 4.6: Spatial analysis of Wnt signalling genes in the Ossification site 127
Figure 4.7: Laser-capture micro-dissection of the normal expression of mechanically regulated genes in distinct territories of the developing humerus. 130
Figure 4.8: Quantitative analysis of differentially expressed genes from Laser-capture Micro-dissection of distinct territories of the developing TS23 control and mutant humerus. 133
Figure 4.9: Spatial analysis of *Sox5* 134
Figure 4.10: Schematic of the Hedgehog pathway including components showing differential expression in the muscle-less embryos, revealed by transcriptomic analysis. 137
Figure 4.11: Schematic of BMP pathway including components showing differential expression in the muscle-less embryos, revealed by transcriptomic analysis, ... 139
Figure 4.12: Schematic of Wnt pathway regulation in the developing joints, including components showing differential expression in the muscle-less embryos, revealed by transcriptomic analysis. 141

Figure 4.13: Schematic of Wnt pathway regulation in the developing ossification site, including components showing differential expression in the muscle-less embryos, revealed by transcriptomic analysis. 142
Figure 4.14: Process of Hyaluronan (HA) Biosynthesis for the regulation of cavitation in the developing joint 146
Figure 5.1: Diagram of the proteins encoded in the constructs. used to activate (**a**) or block (**b**) Wnt signalling. 154
Figure 5.2: *Ex Ovo* cultivation setup. 156
Figure 5.3 Summary of the experimental design and analysis pipeline used to manipulate the Wnt signalling pathway in the developing chick forelimb. 158
Figure 5.4: *Ex ovo* cultivated chick embryos show normal development over time. 164
Figure 5.5: Variability in GFP expression (location and intensity) in forelimbs 24 hours post-electroporation 167
Figure 5.6: The developing cartilaginous skeleton. 169
Figure 5.7: Detection of transgene expression in electroporated limbs 171
Figure 5.8: Three dimensional analysis of *Col2a1* expression in Sham electroporated (EP) forelimbs. 174
Figure 5.9: 3D analysis of *Col2a1* expression in Tcf-β-catenin fusion protein electroporated (EP) forelimbs 176
Figure 5.10: Analysis of *Col2a1* and GFP expression in β-catenin electroporated Specimen 4. 179
Figure 5.11: Analysis of *Sfrp2* expression in the developing chick limb at HH27 180
Figure 5.12: Analysis of *Sfrp2* expression in Tcf-β-catenin electroporated forelimbs. 181
Figure 5.13: Detection of transgene expression in chick limbs electroporated with GFP and Sfrp3 expression vectors in 3 independent specimens 183
Figure 5.14: 3D analysis of *Col2a1* expression in Sfrp3 electroporated (EP) forelimbs 186
Figure 5.15: Analysis of *Sfrp2* expression in specimen 8 electroporated with Sfrp3. 189
Figure 5.16: Similarities in skeletal phenotypes demonstrated in Chick and Mouse studies that have over expressed β-catenin directly or through ectopic expression. 197
Figure 6.1: Picture of a porcine knee joint showing different structures of the joint used for cell extraction. 210
Figure 6.2: Setup of Hydrostatic pressure loading 213
Figure 6.3: Histological sections of Synovial membrane, Fat pad and Chondrocytes derived cell pellets grown in Free swelling (FS) conditions for 14 days of culture. 217
Figure 6.4: Chondrogenic marker gene expression in synovial membrane derived cell pellet cultures with 0, 1, or 10ng/ml TGFβ3 over 14days. 218
Figure 6.5: Histological sections of Synovial membrane derived cell pellet grown in Free swelling (FS) conditions or exposed to hydrostatic pressure (HP) following 14 days of culture. 219
Figure 6.6:The influence of hydrostatic pressure on gene expression in Porcine adult-derived synovial membrane (SM) pellets at day 14 cultured in free swelling (FS) and hydrostatic pressure (HP) conditions with 1 or 10ng/ml TGFβ3 220
Figure 6.7: The influence of hydrostatic pressure on gene expression in Porcine adult-derived fat pad (FP) pellets at day 14 cultured in free swelling (FS) and hydrostatic pressure (HP) conditions with 1 or 10ng/ml TGFβ3 221

Figure 6.8: The influence of hydrostatic pressure on gene expression in articular cartilage derived chondrocyte pellets at day 14 cultured in free swelling (FS) and hydrostatic pressure (HP) conditions with 1 ng/ml TGFβ3. 221
Figure 6.9: Alcian Blue staining of sections of embryonic limb bud cell pellets 222
Figure 6.10: Spatial expression of hypertrophic specific genes *Ihh* (**b**) and *Col10a1* (**c**) in the developing E14.5 humerus. 223
Figure 6.11: Chondrogenic differentiation of embryonic limb bud cells cultured in micromass conditions. 224
Figure 6.12: Alcian Blue staining of micromass cultures kept in Free swelling (FS, **a-d**) or exposed to hydrostatic pressure 225
Figure 6.13: The influence of hydrostatic pressure (HP) on gene expression in embryonic limb bud micromass cultures at day 9 grown in free swelling (FS) and hydrostatic pressure (HP) conditions. 226
Figure 6.14: Isolation of possible Mesenchymal stem cells from adult mouse tissue 228
Figure 7.1: Visual representation of DE genes associated with cytoskeletal components. 243

Appendix Figure B.1: *In situ* hybridisation Images of Genes identified to be differentially expressed, qualitative expression in TS23 control limbs. ..... B.XX
Appendix Figure B.2: *In situ* hybridisation Images of Genes identified to be differentially expressed associated with the BMP (A), Hedgehog (B), Wnt (C) and FGF (D) signalling pathways. ..... B.XXI
Appendix Figure C.1: Restriction map of pCDNA-βcatΔTcf, used for ectopic over-expression of β-catenin ..... C.XXII
Appendix Figure C.2: Restriction map of pCS2mFRZB-HA, containing the HA epitope tag, used for ectopic over-expression of FRZB/Sfrp3. ..... C.XXIII
Appendix Figure C.3: Restriction map and multiple cloning site of pEGFP-C1. ..... C.XXIII
Appendix Figure C.4: Frontal views of upper torso from 3D volume representation of *Col2a1* expression for βcatenin electroporated specimen 1-7. ..... C.XXIV
Appendix Figure C.5: Analysis of *Col2a1* and GFP expression in βcatenin electroporated Specimens 2-7. ..... C.XXVII
Appendix Figure C.6: Frontal views of upper torso from 3D volume representation of *Col2a1* expression sin Sfrp3 electroporated specimen 1-6. ..... C.XXVIII
Appendix Figure C.7: Analysis of *Col2a1* and GFP expression in Sfrp3 electroporated Specimens 1-6. ..... C.XXXI
Appendix Figure C.8: Analysis of *Sfrp2* expression in Sham electroporated forelimbs. ..... C.XXXII

List of Tables

Table 1:1: Identification of mechanosensitive genes using various *in vivo* and *in vitro* experimental regimes. 38
Table 2:1:Pax3 specific primers used to distinguish Splotch (*Sp*) and Splotch-delayed (*Spd*) mutant and wild-type alleles. 45
Table 2:2 Embryos from heterozygote Splotch ($Pax3^{Sp/+}$) and Splotch-delayed ($Pax3^{Spd/+}$) crosses. Genotypes and developmental stages recorded. 45
Table 3:1: Primer sequences for qRT-PCR analysis of differentially expressed genes. 67
Table 3:2: Differentially expressed genes ($p \leq 0.05$) with fold change values ≥ 2 revealed by Microarray and RNA-Seq analysis and combined. 76
Table 3:3: Fold change distribution of differentially expressed genes ≥ 2 fold (p-value ≤ 0.05) from Microarray and RNA-seq analysis. 78
Table 3:4: Fold change distribution of Genes identified by Microarray, with different stringencies for differential selection chosen 78
Table 3:5: Verification of fold change expression levels of selected genes in $Pax3^{Spd/Spd}$ mutant humeri 79
Table 3:6: Enrichment of gene groups down-regulated in muscle-less humeri based on GO term annotations. 82
Table 3:7: Enrichment of gene groups up-regulated in muscle-less humeri based on GO terms under sub-ontologies Biological process and cellular component. 85
Table 4:1: Details of cDNA clones used to generate RNA in situ probes 106
Table 4:2: Differentially Expressed genes associated with specific signalling pathways. 110
Table 4:3: Differentially expressed Wnt signalling pathway genes 111
Table 4:4: The BMP pathway components that were analysed by ISH 114
Table 4:5: The Wnt pathway components that were analysed by ISH. A lists the components of the pathway and B lists targets and potential targets of the pathway that were screened 123
Table 4:6: Hyaluronan biosynthesis associated genes identified to be expressed and differentially expressed upon removal of mechanical stimulation. 145
Table 5:1: Details of Plasmid Expression vectors used in Electroporation 160
Table 5:2 Summary of Antibodies used. 161
Table 5:3: Summary of cDNA clones used to generate RNA in situ probes 162
Table 5:4: Overview of survival and development rate following electroporation 165
Table 5:5 Number and stage of viable embryos with GFP positive cells in limb bud mesenchyme 24 hours post-electroporation. 166
Table 5:6: Stages of electroporated (EP) and non-electroporated (non-EP) forelimbs 172
Table 5:7: Stages of electroporated (EP) and non-electroporated (non-EP) forelimbs 184
Table 5:8: Summary of effects on limb skeletal development following Tcf-β-catenin and Sfrp3 ectopic expression. 194
Table 6:1: Primer sequences for mouse qRT-PCR analysis. 215
Table 7:1: Integration of data on mechanosensitive genes identified in the current work (Column 1) and corroborated in other mechanomodulatory contexts or studies (Columns 2 and 3). 240

Appendix Table A.1: Five uncharacterised proteins/unknown genes identified using Microarray technology. ..... A.I
Appendix Table A.2: Enrichment of muscle associated genes identified in the down-regulated gene category ..... A.I
Appendix Table A.3: List of all DE down-regulated genes and fold change estimated by Microarray and RNA-seq, and evidence of any mesenchyme enrichment (≥3fold)..... A.II
Appendix Table A.4: List of all DE up-regulated genes and fold change estimated by Microarray and RNA-seq..... A.XII

Nomenclature

°C	degrees Celsius
2D	two Dimensions
3D	three dimensions
AER	Apical Ectodermal Ridge
AP	alkaline phosphate
BM	Bone marrow
BMPs	Bone morphogenetic proteins
bp	base pair
c	carpal
CD	Campomelic dysplasia
cDNA	complementary DNA
cl	chondrogenous layer
CO_2	Carbon Dioxide
CS	Carnegie Stage
Ct	cycle threshold
d	digits
DAVID	Database for Annotation, Visualisation and Integrated Discovery
ddH_2O	double-distilled water
DE	differentially expressed
DEPC	diethylprocarbonate
DIG	digoxigenin
Dkk	Dickkopf
DNA	deoxyribonucleic acid
dpc	days post coitum
DTT	DL-Dithiothreitol
Dvl	Dishevelled
E	Embryonic day
ECM	Extra Cellular Matrix
EDTA	Ethylenediaminetetraacetic acid
EJ	Elbow Joint
EMBL-EBI	Eurpoeam molecular biology laboratory- European Bioinformatics Institute
EST	Expressed sequence tag
EtoH	Ethanol
FADS	foetal akinesa deformation sequence
FC	Fold change
FDR	false discovery rate
FE	finite element
FGF	Fibroblast growth factor
FS	free swelling
Fzd	Frizzled
g	gram
GDFs	growth differentiation factors
GO	gene ontology
GPCRs	G protein coupled receptors
GSK3	Glycogen synthase kinase 3
h	humerus
HA	hyaluronan
hc	hypertrophic chondrocytes
HH	Hedgehog
HH23	Hamburger and Hamilton stage 23
HP	Hydrostatic pressure
hrp	horse radish peroxidase
hrs	hours
HS	high sensitivity
HZ	Hypertrophic Zone
IgG	Immunoglobulin G
Ihh	Indian hedgehog
il	intermediate layer
IMAGE	Intergrates Molecular Analysis of Genome and their Expression
IPA	Ingenuity pathway analysis
IPKB	Ingenuity knowledge base
IR	infra-red
ISH	In situ Hybridisation
JF	joint fusion
LB	Luria Bertoni
LCM	Laser Capture Microdissection
LMP	low melting point
m	meniscus
mc	metacarpal
min	minute
ml	millilitre
mM	milliMolar
MSCs	mesecnhymal stem cells
NaCl	sodium Chloride
ng	nanogram
OA	Osteoarthritis
ob	osteoblast
oc	osteocyte
OCT	Optimum cutting temperature
p	perichondrium
p	patella
pai	periarticular
PBS	Phosphate Buffered Saline

PBT	PBS + 0.1% Triton
pc	proliferating chondrocytes
PCP	Planar cell polarity
PCR	polymerase chain reaction
PFA	paraformaldehyde
PHW	post hybridisation wash
pre-hc	prehypertrophic chondrocytes
prehz	pre hypertrophic zone
qRT-PCR	quantitative real time PCR
r	radius
RIN	RNA integrity number
RNA	ribonucleic acid
RNA-seq	RNA sequencing
RT	room temperature
S	scapula
SDS	sodium dodeycle sulphate
secs	seconds
SSC	saline-sodium citrate
Tcf	Transcription factor
TFs	transcription factors
TGFβ	Transforming growth factor Beta
TS	Theiler Stage
u	ulna
UV	ultra-violet
v	vascularisation
Wls	Wntless
µg	microgram
µl	micro litre
µM	micro Molar
µm	micrometer

Chapter 1

1. Introduction

1.1 The Skeleton: Its Role and Importance

The skeletal system is composed of two facets, the axial and appendicular skeletons, both of which are an assembly of a rigid framework of bones, cartilage, ligaments and other connective tissue elements. The rigid framework is a collection of more than 200 bones in the human that interact with muscles, tendons and ligaments as part of the musculoskeletal system (Lefebvre and Bhattaram, 2010) to achieve functional success. The complex shape, size and pattern of each skeletal element work together to provide its functional output, including postural support, movement, protection of vital organs, the site of haematopoiesis and the storage site of minerals. The success of the skeleton is ultimately a product of its mechanical properties, how stiff it is, how resilient to fatigue, and how effectively it withstands the extremes of physical activity. The formation and growth of skeletal cells and tissues during embryonic development produces the elements that are required for skeletal success during postnatal life. To help understand the basis of degenerative diseases that affect the normal functional success of the skeletal system, such as osteoporosis and osteoarthritis, we need not only to uncover the mechanisms of bone and cartilage homeostasis, but also the molecules and cues that drive skeletal formation in the embryo. A deeper understanding of these developmental processes is required to harness the potential of stem cells, in order to

guide them along specific differentiation pathways to regenerate cartilage and bone. This work aimed to provide a greater understanding of the molecular mechanisms involved in coordinating correct skeletal development through the interaction of biophysical stimuli generated by embryo movement and molecular signaling pathways and processes. This knowledge can be used to guide future research addressing the clinical challenges of maintaining healthy skeletal tissue through life and improving regenerative capacities for diseased or damaged skeletal elements such as osteoarthritis and osteoporosis.

1.2 Skeletogenesis

Skeletogenesis is the process of skeleton formation in the embryo. It is the process by which both the axial and appendicular skeletal elements form and grow, initially arising from the mesoderm germ layer during embryonic development. The elements of the skeleton develop through a controlled stepwise progression of diverse cellular processes, including migration, adhesion, proliferation, differentiation and growth (Hall and Miyake, 2000). The specific skeletal elements of the long bones in the limb, and articular cartilage that resides in synovial joints will be the focus of this thesis. There are functional distinctions that define these two elements, for example long bones are solid mineralised structures for protection and support, while articular cartilage is smooth to facilitate articulation and the transmission of load within joints. These structures thus have morphological distinctions which begin during their formation in early development. I will describe how each of these elements develops morphologically and then review how molecular regulation controls their distinct development.

The first step in skeletogenesis is the generation of progenitor cells that display the ability to condense and, under control of certain transcription factors and signalling molecules, have the ability to give rise to mature cell type's specific to the elements of the skeletal system. The skeletal system consists of multiple mature cell types, including chondrocytes in cartilage and

osteoblasts, osteocytes and osteoclasts in bone (Lefebvre and Bhattaram, 2010). The pioneering work of A.J Friedenstein through his observation that bone marrow in postnatal life is a reservoir of stem cells for mesenchymal tissues which have the multi-potential to differentiate into osteoblasts, chondrocytes, adipocytes and haematpoetic supporting stroma (Friedenstein et al., 1987; Friedenstein et al., 1974; Friedenstein et al., 1966), indicates that both chondrocytes and osteocytes generated postnatally arise from an osteochondro progenitor cell. This has been further supported in more recent work identifying such multilineage progenitors as Mesenchymal Stem Cells (MSCs) (Johnstone et al., 1998; Pittenger et al., 1999). Both chondrogenic and osteogenic differentiation from adult stem cells and during skeletogenesis in the embryo have been extensively studied and it is important to understand the similarities and differences involved. The factors responsible for the differentiation to either fate, particularly during development, will be described below in the molecular regulation of chondrogenesis and osteogenesis, but to begin I will describe the morphological changes that osteochondro progenitor cells go through to become mature bone, and mature chondrocytes in articular cartilage within the developing limb.

1.2.1 Morphological development of the Limb

The cells destined to become the vertebrate limb originate early in organogenesis from a combination of the lateral plate and somitic mesoderm. Limb buds first arise as a result of differential proliferation of the body wall at appropriate levels along the anterior posterior (AP) axis of the embryo trunk (Searls and Janners, 1971), this occurs at approximately Hamburger and Hamilton (HH) stage 16 (50-55hrs) for the wing and HH17 (52-64hrs) for the leg of the chick (Hamburger and Hamilton, 1951), Theiler stage (TS) 15 (Embryonic day (E) 9.5) for the forelimb and TS16 (E10) for the hindlimb in the mouse (Theiler. K, 1972), and Carneige stage (CS) 13 (30-33 days post-fertilisation) for the human arm and CS14 (33 days post-fertilisation) for the leg (O'Rahilly et al., 1981). At early stages of development it

consists of undifferentiated mesenchymal cells derived from proliferation of the lateral plate mesoderm and migration from adjacent somites, and is covered at the distal tip by a layer of ectoderm called the apical ectodermal ridge (AER) (Figure 1.1). The mesenchyme then condenses at the core of the limb bud in a y-shaped pattern, and cellular differentiation occurs in a proximo-distal sequence, such that the humerus differentiates first, followed by the radius and ulna and finally the digits (Hindchliffe J.R., 1980) (Figure 1.1).



Figure 1.1 Schematic of limb bud initiation and patterning in the mouse forelimb across developmental time. Limb bud initiation at E9.5. Proximodistal (PD) elongation and presence of the AER at the distal tip at E10; the condensation of mesenchyme and configuration into a y-shape pattern at E10.5; differentiation to cartilage from E11.5 and the progressive differentiation of distal elements that appear at E12.5 and E14.5. Ossification begins at the mid-point of the humerus and scapula at TS23, E14.5 AER; Apical Ectodermal Ridge, s; scapula, h; humerus, u; ulna, r; radius, c; carpal, d; digits. (adapted from description in Shum et al., 2003) .

1.2.1.1 Development of Bone

Bone is formed through two mechanisms: intramembranous and endochondral ossification. Intramembranous ossification is a process in which mesenchymal cells form condensations and develop directly into osteoblasts (bone-forming cells); they do not go through a cartilage phase but go directly to osteogenic differentiation. This process is central to the formation of the flat bones of the skull and face (reviewed in Provot and Schipani, 2005).

Endrochondral ossification differs from intramembranous ossification as it involves the formation of cartilage (chondrocytes) that acts as a template for later replacement by bone (formed by osteoblasts), thus termed transient cartilage. Endochondral ossification is

responsible for the formation of long bones and is illustrated in Figure 1.2 (reviewed in Kronenberg, 2003; Provot and Schipani, 2005). Chondrogenesis is the process by which chondrocytes form as a result of mesenchymal cell condensation followed by chondroprogenitor cell differentiation. Differentiation is first indicated by expression of *Sox9* expression in mesenchymal condensations of the mouse limb from embryonic day 10.5 (E10.5) (Figure 1.2A); *Sox9* encodes a transcription factor that regulates chondrogenesis, it is switched on prior to the onset of cartilage formation reflected by Alcian blue staining (Wright et al., 1995; Zhao et al., 1997). The initial *Sox9* positive, continuous mesenchymal structure is then segmented into individual skeletal elements separated by the sites of future joints as joint specification occurs, as is illustrated in Figure 1.1. Chondrocytes are characterised by the production of specific extracellular matrix (ECM) proteins such as type 2 collagen (*Col2a1*) and aggrecan (*Acan*). Chondrocytes proliferate in one direction and form orderly parallel columns which accumulate a cartilage matrix (Kronenberg, 2003). Ossification initiates at the mid-diaphysis of each rudiment when the chondrocytes progress or mature to a state of hypertrophy (Figure 1.2C), noted by the enlargement of the cells and secretion of collagen type ten (*Col10a1*) in the ECM (Castagnola et al., 1986). The formation of the growth plate, is defined by distinct layers of chondrocytes that are all at different stages of maturation, including the resting zone, a proliferating zone, a pre-hypertrophic zone and a hypertrophic zone (Figure 1.2) (reviewed in Lefebvre and Bhattaram, 2010). The columnar layers of the growth plate form though the proliferation of chondrocytes, until they change shape into pre-hypertrophic chondrocytes, and then enlarge to form hypertrophic chondrocytes. The shape change from round to that of the pre-hypertrophic chondrocytes is typically to flat and is organised into distinct columns (Li and Dudley, 2009). This sequence of events begins in the mid-diaphysis of the rudiment and progresses proximally and distally with growth plates persisting at both epiphyses to allow continued elongation and growth of the bone (also called secondary ossification sites).

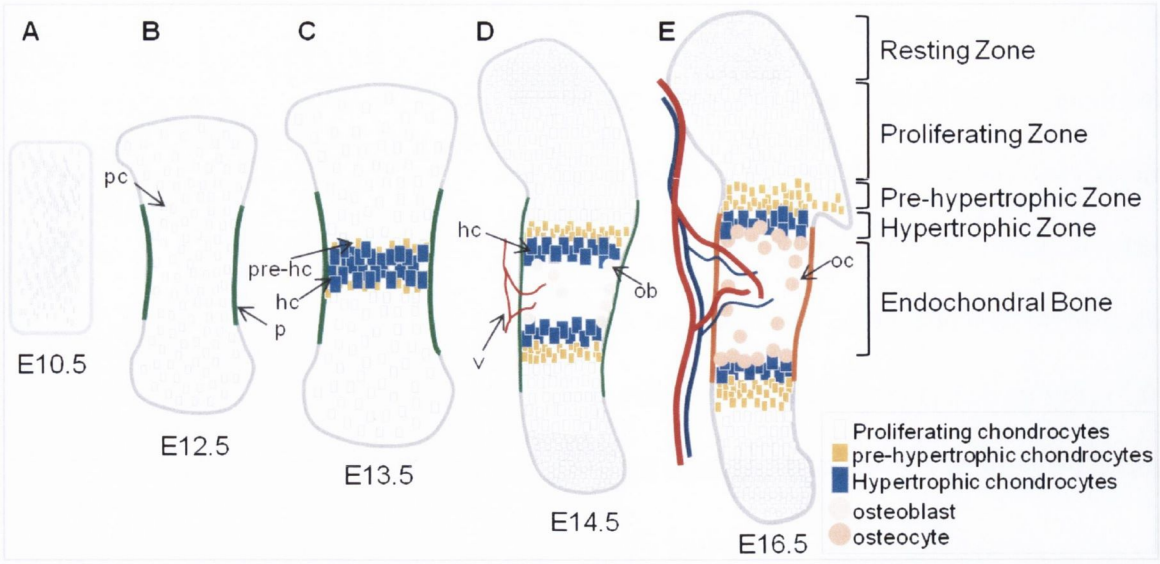

Figure 1.2 Schematic of Endochondral Ossification and the zones in the growth plate. Mesenchymal cells condense in the centre of the limb bud at E10.5 (A). Cells within condensations proliferate to become proliferating chondrocytes (pc) surrounded by a perichondrium (p) (E12.5/ TS20-21) (B). Differentiation of pre-hypertrophic (pre-hc) and hypertrophic chondrocytes (hc) occurs at the mid-diaphysis (E13.5/ TS21-22) (C); followed by proximo-distal separation and development of the primary ossification centre, vascularisation (v) and osteoblast (ob) invasion begins at E14.5/ TS23 (D). Expansion of the marrow cavity occurs at E16.5/ TS24-25 and osteocytes (oc) have invaded to form trabecular bone (E). (adapted from description Kronenberg, 2003).

Concurrently with the differentiation of chondrocytes in the skeletal rudiment, the cells that surround the chondrocytes become perichondrial cells, which typically have two broad functions, firstly to signal to and from the underlying chondrocytes and secondly they provide cells that themselves become osteoblasts. Hypertrophic chondrocytes direct the mineralisation of their surrounding matrix and signal to the adjacent perichondral cells to become osteoblasts, which begins at TS23, approximately E14.5 in the mouse (Figure 1.2D). The hypertrophic cells then undergo apoptosis, however the matrix scaffold that is left behind allows the osteoblasts to invade the cartilage mould and subsequent vascular invasion (Gerber and Ferrara, 2000) occurs to allow osteocytes to be laid down and form trabecular bone (Figure 1.2E) (reviewed in Kronenberg, 2003; Provot and Schipani, 2005).

1.2.1.2 Development of Articular Cartilage

Mature synovial joints that allow articulation between the skeletal elements are made up of multiple cell types, including articular chondrocytes, synovial fibroblasts, tenocytes and fat pad cells. These mature tissues are derived from the same mesenchymal cells that condense to form a template that prefigures bone (Koyama et al., 2008). The cells that will form the joint become distinct during early chondrogenesis; they become flatter, display an increased cell density and become non-chondrogenic (Holder, 1977), forming a distinct joint site termed the interzone. The expression of interzone specific molecules, collagen type 1 (*Col1a1*), Hyaluronan (HA) and the signalling molecule Growth differentiation factor-5 (*Gdf5*) are increased and the overall secretion of ECM molecules, such as Collagen type 2 (*Col2a1*) is reduced in these territories (Francis-West et al., 1999; Holder, 1977). The importance of the interzone region for joint development was demonstrated when it was micro-surgically removed in the developing chick prospective elbow joint, which resulted in no joint formation at later stages (Holder, 1977). However a recent revisitation of this classic experiment showed that a joint will regenerate if the gap is not closed and suggest that cells peripheral to the interzone contribute to the joint at later stages (Ozpolat et al., 2012). As previously mentioned interzone cells express *Gdf5* (Storm and Kingsley, 1996), and lineage tracing studies that marked *Gdf5* expressing cells revealed that they give rise to multiple cell types over developmental time, including articular cartilage, the synovial lining and intra-joint ligaments (Koyama et al., 2008). Mutations in *Gdf5* show defects in digit, wrist and ankle joints in mice and humans (Storm et al., 1994; Thomas et al., 1997). The first phase of joint development involves cell specification from mesenchymal condensations and appearance of the interzone as described (Figure 1.3B). Differentiation then occurs subdividing the interzone into three layers of cells that are histologically and molecularly distinct; the chondrogenous layers (cl) contouring the ends of the rudiments and the intervening intermediate layer (il) where cavitation will later take place (Figure 1.3C) (Ito and Kida, 2000).

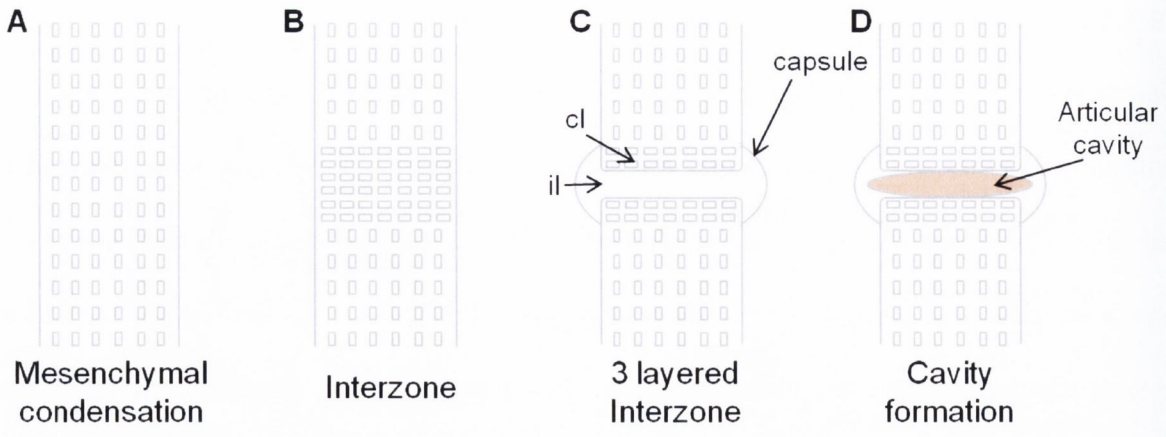

Figure 1.3 The process of joint development. The first indication of the future joint is the appearance of the cell-dense interzone (B) from the mesenchymal progenitor pool (A), the cells of the interzone differentiate and organise to form three layers of cells, bounded by a capsule (C) and ultimately the joint undergoes cavitation, as constituent tissues mature (D). cl; chondrogenous layer, il; intermediate layer.

The second phase in joint development following cell specification and differentiation is cavitation (Figure 1.3D) where the mid-line of the interzone transitions from an area of high cell density to an area consisting of a liquid-filled synovial cell space (reviewed in Pacifici et al., 2005). While cavitation of the elbow joint begins at TS24, the mature joint structure emerges during late embryogenesis, with a synovial cavity that is fluid and lubricant-filled for the unhindered movement of synovial joints. The exact mechanisms that lead to cavitation are not yet known but it is clear that normal joint formation is dependent on sufficient embryo movement. Pharmacologically and micro-surgically induced paralysis, and more recent immobilisation studies has been shown to induce abnormal joint formation (Mikic et al., 2000; Nowlan et al., 2010a; Nowlan et al., 2010b; Osborne et al., 2002). It has been suggested that cavitation occurs as a result of an increase in cell death at the central line of the interzone, however Ito and Kida (2000) found that different joints showed different levels of apoptosis, leading the authors to conclude that cell death does not have a major role in cavitation (Ito and Kida, 2000). An alternative suggestion is that cavitation occurs due to the local accumulation of the non-sulphated glycosaminoglycan hyaluronan (HA) and its interaction with the surface

receptor Cd44, involving cell repulsion contributing to the loss of tissue integrity in the intermediate layer of the interzone, leading to the physical separation of the opposing joint sides and formation of the fluid filled cavity (Chow et al., 1998; Dowthwaite et al., 1998). How the joint acquires its shape is another important aspect to the correct functional output of the joint. Morphogenesis is specific for each anatomical location within the joint and is the least well understood aspect of joint formation. Our research group has shown that morphogenesis occurs early, prior to cavitation in the chick knee joint (Roddy et al., 2009) and biophysical stimuli from muscle contractions are required for correct knee joint shape morphogenesis during development (Roddy et al., 2011b).

Articular cartilage is the tissue that lines the ends of bones within synovial joints and allows for low friction movement. As articular cartilage is aneural and avascular it has a limited capacity to repair, and from a clinical perspective suffers from trauma and disease, such as osteoarthritis and inflammatory rheumatoid arthritis. Osteoarthritis (OA) is a debilitating degenerative joint disease that is characteristed by the degradation of articular cartilage, thus resulting in disruptions of the balanced equilibrium of the ECM that enables joints to resist compression and provide tensile strength (reviewed in Buckwalter and Martin, 2006). The molecular mechanisms underlying this cartilage degeneration is poorly understood; understanding more about how the joint develops and the molecular mechanisms involved during its development could potentially be useful to harness information for regenerative therapies.

1.3 Molecular Regulation of Skeletal Development

While all somatic cells in an individual begin with the same genetic information, molecular and biophysical cues that act on them determine their correct fate within the multi-cellular developing organism. During embryonic development multiple molecular regulatory signalling pathways act to coordinate the correct proliferation and differentiation of tissues.

The morphologies of transient cartilage and articular cartilage are distinct, as described above, yet the regulatory pathways that act on the progenitor cells to produce these tissues are contributed to by many of the same molecules, working differently in different cellular contexts and/or facilitating cross regulation between the emerging tissues. The signalling pathways include Transforming growth factor-Beta (TGF-β) super-family pathways, the Indian Hedgehog (HH) pathway, Wnt signalling, Fibroblast growth factor (FGF) signalling, Notch and retinoid signalling (reviewed in Kronenberg, 2003; Provot and Schipani, 2005). It is the integration of signals from these different pathways that is of central importance for the tight regulation of the growth and proliferation of these territories during skeletal development. I will describe each pathway independently with a focus on how it regulates both ossification and interzone specification for joint development. However, it is the integration of signals from these pathways that regulates the correct proliferation and differentiation of the cell types for the distinct morphological territories.

Specification of the chondrogenic lineage is driven by the Sox (Sex-determining region)-box family of transcription factors (Lefebvre and Smits, 2005), specifically the chondrogenic trio *Sox5*, *Sox6* and *Sox9*. During embryogenesis *Sox9* is expressed in all cartilage primordia along with expression in the nervous system and urogenital system. Later in development all three of these Sox family members are expressed in proliferating chondrocytes, the best characterised being *Sox9*, which is responsible for maintaining proliferation (Akiyama et al., 2002), and directly turning on the expression of the gene *Col2α1* (Bell et al., 1997) resulting in the production of an ECM containing the proteoglycan aggrecan, a marker of chondrocyte differentiation (Han and Lefebvre, 2008). Sox9 has a predominant role in the definition of mouse cartilage as absence of *Sox9* leads to defective cartilage formation and premature skeletal mineralisation (Bi et al., 1999; Bi et al., 2001). Human mutations in SOX9 result in campomelic dysplasia (CD), a rare, lethal, hereditary congenital osteochondral dysplasia

characterised by abnormal bowing and angulations of the lower limbs, with lethality occurring due to pulmonary hypoplasia, distinct from the skeletal abnormalities (Barros et al., 2011; Wagner et al., 1994). Sox9 is thus an important marker during *in vivo* chondrogenesis to indicate that mesenchymal progenitor cells have initiated differentiation to create the transient cartilage template for bone development.

1.3.1 Transforming growth factor-Beta (TGF-β) signalling

Bone morphogenetic proteins (BMPs) are secreted signalling molecules that belong to the transforming growth factor beta (TGFβ) superfamily, implicated in limb growth and patterning and the establishment of the limb axis. At later stages of limb development, expression of multiple Bmp ligands has been reported in the developing forelimb, in the columnar proliferating chondrocytes (*Bmp7*), in the hypertrophic chondrocytes (*Bmp2*, *Bmp4*, *Bmp6*) and in the perichondrium/periosteum (*Bmp3*) (Minina et al., 2002; Minina et al., 2005; Minina et al., 2001). Investigation of the roles of individual Bmp ligands has been performed using multiple mutant models and observations of skeletal defects (Bandyopadhyay et al., 2006; Cao and Chen, 2005). Treatment with Bmp2 in a mouse limb explant model resulted in an expansion of the pre-hypertrophic and hypertrophic domains, indicating that BMP2 promotes the expansion of all differentiation zones in skeletal elements (Minina et al., 2001). Subsequent over-expression of the BMP antagonist noggin, resulted in the inhibition of limb growth in culture, that was shown to be rescued by Bmp2 co-culture treatment (Minina et al., 2001). Over-expression of Bmp2 and Bmp4 through retroviral treatment in the chick limb resulted in similar increases in the size and shape of the long bones, however the ordered arrangement of chondrocyte layers were disrupted and a delay in terminal differentiation shown (Duprez et al., 1996). Noggin knockouts display enlarged cartilage primordia and extended regions of ossification in the anterior-posterior axis in limb elements (Brunet et al., 1998) and noggin over-expression results in decreased trabecular bone with impaired

osteoblast function (Devlin et al., 2003; Wu et al., 2003). The roles that BMPs play in the regulation of proliferation and hypertrophy has been suggested to be as a result of the modulation of the Ihh/PthrP signalling feedback loop, discussed below (Minina et al., 2001).

The noggin knockout mutant shows that BMP signalling requires precise control from this pathway antagonist since the phenotype is similar to what is observed in the over-expression of Bmp2 and Bmp4 in the chick limb with respect to the effect on the joints, demonstrating joint fusion and an absence of *Gdf*-5 expression in the prospective joints (Brunet et al., 1998). *Gdf5* is a divergent member of the Bmp family and as previously mentioned is specifically expressed in presumptive joint sites; it is a valuable marker of forming joints. It is implicated in joint specification through its disruption causing brachypodism in mice (Storm et al., 1994) and chondrodysplasias in humans (Thomas et al., 1996). But it is not only needed for correct joint development; loss-of-function mutations of *Gdf5* present shortening of the long bones of the limb and changes in the pattern of joint and bone formation in the digits, wrists and ankles (Storm et al., 1994; Storm and Kingsley, 1996; Storm and Kingsley, 1999). Transgenic mice expressing *Gdf5* under the control of the collagen type-2 enhancer (so expressed in all chondrocytes) show an increase in cartilage growth and fusion or absence of joints (Tsumaki et al., 2002). As previously mentioned, cell lineage marking of interzone cells in the mouse (*Gdf5* positive cells) shows that they will give rise to all joint tissues including the articular cartilage and synovium with very little contribution to underlying epiphyseal bone (Koyama et al., 2008).

TGFβ signalling through the TGFβ receptor-2 (*Tgfβr2*) was also shown to be critical for interzone formation. Tgfβr2 conditional knockouts showed lack of interphalangeal joint formation, failure of interzone formation and the down-regulation of Noggin, Gdf5 and Wnt9a, all joint markers, indicating that the TGF receptor is necessary to regulate these molecules (Spagnoli et al., 2007). The removal of TGF signalling through the type 2 receptor

results in the ablation of interzone specification but also an increase in proliferative and pre-hypertrophic chondrocytes and a decrease in hypertrophic chondrocytes as demonstrated by the ECM molecule Collagen ten (Spagnoli et al., 2007). These data demonstrate that regulation of the correct pattern of TGFβ signaling is critical for the correct differentiation of the territories involved in both bone and joint specification and development.

1.3.2 Indian Hedgehog (Ihh) Signalling loop

Another important signalling pathway that is central in the transition from cartilage to bone is hedgehog signalling. Indian hedgehog signalling is known to promote endrochondral bone growth through both positive regulation of chondrocyte proliferation and osteoblast differentiation (Karp et al., 2000; Long et al., 2004). The Indian hedgehog (*Ihh*) gene is expressed in the pre-hypertrophic and hypertrophic chondrocytes (Vortkamp et al., 1996) and the *Ihh* null knockout exhibits reduced chondrocyte proliferation, delayed differentiation and disorganised chondrocyte maturation and a complete absence of mature osteoblasts (St-Jacques et al., 1999). Ectopic expression of Ihh in developing chick long bones was shown to induce up-regulation of PthrP (Parathyroid hormone related protein) expression in the articular perichondrium, that led to delayed differentiation of the chondrocytes, and delayed abnormal ossification (Vortkamp et al., 1996). PthrP is expressesed in the peri-articular or resting zone, and it encourages chondrocyte proliferation and its expression is necessary for maintenance of a sufficiently large pool of resting chondrocytes. Knockouts of *PthrP* show significantly shorter limbs, as the orderly transition from proliferative to hypertrophic chondrocytes is altered (Amizuka et al., 1994). This is an example of a negative feedback loop in which the production of Ihh by the pre-hypertrophic chondrocytes induces *PthrP* expression, thereby preventing additional chondrocytes from undergoing differentiation (Vortkamp et al., 1996).

Mutations in the human gene corroborate the importance of the correct balance of Ihh signal in controlling the balance between proliferation and hypertrophy; missense IHH mutations cause brachydactyly type-A1, characterised by shortening or absence of the middle phalanges (Gao et al., 2001), while duplication of the IHH locus presents extensive polysyndactyly of the hands and feet (Yuksel-Apak et al., 2012).

Components of the hedgehog signalling pathway have also been implicated in regulation of joint formation. Two transcriptional effectors of the hedgehog signalling pathway *Gli2* and *Gli3* (Gli family zinc finger 2, 3) have both been shown to be expressed in the developing joint (Niedermaier et al., 2005). As Gli3 is a transcriptional repressor acting in the absence of an Ihh signal, double knockouts of Ihh and Gli3 showed a restoration of the skeletal abnormalities that were shown in the Ihh KO mutants alone, specifically the chondrocyte organisation and maturation within the growth plate and the rescue of joint fusions seen in the Ihh KO mutant (Hilton et al., 2005). These data indicate for a second time that regulation of cartilage development and interzone formation is not mutually exclusive, and it is the correct balance of signals in the correct cells that control the correct development of these tissues within the skeletal system.

1.3.3 Wnt Signalling

Wnt signalling is an evolutionary conserved pathway that has a range of functions during embryonic development including controlling cell fate determination, cell migration, cell polarity and the patterning of individual structures. In classical or canonical wnt signalling, Wnt signals via stabilisation and nuclear localisation of β-catenin to activate the transcription of Wnt target genes, as shown in Figure 1.4. Wnt ligands bind to transmembrane receptors of the Frizzled (Fzd) family of proteins, which can function with the LRP (lipoprotein receptor-related protein) co-receptors. The binding of wnts to a receptor activates the dishevelled (Dvl) protein and this inhibits the activity of the glycogen synthase kinase 3 (GSK3) enzyme. In the

absence of a Wnt signal, this enzyme phosphorylates and degrades β-catenin. Following the inactivation of GSK3, β-catenin accumulates in the cytoplasm and is translocated to the nucleus, where in conjunction with a family of T cell-specific factor/lymphoid enhancer binding factor (Tcf/Lef1) transcription factors, activates the transcription of target genes (reviewed in van Amerongen and Nusse, 2009).

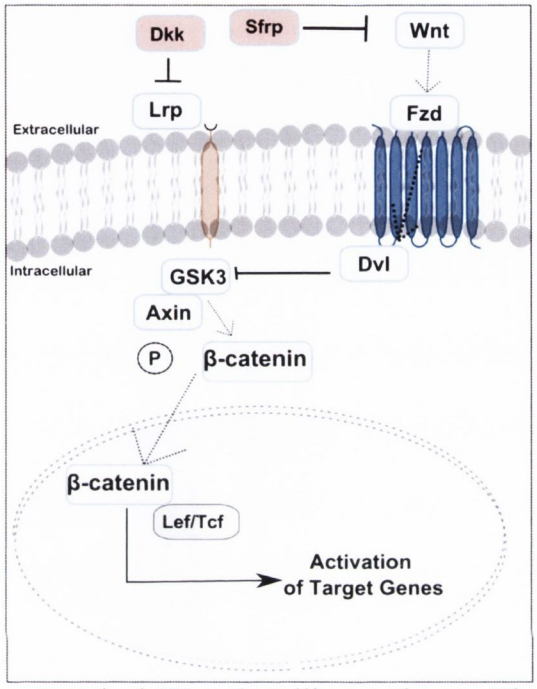

Figure 1.4 Diagram of the canonical Wnt signalling pathway. The wnt signal is transduced through the frizzled receptor (Fzd) and Lrp co-receptor via dishevelled (Dvl) to inhibit the GSK3/Axin complex, which binds and phosphorylates β-catenin in the absence of signal, targeting it for destruction. Signalling leads to inactivation of the destruction complex, allowing translocation of β-catenin to the nucleus. In the nucleus, β-catenin binds to Tcf/Lef transcription factors which in turn bind to the enhancers of and activate or repress target genes. β-catenin provides the transactivation domain while Tcf/Lef provides the DNA binding domain of a functional transactivation complex. Extracellular control is via antagonists Sfrps and Dkks among others. Other membrane and extracellular proteins have been implicated as agonists of the pathway including Rspos (Figure 4.4).

Like BMP signalling, the wnt signalling pathway can be controlled via extracellular antagonists, these include secreted frizzled related proteins (Sfrps) and dickkopfs (Dkks). They antagonise wnt function by binding to the wnt molecule or receptor and preventing receptor activation (Figure 1.4, pink boxes).

Wnt can also signal via pathways independent of β-catenin, and this is termed non-canonical wnt signalling. Non-canonical wnt signalling can be further sub-divided into the planar cell

polarity and the Wnt/Calcium pathways. The non-canonical pathways use different intracellular machinary to the classic canonical pathway. Most non-canonical Wnt signalling has been shown to be imporatant for polarised cell movements and planar polarity of epithelial cells.

1.3.3.1 Wnt signalling regulation of mesenchymal condensation and chondrogenesis

Comprehensive expression analysis of Wnt signalling components in the developing limb over time show multiple ligands and antagonists to be present in a variety of territories, including the AER, the limb mesenchyme, proliferating chondrocytes, hypertrophic chondrocytes, the joint zone and the epithelium (Summerhurst et al., 2008; Witte et al., 2009). During early stages of chondrogenesis when mesenchymal condensation is occurring expression of multiple components of the wnt signalling pathway have been reported in the developing limb. Expression of ligands and receptors have been reported in the mesenchyme surrounding the developing cartilage condensation, these include *Wnt5a*, *Wnt5b* (Kawakami et al., 1999), *Wnt11* (Christiansen et al., 1995; Tanda et al., 1995) and *Wnt9a* ((Hartmann and Tabin, 2000; Hartmann and Tabin, 2001). Four of the 5 Sfrp genes are also expressed in the developing limb, in different territories (unpublished data from our lab). In particular *Sfrp3* was detected first in the ventral region of the developing chick limb bud, and then in the mesenchymal condensations, with restricted expression in the perichondrial tissues of the cartilage template (Wada et al., 1999). Expression of an antagonist in the condensations suggests that negative regulation of wnt activity allows the first steps of chondrogenesis to occur. This is supported by experimental evidence where chondrogensis is inhibited following the ectopic over expression of wnt ligands, *Wnt1*, *Wnt7a*, *Wnt5a* and *Wnt14* (Hartmann and Tabin, 2001; Kawakami et al., 1999; Rudnicki and Brown, 1997). *Wnt1* is not expressed in the limb but is known to signal through the canonical pathway and was shown to be a potent inhibitor of chondrogenesis experimentally in micromass cultures and ectopic expression in

the chick limb, resulting in skeletal abnormalities; this was also seen with *Wnt7a* over-expression (Rudnicki and Brown, 1997). Ectopic expression of *Wnt5a* in the chick limb showed alterations in the length of the radius and ulna (Kawakami et al., 1999). Differences were seen with the ectopic expression of the ligand *Wnt14 (Wnt9a)* in the chick limb, as alterations were shown in the skeletal pattern, not just abnormalities in individual skeletal elements, the authors stated that pre-chondrogenic condensations had formed but there were no further signs of chondrogenic differentiation (Hartmann and Tabin, 2001). The presence of the wnt antagonist in the mesenchymal condensations and the wnt ligand over-expression studies that show a negative effect on chondrogenesis thus suggest that canonical Wnt signalling is low during early chondrogenesis. Wnt-β-catenin signalling in mesenchymal progenitor cells was later shown to play an essential role in determining chondrogenic or osteogenic commitment, with inactivation of β-catenin resulting in ectopic formation of chondrocytes at the expense of osteoblast differentiation, and high level of canonical wnt signalling inhibiting chondrocyte differentiation only allowing osteoblasts to form by intramembraneous ossification (Day et al., 2005).

1.3.3.2 Wnt signalling regulation of Hypertrophy

As chondrocytes proceed through differentiation, the expression patterns of Wnt ligands, receptors and antagonists change. Wnt signalling has been shown to regulate chondrocyte hypertrophy (Akiyama et al., 2004; Day et al., 2005; Hartmann and Tabin, 2000; Yang et al., 2003). *Wnt5a* and *Wnt5b* appear to regulate the rate of cell transition between proliferative and hypertrophic chondrocyte differentiation (Yang et al., 2003), with *Wnt5a* being expressed in the proliferating and pre-hypertrophic chondrocytes and promoting hypertrophy, and *Wnt5b* expressed in the perichondrium and boundary between the pre-hypertrophic and hypertrophic chondrocytes inhibiting hypertrophy (Church and Francis-West, 2002; Hartmann and Tabin, 2000; Yang et al., 2003). Expression of Wnt ligands in the perichondrium has been shown to

work in conjunction with the PthrP-Ihh signalling loop as the perichondrium inhibits chondrocyte differentiation through this loop. It was shown that wnt signalling regulates the rate of chondrocyte hypertrophy by antagonising PthrP signalling, but only PthrP signalling controls when chondrocytes exit the cell cycle to undergo hypertrophy (Guo et al., 2009). Recent work on the Wntless (Wls) conditional mutant has been a useful tool to study bone development (Maruyama et al., 2013; Zhong et al., 2012). Wntless or Gpr177 is a trafficking protein that is essential for the secretion of both canonical and non-canonical Wnt proteins (Banziger et al., 2006). Loss of wnt signalling through inactivation of Wls in chondrocytes and the perichondrium (*Col2a1* positive cells) resulted in delayed chondrocyte differentiation, disorganised chondrocyte arrangement and impaired endochondral bone formation (Lu et al., 2013), supporting the idea of multiple Wnt functions during skeletogenesis. Loss of wnt signalling in the Wls conditional mutant showed features that mimic the defects that were seen in mice with inactivation of β-catenin (Day et al., 2005; Lu et al., 2013).

1.3.3.3 Wnt signalling regulation of Joint development

Wnt signalling is also associated with regulation within the developing joint. Expression of both *Wnt4* and *Wnt9a* (*Wnt14* in the chick) have been associated with joint development. During early joint development, both of these genes are expressed in the presumptive joint regions (Hartmann and Tabin, 2000; Hartmann and Tabin, 2001; Kawakami et al., 1999; Loganathan et al., 2005). Early reports proposed that *Wnt14* (*Wnt9a* in the mouse) is involved in the initial steps of joint formation, as ectopic over-expression of *Wnt14* in pre-chondrogenic regions resulted in these regions becoming morphologically and histologically distinct and taking on histological and molecular properties typical of the early joint interzone (Hartmann and Tabin, 2001). Expression of the ligand *Wnt9a* has been reported in the perspective joints in the developing forelimb (Guo et al., 2004; Hartmann and Tabin, 2001), however only a few synovial joints are abnormally affected in *Wnt9a* knockout mouse

mutants (Spater et al., 2006), maybe due to the expression of other wnt genes *Wnt4* and *Wnt16*. Analysis of *Wnt9a*$^{-/-}$:*Wnt4*$^{-/-}$ double mutant mice also show multiple joint fusions, although results of marker genes *Col2a1*, and *Gdf5* indicate that joints form, fusion occurs secondarily due to the absence of *Wnt9a* and *Wnt4*, suggesting these genes are needed for long-term joint integrity not induction (Spater et al., 2006). Ectopic expression of constitutively active *Wnt9a* and β-catenin under the Col2a1 promoter was then examined in mouse embryos. Endochondral ossification was significantly reduced in both transgenic mice, but not intramembranous ossification. Joint fusions were reported in both transgenic mice, but so were joint-specific markers in territories that were previously cartilage template, indicating that ectopic expression of either *Wnt9a* or *β-catenin* resulted in ectopic joint formation in 'non-joint' regions (Guo et al., 2004). Guo and colleagues suggested from these sets of experiments that *Wnt4*, *Wnt9a* and *Wnt16* expression in the presumptive joint results in the up-regulation of β-catenin protein levels and inhibition of *Sox9*, that leads to interzone formation by reversing or inhibiting chondrocyte differentiation and inducing *Gdf5* expression (Guo et al., 2004). More recent studies agree that wnt signalling is needed for the long term integrity of joints, as cellular organisation and cellular morphology was altered in limbs with conditionally silenced β-cateinn under the *Col2a1* and *Gdf5* promoters (Koyama et al., 2008).

In summary the Wnt signalling pathway has been shown to be involved in early and late phases of skeletal development, for chondrogenesis, hypertrophy of the cartilage template and joint specification and integrity. Low levels of wnt signalling are actively maintained early in mesenchymal condensations to permit chondrogenesis, and then temporally controlled expression of specific wnts in specific locations allows the correct hypertrophy of chondrocytes prior to ossification and specification of joint cells.

1.3.4 Fibroblast growth factor (FGF) signaling

Fibroblast growth factor (Fgf) signalling has also been shown to play an important role in regulating chondrocyte proliferation and differentiation. The Fgf pathway seems to be more involved in chondrocyte maturation. As chondrocytes form they express different components of the Fgf signalling pathway components, including signalling ligands and receptors. The territories of the developing forelimb where expression has been reported include, the low proliferating chondrocytes (resting zone) (*Fgfr1*, *Fgfr2*, *Fgf8*), the high proliferating columnar chondrocytes (*Fgfr3*) the hypertrophic chondrocytes (*Fgfr1*), the perichondrium/ periosteum (*Fgfr1*, *Fgfr2*, *Fgf2*, *Fgf8*, *fgf18*) and the osteoblasts (*Fgfr2*) (Minina et al., 2005). Characterisation of the Fgf18 homozygote mutants revealed that this gene regulates cell proliferation and differentiation positively for osteogenesis and negatively for chondrogenesis (Ohbayashi et al., 2002), and it is suggested to act on the fibroblast growth factor receptor-3, to decrease chondrocyte proliferation, and perhaps on Fgfr1 to delay terminal differentiation (reviewed in Provot and Schipani, 2005). Examination of *Fgfr3*-deficent mice show expansion of proliferating and hypertrophic chondrocytes, resulting in progressive outgrowth of the long bones (Deng et al., 1996). Exogenous application of FGF2 to mouse limb explants caused a shortening of skeletal elements and reduced chondrocyte proliferation, but with larger regions of expression of osteopontin (*Spp1*), a terminal differentiation marker present in the collagenous matrix of mineralised tissues, indicating an acceleration in terminal differentiation (Minina et al., 2002). Co-treatment of exogenous FGF2 and BMP2 on mouse limb explants resulted in territories that were Ihh positive (pre-hypertrophic and hypertrophic chondrocytes) that were larger than when the limbs were treated with either FGF2 or BMP2 alone, indicating that the signalling ligands were working in opposition to each other to regulate endochondral ossification (Minina et al., 2002). Excessive FGF signaling has been shown to cause decreased proliferation at the growth plate of the appendicular skeleton, resulting in achondroplasia (reviewed in Baldridge et al., 2010). This complex regulation by

two pathways indicates the tight regulatory mechanisms that are in place to co-ordinate the correct differentiation of chondrocytes for bone formation. It is interesting to note that both Fgf2 and Bmp2 are also expressed in the joint line (Roddy et al., 2011b).

1.3.5 Other signalling molecules involved in Joint Morphogenesis

Down regulation of expression of the master chondrogenic transcription factor *Sox9* is indicative of joint line specification but joint morphogenesis has been shown to rely on *Sox5* and *Sox6*, as severe interzone, joint and growth plate defects are seen in double mutants (*Sox5*$^{-/-}$,*Sox6*$^{-/-}$) (Dy et al., 2010). The transcription factor *Sox11* has also been shown to be expressed in the interzone, and it was shown to directly activate *Gdf5* expression (Kan et al., 2013). However ectopic expression of *Sox11* in non-joint regions, did not result in *Gdf5* expression, indicating that *Sox11* expression alone is not enough to drive *Gdf5* expression in ectopic locations (Kan et al., 2013). *Osr1* and *Osr2* (odd-skipped related 1 and 2) are examples of two other transcription factors that when absent result in joint fusion, their expression has been shown to be required for the expression of signalling molecules critical for joint formation, including *Gdf5*, *Wnt4* and *Wnt9b* (Gao et al., 2011). More recent studies have used laser-capture microdissection as a means of profiling the distinct layers in the developing interzone in different joints, both identifying genes related to inflammation and actin cytoskeletal organisation, which could provide more detail into the differentiation mechanisms involved in joint differentiation prior to cavitation (Jenner et al., 2014; Longobardi et al., 2012).

The intrinsic cyclic nature of gene expression, which in turn can promote or prevent signalling cascade activation in a spatially and temporally controlled manner, determines the correct development of all organ systems during embryonic development. More recently, accumulating evidence on the impact of embryonic movement on skeletal development (reviewed below) has led to the proposal that molecular cell signalling and gene expression

mechanisms (intrinsic cues) are integrated with mechanical signals generated by movement (extrinsic cues) in guiding certain events in skeletogenesis (reviewed in Roddy et al., 2011b; Rolfe et al., 2013a).

1.3.6 Mechanosensory proteins: the potential link between mechanical stimulation and molecular regulation

How cells perceive and relay dynamic mechanical signals to illicit an intracellular response via alteration of cell signalling pathways still remains yet unclear. Cells that perceive mechanical signals have thus been termed mechanosensors and are defined as any molecule, protein complex or biological structure that has the ability to detect alterations in force. Candidate mechanoreceptors include integrin complexes, ion channels and G-protein coupled receptors.

Integrins are protein complexes that couple the cell to the external environment by spanning the plasma membrane and forming attachments with the ECM. The binding of extracellular ligands to integrins may initiate intracellular signalling events (reviewed in Docheva et al., 2014). Integrin complexes have previously been identified to be potential mediators of mechanotransduction. Articular chondrocytes have been shown to express both integrin ECM receptors (Knudson et al., 1996; Woods et al., 1994). Under physical loading, integrins are activated on the surface of chondrocytes and have been shown to enhance cell proliferation (Chowdhury et al., 2004). Removal of loading in this system has resulted in the down-regulation of cell-adhesion associated integrins and cadherins, supporting the suggestion that they are involved in surface reception of mechanical stimuli.

1.4 Mechanical Influences on Developmental Processes

The pioneering work of Wilhelm His, Julius Wolff and Wilhelm Roux in the 18th and 19th centuries demonstrated the importance of mechanical stimulation for functional adaptation of

the structure and mass of bone at a tissue level (reviewed in Chen et al., 2009; Nowlan et al., 2010b; Rubin et al., 2006). The ability of the skeleton to adapt to its loading environment is reflected in an increase in thickness of cortices in the humeri of the dominant arm of elite tennis players (Kontulainen et al., 2003). In contrast, a reduction in biophysical stimulation on the skeletal system, as experienced in low-gravity environments for long durations (space-flight), results in loss of bone mass (Carmeliet et al., 2001); this phenomenon is analogous to the reduction in bone mass that is seen following paralysis or prolonged bed-rest, identified as disuse osteoporosis (Takata and Yasui, 2001). The role of mechanical stimuli on bone maintenance and adaptation was incorporated into Harold Frost's Mechanostat theory in which he proposed that local mechanical effects are integrated with molecular processes at a cellular level (Frost, 1987; Frost, 2000). Mechanical forces have been shown to be important in various aspects of skeletal health, including: fracture healing in which application of compressive forces promoted bone formation (Claes et al., 2008) and bone remodeling (Isaksson et al., 2007).

The mechanical regulation of tissue differentiation has more recently been studied in a variety of developing tissues, and it has become apparent that molecular pathways are tightly integrated with physical /mechanical signals to guide correct cellular differentiation. Elegant work on mesenchymal condensations during tooth development have shown that classic signaling from epithelium to mesenchyme leads to cell compression as a necessary step for the modulation of gene expression and cell differentiation (Mammoto et al., 2011). Mechanical cues have been shown to be involved in development of multiple organ systems, including angiogenesis of vasculature (Mammoto et al., 2009), alveolar differentiation into lung tissue (Gutierrez et al., 2003) and haematopoiesis (Adamo et al., 2009). Several recent studies on Drosophila development have also shown the importance of mechanical stimulation in cell polarisation, in particular impacting the Planar Cell Polarity (PCP)

pathways (Aigouy et al., 2010; Olguin et al., 2011). In recent years there has been a dramatic increase in interest in the interactions between mechanical forces and the differentiation of cells by tissue engineers, who aim to recreate tissue for regenerative therapies (reviewed in Johnstone et al., 2013; Kelly and Jacobs, 2010). Multiple approaches have been used to investigate how mechanical forces that are applied to tissues or cells have an effect. These include *in vivo* animal models that have an alteration in their mechanical environment thus impacting developmental processes, and *in vitro* culture systems that apply distinct types of mechanical stimulation on to progenitor cells in culture as to assess their affect.

1.5 The Mechanical influence on Skeletal Development

Although the effect of mechanical stimulation on the formation of the skeletal system in the embryo has been less widely considered in the past (reviewed in Nowlan et al., 2007), evidence has existed for some time that mechanical forces generated by embryonic muscle contractions are required for normal skeletogenesis. The musculoskeletal system develops in the limb in a co-ordinated fashion with the muscle forming from cells that migrate into the limb bud adjacent to the condensing mesenchyme (Kardon, 1998). In situations where muscle does not function correctly as seen in rare human *in utero* neuromuscular disorders, a range of skeletal anomalies occur including permanent joint flexion (comptodactly), multiple joint fusions (ankylosis), craniofacial abnormalities and pulmonary hypoplasia along with thin hypomineralised bones (Rodriguez et al., 1988a; Rodriguez et al., 1988b). These anomalies were caused by a reduction in foetal movement due to congenital muscular atrophy and other myopathies and dystrophies and form part of a spectrum of defects referred to as Foetal Akinesa Deformation Sequence (FADS) (Moessinger, 1983). It was said from these observations that immobilisation *in utero* resulted in bone osteoporosis of the foetus due to hypomineralisation (Rodriguez et al., 1988a; Rodriguez et al., 1988b).

Evidence from animal models has been key to help our understanding of the importance of movement as a regulatory tool in sculpting skeletal development. In animal models the mechanical environment can be altered in a number of ways including *in vivo* immobilisation of the musculature or the use of mutant mouse embryos in which the skeletal rudiments develop with reduced, absent or non-contractile muscle (reviewed in Nowlan et al., 2010b; Rolfe et al., 2013a). Both the chick and mouse are valuable vertebrate models used to investigate the effect of mechanical stimulation on embryonic skeletal development, due to their similarities with human musculoskeletal development. A schematic summary of abnormalities described in the chick and the mouse is shown in Figure 1.5.

1.5.1 Analysis of *In Ovo* Immobilisation

An advantage of the chick embryonic model is that it can be physically manipulated in ways that are impossible in the mammalian embryo (Nowlan et al., 2007). The chick shares many features of embryonic development with mammals and has a huge advantage of development external to the mother, *in ovo* (in the egg); which allows procedures and alterations to the embryos and resulting effects to be examined (reviewed in Stern, 2005). During chick development, innervations of chick myotomes occurs at approximately embryonic day 3 (King and Munger, 1990), and it has been reported that spontaneous limb movements occur from E3.5 to hatching (Hamburger, 1963). During egg incubation variables such as incubation temperature and humidity can have effects on the rate of development. When egg incubation temperature was increased by one degree, from 37.5°C to 38.5°C during incubation days 4 to 7, an increase in embryonic movement as well as an increase in muscle mass and bone length were reported, and it was suggested that the increase in muscle mass and resultant movement from these muscles caused an increase in bone growth (Hammond et al., 2007). An interesting observation in this study was that the increase in incubation temperature was only between day 4 and day 7, yet the differences in bone growth were recorded at E12.5 onwards,

indicating that the early period of incubation programmed the later bone development (Hammond et al., 2007).

Immobilisation can be achieved in the developing chick embryo either surgically, by extirpation of the spinal nerves, or by application of pharmaceutical agents which block neuromuscular signals (for example Nowlan et al., 2008b; Osborne et al., 2002). Immobilisation studies on the chick have shown that biophysical stimuli are required for correct initiation of ossification (Nowlan et al., 2008b) and several aspects of joint formation leading to joint fusions in extreme cases, but also loss of associated structures such as articular surfaces, menisci and patella (Drachman, 1966; Murray and Drachman, 1969; Osborne et al., 2002; Persson, 1983; Roddy et al., 2011b).

1.5.1.1 *In ovo* Immobilisation: Analysis of Ossification and skeletal rudiment length

Immobilisation of the embryonic chick has been used to study the effect of muscle contractions on bone development. Multiple studies have reported defects in growth of skeletal rudiments following immobilisation of the embryonic chick (Drachman, 1966; Hall and Herring, 1990; Hosseini and Hogg, 1991a; Hosseini and Hogg, 1991b; Nowlan et al., 2008a; Osborne et al., 2002). Hall and Herring in 1990 compared the effect of paralysis on individual skeletal elements during development and showed that while there was variation from site to site, the growth rates of the long bones (humerus, tibia, femur and ulna) were decreased by over 50% (Hall and Herring, 1990). Hosseini and Hogg (1991a) also reported reductions in the length and the size of the calcified diaphyses suggesting that a reduction in cellular proliferation was the cause (Hosseini and Hogg, 1991a). Further histogenic analysis of the immobilised tibia showed that there was a reduction in the spread of cartilage resorption in the marrow cavity (Hosseini and Hogg, 1991b). A reduction in the width of mineralised bone was shown in the tibiotarsus and the metatarsus following rigid paralysis, with a concurrent reduction in tibiotarsal cartilage volume being identified and no reduction in

mineralised bone (Osborne et al., 2002). Paralysis of zebrafish exhibited a reduction in the size of all pharyngeal cartilage; establishing muscle loading in this model as a regulator of chondrocyte intercalation (Shwartz et al., 2012).

Nowlan and colleagues showed a significant decrease in bone length in the tibiotarsus by embryonic day 11 following immobilisation. Using finite element (FE) analysis to model the effect of mechanical forces due to muscle contractions it was shown that as normal development proceeds in the tibiotarsus of the chick the patterns of stress, strain, hydrostatic pressure and fluid velocity stimuli change, with peak stimuli experienced by cells that undergo hypertrophy and initiate ossification some hours later- i.e. the peak stimuli spread from the mid-diaphysis, moving proximally and distally in advance of the wave of ossification (Nowlan et al., 2008a). It was therefore hypothesised that the spatial and temporal pattern of peak stimuli is required for the later initiation and progression of ossification. This was tested by immobilisation, which would remove the spatial and temporal pattern of stimuli, and was supported by the finding of reduced ossification as well as reduction in the expression of the molecular markers type ten Collagen in the hypertrophic zone and the perichondrium, and Indian Hedgehog in the pre-hypertrophic chondrocytes (Nowlan et al., 2008b).

1.5.1.2 *In ovo* Immobilisation: Analysis of Joint development

In addition to the alterations in skeletal rudiments following immobilisation described above, there is also a change to the cellular organisation and definition of tissue territories and corresponding regulatory gene expression in the developing joint (Roddy et al., 2011b). Early experimental manipulations of the chick embryo showed that joints are affected; as early as 1958 Lelkes grew mesenchymal condensations in *in vitro* explant cultures and showed that application of movement induced the formation of well-formed articular surfaces and even articular cavity formation, compared to unmoved control explants that showed cartilaginous

fusion and irregular proliferation (Lelkes, 1958). Removal of all mechanical stimulation was shown to result in the absence of nearly all of the articular cavities in the head and neck (Murray and Drachman, 1969). Paralysis has been shown to result in the complete absence of an articular cavity in the ankle joint, in parallel with the absence of the capsule, ligaments and the meniscus (Persson, 1983). Several studies have reported that immobilisation causes a failure of cavity formation (Murray and Drachman, 1969; Osborne et al., 2002; Ruano-Gil et al., 1978), with the interzone becoming occupied with cartilaginous tissue and no cavity forming. A reduction in cavity formation has also been reported in the developing knee joint following immobilisation (Sawamura et al., 2006). More recently, examining morphological changes in the knee joint using 3D imaging, and molecular changes through gene expression analysis, Roddy et al (2011b) showed dramatic changes to the shape of the condyles on the rudiment termini (Roddy et al., 2011b) (Figure 1.5c). They again used FE modelling to predict patterns of mechanical forces generated during avian embryo knee joint flexion–extension contraction and showed specific dynamic patterns in the emerging tissues of the joint. Modelling the state of rigid paralysis, predicted a change in biophysical stimuli, from tension and compression to largely compression in immobilisation (Roddy et al., 2011b). Increased levels of cell proliferation were reported in femoral condyles that had the highest level of biophysical stimuli in control knee joints, indicating mechanical loading to have a stimulatory effect on outgrowth of condyles (Roddy et al., 2011a). The expression of genes encoding the signalling molecules Bmp2 and Fgf2 were lost following immobilisation of the chick knee joint, as well as genes involved in hyaluronan synthesis (*Has2*) and reception (*Cd44*) implicated in the cavitation process (Roddy et al., 2011b) (Figure 1.5b). Expression of *Pthlp* was disrupted following immobilsation from the clear peri-articular region in normal knee joints, to "fuzzy" expression across the interzone (Roddy et al., 2011b) (Figure 1.5b). Identification of genes that are disregulated upon alteration of mechanical stimulation are thus termed mechanosensitive genes and were revealed as potential key mediators of mechanical

stimulation in joint development (Roddy et al., 2011b). Following these findings of the alteration in tissue organisation observed in the knee joint region it was proposed that the correct spatial patterning of tissue territories within the developing joint is dependent on the appropriate dynamic mechanical environment (Roddy et al., 2011b). This is in contrast to previous proposals that mechanical stimulation is only required for the relatively late event of cavitation, without affecting joint specification or patterning (Lamb et al., 2003; Osborne et al., 2002; Pitsillides and Ashhurst, 2008).

1.5.2 Analysis of the Role of Mechanical stimulation in Mammalian Mouse Models

Essential information about regulatory genes and the role of environmental stimuli for skeletal development has emerged using the developing chick model; however for appropriate comparison with human development the mammalian murine model has been utilised. Muscle contractions begin relatively early in development, at approximately the same time as the cartilage template is taking shape, after approximately E12.5 in the mouse (Suzue, 1996). Genetic manipulation has produced mouse models that can be used to study the effect of mechanical stimulation from movement on skeletal development; they include mice with reduced (*Myf5*$^{nlacZ/+}$*:MyoD*$^{-/-}$ (Rudnicki et al., 1993)) or immobile (Mdg$^{-/-}$ (Pai, 1965), Dock1$^{-/-}$ (our unpublished results)), or absent (*Splotch* (Franz et al., 1993; Tajbakhsh et al., 1997), *Splotch-delayed* (Franz, 1993; Vogan et al., 1993), *Myf5*$^{nlacZ/nlacZ}$*:MyoD*$^{-/-}$ (Kablar et al., 2003; Kassar-Duchossoy et al., 2004), *Six1*$^{-/-}$*:Six4*$^{-/-}$ (Grifone et al., 2005)) skeletal muscle. These mouse models that lack normal muscle contraction show similar skeletal phenotypes to those observed in the chick immobilisation studies including; joint fusions and alterations in the ossification pattern (Nowlan et al., 2010a).

1.5.2.1 Analysis of Ossification in Muscle-less mutants

Initial reports using the Myf5/MyoD double null mutants which develop no skeletal muscle showed reductions in the length of the scapula, the tibia and the femur, and in the shape of the

femur at E18.5 (Rot-Nikcevic et al., 2006), and significant differences in the dimensions of the diameter of the humerus, the humeral head and condyles, the total length of the ulna and the deltoid tuberosity at E18 (Gomez et al., 2007). Using two gene mutation models that lack limb muscle for different reasons, including Myf5/MyoD double null mutants and Splotch (Pax3 mutation) mutants that lack migration of myogenic precursor cells into the limb, Nowlan et al (2010a) showed altered ossification in the scapula, the humerus and the femur, with a reduction in the extent of hypertrophy shown in the humerus in the primary ossification center (Nowlan et al., 2010a) (Figure 1.5a). So although ossification proceeds, the altered pattern of initiation and progression shows that this process is not normal. Sharir *et al* (2011) used microCT of late stage long bone from non-contractile muscle mutants ($Cacnas^{mdg}/Cacnas^{mdg}$) to show that the normal pattern of mineral deposition specific to each bone is lost in the absence of contractions, thus compromising the mechanical properties of the bone (Sharir et al., 2011). This is associated with a difference in osteoblast distribution. So muscle generated mechanical stimuli are required for normal initiation of ossification, for normal local bone growth and bone strength. Analysis of expression patterns of candidate mechanosensitive genes were compared in the humerus and femur across three time-points TS23, TS24 and TS25, with more severe changes seen in the humerus than the femur (Nowlan et al., 2012). A decrease in the expression pattern was seen for *Col10* at each time-point examined, with a suggested lagging behind of expression in mutants compared to stage-matched controls (Nowlan et al., 2012). Examination of the *Ihh* expression pattern across time revealed that it was not just a delay as with collagen 10 expression, but a more complex deregulation (Nowlan et al., 2012). As the humerus was reported to be more severely affected than the femur, FE modelling of the control humerus and femur over three developmental time-points TS22, TS23 and TS24 were performed in order to identify if one element received a higher level of biophysical stimuli from muscle contraction that could account for the differences seen in muscle-less mutants. Peak biophysical stimuli were shown to be in the

region where bone forms, similar to what was seen in the chick tibiotarsus (Nowlan et al., 2008a), suggesting that a pulse of biophysical stimuli contribute to the normal initiation of osteogenesis (Nowlan et al., 2012). No differences were seen in the biophysical stimuli patterns and extent in the humerus and femur, indicating that the loss of muscle contractions alone could not explain the more severe effect seen in the humerus than the femur. The application of displacement, that mimics passive movement of the embryonic limb, caused by maternal or littermate movement, was applied to the FE model to test whether this could account for the discrepancies seen between the humerus and femur. It showed that higher biophysical stimuli were generated by passive displacement of the hindlimb compared to the forelimb (Nowlan et al., 2012) suggesting that stimuli generated by passive movement of the hindlimb might compensate for the loss of muscle contractions.

1.5.2.2 Analysis of Joint development in Muscle-less mutants

Joint development has also been shown to be affected in muscle-less mouse mutants (Kahn et al., 2009; Nowlan et al., 2010a). Joint loss was shown in three muscle-less mutants with effects seen in the elbow joint, the shoulder joint, partial loss in the carpal joints of the wrist and an absent joint in the ankle and metacarpals (Kahn et al., 2009). To assess whether the interzone cells were specified in the absence of limb musculature examination of the joint specific marker Gdf5 was performed over developmental time, with expression present in muscle-less elbow joints at E12.5 and E13.5 but an absence of expression by E14.5 in parallel with an absence of joint cavitation, as shown by expression of cartilage markers in the joint region (Kahn et al., 2009). To understand the potential mechanistic basis of the abnormalities seen in the joints, they crossed mouse lines to generate muscle-less *Spd* embryos that also carry a reporter construct indicating which cells are actively responding to a canonical Wnt signal. They showed apparent reduced canonical Wnt activity in some joints in muscle-less embryos. The study by Nowlan et al (2010a) identified that the shoulder and elbow joints in

muscle-less mice showed a dramatic reduction in the shape definition of the rudiment territories in conjunction with a complete loss of cellular organisation of the interzone between the cartilage rudiments (Nowlan et al., 2010a). In addition, the conclusion that reduced movement was responsible for the alterations was supported by examining an intermediate phenotype (reduced muscle in $Myf5^{+/-}/MyoD^{-/-}$ embryos). Similarly to the effect on ossification, a difference was seen in impact on fore and hind limbs which could similarly be explained by greater stimulation from passive movements experienced in the hindlimbs (Nowlan et al., 2010a; Nowlan et al., 2012). So the spectrum of effects on skeletal development through immobilisation of both chick and mouse embryos are similar (summarised in Figure 1.5).

Since a range of mouse mutants where muscle is immobile, reduced or absent (as described above) have similar skeletal phenotypes, alteration of the mechanical environment, rather than other aspects of the physical absence of muscle, such as trophic support, could be concluded (Kahn et al., 2009; Nowlan et al., 2010a; Sharir et al., 2011). It was suggested that as intermediate skeletal effects were seen in 'reduced muscle' environment, there may be a minimum threshold of mechanical forces that are required for normal skeletal development to occur (Nowlan et al., 2010a). This is supported by the chick immobilisation studies where reduced movement had similar effects, as previously reviewed (Section 1.5.1). From these results it is clear that skeletogenesis is affected by reducing mechanical stimulation.

Similar findings in different animal models (chick, mouse, zebrafish), using either immobilisation or absence/reduction of muscle, definitively separate paracrine and mechanical influences. Integrating these findings allows us to draw general conclusions about the specific aspects of skeletogenesis that require appropriate mechanical stimulation from adjacent twitching muscles for normal progression, including joint formation, ossification and rudiment shape (morphogenesis) (Rolfe et al., 2013a).

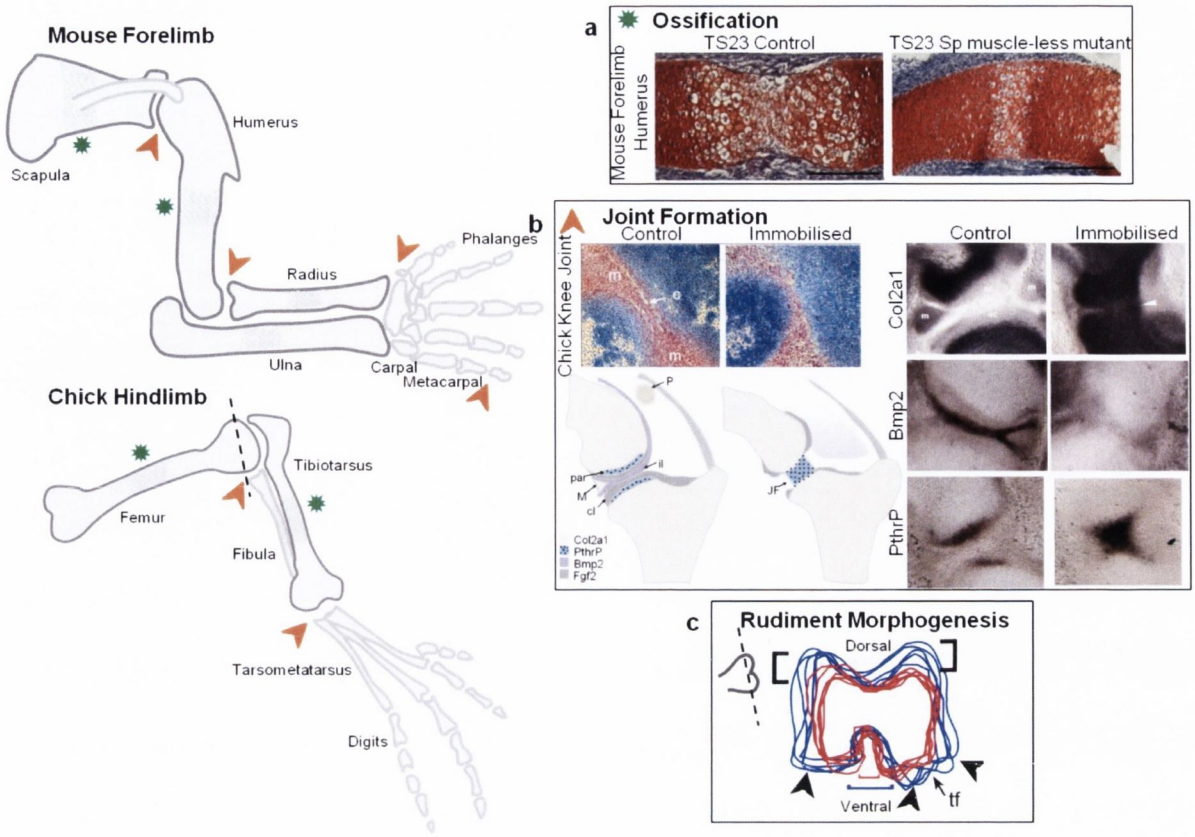

Figure 1.5: Lack of mechanical stimulation from muscle contractions impacts several aspects of skeletogenesis during embryonic development: the mouse forelimb and chick hindlimb are used here to summarise the effects on (✸) ossification, (▲) joint formation and (ᔓ) rudiment shape. The data shown in boxes **a**, **b** and **c** serve as examples of the evidence of impact on each process. (**a**) mid-diaphysis of the mouse humerus at TS23 (E14.5) in control and Sp muscle-less, stage matched embryos, showing reduction in the hypertrophic zone by safranin-o staining. (**b**) In the knee joint of immobilised chick embryos, lack of definition of joint territories is shown by histology (note the absence of organised cell layers within the presumptive joint) and gene expression patterns (as indicated) which normally define the territories of the forming joint, the cartilaginous rudiment (*Col2a1*), the peri-articular cartilage of the rudiment (*PthrP*), the intermediate layer of the interzone (Bmp2). The schematic in box **b** summaries effects of immobilisation on the knee joint, p; patella, pai; peri-articular, m; meniscus, il; indermediate layer, cl; chondrogenous layer, JF: joint fusion. (**c**) The effect on rudiment morphogenesis is exemplified by the change in shape of the distal femur; the diagram represents outlines of control (blue) and immobilised (red) sections, overlaid. Images are adapted from (Rolfe et al., 2013a).

1.5.3 Response of Progenitor Cells *in vitro* to Mechanical Stimulation

A major challenge for the successful development of stem cell therapies for skeletal disorders is defining the conditions required for priming stable differentiation of progenitor cells into the appropriate tissues required for repair and regeneration. The differentiation of transient cartilage that undergoes hypertrophy and is replaced by bone in the developing skeletal rudiments is distinct from the differentiation of mature chondrocytes that are housed at the

rudiment termini to form permanent articular cartilage, as previously described. Each of these distinct processes are highly regulated through the coupling of biochemical and biomechanical factors that the cells experience *in vivo*. Bioengineering approaches use *in vitro* culture systems that allow for the preliminary screening of cell specific responses prior to scaling up for repair strategies, and there is current widespread interest in testing combined biochemical and biomechanical factors for their influence on cartilage differentiation. It is clear from preceding sections that chondrogenesis is a tightly regulated process that relies on signalling cues and biophysical signals for correct cellular differentiation. In the embryonic limb *in vivo*, the cells that form mesenchymal condensations are the progenitors of the entire skeletal system. In culture, chondrocytes derived from cartilage tissue can provide a limited source of progenitor cells for cartilage therapies. However the existence of multipotent stem cells that can be induced to differentiate to cartilage hold great promise for more extensive therapies.

Stem cells are defined as undifferentiated cells capable of self renewal that can differentiate into more than one specialised cell type, but the cellular differentiation potential varies among different stem cell populations. The differentiation potential of progenitor cells can be described as either; (1) totipotent- capable of giving rise to all cell types of the embryo as well as the embryonic component of the placenta; (2) pluripotent- can give rise to all cell types of the embryo arising from the three germ layers, endoderm, mesoderm and ectoderm, (3) multipotent- can give rise to multiple lineage-restricted, tissue specific cell types, for example the mesengenic process giving rise to bone, cartilage, muscle, tendon, ligament, and other connective tissues, and (4) unipotent cells- can only generate one cell type. Embryonic stem cells are derived from the early embryo and are pluripotent whereas adult derived stem cells such as Mesenchymal Stem Cells (MSCs) are generally multipotent. Due to the social, ethical and legal constraints surrounding the use of embryonic stem cells, much work has been

performed over the past 20 years on multipotent, adult derived stem cells. The discovery that adult bone marrow (BM) derived stem cells demonstrate a multi-lineage capacity to differentiate into multiple tissue types has promoted them as an attractive source to study (Johnstone et al., 1998; Pittenger et al., 1999). More recent reports have provided further insights into stem cell populations derived from a variety of adult tissues including infrapatellar fat pad (Dragoo et al., 2003; Wickham et al., 2003), synovial membrane (De Bari et al., 2001) and subcutaneous adipose tissue (Vidal et al., 2008). The more recent discovery that adult derived cells can be altered by forced expression of pluripotency genes to resemble embryonic stem cells (induced pluripotent stem (iPS) cells) will no doubt provide new improved stem cell populations with greater proliferation and differentiation potential for cartilage regeneration (Ko and Im, 2014; Ko et al., 2014; Okita and Yamanaka, 2010; Takahashi and Yamanaka, 2006; Tsumaki et al., 2015).

Cumulative evidence shows that various mechanical stimuli influence the differentiation of stem cells isolated from adult sources (reviewed in Kelly and Jacobs, 2010; Responte et al., 2012). These studies demonstrate the importance of mechanical stimuli but have varied results depending on the cell context. Tissue engineering strategies have incorporated bioreactors to apply mechanical loading regimes to progenitor cells *in vitro* in order to maximise cell proliferation and differentiation to guide specific tissue development. For example compression can enhance chondrogenesis in BM derived MSCs but it depends on when the load is applied and in what cellular environment (Angele et al., 2004; Mouw et al., 2007; Thorpe et al., 2008). The cell source and heterogenitiy among MSC populations from different sources may also contribute to variable responses (Phinney, 2012).

Despite variability in response, some generalities can be drawn from the work on biophysical stimulation of stem cells to date. The computational model generated by Prendergast et al (1997) proposed that a balance of fluid flow and shear strain determines the spatial and

temporal pattern of MSC cell fate and this prediction has been corroborated by various experimental results including work in bone chambers or 3D scaffolds (Khayyeri et al., 2009; McMahon et al., 2008b). Hydrostatic Pressure (HP) has been largely associated with chondrogenic differentiation whereas tensile strain and fluid induced shear stress are generally shown to induce osteogenesis (Carter et al., 2004). Experimentally cyclic HP applied to MSCs in defined medium was found to enhance chondrogenesis, increasing expression of chondrogenic markers (Angele et al., 2003; Miyanishi et al., 2006b; Sakao et al., 2008; Wagner et al., 2008). Several parameters, including magnitude, frequency, onset and duration of HP stimuli are important in the response (Elder et al., 2005; Ikenoue et al., 2003; Miyanishi et al., 2006a). Application of HP has recently been shown to increase the functional properties of cartilageous tissues (Huang et al., 2010; Meyer et al., 2011; Steward et al., 2013).

Cyclic tensile strain is prominent in the superficial region of cartilage tissue and at the cartilage-bone interface and is predicted (with octahedral shear stress) to stimulate maturation and ossification (Carter and Wong, 2003) and is experimentally associated with enhanced osteogenic differentiation of stem cells. Tensile strain applied in a two-dimensional culture caused a switch in cell fate from adipogenic to osteogenic differentiation via up-regulation of canonical Wnt responsive genes (Sen et al., 2008). Wnt signalling (through β-catenin) was also implicated in the osteogenic differentiation of bone marrow derived cells embedded in alginate-gels exposed to dynamic tension (Haudenschild et al., 2009). Similarly short-term cyclic tensile strain reduced the rate of MSC proliferation and induced osteogenic differentiation (Kearney et al., 2010). Conversely, it has also been shown that cyclic tensile loading on BM MSCs promotes fibrocartilage-like differentiation (Connelly et al., 2010). Fluid-induced shear stress has also been shown to promote osteogenic differentiation (Arnsdorf et al., 2009a; Arnsdorf et al., 2009b; Sharp et al., 2009) through RhoA/ROCK2 and enhanced tension in the actin cytoskeleton (Arnsdorf et al., 2009b). In a similar study

oscillatory fluid-flow induced β-catenin nuclear translocation and up-regulation of Wnt associated proteins, Wnt5a and Ror2, which are both involved in RhoA activation (Arnsdorf et al., 2009a) and ultimately Runx2 expression (Arnsdorf et al., 2009b).

1.6 Identification of Mechanosensitive Genes during embryonic skeletal development

The molecular response following alterations in the mechanical environment have been previously reported in various *in vivo* and *in vitro* studies in an attempt to understand in more detail the means by which mechanical stimuli modulate the cellular response during differentiation. Gene expression profiling has the potential to uncover hundreds of genes that respond to mechanical stimuli simultaneously, termed mechanosensitive genes. A non-exhaustive list of studies that have identified potential mechanosensitive genes using both *in vivo* and *in vitro* experimental regimes following alterations in the mechanical environment is presented in Table 1:1. Gene expression profiling to identify genome wide changes under altered mechanical environments has been carried out using *in vitro* culture systems in conjunction with microarray technology, including osteoblast cell-lines subjected to weightlessness or microgravity conditions (Patel et al., 2007), chondrocyte-laden constructs and murine cartilage explants to which dynamic compression was applied (Bougault et al., 2012) and chondrocyte cell lines exposed to hydrostatic pressure (Sironen et al., 2002).

Previously mentioned studies that have altered the mechanical environment *in vivo* have investigated candidate genes for altered expression, in order to assess the molecular response to alterations in biophysical stimuli (Kavanagh et al., 2006; Nowlan et al., 2012; Nowlan et al., 2008b; Roddy et al., 2011b). Application of various forms of mechanical stimulation during *in vitro* culture regimes is a major goal of bioengineering techniques in order to create tissue suitable for regeneration applications. Revealing molecular responses to mechanical stimulation is useful to aid in our understanding of the molecular responses at a cellular level.

Table 1:1: Identification of mechanosensitive genes using various *in vivo* and *in vitro* experimental regimes.

Gene/Protein showing altered expression	**Experimental approach**	**Reference**
Col10, Fgfr3, Ihh, Runx2	*In vivo,* muscle-less murine models, humerus and elbow joint	(Nowlan et al., 2012)
325 candidate genes (FC ≥1.4≤, p≤0.01)	*In vito*; primary mouse chondrocytes subjected to short-term dynamic compression	(Bougault et al., 2012)
Cd44, Pthlp, Col2a1, Fgf2, Bmp2, Has2	*In ovo* immobilisation of chick, knee joint	(Roddy et al., 2011b)
Gdf5, Noggin	*In vivo,* muscle-less murine models, elbow joint	(Kahn et al., 2009)
Runx1	*In vitro*: fluid shear stress on embryonic stem cells promoting haemoatopoietic development	(Adamo et al., 2009)
Col10, Ihh	*In ovo* immobilisation, chick tibiotarsus	(Nowlan et al., 2008b)
106 candidate genes (FC ≥2≤, p≤0.05)	*In vitro*: 2T3 murine osteoblast precursor cells subjected to rotating wall vessel to stimulate microgravity	(Patel et al., 2007)
Fgfr3, Fgfr1, Fgfr4, Fgf1	Four point bending to create fluid shear and strain forces in an osteoblast cell line	(Jackson et al., 2006)
Itgbp1, Cox2, Igf1, Hyal2	*In vitro* Steady fluid shear stimulation of C3H and B6 murine osteoblasts	(Lau et al., 2006)
Runx2, Opn, Col10, Col2	*Ex vivo*: Cyclic compression of whole rabbit femoral condyle explant	(Sundaramurthy and Mao, 2006)
Erg1, Fgf2, Cox2, cFos	*In vitro*: mechanical force induced changes in gene expression in osteogenic cell line	(Hatton et al., 2003)
51 candidate genes (FC ≥2≤, p≤0.05)	*In vitro*: chondrocyte cell line under continuous hydrostatic pressure	(Sironen et al., 2002)
Igf1, Tgfβ1, Fgf2, IL6	*In vitro* mechanical cyclic tensile stretch on human osteoblast-like cells	(Cillo et al., 2000)
Cd44, Has2	*In vitro*: application of mechanical strain to chick fibrocartilage	(Dowthwaite et al., 1999)
Il1b	*In vitro*: compression of micromass cultures	(Takahashi et al., 1998)
Igf1, Tgfβ, cfos, Opn, Ocn, Alp	*Ex vivo*: Four point bending of rat tibia	(Raab-Cullen et al., 1994)

Multiple developmentally important molecular signalling pathway component genes have been identified to be altered in abnormal mechanical environments, for example components in the Tgfβ pathway have been shown to be altered, including Bmp2 expression in the immobilised chick knee joint (Roddy et al., 2011b), Bmp4 was down-regulated following exposure to microgravity (Patel et al., 2007) and Tgfβ1 was increased following mechanical stretch on an osteoblast cell line (Cillo et al., 2000). Components of the Wnt signalling pathway were previously linked to mechanosensitivity including a down-regulation of Wnt9a in the elbow joint in muscle-less mice (Kahn et al., 2009), a down-regulation of the antagonist

Sfrp2 was identified in microgravity conditions (Patel et al., 2007), a down-regulation of the receptor frizzled 10 (Fzd10) following compression of agarose-embedded chondrocytes (Bougault et al., 2008) and an up-regulation of Wnt8b and a concurrent down-regulation of the Fzd7 gene following dynamic tension of human BM MSCs (Haudenschild et al., 2009). An alteration of components of the Fgf pathway have similarly been identified to be altered following alteration of mechanical stimulation (shown Table 1:1), and that may be due to its role in regulation of chondrocyte maturation that is altered as previously described in section 1.3.4.

1.7 Objectives of the Thesis

Despite strong evidence, laid out above, that mechanical cues impact skeletal development, we have very little insight into the mechanisms that sense and integrate this information during cell differentiation and patterning of tissues. This project used a combination of embryonic animal models, transcriptome profiling, molecular analysis, gene function analysis and differentiation of cells in culture to investigate how mechanical stimulation influences key developmental regulatory genes that control cellular differentiation in the developing skeletal system. Understanding the role of mechanical stimulation as a regulator of cartilaginous and skeletal development is important not only because it aids our knowledge of a complex developmental process and the fundamentals of cellular regulation but also because of its implication for regenerative therapies. The ability to guide the process of cellular differentiation through exogenous application of biochemical cues combined with mechanical stimulation may aid the *in vitro* recreation of conditions that exist within a developing joint or rudiment in order to promote progenitor cell differentiation towards a specific lineage, and to produce a functional tissue phenotype. Before this knowledge can be applied to the generation of tissues *in vitro,* a greater understanding of the complex signalling pathways and stimuli that control normal growth and development are required.

Central Hypothesis: That mechanical stimulation of progenitor cells in the embryonic skeletal system influences tissue patterning and cell differentiation through altering the activity of key developmental regulatory genes.

Central Objective: To uncover molecular mechanisms underlying the response of developing skeletal cells to mechanical stimulation.

Aim 1: To carry out a genome wide analysis of gene expression differences in skeletal rudiments (humeri) from muscle-less compared to control littermate mouse embryos, with a view to identifying mechanosensitive genes during skeletal development.

Very little is known about how mechanical stimulation can influence gene expression. Chapter 3 reports Microarray and RNA transcriptome sequencing analyses of *Spd/Spd*$^{-/-}$ muscle-less humeri and associated joints. This chapter tests the hypothesis that mechanical cues generated by muscle contractions exert influence on gene transcription directly and/or indirectly, particularly through known signalling pathways.

Aim 2: To explore potential molecular mechanisms impacted by mechanical stimuli in the developing limb skeleton.

Chapter 4 reports the characterisation of selected genes that are differentially expressed in developing humeri of muscle-less compared to control embryos, examining in particular the alterations to specific signalling pathway component genes and examining distinct effects on different developmental processes; ossification and joint development.

Aim 3: To examine the effects of altering Wnt signalling on limb skeletal patterning as a candidate integration point for mechanical cues.

Chapter 5 reports establishment of techniques to disturb Wnt signalling in embryos *in vivo* using mis-expression of pathway activators and repressors. Building on the findings of

Chapters 3 and 4 which implicated Wnt signalling as a key point of integration for mechanical cues, the initial objective was to assess whether manipulation of the Wnt pathway phenocopies what is seen following the removal of mechanical stimulation.

Aim 4: To examine the influence of mechanical stimulation (hydrostatic pressure) on chondrogenesis *in vitro* from adult derived stem cells and embryonic skeletal precursor cells.

Chapter 6 reports that application of hydrostatic pressure on embryonic and adult derived stem cells show similar responses in gene expression that are indicative of a maintenance of a stable cartilage phenotype. This tests the hypothesis that the correct combination of mechanical and biochemical signalling is required to direct appropriate differentiation and maintenance of stable cartilage, preventing maturation and hypertrophy.

Chapter 2

2. Methods

General methods used throughout the project are reported here. Additional methods specific to the work presented in each subsequent chapter, as well as experimental design for chapter specific experiments, are presented in the relevant chapter..

2.1 Embryo Collection

Male and female heterozygote C57BL/Pax3$^{Spd/+}$ mice were purchased from the Jackson Laboratory (Strain Name: C57BL/6J-*Pax3*$^{Sp\text{-}d}$/J, Stock Number 000565) and were housed in the Bioresources Unit TCD, were mated over-night and vaginal plugs were checked the following morning. The morning of finding a vaginal plug, indicating mating had taken place, was designated embryonic day (E) 0.5 (0.5 days post coitum (dpc)). Embryonic material was collected from timed pregnancies of heterozygote dams on the afternoon of E14.5. The pregnant females were humanely sacrificed by CO_2 intoxication and followed by cervical dislocation and the maternal uteri containing the embryonic material were dissected and placed in ice cold Phosphate buffered saline (PBS). Individual embryos were dissected from each decidua using RNase-free equipment. Each individual embryo was accurately staged, according to Theiler staging criteria (Theiler. K, 1972) and any visible phenotype was recorded (spina bifida; exencephaly; thin, muscle-less limbs). Genomic DNA from each embryo was obtained from the head tissue, using standard protocols (Sambrook & Russell 3rd

Ed; detailed below) for genotyping. The body of the embryo was then either: (1) fixed in 4% paraformaldehyde (PFA) in PBS overnight and dehydrated through a graded series of methanol/ PBS plus 0.1%Triton (PBT) (25%, 50%, 75% methanol; 1x10min, 100% methanol; 2x10min) washes and stored individually at -20°C according to assigned embryo number; or (2) the humeral rudiments were micro-dissected, pooled according to genotype and RNA extracted; In total RNA was extracted from 18 ($^{+/+}$), 44 ($^{+/-}$) and 38 *Spd*/*Spd*$^{-/-}$ humeri (sections 3.2.3).

2.2 Genotyping of Embryos

Embryonic head tissue was obtained from each individual embryo, digested overnight with proteinase K (100µg/ml) in extraction buffer containing 100mM Tris pH7.5, 1mM EDTA (Ethylenediaminetetraacetic acid), 250mM NaCl (Sodium Chloride), 0.2% SDS (Sodium dodecyl sulphate), at 37°C, extracted with equal volumes of phenol (Sigma-Aldrich, Ireland: Cat no: P1037) and chloroform (Sigma-Aldrich, Ireland: Cat no: C2432). DNA was precipitated with ice-cold 70% ethanol (Sigma-Aldrich, Ireland: Cat no: E7023), the purified pellet was washed with 70% ethanol and re-suspended in 10mM Tris-EDTA. For each embryo the DNA was used as template in two specific polymerase chain reaction (PCR) amplifications; one using wild-type Pax3 primers and the other using an upstream Pax3 primer specific for the *Spd* mutation (Table 2:1) (as previously designed by Keller-Peck and Mullen, 1997) to detect the one base pair difference between mutant and wild-type alleles; all primers used at 500µM. The amplification program consisted of an initial denaturation at 94°C for 4 minutes, then 30 cycles of: denaturation at 94°C for 30 seconds, annealing 63°C for 30 seconds, and extension 74°C for 30 seconds. For the Spd genotyping the wild-type (+/+) (130bp) and mutant (-/-)(150bp) amplicons were distinguished following separation by electrophoresis on a 2.5% agarose-gel, compared to hyperladder ^{TM} IV size standard (Bioline, UK). In all cases the established genotype confirmed the observed phenotype for homozygous

mutant *Spd/Spd* embryos. The total number of embryos obtained and their respective stage and genotype can be seen in table 2.2. In accordance with Mendialian inheritance the homozyogote mutant alleles displayed a 23.2% occurrence in the Splotch-delayed strain.

Table 2:1:Pax3 specific primers used to distinguish Splotch (*Sp*) and Splotch-delayed (*Spd*) mutant and wild-type alleles.

Splotch (*Sp*)	**Primer Sequence**
Forward Pax3 Primer	5'-CAGAGACAAATTGCTCAAGGACG-3'
Reverse Wild-type Pax3 Primer	5'-GCGGCTGATAGAACTCACTG- 3'
Reverse Sp Mutant Primer	5'-GCGGCTGATAGAACTCACAC- 3'
Splotch-delayed (*Spd*)	
Forward Wild-type Pax3 Primer	5`-AGGGCCGAGTCAACCAGCACG- 3`
Forward Spd Mutant Primer	5` AGTGTCCACCCCTCTTGGCCTCGGCCGAGTCAACCAGGTCC -3`
Reverse Pax3 Primer	5'-CACGCGAAGCTGGCGAGAAATG-3

Table 2:2 Embryos from heterozygote Splotch ($Pax3^{Sp/+}$) and Splotch-delayed ($Pax3^{Spd/+}$) crosses. Genotypes and developmental stages recorded.

Developmental Stages									
	TS20	**TS21**	**TS22**	**TS23**	**TS24**	**TS25**	**TS26**	**TS27**	**Total**
Splotch: *Sp* Genotype									
+/+		-	4	7	-	-	-	-	11
+/-		3	15	53	-	-	-	-	71
-/-		3	9	6	-	-	-	-	18
Total	**4**	**6**	**28**	**66**	**-**	**-**	**-**	**-**	**104**
Splotch-delayed: *Spd* Genotype									
+/+		1	26	158	3	1	4	2	195
+/-		-	46	339	14	1	3	3	406
-/-	1		14	152	14		2		183
Total	**5**	**1**	**86**	**649**	**31**	**2**	**9**	**5**	**788**

2.3 Histological Analysis

Preparation of sections for histological analysis all followed the protocol below. The upper body of the embryo that had been fixed in 4% PFA and stored at -20°C in 100% methanol were rehydrated by a series of 10min washes of 75%, 50% and 25% methanol/PBT followed by a 10min wash in PBS. The forelimbs were then dissected off the body cavity and were dehydrated through serial washes of ethanol (EtOH): twice for 15mins in 50% EtOH, twice in 70% EtOH, first for 15mins and the second for 30mins, then 1hr in 90% EtOH and twice in 100% EtOH for 1hr. De-calcification was performed on TS24 limbs in 10%

Ethylenediaminetetraacetic acid (EDTA) over two nights prior to dehydration in EtOH. All steps were performed at room temperature (RT). The limbs were then placed in Histoclear at RT over night in glass jars. The limbs were then washed in 50% histoclear: 50% paraffin wax for 1h at 60°C; followed by two 1hr washes in 100% paraffin wax at 60°C. The limbs were then aligned to be sectioned longitudinally and embedded in 100% wax that was left to harden over night on a cold plate. The hardened wax block was then serially sectioned using a microtome (Leica RM2255) at a thickness of 5-10μm. Consecutive serial sections of the regions of interests were floated over ddH_2O at 50°C in a pre-warmed water-bath (Leica HI1210) and collected on a microscope slide and allowed to dry at RT prior to staining. De-waxing and re-hydration of the slides was performed prior to staining with 3min washes in Histoclear and serial washes in 100% EtOH, 90% EtOH and 70% EtOH.

2.3.1 Safranin-O staining

For the Safranin-O staining slides were incubated in 0.005% Haemotoxylin solution (Equal Parts Haematoxylin: Ferric chloride solution; 1g Weight's Iron Haematoxlin Solution in 100ml of 95%Ethanol; 4ml 29% Ferric chloride + 1ml HCL in 95ml ddH_2O) (40sec) and then washed with running tap water before being incubated with 0.001% Fast Green Solution (5mins) (0.01 g of Fast green (FCF, C.I. 42053) in 1000ml of ddH_2O). The slides were then quickly washed in 1% acetic acid (15secs) (1ml of glacial acetic acid in 99ml ddH_2O) and then counterstained with 0.1% Safranin-O Solution (0.1g Safranin-O (C.I. 50240) in 100ml of ddH_2O), the duration of counterstaining was dependent on the stage of the tissue (≤TS23 5mins, ≥TS24 2mins). The slides were then dehydrated in serial washes of EtOH for 2mins each (70%, 90%, 100%) followed by a final wash in 100% histoclear (5mins) prior to being mounted using DPX synthetic resin. The Safranin-O stains the hyalurnoic acid components contained in cartilage and mucins orange, the hematoxylin stains the nuclei purple, fast green stains mast cells green and the background cytoplasm of other cells grey green.

2.4 Embedding and Sectioning of embryonic tissue for *in situ* hybridisation

Preparation of sections for *in situ* hybridisation staining followed the same initial re-hydration and dissection protocols. The upper body of the embryo that had been fixed in 4% PFA and stored at -20°C in 100% methanol were rehydrated by a series of 10min washes of 75%, 50% and 25% methanol/PBT followed by a 10min wash in PBS. The forelimbs were then dissected off the body cavity and embedded using different techniques, as described below for the two sectioning techniques. The two techniques that were used were in order to prepare thick (60-100μm using a Vibratome) and thin (10-30μm using a Cryostat) longitudinal sections for mRNA transcript identification.

2.4.1 Vibratome sectioning

Following rehydration the right and left limbs were embedded in 4% Low Melting Point (LMP) Agarose (Invitrogen, UK) in PBS. The limbs were orientated for longitudinal sections throughout the rudiments. 60μm, 80μm and 100μm sections were cut in PBS with a vibrating microtome (Leica™, VT1000S) and floating sections were collected in PBS in 12-well plates and pre-hybridised for *in situ* hybridisation, described in section 2.5.2

2.4.2 Cryosectioning

Following rehydration the limbs were equilibrated in 30% Sucrose/ PBS overnight at 4°C and flash frozen in a dry ice/ethanol bath and stored at -20°C immediately. Limbs were mounted onto the chuck within the frozen chamber of the cryostat (Leica CM1860) using OCT (optical cutting temperature compound), orientation of the limb on the mount was adjusted and 10-30μm sectioning was performed. Serial sections were mounted onto Superfrost plus slides (VWR; Cat #631-0108) and stored at -20°C prior to pre-hybridisation.

2.4.3 Paraffin sectioning

Following methanol rehydration the limbs were dehydrated though a graded series of ascending concentrations of ethanol solutions comprising 50% twice for 15mins, 70% twice for 30mins, 90% for 1hr, 100% twice for 1hr each. Ethanol dilutions were prepared using absolute ethanol (100%) and ddH_2O. Prior to the introduction of paraffin wax limbs were placed in glass vials and washed in histoclear at RT overnight. A 50:50 histoclear: liquid paraffin wax wash then performed at 60°C for 1hr, followed by two pure wax washes for 1hr each at 60°C. Limbs were embedded longitudinally in pre-warmed plastic moulds and left to harden on a cold plate prior to sectioning. Sectioning was performed using a standard rotary microtome (Leica, RM2255). Sections of 5-10μm were obtained on a slide series, with consecutive sections stretched onto each slide using a pre-warmed 50°C waterbath (Leica HI1210).

2.5 *In Situ* Hybridisation

2.5.1 Probe Preparation

An I.M.A.G.E (Integrated Molecular Analysis of Genome and their Expression) consortium (http://www.imageconsortium.org/) expressed sequence tag (EST) mouse cDNA clone bank (IRAV) was used to generate the plasmid DNA of the genes of interest. To amplify and purify the plasmids an inoculate of the EST bank E.coli bacterial clone was grown on Luria Bertoni (LB) agar plates (1% Peptone, 0.5% Yeast Extract, 1% NaCl, 1.5% Bacto-Agar in ddH_2O) supplemented with 100μg/ml amplicillian (Sigma). Details of the cDNA clones used to generate RNA probes are summarised in Table 4:1.

Single colonies of each *E.coli* bacterial clone were expanded in LB broth cultures (100ml; plus ampicillan 100μg/ml) and then plasmid DNA was extracted and purified using a PureYield™ Plasmid Midiprep system (Promega) according to manufacturer's protocol. Each plasmid DNA was sequence verified (Source Biosciences) using vector primer sites flanking

the insert. Sequences were analysed using tools provided by the National centre for Biotechnology Information (http://www.ncbi.nlm.nih.gov) to ensure it represented a cDNA clone of the correct gene and to identify the size and exact identity of the clone that was present (detailed in Table 4:1). Plasmid DNA was linearised with appropriate restriction enzymes to produce template DNA for *in vitro* transcription. Antisense and sense digoxigenin (DIG)-labelled RNA probes were generated, according to vector and insert orientation, from 1µg linearised plasmid DNA using T7, T3 and SP6 RNA polymerase binding sites in the relevant plasmid vector (all reaction components from Roche) in a 20µl volume at 37°C for 3hrs. Other components included DigRNA labelling mix (Roche), RNase inhibitor (Roche), 10x Transcription Buffer (Roche) and 0.2M DTT (DL-Dithiothreitol). RNA production and integrity was checked by running 1µl on a 1% agarose gel. If visible RNA production was present (at equal or up to approximately 5 fold intensity compared to the DNA band) the DNA template was degraded by incubation with 1µl of RNase free DNase (Roche) for 15mins at 37°C. The *in vitro* transcribed RNA was purified on a G25 column (Amersham Biosciences) as per manufacturer's instructions, quantified by Qubit RNA assay kit spectrophotometry, as per manufactures instructions and stored at -20°C in an equal volume of hybridisation solution (2% blocking reagent (Boehringer), 50% deionised formamide, 5x Saline-sodium citrate (SSC) (Sigma), 0.5% [(3-Cholamidopropyl-[(3-Cholamidopropyl) dimethylammonio]-1-propanesulfonate (CHAPS), 50µg/ml Heparin, 100µg/ml yeast RNA, 0.1% Trition and 5mM EDTA (ethylenediamine tetra-acetic acid)).

2.5.2 Fixation and pre-treatment of floating tissue sections

For testing probes and preliminary analysis of expression patterns within the developing forelimb, vibratome sections of thickness 60-100µm were prepared, as described above (section 2.4.1). After two 10min washes in PBT the free floating sections were treated with proteinase K (10µg/ml in Tris-HCL, 5mM EDTA pH7.5) for 5 mins at RT. Sections were

then washed twice in PBT (10mins) at 4°C and fixed in 4% PFA/0.2% Glutaraldehyde for 20mins at 4°C. Following fixation, 3 x 5min washes in PBT were performed at RT and a further 30min wash in PBT at 55°C. The sections were then pre-hybridised at 55°C overnight in hybridisation solution (section 2.5.1). Sections were then ready for hybridisation with antisense or sense RNA probes or they were stored at -20°C for future hybridisation.

2.5.3 Fixation and pre-treatment of Frozen and Paraffin sections

Following selection of slides, paraffin was removed with histoclear and rehydrated through a series of ETOH washes, opposite to those described in section 2.4.3; two 10min washes in PBS was performed in a glass trough with slides facing back to back. Sections were then treated with proteinase K (10µg/ml in Tris-HCL, 5mM EDTA pH7.5) on each slide for 5 mins at RT. Sections were then washed twice in PBS (5mins) at 4°C and fixed in 4% PFA/0.2% Glutaraldehyde for 20mins at 4°C. Following fixation, 2 x 5min washes in PBS were performed at RT. An acetlyation step was then performed using triethanolamine (Sigma Aldrich, Ireland. Cat no: 90279) (1:75) in DEPC ddH_20, pH8.0 and Acetic Anhydride (Sigma Aldrich, Ireland. Cat no: 242845) (1:400) with constant stirring for 10mins at RT. The sections were then washed twice in PBT (5mins) and allowed to air dry for ~15mins at RT. The sections were then ready for hybridisation by overlaying the slides with 1µg/ml denatured RNA probe in hybridisation solution. Incubation with probe was performed under coverslips in a humid chamber containing tissues soaked in 5xSSC, so the sections did not dry out. The slides were supported on struts. All further washing, hybridisation and antibody staining was performed on the slide.

2.5.4 Hybridisation, washing and detection of probe on vibratome sections

Antisense and sense probes were denatured at 80°C for 3mins in hybridisation solution (described in section 2.5.1), and sections were incubated at 55°C over 2-3 nights in hybridisation solution containing either antisense or sense probe at minimum concentrations

of 1μg/ml. After hybridisation the un-hybridised probe was removed and stored at -20°C for reuse up to 3 times.

Post hybridisation washes were carried out at 65°C as follows, 1 x 5mins in post-hybridisation wash (PHW) solution (50% formamide, 5x SSC and 0.5% CHAPS), then three serial 30min washes in decreasing concentrations of formamide, SSC and CHAPS and increasing concentrations of Wash 1 (W1) solution containing (2x SSC and 0.1% CHAPS), (75% PHW/25% W1, 50% PHW/50% W1, 25% PHW/75% W1). This was followed by two 30min washes in W1 followed by two 30min washes in Wash 2 (W2) containing 0.2xSSC and 0.1% CHAPS. Two ten min washes were then performed in TNT (100mM Tris-HCL pH7.5, 150mM NaCl, 0.1% Trition X-100) at RT. After washing, the sections were then blocked in Maleic Acid buffer (100mM Maleic Acid, 150mM NaCl) containing 3% blocking powder (Boehringer) for 3hrs at 4°C followed by incubation in fresh blocking buffer with 1/3000 dilution of anti-digoxigenin Fab fragments conjugated with alkaline phosphatase (AP) (Roche) for 12hrs at 4°C with rocking. Post-antibody washes were then performed at RT in TNT, 2x 5mins washes followed by 3x 1hr washes then a 16hr fresh TNT wash at 4°C. Following this the sections were washed 3x 15mins in NMT (100ml Tris-HCL pH9.5, 50mM $MgCl_2$, 100mM NaCl) as this provides the optimal pH for staining. The chromogenic reaction was carried out in half strength stain in NMT containing 1675ug/ml 4-nito blue tetrazolium chloride (NBT; Roche) and 175ug/ml 5-bromo-4-chloro-3-indolyl-phosphate (BCIP; Roche). Sections were developed in the dark at RT with rocking. Fresh staining solution was replaced after 1 hour. The staining was monitored and once a strong signal had been produced (4-24hrs) the reaction was stopped in PBS. The sections were then fixed in 4% PFA (1hr to overnight) before mounting of the free-floating sections on slides with Aqua-polymount (Polysciences, Inc) and coverslips.

2.6 RNA Preparation for gene expression analysis

The humeri, including the associated joint regions, were finely, manually micro-dissected from control and mutant (*Pax3*$^{Spd/Spd}$) embryos at stage TS23. Pooling of rudiment tissue from multiple embryos of the same genotype (n=2-4) was performed, totalling between 4-8 humeri for extraction. Tissue was mechanically homogenised and total RNA extracted (SV Total RNA Isolation System: Promega). RNA integrity was assessed on the 2100 Bioanalyser (Agilent Technologies). RNA samples with RIN (RNA integrity number) values of 8.2-9.6 were used for Microarray and RNA-seq analysis.

2.7 Quantitative Gene Expression

Quantitative real-time reverse transcription-polymerase chain reaction (qRT-PCR) was used to determine the relative gene expression levels in control and mutant embryonic tissue and also in cell preparations that were differentiated *in vitro* under different mechanical loading regimes. All primers were designed using Primer Express Software®, version 3.0, under default settings for TaqMan® quantification and purchased through Sigma (Sigma-Aldrich, Ireland), or purchased directly as pre-designed pre-validated TaqMan® gene expression Assays from Applied Biosystems. Total RNA concentrations were determined using the Quant-iT™ RNA assay and a Qubit® fluorometer (Invitrogen, UK) and/or NanoDrop® ND-1000. To quantify mRNA expression a standardised quantity of total RNA was reverse transcribed (generally 100ng) into cDNA using iScript™ cDNA synthesis kit (BioRad, UK) as per manufacturer's instructions. Samples were assayed in triplicate in one run (40-45cycles), which was composed of three stages, 95°C for 10 min, 95°C for 15secs for each cycle (denaturation) and 60°C for 1min (annealing and extension). Real-time PCR was performed using an ABI 7500 Sequence Detection system (Applied Biosystems). qRT-PCR data was analysed using relative quantification and the C^t method as described previously (Livak and Schmittgen, 2001), with the *Gapdh* gene as the endogenous control. The level of

gene expression was calculated by subtracting the averaged C^t values (C^t is the threshold cycle) for *Gapdh* from those of the gene of interest. The relative expression was calculated as the difference ($\Delta\Delta C^t$) between the C^t of the test sample (mutant) and that of the control sample. The relative expression of genes of interest were calculated and expressed as $2^{-\Delta\Delta Ct}$. Relative quantification values are presented as fold changes plus/minus the standard error of the mean relative to the control group, which was normalised to one

2.8 Microarray

Four independent pooled sets of samples were used for microarray (n=4 biological replicates) analysis. All microarrays were processed at IMGM® Laboratories (Martinsried, Germany). 100ng of total RNA per sample was reverse transcribed into cDNA and then converted into labelled cRNA by *in vitro* transcription incorporating cyanine-3-CTP (Low input quick-amp labelling kit one-colour, Agilent Technologies). Genome wide expression profiling was carried out using the Agilent Mouse GE v2 Microarrays (4x44K format) (G4846A, Agilent Technologies) which contains 39,485 coding and non-coding sequences of the mouse genome (outlined in Figure 3.1B). A one-colour based hybridisation protocol was performed at 65°C for 17 hrs on separate mouse GE v2 microarray platforms. Microarrays were then washed with increased stringency using Gene Expression Wash Buffers (Agilent Technologies) followed by drying with Acetonitrile (Sigma). Fluorescent signal intensities were detected with Scan Control A.8.4.1 software (Agilent Technologies) in the Agilent DNA microarray scanner and extracted from the images using Feature Extraction 10.7.3.1 software (Agilent Technologies). The software tools Feature Extraction 10.7.3.1, GeneSpring GX 11.5.1 and Spotfire Decision Site 9.1.2 (TIBCO) were used for quality control and statistical data analysis. Quantile normalisation was applied to each data set in order to impose the same distribution of probe signal intensities for each array (Bolstad et al., 2003), thus adjusting them to a uniform level that can allow for comparable downstream analysis. Welch's

approximate t-test ("unpaired unequal variance", parametric) was applied to compare the control and mutant groups. A corrected p-value was calculated based on the algorithm of Benjamini and Hochberg (Benjamini Y., 1995), based on control of the False Discovery Rate (FDR). A fold change (FC) of ≥ 2 and FDR-adjusted p-value of ≤ 0.05 were used as criteria to indicate differential expression between the two groups.

2.9 RNA-sequencing: Alignment and Differential expression analysis

Three independent pooled sets of samples were used for RNA-seq (n=3 biological replicates) analysis. The DNase-treated RNA (3μg) was used to prepare RNA-Seq libraries with the TruSeq RNA Sample Prep kit. A total of six cDNA libraries were constructed, representing triplicate biological replicates for each group. 40bp single end reads were obtained from an Illumina GAII in FASTQ format, one sample per sequencing lane. The Tophat aligner (http://tophat.cbcb.umd.edu/) was used to align the reads to the mouse reference genome (mm9). After alignment the read counts for each gene were extracted using htseq-count (http://www-huber.embl.de/users/anders/HTSeq/) based on an mm9 Refseq gff file. Differential expression in our two groups was evaluated using DESeq version 1.4.1, implemented in R 2.14.1. DESeq uses a negative binomial distribution to model genic read counts following normalisation based on size factors and variance. As for the microarray analysis, p-values were adjusted by the procedure of Benjamini and Hochberg to control the type I error rate, and a cut off of $p \leq 0.05$, and a fold change of ≥ 2 were used as a threshold to define differential expression.

2.10 Immunohistochemistry

Immunohistochemistry was performed on 5μm longitudinal paraffin TS23 control and mutant sections. Slides were washed three times in PBS prior to blocking in 5% goat serum in PBT for 1hr at RT. Incubation with Primary antibody in 5% blocking solution was performed in a humid chamber O/N at 4°C. Three 15mins post-antibody washes were performed in PBS at

RT. Incubation with secondary antibody was performed in 5% blocking solution for 1hr at RT in the dark. Post secondary antibody washes, 3 x 10mins in PBS were performed in the dark. Primanry and secondary antibody dection concentrations are listed in each relevant chapter.

Mounting of fluorescent samples was performed using DAPI counter-stain (DAPI Prolong Anti-fade Mounting Medium, P-36931, Invitrogen) and colourometrically stained samples with Aquapolymount (Polysciences Inc).

2.11 Laser capture Micro-dissection

Unfixed, frozen tissue sections were prepeared for LCM: Collection and dissection of fresh forelimb samples from homozygous *Pax3*$^{Spd/Spd}$ mutant embryos and littermate controls was performed as described in section 2.1. The right and left forelimb were finely dissected in DEPC PBS and were laid on to individual pieces of aluminium foil and flash frozen over a dry-ice and absolute ethanol bath, until the tissue was fully frozen, white in colour and hard. The frozen tissue was then stored immediately at -80°C until it was sectioned on a Leica CM1860 cryostat (at -30°C) prior to LCM. In order to reduce RNase activity before sectioning, the cryostat was wiped down with 100% ethanol, and a new disposable blade was used to cut the tissue. Forelimbs were mounted onto metal chucks within the cryostat chamber in OCT embedding compound. 10μm longitudinal sections were cut through the humerus, elbow joint and radius and ulna of the forelimb. Sections were mounted on PEN membrane coated slides (Applied Biosystems® LCM0522), with two slides used for each limb, increasing the number of sections on a slide allowed for capturing of more tissue of interest during LCM. Slides were dehydrated through a series of 70% and 100% ethanol washes prior to being dried fully and stored in an air-tight container at -80°C prior to LCM sub-dissection. Staining of the tissue using cresyl violet was tested in order to assess whether the tissue required added visualisation during LCM. Results showed no additional benefit of staining

compared to unstained tissue, as the distinct regions were visible unaided, based on cell shape and size.

LCM was performed using an ArtucusXT™ micro-dissection system (Applied Biosystems) and software (Artucus). The system works by pulsing an adjustable strength infrared (IR) laser in combination with an ultraviolet (UV) laser through a thermoplastic film located at the base of the cap, resulting in extension of the film directly on the area of interest. When the cap is lifted from the tissue, the cells remain captured on the cap. A standard protocol was followed and adapted for the tissue of interest (as detailed in Espina et al., 2006). In Brief, the slides containing the fresh frozen tissue were loaded on to the microscope instrument platform, and held in place with the locking pins. The CapSure® HS (high sensitivity) LCM caps (#LCM 0214) were inserted into the cap holder assembly. Using the manually controlled joystick the regions of interest were located and the cap was loaded on the tissue area of the slide. The Laser spot was then focused and aligned on the screen and the exact location calibrated. The UV laser power and spot size was also calibrated. Following delineation of the territory for capturing, using the connected software, both IR and UV lasers were used to capture the tissue. The IR laser cuts out the region of interest following marked lines, while the UV laser promotes adherence of the tissue to the film on the cap with circular rings. Moving of the cap to another region on the slide allows pooling of multiple sections of the same territory on to one cap. Approximately 12-15 10μm sections of the regions of interest were pooled on the same cap for downstream transcript analysis. Following completion of an area of interest, the cap was removed from the system and the film containing the micro-dissected tissue was coated in RNA Extraction buffer (Promega), and placed in a 0.5ml tube, where the cap fit fully.

2.12 Optical Projection Tomography

Whole embryos were prepared for OPT by embedding in 1% Low melting point agarose in ddH_2O, dehydrated overnight in 100% Methanol and cleared in BABB (1:2 Benzyl alcohol: Benzyl benzoate) overnight. Optical Projection Tomography constructs a 3D scan by measuring the amount of light transmitted or emitted by an object when light is shone on it. Specimens were placed in the scanner and rotated through 360degrees, a scan is produced which is composed of 400 projected images of the specimen. At least two scans were performed for each specimen using visible light and UV light with either a GFP1 filter (425/60nm excitation) or a TXR filter (560/40nm excitation). An auto-fluorescence image was subsequently captured from the tissue following each scan to reconstruct specimen morphology. For the visible light either a 700nm or 750nm filter was used in some cases when colourimetric staining was very intense. The raw data from each scan (400 projected images) were loaded onto a Linux workstation and reconstructed using a set of programs provided by the Edinburgh Mouse Atlas Project (EMAP) and analysed using custom made software MAPaint and MA3DView (Mouse Altas (MA)) provided by EMAP. MAPaint is a program that enables the user to navigate through 3D data and select comparable sections in any orientation. Physical landmarks such as the humerus, ulna and radius were used to ascertain the position of the section to ensure consistent comparisons between EP and non-EP limbs.

Chapter 3

3. Identification of Mechanosensitive genes during Skeletal Development[1]

[1]Most of the data in this chapter have been published in:

Rolfe, R.A., Nowlan, N.C., Kenny, E.M., Cormincan, P., Morris, D.W., Prendergast, P.J., Kelly, D., Murphy, P. Identification of Mechanosensitive genes during skeletal development: alteration of genes associated with cytoskeletal rearrangement and cell signalling pathways. BMC Genomics, 2014, Jan 20;15:48. doi: 10.1186/1471-2164-15-48

Rolfe R.A., Kenny E.M., Cormican P., Murphy P.: Transcriptome analysis of the mouse E14.5 (TS23) developing humerus and differential expression in muscle-less mutant embryos lacking mechanical stimulation. *Genomics Data*, December 2014, Vol 2 pages 32-36, doi: 10.1016/j.gdata.2014.03.003

I produced and analysed all of the data, with the exception of raw RNA-seq and Microarray carried out as commercial services by Trin-Seq and IMGM® Laboratories respectively, on RNA samples I provided.

3.1 Introduction

Mechanical stimulation plays an important role in skeletal growth and repair (reviewed in (Chen et al., 2009)) and, although much less well understood, it is also required for normal skeletal development, as described in section 1.5. This was initially indicated by observations that infants who experience a decrease in foetal movement *in utero* due to neuromuscular disorders, present a range of skeletal anomalies including multiple joint fusions, craniofacial abnormalities and thin hypo-mineralised bones (Rodriguez et al., 1988a; Rodriguez et al., 1988b). Direct evidence that mechanical stimuli generated by embryonic muscle contractions impacts skeletal development comes from several experimental animal models that show similar abnormalities in ossification and joint formation; in immobilised chicks, and in mouse embryos lacking muscle or with reduced or immobile muscle (reviewed in Nowlan et al., 2010b; Rolfe et al., 2013b), as discussed in section 1.5.1 and 1.5.2. However little is known about the molecular mechanisms through which mechanical stimuli influence cellular events during skeletal development.

A number of different strains of mutant mice have been used that phenotypically lack limb muscle or show reduced stimulation from muscle contraction during development (Kahn et al., 2009; Nowlan et al., 2010a; Nowlan et al., 2012), including *Splotch* ($Pax3^{Sp}$) and *Splotch-delayed* ($Pax3^{Spd}$), where muscle precursor cells fail to migrate to the developing limbs and no limb muscle forms (Franz et al., 1993; Vogan et al., 1993). Common defects in muscle-less and immobilised embryos include abnormal initiation and/or progression of ossification, loss of definition of tissue territories in the joint region and altered rudiment morphology, associated with reduced local cell proliferation (Kahn et al., 2009; Nowlan et al., 2010a; Roddy et al., 2011a), as outlined in section 1.5.2. It has been shown that mechanical stimuli thus impact a variety of developmental processes and presumably must influence or integrate with signalling pathways and molecular changes known to guide these events. One clue to a signalling pathway impacted by mechanical stimulation comes from the work of Kahn *et al*

(2009) who have shown that canonical Wnt signalling is altered in the elbow joint of *Splotch-delayed* embryos. Several regulatory genes have been shown to have dramatically altered expression patterns in reduced mechanical stimuli including, *Ihh* and *Col10a1* at the site of ossification (Nowlan et al., 2012; Nowlan et al., 2008b) and *Bmp2*, *Fgf2*, and *Pthlp* at the joint line (Roddy et al., 2011b), although whether expression of these genes is directly affected by the mechanical stimuli or as a more indirect consequence of altered cell behaviour is not known. We need to know more about the spectrum of molecular changes that occur when mechanical stimuli are altered.

Gene expression profiling to identify genome wide changes under altered mechanical environments has been carried out on cells in culture using microarray technology, including osteoblast cell-lines subjected to weightlessness or microgravity conditions (Patel et al., 2007), chondrocyte-laden constructs and murine cartilage explants to which dynamic compression was applied (Bougault et al., 2012) and chondrocyte cell lines exposed to hydrostatic pressure (Sironen et al., 2002). Gene expression profiling has the potential to uncover hundreds of genes that respond to mechanical stimuli simultaneously (mechanosensitive genes); however no direct analyses of *in vivo* changes in gene expression during skeletal development following alteration of the mechanical environment have been performed. This is required to begin to assemble a picture of the molecular landscape impacted by mechanical stimuli in a developmental context.

The experiments reported in this chapter were designed to addresses the relationship between mechanical stimulation and alterations in the biochemical environment in an *in vivo* context while the processes of ossification and joint development are occurring in the developing forelimb rudiment at TS23; as it was previously established that the humerus was the most strongly affected rudiment and TS23 the earliest time point at which the specific effects on ossification and joint line reduction were clearly detected when mechanical stimulation was

altered (Nowlan et al., 2010a; Nowlan et al., 2012). Both RNA whole transcriptome sequencing analysis (RNA-seq) and Microarray technology were used to investigate the altered transcriptome in humerus tissue from muscle-less mutant embryos compared to phenotypically normal littermate controls. Microarray analysis is a more established technique (Malone and Oliver, 2011), but RNA-seq offers the potential of greater sensitivity (Lahiry et al., 2011) and by analysing the same tissues in parallel allows direct comparison of the two methods. In addition RNA-seq analysis of the normal developing skeletal rudiment would in itself produce valuable data about the entire profile of genes that are active at this key stage of skeletal development when ossification and joint formation are at early stages. The comparison with immobile embryonic tissue further profiles genome wide transcriptional changes, giving an overview of the molecular processes and pathways most affected and identifying a set of putative direct target genes responding to mechanical stimulation during ossification and joint formation.

Given the importance of appropriate mechanical stimulation generated by embryo movement on skeletal development I postulate that mechanical stimulation of the embryonic skeletal system impacts expression levels of genes implicated in a variety of regulatory pathways and biological processes, as would be expected when an integrated regulatory system is disturbed. With the ultimate objective of testing this postulation, the specific aims of the work presented here were as follows:

1. To characterise the skeletal phenotype in muscle-less *Splotch-delayed* ($^{Spd/Spd}$: Vogan et al., 1993) humeri and associated joints. Previous work in the research group had used the related genetic mutation *Splotch* ($^{Sp/Sp}$: Franz et al., 1993) to identify skeletal abnormalities in the absence of muscle. Splotch-delayed embryos offer extra advantages for the production of tissue samples but the skeletal phenotype first needed to be confirmed.

2. To describe the transcriptome of control TS23 humerus and associated joints through the use of RNA-sequencing technology. Results from this work aim to provide a valuable resource to help to understand the molecular processes occurring at this developmental time when chondrocytes are undergoing hypertrophy, the cartilage rudiment is beginning to ossify and joints are forming.

3. To identify global gene expression changes in skeletal tissue from muscle-less embryos. A comprehensive investigation of the altered transcriptome in humerus tissue from muscle-less mutant embryos compared to phenotypically normal littermate controls, using both RNA whole transcriptome sequencing analysis (RNA-seq) and Microarray technology. The genes that show altered expression would include direct and indirect targets of mechanical stimulation. A genome wide analysis of altered transcript levels is required to indicate the principal molecular mechanisms disturbed and the most likely candidates for direct regulation.

3.2 Methods

3.2.1 Embyro Collection

Heterozygous C57BL/Pax3$^{Spd/+}$ (Vogan et al., 1993) mice were time-mated to produce homozygous *Pax3*$^{Spd/Spd}$ mutant embryos, as per section 2.1. All embryos were genotyped following PCR amplification to confirm homozygote mutants and distinguish heterozygote and homozygote controls, as described in section 2.2.

3.2.2 Histology of TS23 limbs

Histological staining was performed following paraffin embeddeding as described in section 2.4.3 and Safranin-O/Fast green staining according to section 2.3.1. This method detects cartilage and mast cell granules. The hyaluronic acid in cartilage stains orange to red, nuclei purple and mast cells green.

3.2.3 RNA preparation

The humeri, including the associated joint regions, were finely, manually micro-dissected from control and mutant (*Pax3*$^{Spd/Spd}$) embryos at stage TS23 as shown in Figure 3.1A. RNA was extracted as described in section 2.6.

3.2.4 Microarray

Four independent pooled sets of samples were used for microarray (n=4 biological replicates) analysis. All microarrays were processed at IMGM® Laboratories (Martinsried, Germany). The preparation of RNA and processing for microarray analysis is described in section 2.8. Genome wide expression profiling was carried out using the Agilent Mouse GE v2 Microarrays (4x44K format) (G4846A, Agilent Technologies) which contains 39,485 coding and non-coding sequences of the mouse genome (outlined in Figure 3.1B).

3.2.5 RNA-sequencing: Alignment and Differential expression analysis

Three independent pooled sets of samples were used for RNA-seq (n=3 biological replicates) analysis. The processing of RNA for RNA-sequencing analysis is described in section 2.9. Sequence reads were aligned to a reference mouse genome (mm9) to identify expressed transcripts (outlined in Figure 3.1B).

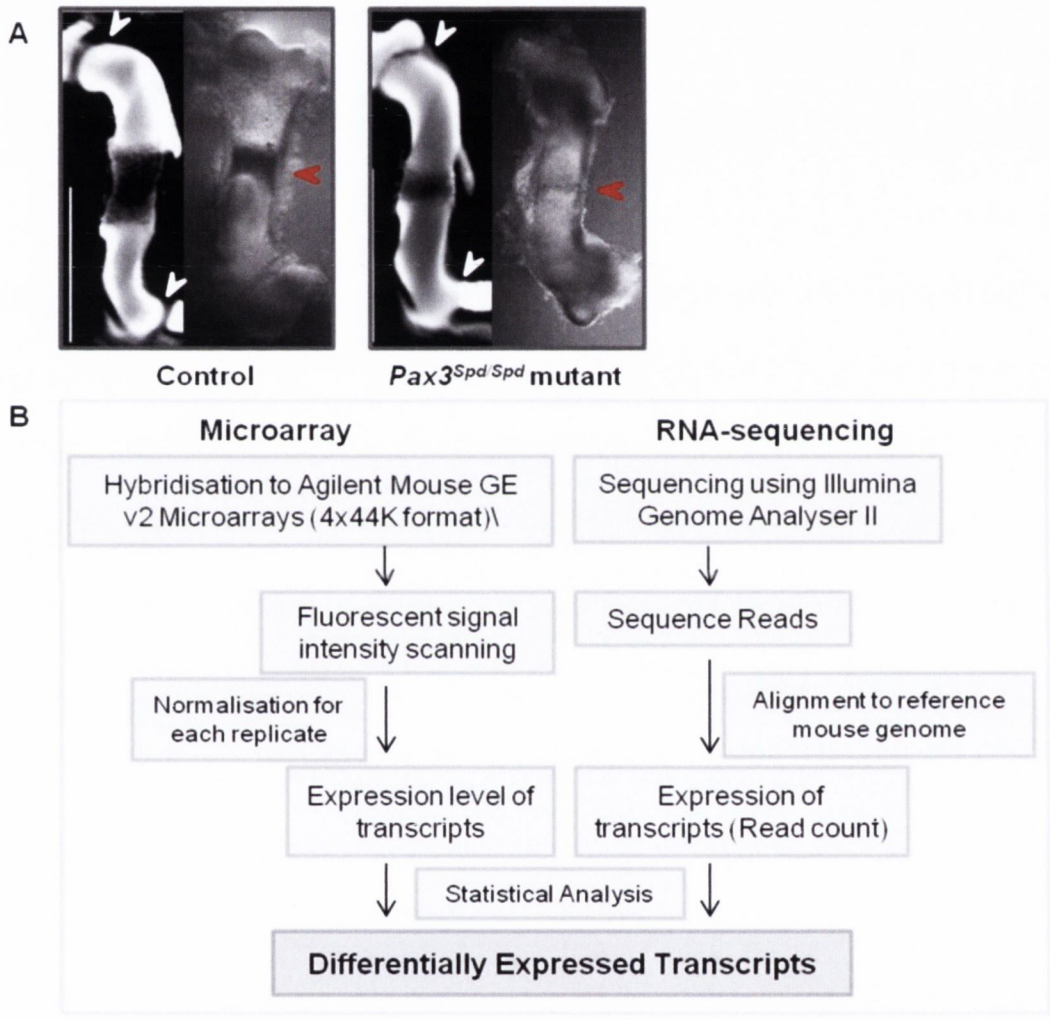

Figure 3.1: Overview of gene expression profiling approach used. (**A**) Images of control and Pax3$^{Spd/Spd}$ mutant humeri at Theiler stage 23 dissected prior to RNA extraction (right hand image); the images on the left are external views of stage and genotype matched 3D scanned specimens stained to reveal the morphology and ossification more clearly. White arrow heads indicate the elbow joint and shoulder joint line and red arrow heads the ossification site, a visible reduction is apparent in the mutant compared to the control in each case. (**B**) Work-flow of Microarray and RNA-sequencing data analysis.

3.2.6 Quantitative real-time-polymerase chain reaction

Quantitative real-time reverse transcription-polymerase chain reaction (qRT-PCR) was used to verify the relative gene expression changes in nine genes indicated to be differentially

expressed (DE) by microarray and RNA seq analysis; Fgf4, Cilp, Rxrg, Dll1, Spp1 Vstm2a, Figf, Fgf10 and Sfrp2 (primer sequences detailed in Table 3:1). All primers were designed using Primer Express Software®, version 3.0, under default settings for TaqMan® quantification and purchased through Sigma (Sigma-Aldrich, UK). Primers sets were designed with a primer Tm range of 58°-60°C, an optimal length of 20bp and an amplicon range of 50-150bp. Total RNA was reverse transcribed (100ng) into cDNA using iScript™ cDNA systhesis kit (BioRad) as per manufacturer's instructions. SYBR green gene expression quantification was performed using QuantiTect SYBR green kit. 5µl of cDNA preparation was diluted 1:5 with RNase free water, 10µl of 2x QuantiTect SYBR green PCR master mix, 0.5ul (10µM) of each primer and 4ul RNase free water. Samples were assayed in triplicate in one run (40cycles), which was composed of three stages, 95°C for 10 min, 95°C for 15sec for each cycle (denaturation) and 60°C for 1min (annealing and extension). Real-time PCR was performed using an ABI 7500 Sequence Detection system (Applied Biosystems). qRT-PCR data was analysed using relative quantification and the Ct method as described previously (Livak and Schmittgen, 2001), with the Gapdh gene as the endogenous control, as section 2.7.

3.2.7 Gene Ontology Annotation Analysis

Gene Ontology (GO) terms were utilised to reveal significant enrichment of groups of genes among the DE datasets from the microarray and the RNA-seq analysis using the Database for Annotation, Visualisation and Integrated Discovery, DAVID (http://david.abcc.ncifcrf.gov/) (Huang da et al., 2009), and GOstat (http://gostat.wehi.edu.au/) software. Analysis of GO terms associated with biological process, molecular function and cellular component was performed on all data-sets independently and combined to identify significantly ($p \leq 0.05$) enriched gene sets. The strength of the enrichment of any GO term-associated gene set is reflected in the calculated p-values, comparing the proportion of genes in the data-set and the proportion of genes in the genome bearing that annotation. Ingenuity pathway analysis

(http://www.ingenuity.com/) was also used to analyse and interpret the biological meaning in the DE datasets.

Table 3:1: Primer sequences for qRT-PCR analysis of differentially expressed genes.

Gene	RefSeq	Primer Sequence		Amplicon length
Fgf4	NM_010202	Fwd	CCGACGAGTGTAAATTCAAAGAAA	97
		Rv	TTCTTACTGAGGGCCATGAACA	
Cilp	NM_173385	Fwd	AAAAAGACGGCTTTCCAAATCA	78
		Rv	GGCATAGATAGGCCCATTGC	
Rxrg	NM_009107	Fwd	CGTTGAGTGGGCCAAACG	75
		Rv	CCTGCCCGGAGTAGAATGAC	
Dll1	NM_007865	Fwd	GACCGCCGCTTCCTAATAGG	74
		Rv	GCCCAGATGTTCAGCTTAATTCC	
Cd44	NM_009851	Fwd	CCCCCCTACCCCAAGTGA	92
		Rv	TCTGTGTTGTTATTCTTTGACTTGGAT	
Vstm2a	NM_145967	Fwd	GTGGAGCTCTTACCCGACAGA	73
		Rv	CATTGCCTTGGACTTTCACTGTAC	
Pcdh8	NM_021543	Fwd	GATACAGCACGTTCGAAGAGGAT	122
		Rv	CAGAGAGCTGTTGAATTGCTTC	
Figf	NM_010216	Fwd	GGTTGCCTGAAACAGAGTAGTAGGT	71
		Rv	AGCATTGCCCTTGGACTTTG	
Fgf10	NM_008002	Fwd	GGGCTGCTGTTGCTGCTT	94
		Rv	GGCCTCCTGTGACACCATGT	
Sfrp2	NM_009144	Fwd	CAGAGAGAGTTCAAGCGCATCTC	68
		Rv	GCCACCCCACTGGGAAAC	
Spp1	NM_001204201	Fwd	CCCTCGATGTCATCCCTGTT	69
		Rv	TGCCCTTTCCGTTGTTGTC	
Sox5	NM_011444.3	Fwd	GACGGCAAGAAACTGCGTATC	79
		Rv	CGTTGAAGTACTGTCGCATTTCC	
Wnt4	NM_009523.2	Fwd	GGTCAGGATGCCTCGGACAA	65
		Rv	CCGGACGTCCACAAAGGA	

3.2.8 Chromosome position of Differentially Expressed genes

Freely available software (available at http://www.ncrna.org/idiograhica/) was used to generate idiograms to visualise the genome localisation of all differentially expressed genes; combined from the Microarray and RNA-seq data (Kin and Ono, 2007). These were used to assess any gene clustering.

3.3 Results

3.3.1 Establishment of the developmental defects in *Spd/Spd* muscle-less humeri and associated joints.

The phenotypic effects on skeletal development caused by lack of muscle were previously established in *Splotch* mutant embryos ($Pax3^{Sp/Sp}$) (Epstein et al., 1993; Nowlan et al., 2010a). The *Splotch-delayed* (Pax3 *Spd*) mutation is caused by a single point mutation at position 421 in the *Pax3* gene (Vogan et al., 1993) that leads to a defect in migration of muscle progenitor cells in the developing limb (Franz, 1993). Similar to *Sp* mutants, *Spd* mutants have entirely muscle-less limbs but have a milder phenotype in other respects. They offer an advantage in this study because they do not die *in utero* and give a better recovery of mutant samples, especially at later stages of development. For this reason *Spd* heterozygous mice were purchased from Jackson laboratories and used to generate muscle-less embryos. A necessary prerequisite to using *Spd* specimens in this research was to verify the phenotypic effects on skeletal development. Assessments of the phenotypic changes were carried out across three developmental stages, TS22, TS23, which was the stage previously established to be first clearly affected, and TS24. These correspond to E13.5-E14, E14.5-E15 and E15.5-E16 respectively. Histological analysis of forelimb rudiments was performed using Safranin-O/fast green to detect cartilage. Comparisons were made between muscle-less homozygous mutant ($Spd^{-/-}$) limbs and two types of stage-matched littermate controls; homozygous wild-type ($^{+/+}$) and heterozygous for the *Spd* allele ($Spd^{+/-}$). A reduction and loss of cellular organisation in the humero-ulnar (Figure 3.2b, f) and humero-radial (Figure 3.2 d, h) elbow joint was observed at both TS22 and TS23, compared to both littermate controls (Figure 3.2 a, e & c, g, and homozygous wild-type (not shown). At TS24 the humero-ulnar (Figure 3.2 i) and humero-radial (Figure 3.2k) elbow joints had begun to cavitate in control specimens but there was no cavitation observed in $Spd^{-/-}$ embryos (Figure 3.2j & l). A loss of cellular organisation

and joint line reduction was also observed in the shoulder joint at TS22 (Figure 3.3b), TS23 (Figure 3.3d) and TS24 (Figure 3.3f) compared to stage-matched controls (Figure 3.3a, c, e).

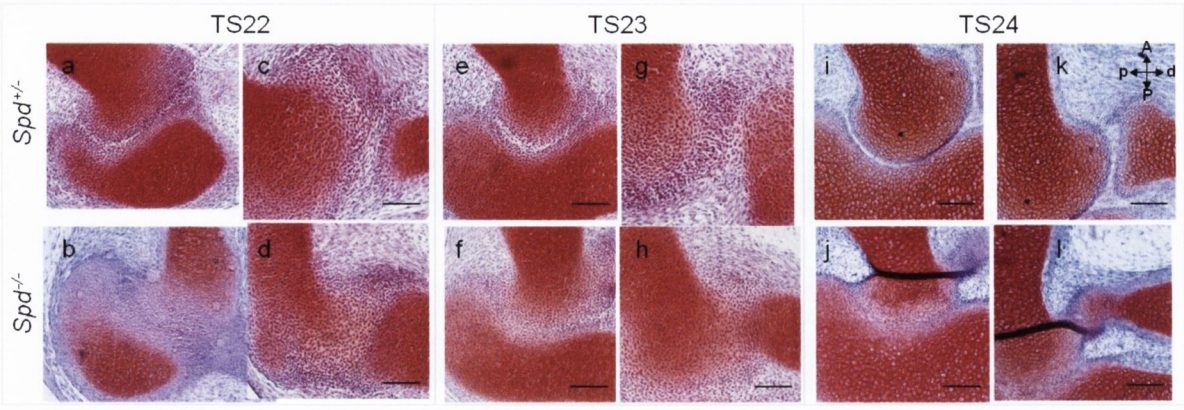

Figure 3.2: Elbow joint line reduction and loss of interzone layer organisation in Spd/*Spd*$^{-/-}$ muscle-less mutants. The joint line of the humero-ulnar (**a-b, e-f, i-j**) and humero-radial (**c-d, g-h, k-l**) joints is visibly reduced in the mutant limbs as shown by histological sections across developmental stage, TS22 (**a-d**), TS23 (**e-h**) and TS24 (**i-l**). Cell organisation is altered in **b**, **d**, **f**, and **h**, while no cavitation is seen in **j** and **l** compared to stage-matched litter-mates. Histological sections stained with Safranin-O/Fast green. Scale bars 100μm.

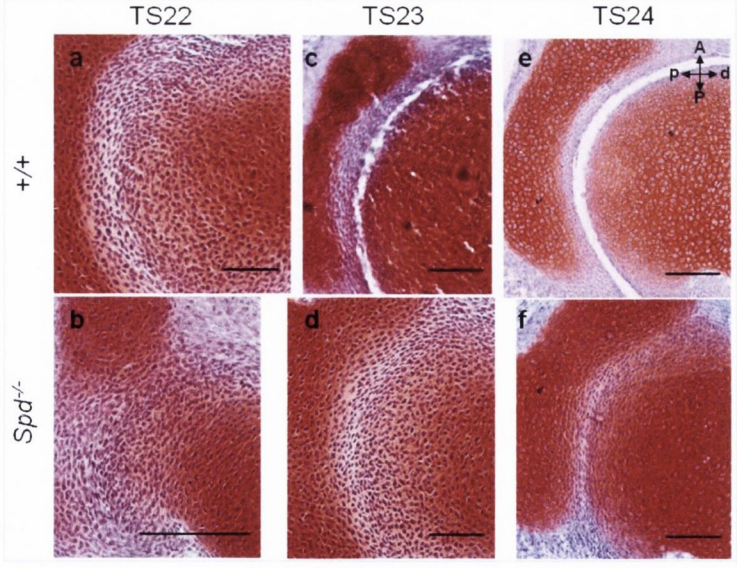

Figure 3.3: Loss of cellular organisation, and shoulder joint line reduction in Spd/*Spd*$^{-/-}$ muscle-less mutants. Developmental stage as indicated; TS22 (**a-b**), TS23 (**c-d**) and TS24 (**e-f**). Histological sections stained with Safranin-O/Fast green. Scale bars 100μm.

Analysis of the primary ossification centres in humerus sections (Figure 3.4**A, B**) showed the initiation of hypertrophy at TS22 in control embryos (Figure 3.4**A**a, **B**g, h), by the distinct enlarged cells that are safranin-O negative in the mid-diaphysis of the rudiment. At TS23 there are two distinct fronts of hypertrophic chondrocytes spreading proximally and distally (Figure 3.4**A**c, **B**j, k). At TS24 there are signs of matrix degradation indicative of bone deposition (Figure 3.4**A**e, **B**m, n). In contrast, a reduction in the number and spread of hypertrophic chondrocytes was detected in the muscle-less mutants across all stages (Figure 3.4**A**b, d, f, **B**i, l, o). The more distal elements of the forelimb comprising the ulna and radius showed no visible reduction in hypertrophic chondrocytes or in the proximal distal spread of hypertrophy in the muscle-less mutants compared to control, in any of the stages compared; data is only shown for TS23 (Figure 3.4**C**). Therefore in all aspects the *Spd/Spd*$^{-/-}$ mutant shows the same phenotypic effects as the *Sp/Sp* mutant previously described (Nowlan et al., 2010a) with effects on ossification and joint interzone cellular organisation and joint formation.

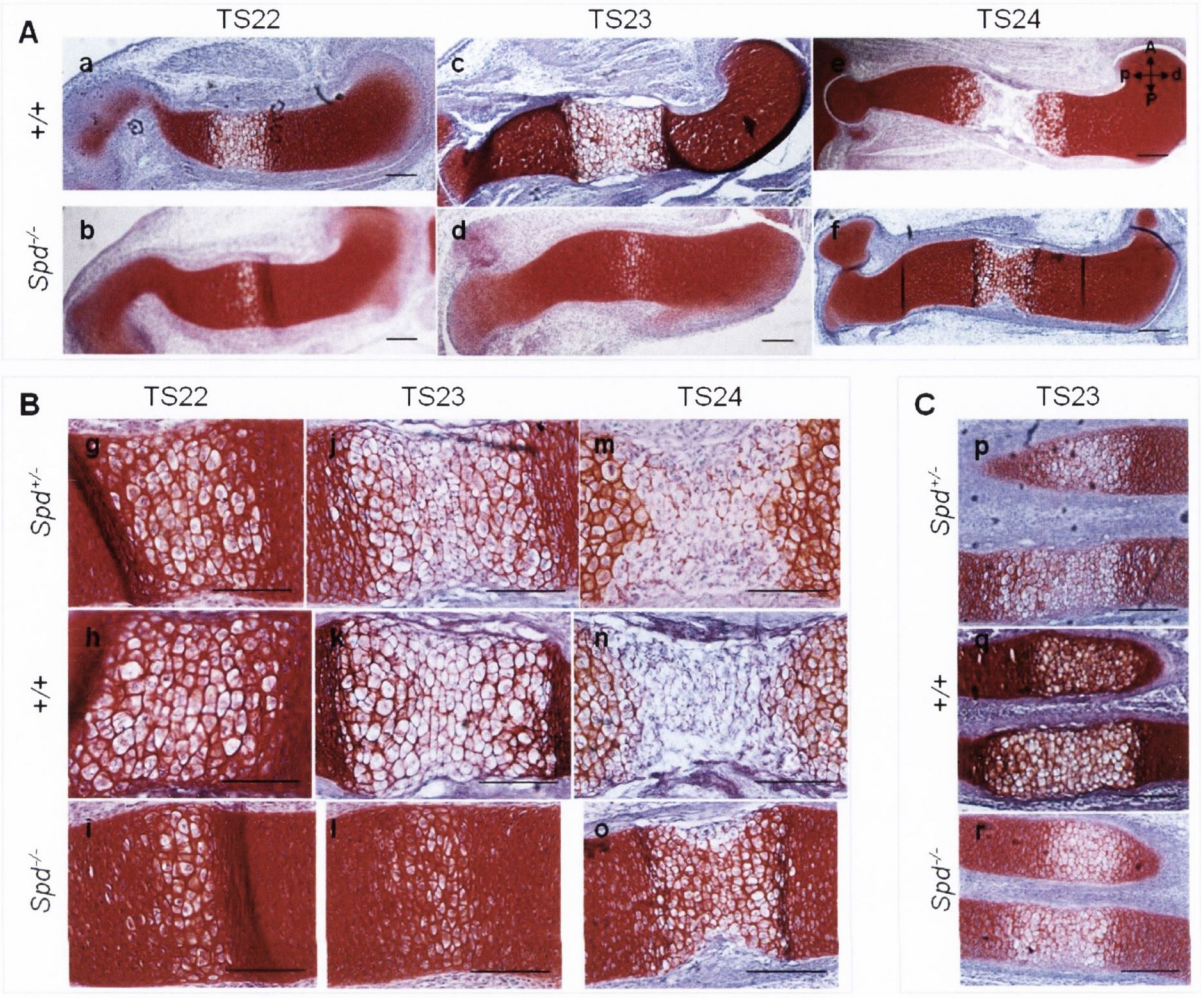

Figure 3.4: Histological analysis of primary ossification centers in proximal humeri (**A,B**) and distal ulna and radius (**C**) in *Spd/Spd*$^{-/-}$ muscle-less mutants and stage-matched controls across developmental stages, TS22 (a-c, g-i), TS23 (c-d, j-l) and TS24 (e-f, m-o). Orientation of sections is indicated at the top left corner (d; distal, p; proximal, A; anterior P; posterior). The zone of hypertrophic chondrocytes in the mid-diaphysis of the humerus in reduced in muscle-less mutants (**A**: b, d, f, **B**: i, l, o) compared to stage-matched controls (**A**: a, c, e, **B**: g-h, j-k, m-n) Histological sections stained with Safranin-O/Fast green. Scale bars 100μm.

3.3.2 Transcriptome Profiling of the developing humerus and associated joints during early Ossification and Joint formation

RNA sequencing of control humeri at TS23 gives an insight into the transcriptome at this key stage of development when the rudiment is undergoing early stages of ossification and tissue zones in the joint are being defined. Transcripts from 15,214 individual genes (n=3 biological replicates; data submitted to EMBL-EBI ArrayExpress repository: [E-MTAB-1745]) were detected in this tissue at this stage. A minimum of 5 transcript reads (on average), with at least one read from each replicate sample, was chosen as the cut off point to reliably indicate

reproducible expression across biological replicates (Bottomly et al., 2011). Expressed genes were divided into groups according to their relative expression level, as shown in Figure 3.5. Genes that represented the lowest level of expression are shown between 5 and 10 read counts, while the majority of genes (71%; 10,789/15,214) showed expression levels between 100 and 5,000 read counts. Only 732 genes are in the most highly expressed categories (≥5,000 read counts) (Figure 3.5), representing 4.8% of expressed genes. Expression levels of selected individual genes are represented in Figure 3.6. The most abundantly transcribed gene was *Col2a1* (collagen 2, alpha 1) with a read count of 452,576, and, among the 8 genes with read counts of more than 100,000, there are 4 other collagen encoding genes. In total, 42 collagen subtype genes are expressed, as shown in Figure 3.6.

The relative levels of expression of genes associated with signalling pathways involved in regulating skeletal development (reviewed in Kronenberg, 2003; Provot and Schipani, 2005) are highlighted in Figure 3.6. This shows the potential components that can contribute to these signalling pathways at this stage of skeletal development. For example the hedgehog (HH) pathway is known to play an important role in ossification through the action of Ihh (640 reads), binding to its receptor Ptch1 (1,342 reads) activating Smo (5,154 reads). Similarly, 14 FGF ligand encoding genes and 5 FGF receptor encoding genes were detected, highlighting the potential for multiple FGF signalling interactions. The BMP signalling pathway genes also reveal potential for multiple signalling interactions with nine BMP encoding genes expressed. *Bmp1* is by far the most highly expressed (5719 reads); although it is not previously reported in this tissue at this stage in gene expression databases (http://www.informatics.jax.org/).

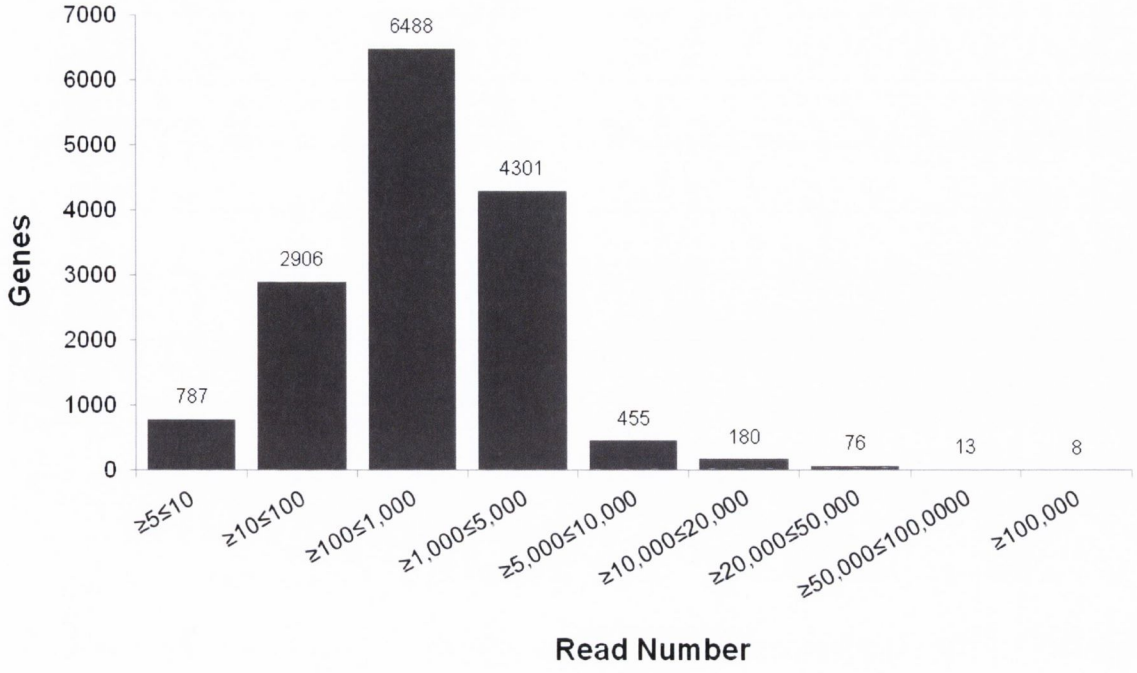

Figure 3.5: Transcriptome Profiling of the developing humerus at TS23 by RNA-seq. The number of genes (y-axis) with increasing relative expression levels represented by transcript read counts (x-axis) as indicated.

The relative expression levels of Wnt ligand (Wnt), Wnt receptor (Fzd, Lrp, Kremen), extracellular Wnt interactor (Sfrp, Dkk, Rspo, Sost), intracellular Wnt pathway component (Dvl, Axin, Ctnnb) and Wnt pathway transcription factor (Tcf, Lef) encoding genes are represented. The detection of previously unreported Wnt gene expression in the humerus (e.g. *Wnt2* and *Wnt2b*) opens up new considerations for functional roles, especially as both genes are up-regulated in muscle-less rudiments (described below). The low density lipoprotein receptor-related genes Lrp5 and Lrp6, which are Wnt co-receptors, are most highly expressed among the Lrp gene family (4,727 and 3,310 reads respectively). Interestingly eight Fzd receptor encoding genes are detected. Other genes known to be involved in skeletal development are highly expressed; *Sox9* (4,550 reads), *Runx2* (1,285reads), *Spp1* (8,155 reads) and *Mmp13* (1,103 reads).

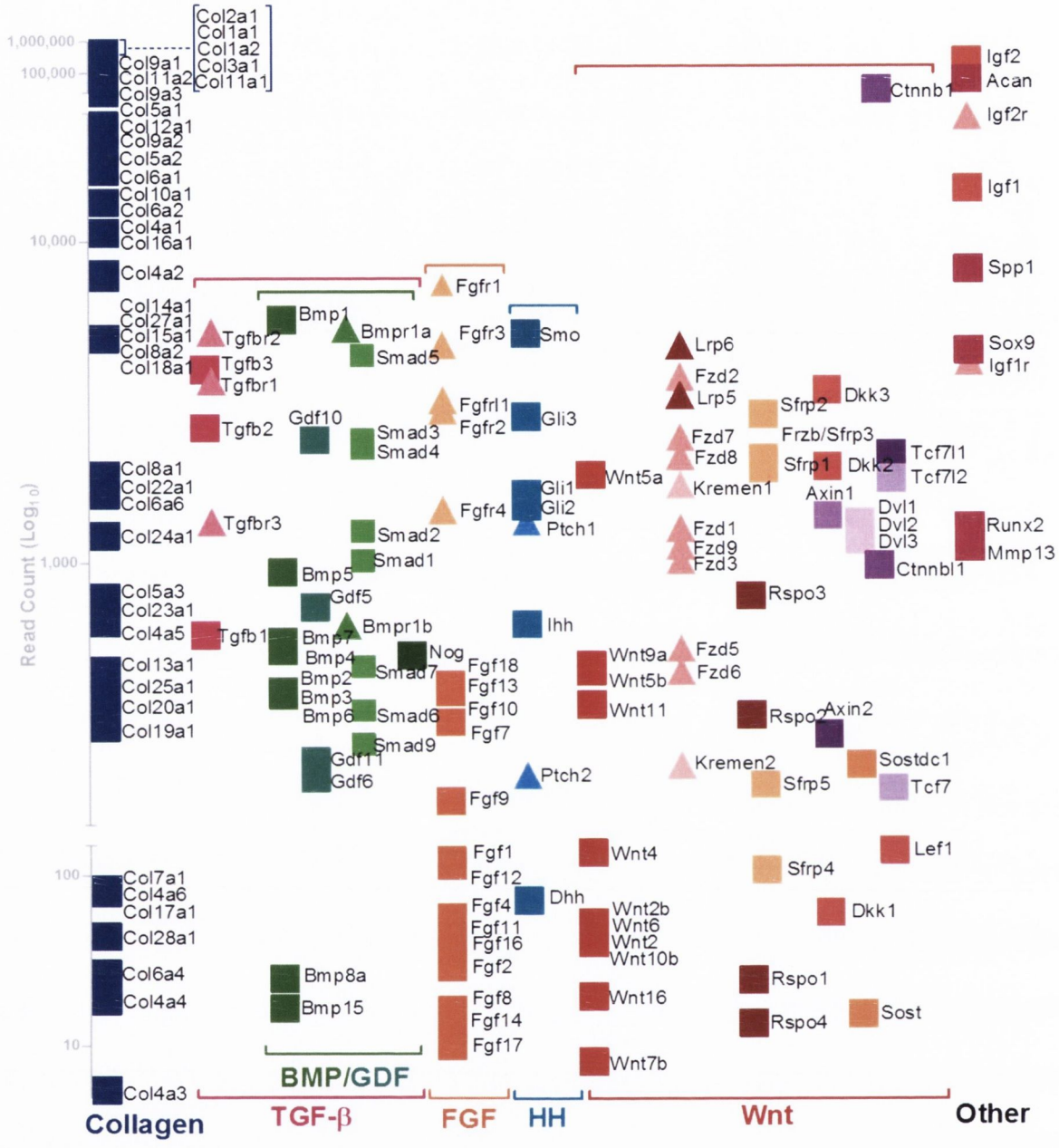

Figure 3.6: Transcriptome Profiling of the developing humerus at TS23 by RNA-seq. The relative expression of selected genes represented by read counts (Log10) (y-axis). Collagen genes and signalling pathways genes are grouped: TGFβ (including TGFβ, BMP and GDF ligands, receptors and agonists), FGF (ligands and receptors), HH (ligands, receptors and intracellular modulators), Wnt (Wnt ligands and agonists (Wnt, Rspo), receptors (Fzd) and co-receptors (Kremen, Lrp), antagonists (Sfrp, Dkk) Intracellular components (Sost, Dvl, Ctnnb) and nuclear components (Tcf, Lef)) and a selection of 'other' genes associated with skeletal development. Squares indicate ligands and modulators, triangles indicate receptors.

3.3.3 Identification of differentially expressed genes in muscle-less versus control developing humeri and associated joints

Microarray analysis of RNA extracted from control and *Pax3*$^{Spd/Spd}$ muscle-less humeri (n=4 biological replicates) detected expression of a similar proportion of individual genes on the array; 20,697 independent genes from the control and 20,949 from the muscle-less humeri (data submitted to EMBL-EBI ArrayExpress repository: ref E-MTAB-1744). Comparing hybridisation intensity between control and mutant derived cDNAs, using cut off points of at least a 2-fold change (FC) and corrected p-value ≤ 0.05 (Benjamini Y., 1995) for significance across replicates, identified 374 independent genes as differentially expressed (DE). Of these, 282 genes (76.4%) were down-regulated and 87 genes (23.6%) were found to be up-regulated, as shown in Table 3:2. Five putative uncharacterised proteins/unknown genes were identified using microarray technology; details shown in Appendix Table A.1, as these were predicted/ uncharacterised genes they were omitted from any downstream analysis.

RNA-sequencing analysis (n=3 biological replicates) detected 15,031 independent genes (with ≥5 read counts) in muscle-less humeri, compared to 15,214 in control tissue (data submitted to EMBL-EBI ArrayExpress repository: ref E-MTAB-1746). To determine differential expression, the same cut off points of a corrected p-value ≤ 0.05 and at least a 2-fold change were applied to the RNA-seq data-set, identifying 1,037 genes as DE across replicates. Of these, 618 (59.6%) were down-regulated and 419 (40.4%) were up-regulated in the muscle-less humeri and associated joints compared to that of phenotypically normal littermate control humeri (Table 3:2).

Table 3:2: Differentially expressed genes ($p \leq 0.05$) with fold change values ≥ 2 revealed by Microarray and RNA-Seq analysis and combined.

	Microarray		**RNA-Seq**		**Combined**	
Total number of differentially expressed transcripts	**374**		**1,037**		**1,132**	
	Down-regulated	**Up-regulated**	**Down-regulated**	**Up-regulated**	**Down-regulated**	**Up-regulated**
Independent named genes	282	87	618	419	680	452
Putative uncharacterized/ unknown genes	2	3	-	-	-	-
	284	**90**	**618**	**419**		

The individual datasets from the microarray and the RNA-seq were then compared and there was a 24.2% overlap in the genes identified as DE across the two platforms. In total 1,132 independent genes were identified as DE in the muscle-less mutant compared to its phenotypic control (Table 3:2 and Figure 3.7). There were 220 independent genes in common in the down-regulated category and 54 independent genes in common in the up-regulated category as visualised on the venn diagram in Figure 3.7. Of the 374 genes identified by microarray (Table 3:2), 73.2% of these genes are also represented in the RNA-seq data.

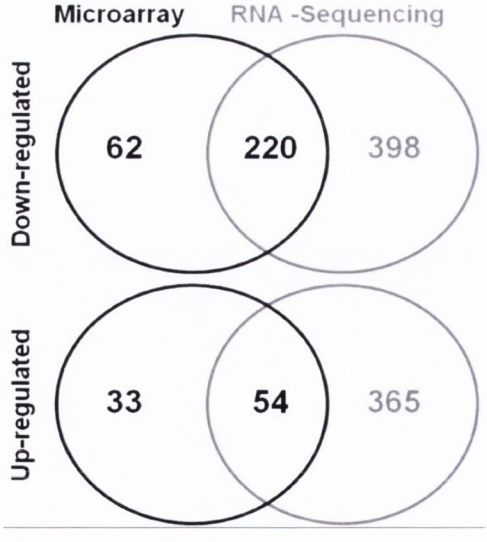

Figure 3.7: Venn diagrams representing the overlap of independent genes detected as differentially expressed (up-regulated and down-regulated; cut off criteria $p \leq 0.05$, and fold change ≥ 2) from the Microarray and RNA seq analysis, as indicated.

RNA-seq detected a greater total number of DE genes than the microarray (1,037 versus 374, respectively, using the standard cut off criteria). In addition, if the stringency for DE gene selection is weakened for the microarray data by moving the cut-off point to corrected p-value of ≤ 0.08, then the number of genes detected as DE in common by the two platforms, increases to 426 from 274 (data not shown). This suggests that the RNA-seq approach is more sensitive in detecting differential expression. Grouping genes based on the degree of change showed that the spread of fold change values was similar across platforms although there were differences in the number of genes in different categories, (Table 3:3). Note that 25 DE genes (2 up-regulated and 23 down-regulated) detected by RNA-seq could not be assigned a numerical fold change value because no reads were mapped in one of the sets of samples (Table 3:3). The up-regulated genes from both microarray and RNA-seq showed a reduced degree of alteration compared to down-regulated genes, as indicated by fold change levels. In each of the categories between 50 and 5 fold change, there is a similar proportion of total differentially expressed genes with both platforms, however this is disturbed in the lowest fold change category of $5 \leq 2$, with the microarray representing 192 genes but the RNA-seq totalling 671 (Table 3:3). This increase in gene number specifically close to the lower cut off point, again indicates that the RNA-seq platform was more sensitive in identifying significantly DE genes. There is again further support for this if the criteria for selection of differential expression are relaxed for the microarray data; using a corrected p-value of ≤ 0.08 and fold change ≥ 2, as shown in (B) and (B`) in Table 3:4, the total number of genes with a fold change $5 \leq 2$ increases to 331 from 192. Similarly if the selection criteria for differential expression is relaxed based on the fold change alone and maintaining a significance level of p-value ≤ 0.05, for example fold change of ≤ 1.5 and ≥ 1.5, then the total number of DE genes would increase to 1,005 in the down-regulated category, from 284 genes ($FC \geq 2$, $p \leq 0.05$) and 1,164 in the up-regulated category, compared to 90 using the standardised cut off criteria of $FC \geq 2 \leq$, $p \leq 0.05$, as used in this study for DE.

Table 3:3: Fold change distribution of differentially expressed genes ≥ 2 fold (p-value ≤0.05) from Microarray and RNA-seq analysis.

	Platform	Fold Change						
		# Not determined	≥100	100≤50	50≤25	25≤10	10≤5	5≤2
Up-regulated	Microarray		0	0	0	0	7	83
	RNA-seq	2	0	0	2	7	35	373
Down-regulated	Microarray		2	16	32	59	67	108
	RNA-seq	23	17	57	59	80	84	298
Total differentially expressed genes	**Microarray**		**2**	**16**	**32**	**59**	**74**	**192**
	RNA-seq		**42#**	**57**	**61**	**87**	**119**	**671**

#Not determined as no expression in the control so the precise fold change cannot be assigned

Table 3:4: Fold change distribution of Genes identified by Microarray, with different stringencies for differential selection chosen. (**A**) Fold change ≥ 2, p-value ≤0.05, (**B**) Fold change ≥ 2, p-value ≤0.08, (**C**) Fold change ≥ 1.5, p-value ≤0.05, (**A`**) Fold change ≤2, p-value ≤0.05, (**B`**) Fold change ≤2, p-value ≤0.08, (**C`**) Fold Change ≤1.5, p≤0.05

	Microarray Platform	Fold change distribution						
		≥100	100≤50	50≤25	25≤10	10≤5	5≤2 / 5≤1.5	Total no of genes
Up-regulated	(**A**) Fold Change ≥2,p≤0.05	0	0	0	0	7	83	90
	(**B**) Fold Change ≥2, p≤0.08	0	0	0	0	9	153	162
	(**C**) Fold Change ≥1.5, p≤0.05	0	0	0	1	28	1135	1164
Down-regulated	(**A`**) Fold Change ≤2, p≤0.05	2	16	32	59	67	108	284
	(**B`**) Fold Change ≤2, p≤0.08	7	25	45	70	88	178	413
	(**C`**) Fold Change ≤1.5, p≤0.05	14	35	50	77	104	725	1005

3.3.4 Verification of differentially expressed genes

Verification of fold change values for differentially expressed genes was performed using qRT-PCR. The differentially expressed genes chosen include *Fgf4*, *Cilp*, *Rxrg*, *Dll1*, *Spp1*, *Vstm2a*, *Figf*, *Fgf10* and *Sfrp2* which represent both down-regulated and up-regulated genes, as shown in Figure 3.8. The direction and degree of fold changes were similar in all cases for the microarray and the RNA-seq. For all genes analysed there was a good correspondence across all platforms (Microarray, RNA-seq and RT-PCR), as can be compared in Figure 3.8.

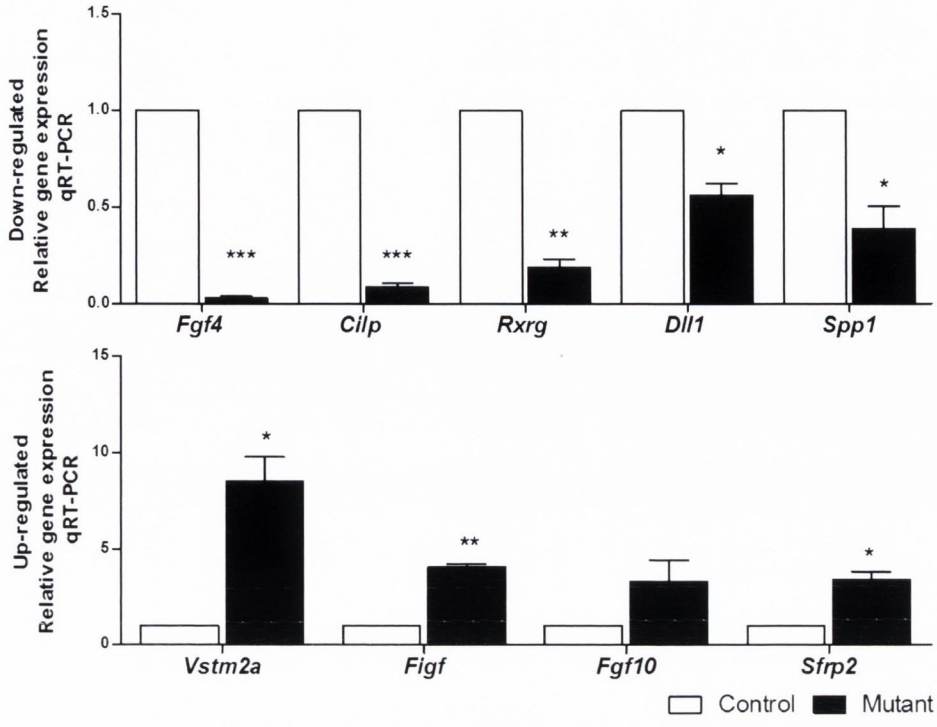

Figure 3.8: Quantitative Real time PCR relative expression values of selected differentially expressed genes revealed by microarray and RNA-seq. White bars show control and black bars show mutant expression. *Fgf4*, *Cilp*, *Rxrg*, *Dll1*, *Spp1* are down-regulated genes (<0.5), and *Vstm2a*, *Figf*, *Fgf10* and *Sfrp2* represent up-regulated genes (>2). All data is normalised to the endogenous control gene *Gapdh*. ***p≤0.001, **p≤0.01, *p≤0.05 indicates significance of differential expression.

Table 3:5: Verification of fold change expression levels of selected genes in $Pax3^{Spd/Spd}$ mutant humeri compared to control humeri revealed by Microarray, RNA seq and qRT-PCR.

Gene Symbol	Gene Name	Regulation status	Microarray (Fold Change)	RNA-seq (Fold change)	qRT-PCR (Fold change)
Fgf4	Fibroblast growth factor 4	Down-regulated	41.05	#No numerical value	35.24^{***}
Cilp	Cartilage intermediate layer protein	Down-regulated	9.73	9.76	11.3^{***}
Rxrg	Retinoid X receptor gamma	Down-regulated	7.05	12.29	5.25^{**}
Dll1	Delta-like 1	Down-regulated	2.21	3.16	1.78^{*}
Spp1	Secreted phospoprotein 1	Down-regulated	$5.23^{(ns)}$	2.9	2.59^{*}
Vstm2a	V-set and transmembrane domain containing 2A	Up-regulated	8.56	3.09	8.52^{**}
Figf	c-fos induced growth factor	Up-regulated	3.52	3.17	4.06^{**}
Fgf10	Fibroblast growth factor 10	Up-regulated	2.48	2.14	3.28
Sfrp2	Secreted frizzled-related protein 2	Up-regulated	2.62	2.09	3.38^{*}

#No numerical value for fold change as no transcripts detected in the mutant

*** p≤0.001, **p≤0.01, *p≤0.05 indicates significance of differential expression from qRT-PCR. p≤0.05 for all microarray and RNA-seq differences except *Spp1* in the Microarray (ns)

3.3.5 Biological Interpretation of Differentially expressed genes.

To reveal any enrichment of functionally related genes among the DE data sets, two web based tools, DAVID and GOstat, were used to analyse Gene Ontology (GO) term associations (Beissbarth and Speed, 2004; Huang da et al., 2009). A significant enrichment (normalised by the number of genes in the genome with that associated GO term) indicates specific biological processes and cellular components that are affected when mechanical stimuli are reduced. The strength of the enrichment is indicated by the calculated p-value. Independent analysis of data sets from both the microarray and RNA-seq showed the same enriched groups so analysis of the combined DE gene sets is presented; 680 independent down-regulated genes and 452 independent up-regulated, as described above in section 3.3.3. The individual GO terms found to be enriched have been grouped for the purpose of interpretation as indicated in Table 3:6 and Table 3:7. Down-regulated genes are associated with development and differentiation, cytoskeletal architecture and cell signalling.

Analysis of the down-regulated gene set (Table 3:6) indicated that genes associated with Development and Differentiation are most highly enriched (total of 155/680 with p-values down to 2.73×10^{-15}). The gene ontology groups that are included in the development and differentiation category include; for example, organ development (GO:0048513), and cell differentiation (GO: 0030154), more detail listed in Table 3:6. The categories within this group are involved in signal transduction, and include genes that encode signalling molecules, receptors, and transcription factors (TFs), for example signalling ligands Fgf4,Fgf5, Fgf6, Fgf8 from the fibroblast growth factor signalling pathway; receptors Fzd10 and Rxrg from the Wnt and Retinoic acid pathways respectively. 28 of these genes encode TFs including; Barx2, Scx, Hes6, Pitx2, Pitx3 and Tead4. The down-regulation of such signalling pathway component genes also underlines the enrichment of ontology groups related to Cell Signalling (Table 3:6: p-value down to 4.78×10^{-5}).

There were 110 independent genes associated with the Cytoskeleton that were down-regulated in $Pax3^{Spd/Spd}$ humeri, including those encoding microfilament, microtubule and intermediate filament components, these showed enrichment in both biological process and cellular component annotation (Table 3:6). 33 are directly associated with microfilaments (e.g. Acta1, Ablim2, Pdlim3), 13 with microtubules (e.g. Rassf5, Tubb2b, Tppp) and 4 with intermediate filaments (Des, Krt33b, Sync, Tchh); other DE genes associated with the cytoskeleton encode proteins that interact with myosin, or the extracellular matrix (ECM), including integrin and cadherin encoding genes (e.g. Lamb3, Cdh4, Itga4 and Pdgfa).

Table 3:6: Enrichment of gene groups down-regulated in muscle-less humeri based on GO term annotations. All GO terms are associated with the sub-ontology "Biological Process" except where indicated under Cytoskeleton, where Cellular Component was also used.

Gene Ontology Term			Gene count in study	Enrichment[1]
Development/ Differentiation			**[155]**	**2.73×10^{-15} to 0.0084**
	GO:0048856: anatomical structure development		134	2.73×10^{-15}
	GO:0032502: developmental process		155	1.52×10^{-14}
	GO:0048513: organ development		107	4.23×10^{-13}
	GO:0007275: multicellular organismal development		142	4.92×10^{-13}
	GO:0048731: system development		122	5.57×10^{-13}
	GO:0009888: tissue development		58	8.37×10^{-13}
	GO:0030154: cell differentiation		94	8.86×10^{-10}
	GO:0048869: cellular developmental process		96	1.67×10^{-9}
	GO:0048468: cell development		45	2.66×10^{-7}
	GO:0009887: organ morphogenesis		38	6.12×10^{-5}
	GO:0001756: somitogenesis		8	2.61×10^{-4}
	GO:0035282: segmentation		9	2.66×10^{-4}
	GO:0009952: anterior/posterior pattern formation		13	0.0033
	GO:0009790: embryonic development		34	0.0074
	GO:0043009: chordate embryonic development		24	0.0075
	GO:0009792: embryonic development ending in birth		24	0.0084
Cytoskeleton			**[110]**	**5.30×10^{-19} to 0.0995**
Biological process	GO:0030029:actin filament-based process		**25**	1.45×10^{-9}
	GO:0030036:actin cytoskeleton organization		**23**	1.08×10^{-8}
	GO:0007010: cytoskeleton organization		**31**	1.50×10^{-7}
	GO:0007015: actin filament organization		**5**	0.0995
	GO:0015629: actin cytoskeleton		**39**	**5.30×10^{-19}**
Cellular componetnet	GO:0005856: cytoskeleton		**86**	**2.20×10^{-14}**
	GO:0016459: myosin complex		**21**	**1.26×10^{-15}**
	GO:0032982: myosin filament		**11**	**2.32×10^{-12}**
	GO:0044430: cytoskeletal part		**51**	**1.16×10^{-6}**
	GO:0005884: actin filament		**5**	**0.0134**
Cell Signalling			**[52]**	**4.78×10^{-5} to 0.0899**
	GO:0007154: cell communication		32	4.78×10^{-5}
	GO:0007267: cell-cell signalling		23	1.33×10^{-4}
	GO:0007169: transmembrane protein tyrosine kinase signalling		17	3.85×10^{-4}
	GO:0007167: enzyme linked receptor protein signalling pathway		20	0.0011
	GO:0008543: fibroblast growth factor recp signalling pathway		5	0.0139
	GO:0045168: cell-cell signalling involved in cell fate		4	0.0271
	GO:0040036: regulation of fibroblast growth factor signalling		3	0.0451
	GO:0043409: negative regulation of MAPKKK cascade		3	0.0614
	GO:0007219: Notch signalling pathway		5	0.0899

1. P-value enrichment of GO terms using DAVID analysis software; similar results were found with GOstat

3.3.5.1 Up-regulated genes are associated with cell adhesion, cell signalling and development and differentiation.

Genes up-regulated in muscle-less humeri revealed by microarray and RNA-seq were similarly analysed for enrichment of genes associated with particular biological processes or cellular components, using associated GO terms (Table 3:7). For terms within the sub-ontology "biological process", the strongest enrichment was for cell adhesion and ECM associated genes (total of 50/447 genes, with p-values down to 1.99 $x10^{-10}$). The genes identified in this category include ECM glycoproteins (*Lsamp, Svep1*), ECM structural constituents (*Col8a1, Col8a2, Frem3*), cell-adhesion molecules (*Cntn1, Cntn4, Cntn5*) and calcium-dependent cell adhesion proteins (*Pcdh8, Pcdhb2, Pcdhga1*). This grouping in addition included genes involved in signalling pathways which overlap with the next most enriched terms; cell signalling (GO:0007154) and cell-cell communication (GO:0007267). The signalling pathway components identified in this category include: Hedgehog (*Hhip, Ptch1*), fibroblast growth factor (*Fgf10, Fgf2*), transforming growth factor (*Frem2, Bmp3*), Notch (*Ctn1, Nrg1*) and Wnt signalling (*Dkk2, Cpz Rspo2, Rspo3, Sfrp2, Wnt2, Wnt2b, Wnt4* and *Wnt16*) and others, including receptors (*Epha3, Epha4, Epha5, Grin2a, Grm4, Grm7, Grm8, Gfra2,* and *Pdgfra*). Other signals identified as up-regulated included c-fos induced growth factor (*Figf),* hepatocyte growth factor *(Hgf)* and Insulin-like growth factor (*Igf1*). The gene lists in the next most enriched set, Development and Differentiation, similarly show large overlap due again to the presence of the signalling pathway genes mentioned above, and also transcription factors *Foxc2, Foxo3, Lmx1a, Lmx1b.*

Under the sub-ontology Cellular Component there was also striking enrichment of extracellular (total 81/447; with p-values down to 2.34 $x10^{-10}$) and membrane associated gene products (total 227/447 p-values down to 2.46 $x10^{-16}$), including cell adhesion molecules (*Cadm2, Cntn1*), receptors (*Fat2, Fat4, Grin2a, Grm4, Gfra2, Pdgfra, Robo2, Sorcs1, Sstr4*), cell surface molecules (*Cd83, Cd96*), cadherins (*Cdh20, Cdh8*), trans-membrane proteins

(*Tmem26, Tmem28*), voltage gated channels (*Kcna1, Kcna2, Kcnc2*) and cell adhesion and extracellular components: *Alcam, Cntn4, Epha4, Col8a1, Col8a2, Pappa, Pcdh8*.

3.3.6 Pathway Analysis of DE datasets

Following the identification of the biological processes affected in the DE datasets, I performed Ingenuity pathway analysis (IPA). The IPA program is based on the Ingenuity knowledge base (IPKB) which is derived from known functions and interactions of genes in published articles, that is accurately updated (used in: Wang et al., 2014). The IPA analysis revealed total agreement with the GO annotation analysis using DAVID and GOstat (Table 3:6 and Table 3:7) with regard to top biological functions identified, using the microarray and RNA-seq datasets independently.

IPA was applied to datasets from the two platforms separately but independent of regulation status, to identify in more detail the pathways that are most highly enriched. The top five pathways identified for the microarray and RNA-seq data are identical, including Calcium signalling, Actin cytoskeleton signalling and ILK (Integrin-linked kinase) signalling.

Table 3:7: Enrichment of gene groups up-regulated in muscle-less humeri based on GO terms under sub-ontologies Biological process and cellular component.

Gene Ontology:Biological Process	**Gene Count in study**	**Enrichment[1]**
Adhesion/ Extracellular Matrix	**[50]**	**1.99×10^{-10} to 0.0842**
GO:0007155: cell adhesion	41	1.99E-10
GO:0022610: biological adhesion	41	2.12E-10
GO:0007156: homophilic cell adhesion	15	4.95×10^{-7}
GO:0016337: cell-cell adhesion	19	9.38×10^{-6}
GO:0043062: extracellular structure organization	9	0.0223
GO:0030198: extracellular matrix organisation	6	0.0842
Cell Signalling	**[119]**	**3.45×10^{-9} to 0.0148**
GO:0007267: cell-cell signalling	27	3.45×10^{-9}
GO:0007154: cell communication	33	2.05×10^{-9}
GO:0007223: Wnt receptor signalling pathway, calcium modulated	7	0.0092
GO:0016055: Wnt receptor signalling pathway	4	0.0104
GO:0008589: regulation of smoothened signalling pathway	9	0.0105
GO:0010648: negative regulation of smoothened signalling	4	0.0135
GO:0048010: vascular endothelial growth factor receptor signal	10	0.0288
GO:0007169: transmembrane receptor protein tyrosine kinase sig	3	0.0402
GO:0007167: enzyme linked receptor protein signalling pathway	12	0.0051
GO:0007165: signal transduction	80	0.0148
Development/ Differentiation	**[93]**	**4.38×10^{-6} to 0.0083**
GO:0048731: system development	78	4.38×10^{-6}
GO:0048856: anatomical structure development	81	8.42×10^{-6}
GO:0007275: multicellular organismal development	87	6.80×10^{-5}
GO:0048468: cell development	31	8.17×10^{-5}
GO:0032502: developmental process	91	1.82×10^{-4}
GO:0048869: cellular developmental process	59	5.41×10^{-4}
GO:0030154: cell differentiation	57	5.74×10^{-4}
GO:0048513: organ development	56	0.0036
GO:0045595: regulation of cell differentiation	18	0.0083
Gene Ontology: Cellular Component	**Gene count in study**	**Enrichment[1]**
Extracellular Region	**[81]**	**2.34×10^{-10} to 0.022**
GO:0005576: extracellular region	81	2.34×10^{-10}
GO:0044421: extracellular region part	43	2.70×10^{-7}
GO:0031012: extracellular matrix	22	1.16×10^{-5}
GO:0005578: proteinaceous extracellular matrix	21	2.14×10^{-5}
GO:0005615: extracellular space	24	0.0020
GO:0044420: extracellular matrix part	7	0.0202
Membrane Association	**[227]**	**2.46×10^{-16} to 1.01×10^{-6}**
GO:0005886: plasma membrane	134	2.46×10^{-16}
GO:0031224: intrinsic to membrane	191	1.07×10^{-8}
GO:0044425: membrane part	215	2.08×10^{-8}
GO:0016020: membrane	226	7.80×10^{-8}
GO:0031224: intrinsic to membrane	178	1.01×10^{-6}

1. P-value of enrichment of GO terms using DAVID analysis software; similar results were found with GOstat.

3.3.7 Genomic localisation of DE genes

The genomic localisation of all DE genes with fold change of 2 and p-value ≤ 0.05 were analysed using an ideogram; a diagrammatic view of the chromosomes with DE gene locations indicated according to cytogenetic banding positions (Kin and Ono, 2007). Ideograms are useful to reveal genomic clustering of genes and their associated elements, which might indicate common regulation/ co-expression. There was no clear association of the DE genes with specific chromosomes or chromosome regions (Figure 3.9). Chromosome 1 is most densely populated with 91 DE genes (8.05% of total genes), chromosome 15 is lowest with 32 DE genes (2.83% of total genes). Two regions that are relatively enriched for DE genes are highlighted in Figure 3.9.

The data sets supporting the results of this article are available in the EMBL-EBI ArrayExpress repository (http://www.ebi.ac.uk/arrayexpress/). The differential expressed data set from the Microarray [ref: E-MTAB-1744], the differential expressed data set from the RNA-sequencing [ref: E-MTAB-1746] and for the transcriptome [ref: E-MTAB-1745]. Lists of differentially expressed genes are available in Appendix Table A.3 and Appendix Table A.4.

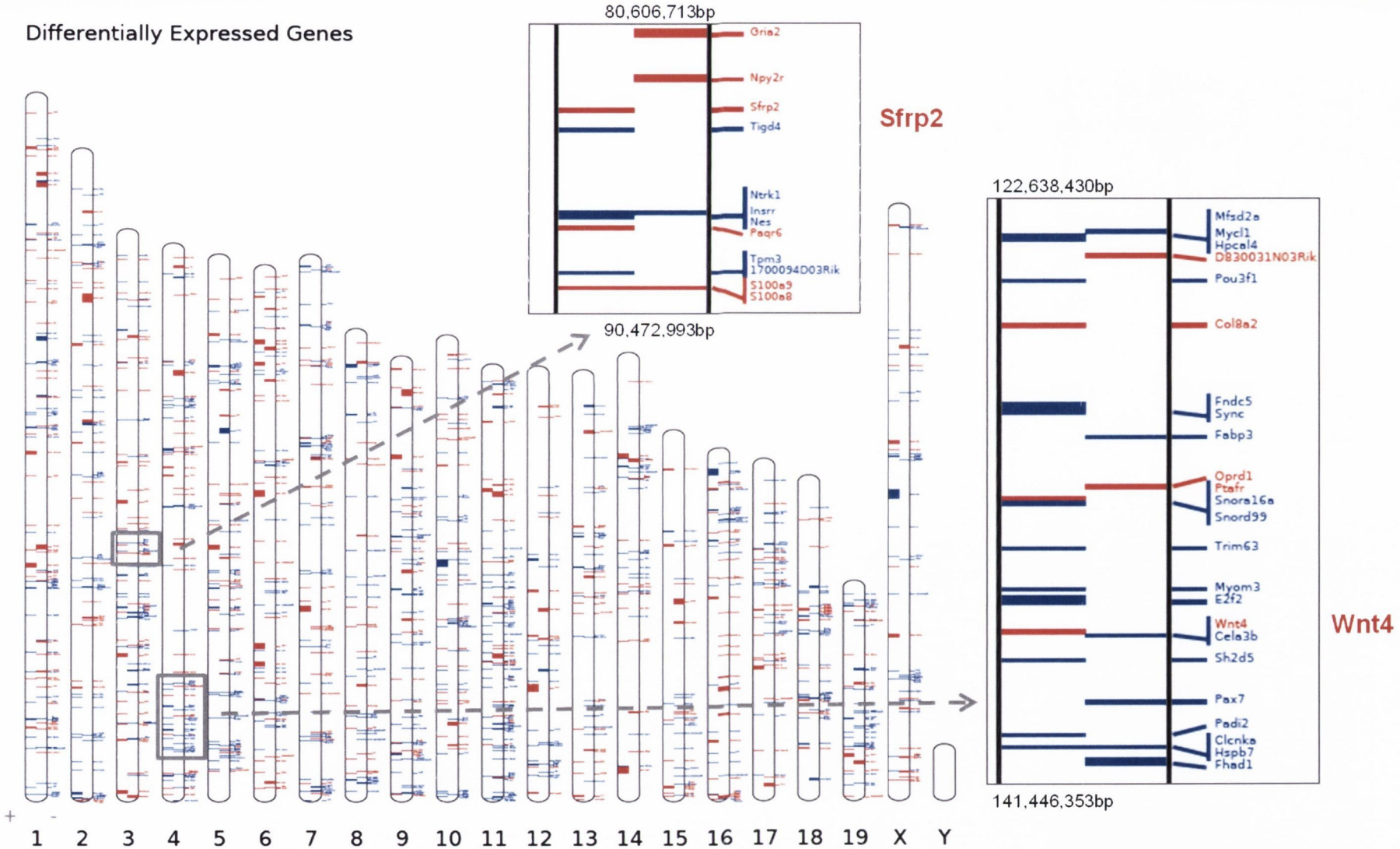

Figure 3.9: Ideogram of differentially expressed genes. Red shows up-regulated and blue down-regulated genes on each chromosome, Boxes show regions of clustering around selected Wnt component genes (Sfrp2; chromosome 3, Wnt4; chromosome 4).

3.4 Discussion

Here I describe the spectrum of genes expressed in the developing humerus at TS23, early in the process of ossification and when territories of differentiating cells are being defined in the developing joint region. I also use microarray and RNA-sequencing to identify genes that are differentially regulated when mechanical stimulation of the developing skeletal rudiment is altered, giving an insight into the genes that respond to mechanical stimuli generated by muscle contractions. Analysis revealed that the genes altered are highly enriched for genes that regulate development and differentiation, are involved in cytoskeletal rearrangement and components of extracellular matrix including cell adhesion and signalling molecules. Although it is clear that appropriate mechanical stimulation from *in utero* muscle contractions is required for normal development of bone and cartilage, we know very little about the molecular mechanisms that incorporate mechanical cues with classical biochemical signalling pathways. The differentially regulated genes identified here, particularly those associated with signalling pathways and cytoskeletal changes represent a valuable focus for dissecting integrated regulation by biochemical and mechanical signals. These data represent an important resource that can be utilised to understand the molecular basis of mechanoregulation.

3.4.1 The transcriptome of a developing skeletal rudiment

Utilising RNA-sequencing technology to reveal the transcriptome in the normal developing humerus and associated joints at TS23 provides an insight to the processes that are occurring during this stage of skeletal development when chondrocytes are undergoing hypertrophy, the cartilaginous rudiment is beginning to ossify at the mid diaphysis (reviewed in Karsenty et al., 2009) and specific zones within the joint are differentiating (reviewed in Pitsillides and Ashhurst, 2008). This adds a valuable resource to a growing set of data that can be combined to explore skeletal development. Previous transcriptome profiling studies have examined

cartilage condensation in the tibia-fibula from E11.5 to E13.5 (Cameron et al., 2009), ossification of metatarsals (Sugars et al., 2006), in different zones of the growth plate in 2 week old mice (Belluoccio et al., 2008) and in $Runx2^{-/-}$ mutant mice (Hecht et al., 2007). Earlier stages of limb development, although not specific to skeletal development, are informed by whole limb bud profiles between E9.5 and E11.5 (Taher et al., 2011). Another important resource that has recently become available examines the spatial expression patterns of 18,000 coding genes and over 400 microRNAs within the whole mouse embryo at the same developmental stage examined here (Diez-Roux et al., 2011). This digital transcriptome atlas is a powerful tool (Eurexpress; http://www.eurexpress.org/ee/intro.html) that can be used to examine spatial analysis of specific genes, exploring possible functional associations. Combining these resources gives information on quantitative and spatial expression of individual genes providing the basis to explore regulatory networks active during the development of skeletal rudiments.

Several of the findings of the transcriptome analysis are as expected; the most highly expressed genes (8 with ≥100,000 read counts) include 5 collagen encoding genes (Figure 3.6); collagens have been shown to be the most abundant structural proteins in cartilage and show characteristic distribution patterns as skeletal rudiments develop (Aigner and Stove, 2003; Olsen, 1996). The Insulin-like growth factor genes *Igf2* and *Igf1* and their associated receptors *Ifg2r* and *Igf1r* are also highly expressed (4,194 to 221,194 read counts); these are reported to play a prominent regulatory role in skeletal development (reviewed in Yakar et al., 2010). Similarly, aggrecan (*Acan)* and osteopontin (*Spp1*), both involved in skeletal development, are highly expressed (Figure 3.6). Although much is known about the regulatory network that controls early chondrogenesis and joint formation (Kronenberg, 2003; Provot and Schipani, 2005), open-ended whole transcriptome studies are required to add new information. Centred on regulatory signalling pathways known to be involved in skeletal

development; HH, FGF, TGFβ (including BMP) and Wnt; a complete list of components of these pathways expressed in the humerus as TS23 was extracted (Figure 3.6) indicating the potential role players in each of these pathways at this specific stage. The importance of Indian hedgehog (*Ihh)* expression in the early prehypertrophic and hypertrophic chondrocytes of cartilage condensations is well established (Hecht et al., 2007; Minina et al., 2005; St-Jacques et al., 1999). The full spectrum of possible interacting molecules in HH signalling (Figure 3.6) include the receptors *Ptch1, Ptch2, Smo* and transcription factors *Gli1, Gli2,* and *Gli3.* In addition to *Ihh,* Desert hedgehog (*Dhh*) expression was also detected (read count 70) and, examining the data presented by Cameron et al confirms that Dhh is up-regulated (≥3 fold) in E13.5 fibual and tibual cartilage (Cameron et al., 2009). *Dhh* has not previously been functionally linked to skeletogenesis but this opens the possibility of regulatory contribution, perhaps co-operating with Ihh. No expression of *Shh* was detected.

Similarly, novel components of the FGF, TGBβ and Wnt pathways were identified (Figure 3.6). FGF signalling is known to be crucial for hypertropic differentiation (Ornitz and Marie, 2002) but may also be important in other aspects of skeletal development. In the FGF pathway the most highly expressed transcripts identified were associated with receptor encoding genes (*Fgfr1, Fgfr3, Fgfrl1, Fgfr2, Fgfr4)*. Fgfr1 and Fgfr3 have previously been reported to be expressed in pre-hypertrophic/ hypertrophic and proliferating chondrocytes respectively (Minina et al., 2002; Peters et al., 1992). The higher expression level of fibroblast growth factor receptor encoding genes relative to corresponding ligands might be related to a generally more restricted expression pattern of ligand encoding genes and more widespread expression of Fgf receptor genes, as was seen in spatial studies at E14.5 and E16.5 (Minina et al., 2005). The most highly expressed Fgf ligand encoding gene identified was *Fgf18*, also identified as up-regulated in E13.5 compared to E11.5 cartilage tissue (Cameron et al., 2009); expression is in the perichodrium and joints of long bones and appears to regulate cell

proliferation and differentiation. It acts by promoting osteogenesis and negatively regulating chondrogenesis through the Fgfr3 receptor (Ohbayashi et al., 2002) with mutations in Fgfr3 resulting in constitutive activation of Fgf signalling in chondocytes, impairment of cell proliferation and dwarfism (Naski et al., 1996). The detection of other FGF genes is novel; *Fgf10*, the second most highly expressed ligand, was not detected in a previous study at E14.5 and E16.5 (Minina et al., 2005); however searching the Eurexpress database corroborates forelimb expression at E14.5 (Diez-Roux et al., 2011). Similarly *Fgf7* and *Fgf9* expression was detected here and corroborated by Eurexpress. The transforming growth factor β (TGFβ) family of signalling molecules also includes bone morphogenetic proteins (BMPs) and growth differentiation factors (GDFs), functionally implicated in various aspects of skeletogenesis. The large number of components of this signalling pathway family expressed (Figure 3.6) underlines the huge potential for component interactions during skeletal development. The most highly expressed TGFβ receptor encoding gene identified here is *Tgfβr2,* with limited previous expression data linked to skeletogenesis. All TGFβ ligands detected were previously reported to be expressed in skeletal elements at E14.5; *Tgfβ3* in the perichodrium and in distinct stripes of early hypertrophic chondrocytes and *Tgfβ2* and *Tgfβ1* in early hypertrophic chondrocytes (Minina et al., 2005).

Bmp1 was the most highly expressed BMP ligand (5417 read counts) indicating its potential role; although associated with osteogenesis in zebrafish (Asharani et al., 2012) and an early study indicated mammalian skeletal expression (Scott et al., 1999), it is more associated with neural development (www.informatics.jax.org). Detection of *Bmp5* expression in the humerus at TS23 is corroborated in the Eurexpress database. Other components of the BMP pathway have been well characterised during skeletal development (Minina et al., 2005), with expression of several of the components associated with positive regulation of hypertrophy (Kobayashi et al., 2005); *Bmp2* (530 reads) and *Bmp6* (395 reads) were previously detected in

hypertrophic chondrocytes, with *Bmp7* (566 reads) in proliferating chondrocytes (Minina et al., 2005). However there are no previous reports of skeletal expression of *Smad2,4, 6, 7* and *8;* Smad6 in particular can bind type 1 BMP receptors and prevent the activation of downstream Smads (Imamura et al., 1997), suggesting complex regulatory interactions.

The Wnt signalling pathway plays a central role during embryonic development and is known to be an important regulator of bone formation and bone remodelling (reviewed in Macsai et al., 2008). It also plays a pivotal role in joint formation and maintenance, shown through gain and loss of function experiments (Guo et al., 2004; Spater et al., 2006). The key intracellular mediator of canonical Wnt signalling, β-catenin (*Ctnnb1*; 28,608 read counts) is the most highly expressed Wnt signalling component in the TS23 humerus and associated joints. The most highly expressed Wnt ligand is *Wnt5a*, previously associated with expression in joints and perichondrium (Church et al 2002) and proliferating chondrocytes (Yang et al 2005). Other highly expressed ligands include *Wnt9a, Wnt5b, Wnt11,* and *Wnt4. Wnt5b* and *Wnt11* expression has been shown in the pre-hypertrophic chondrocytes and *Wnt4, Wnt9* and *Wnt16* in the developing joints (Church et al., 2002; Guo et al., 2004; Hartmann and Tabin, 2000; Hartmann and Tabin, 2001). High expression of *Wnt9a* could be due to its role in the temporal and spatial regulation of *Ihh* (Spater et al., 2006).

Numerous extracellular modulators of the pathway were detected; all five secreted frizzled related protein (*Sfrp)* genes, Dickoff (*Dkk)* 1, 2 and 3 genes and four R-spondins (*Rspos)*, indicating a huge potential for pathway modulation. The most highly expressed antagonist modulators of the pathway were *Dkk3* and *Sfrp2* both of with are detected in joint cells at E13.5 and E15.5 (Witte et al., 2009). The most highly expressed R-spondin agonist of the pathway was *Rspo3*, previously detected in phalanges (Nam et al., 2007).

3.4.2 Identification of Mechanoresponsive genes

The identification of differentially expressed genes between humeri from control and muscle-less embryonic limbs allows an investigation of the biological processes and the developmental regulatory signalling pathways that are affected by the removal of mechanical stimulation on skeletogenesis *in vivo*. It was previously reported that muscleless (*Splotch*) mutants display abnormal ossification in the humerus, altered humeral morphogenesis and altered elbow and shoulder joint formation and these effects were most strongly identified at TS23 (Nowlan et al., 2010a). These phenotypic disturbances were confirmed for the TS23 muscle-less (*Splotch-delayed*) mutant. Alteration in expression pattern of some selected candidate genes and pathways was revealed (Kahn et al., 2009; Nowlan et al., 2012), but here we carry out the first genome wide study identifying a total of 1,132 independent genes as differentially expressed: with approximately 60% down-regulated and 40% up-regulated. The finding of more genes being down-regulated than up-regulated and to a greater extent is consistent with the proposal that mechanical stimuli supports the correct differentiation of cells, as observed in the ossification phenotype (Nowlan et al., 2010a), and for the maintenance of tissue patterning, as seen in the developing joint (Roddy et al., 2011b).

To identify biological functional enrichment of these genes I used gene ontology (GO) annotation analysis to identify specific biological processes that are affected when mechanical stimuli are removed. This type of analysis has been used previously to interpret biological processes associated with developing skeletal tissue (Hecht et al., 2007; Sohn et al., 2010; Sugars et al., 2006). Analysis of the down-regulated DE gene set identified genes associated with development and differentiation as the most highly enriched categories, including developmental regulatory signalling pathway molecules and transcription factors. Similarly, analysis of up-regulated DE gene sets indicated genes associated with cell signalling and

development and differentiation. Signalling pathway disturbances are explored in more detail in chapter 4.

DE genes were also highly enriched for genes associated with the cytoskeleton. The cytoskeleton controls cell shape, organelle transport, cell motility and division, and connects the extracellular matrix to internal cell processes (reviewed in Alenghat and Ingber, 2002). It maintains the mechanical integrity of cells and has been implicated in relaying mechanical signals to downstream biochemical responses (Mammoto et al., 2012; Wang et al., 1993). This was seen in the embryonic lung where cytoskeletal network inhibitors resulted in altered tissue morphogenesis and conversely when cytoskeletal tension was activated lung development was accelerated (reviewed in Ingber, 2006), indicating the dynamic role the cytoskeleton has in morphogenesis.

In chondrocytes the actin microfilaments are predominantly located at the periphery of the cytoplasm (Idowu et al., 2000), tubulin microtubules are uniformly distributed throughout the cytoplasm (Jortikka et al., 2000) as are intermediate filaments, connecting the nuclear membrane with the cell periphery (Blain et al., 2006). In this study 84 genes annotated as cytoskeletal were down-regulated when mechanical stimulation was removed. These include 33 genes directly associated with actin microfilaments, 13 with microtubules and 4 with intermediate filaments. The most highly affected group, the Filamentous-actin cytoskeleton, has been shown to be involved in articular cartilage chondrocyte mechanotransduction, converting a mechanical stimulus into a biochemical response (Guilak, 1995; Knight et al., 2006; Parkkinen et al., 1995; Wang et al., 1993). Other studies have confirmed the involvement of the actin cytoskeleton in cartilage chondrocyte mechanotransduction via manipulation of the actin accessory proteins (Campbell et al., 2007; Knight et al., 2006), but there are few reports on the affect of mechanical stimulation on microtubule and intermediate filaments (Steward et al., 2013). Among the DE genes is an actin-binding protein, cofilin2

(Cfl2); cofilin was previously shown to be increased following cyclic mechanical loading of chondrocytes (Campbell et al., 2007).

The identification of cytoskeletal genes down-regulated following the removal of mechanical stimulation indicates that the cytoskeleton is affected, but is this because the mechanical integrity of the cell is altered or because mechanotransduction from the ECM is affected, or perhaps a combination of both? The finding that ECM and cell adhesion associated genes are also affected further supports changes in mechanotransduction pathways. The cell-adhesion associated integrins (*Itga4, Itga7, Itgb6*) and cadherins (*Cdh4, Cdh15, Cdhr3*) are down-regulated and these proteins potentially function to physically couple cells to the ECM and play a role in mechanical signal transduction (Ingber, 2006; Wang et al., 1993). Articular chondrocytes have been shown to express both integrin (Woods et al., 1994) and non-integrin (Knudson et al., 1996) ECM receptors. Another actin-associated protein identified to be down-regulated is actinin-α2 (*Actn2*); this protein also couples the cytoskeleton to the ECM and may be involved in transducing mechanical stimulation.

In this study differential expression in developing skeletal rudiments is documented in the absence of limb muscle; this will include genes that respond to lack of mechanical stimulation but perhaps also as a paracrine response to adjacent muscle cells. We know that phenotypic effects on ossification and joint formation are due to the lack of mechanical stimulation rather than physical absence of muscle cells because phenotypic analysis of a range of mouse mutants where muscle is immobile (Kahn et al., 2009), reduced (Nowlan et al., 2010a) or absent (Kahn et al., 2009; Nowlan et al., 2008a) have similar effects and we see similar effects in immobilised chick embryos (Nowlan et al., 2008b; Roddy et al., 2011b). Therefore, although some of the genes identified here may respond to lack of adjacent muscle tissue, many must underlie the phenotypic effects seen in response to lack of mechanical stimulation. This is further supported by the overlap of some of the genes identified here and in skeletal

cells in culture or adult tissues, in response to mechanical stimulation (Bougault et al., 2012; Patel et al., 2007).

Although Genomic localisation of DE genes revealed dispersal of genes across the genome with no predominance of individual chromosomes or regions, there is evidence for finer scale gene clustering, for example at the lower end of chromosome 3 (24 genes) and on chromosome 4 (12 genes) (Figure 3.9). These represent regions worthy of further analysis since each included a DE Wnt pathway component gene (Sfrp2 and Wnt4) and identify potential regulatory regions and co-regulation of genes base on positional arrangement.

3.4.3 Limitation of Approach

An important limitation in this work is the possibility that a proportion of the down-regulated genes may be due to contamination of the dissected control humeri with adjacent mesenchyme/muscle, since this is being compared to tissue from muscle-less embryos. Although care was taken with the dissections, it is impossible to be sure that all muscle tissue was eliminated from the control. The down-regulated gene set also showed enrichment for muscle associated genes (Appendix Table A.2), consistent with possible contamination of the dissected control humeri by neighbouring muscle. To inform this we also sequenced the transcriptome of mesenchyme adjacent to the humerus of control embryos at TS23 and compared it to the transcriptome of control humeri. We then cross referenced this to the down-regulated gene set in control versus muscle-less humeri (Appendix Table A.3), noting any genes enriched more than 3 fold in mesenchyme compared to control humeri; these are indicated in column 2 of Appendix Table A.3. It is possible that these genes are involved in both cartilage and muscle development so no genes have been removed from the data set, however, DE genes also showing higher expression in mesenchyme compared to control humeri must be treated with caution with respect to a skeletal specific response to mechanical

stimulation. Such genes have not been prioritised in any of our subsequent exploration of candidate mechanosensitive genes.

3.4.4 Technical Comparison

This study used both RNA-sequencing (Illumina) and Microarray (Agilent) technologies in parallel to determine differential expression. Microarray technology has been utilised to determine expression of chondrogenic and osteogenic genes from developing whole tissues (Hecht et al., 2007; Sugars et al., 2006; Taher et al., 2011), and from *in vitro* differentiation procedures (Bernstein et al., 2010; Bougault et al., 2012; Chen et al., 2010b; James et al., 2005; Tallheden et al., 2004). The use of RNA-seq technology to describe the transcriptome is more recent (Li et al., 2010a; Mortazavi et al., 2008; Wilhelm and Landry, 2009). Previous direct comparisons between microarray and RNA sequencing-based approaches to reveal alterations in gene expression between tissues reported that RNA-seq identified more DE genes (Bottomly et al., 2011; Lahiry et al., 2011; Marioni et al., 2008). It was found that RNA-seq is more sensitive in reproducibly detecting alterations in gene expression, detecting more genes altered at lower quantitative levels (Table 3:4). This was further emphasised by reducing the stringency of the statistical analysis to $p \leq 0.08$, which increased the number of genes detected by microarray specifically. The larger dynamic range (Bottomly et al., 2011) and higher reproducibility across replicates (Marioni et al., 2008) has also been found in other studies.

3.5 Conclusion

This study examined the set of genes active at a key stage of skeletal development (TS23) and revealed the genes that are differentially regulated in the developing humerus when skeletal muscle is absent. Since it was previously shown that the lack of muscle contractions leads to common phenotypic defects in both ossification and joint formation in several chick and mouse models, this provides an insight into the genome wide alterations in gene transcription

that take place when the mechanical environment is altered. Given the importance of appropriate mechanical stimulation generated by embryo movement on skeletal development I postulated that mechanical stimuli must integrate with biochemical cell signalling pathways known to be essential for normal development. I showed that multiple signalling pathways are affected and this is further explored in Chapter 4. This finding, together with alteration of cytoskeletal components, indicates the biological processes involved in integrating biophysical stimuli during cell differentiation and patterning. Understanding the mechanistic basis for how developing cells interpret and respond to biophysical cues is a major challenge, relevant to all developing systems, and will impact our ability to control differentiation of progenitor cells for regenerative therapies. This work is an early step in unravelling the mechanistic basis of biophysical regulation of skeletal development and provides a focus for future studies.

Chapter 4

4. Characterisation of Mechanosensitive genes: signalling pathways and developmental processes

4.1 Introduction

Immobilisation of both mouse and chick embryos showed that movement is required for multiple aspects of skeletal development; for endochondral ossification, for morphogenesis of the cartilage rudiment and for definition of tissue territories in the joint (Nowlan et al., 2010a; Nowlan et al., 2008a; Roddy et al., 2011b; reviewed in Rolfe et al., 2013a). Chapter 3 reported transcriptome profiling of the developing humerus and associated joints from muscle-less Splotch-delayed mutant embryos compared to heterozygous littermates at TS23, the earliest stage at which the phenotypic effects are evident. This was designed as an open-ended approach to identifying genes that are impacted by mechanical stimulation resulting from movement, with the objective of revealing the molecular mechanisms involved in sensing and transducing such mechanical signals. This list of differentially expressed genes generated by transcriptome profiling was analysed to reveal enrichment of particular categories of genes and showed strong enrichment of genes associated with Development and differentiation (Table 3:6 and Table 3:7) including genes associated with cell signalling pathways. This shows that cell signalling pathways that guide cell differentiation and tissue organisation are disturbed in an altered mechanical environment. Establishing precisely which pathways are disturbed and to what extent would bring insights into the molecular processes involved and potentially reveal the mechanistic basis of mechanical control of skeletal development.

Previous mechano-modulatory studies have identified components of multiple signalling pathways to be mechanosensitive, including BMP signalling in an immobilisation study focusing on joint development (Roddy et al., 2011b), the FGF signalling in an immobilisation study (Roddy et al., 2011b), in an *in vitro* four point bending study of osteoblasts (Jackson et al., 2006) and when mechanical forces were applied to osteoblasts (Cillo et al., 2000) and an osteogenic cell line (Hatton et al., 2003). Microgravity conditions have also been associated

with alteration of cell signalling components, including the Wnt signalling pathway and the BMP pathway (Patel et al., 2007).

While the annotation tags on genes in the mouse genome were used to reveal enrichment of signalling pathway genes, such annotations are not detailed or complete enough to reliably reveal associations with specific signalling pathways. One of the objectives of the current chapter is to examine differentially expressed genes for any known association with specific signalling pathways.

A developing skeletal rudiment at any particular point in development is made up of cells undergoing different developmental processes related to ossification and joint definition at the rudiment termini. In particular, endochondral ossification is spatially dynamic with cells in different positions along the length of the rudiment undergoing different phases of the process (Figure 1.2). In chapter 3 the transcriptome of the developing humerus and associated joints at stage TS23 was analysed. The genes expressed reflect the molecular activities of the constituent cells and the differentially expressed genes reflect the molecular processes impacted by movement. However this is a complex set of developing tissues made up of chondrogeneic cells undergoing different phases of endochondral ossification, as well as joint tissue patterning. Transcriptome profiling for the whole tissue sample does not identify which cell type or developmental process a given gene is involved in. Therefore to be able to further interpret the differential expression data, it is important to reveal where in the developing humerus and joints a differentially expressed gene is active and precisely how it is disturbed in the muscle-less mutant.

In situ hybridisation (ISH) is a powerful technique that allows individual gene expression visualisation in particular tissues of interest; it is widely used to piece together information about where particular mRNAs are located, and therefore which cells are expressing a particular gene in a complex tissue context. This information, combined with information

about the type of molecule it encodes and changes that take place in those cells, can give valuable clues to functional possibilities for that gene and the proposal of testable hypotheses to give insight into cellular differentiation and morphogenesis. It is particularly valuable in the temporally and spatially dynamic context of developing tissues. Despite its valuable advantages the technique is associated with limitations including the lengthy period it takes to obtain results for one gene, and a threshold level of gene expression per cell is required for detection, i.e. if there is a very low number of transcripts per cell, it will not be detected.

Another method of distinguishing which tissue territories within the developing humerus express a specific gene is Laser Capture Microdissection (LCM), coupled with detection of gene transcripts. LCM enables selective harvesting of pure cell populations from distinct territories, which are highly enriched for specific cell types thus having the potential of yielding information about the developmental processes that are occurring in a particular tissue at a particular point in time. LCM technology has been used in a wide variety of applications (reviewed in Liu, 2010). Recent studies have used LCM technology to analyse the molecular profiles of developing cartilage (Akavia et al., 2012; Jenner et al., 2014), of pathological cartilage (Fukui et al., 2011; Judex et al., 2004) and the developing meniscus (Pazin et al., 2014). Through the careful sub-dissection of tissue territories and the downstream analysis of transcript expression, it is possible to use LCM to quantify small expression changes in distinct cellular regions of interest. Laser-capture micro-dissection has the potential to be a more high through-put approach, analysing more genes and with a higher level of sensitivity than ISH.

Given the importance of appropriate mechanical stimulation generated by embryo movement on skeletal development we postulate that mechanical stimuli must integrate with biochemical cell signalling pathways known to be essential for normal development. This chapter reports

analysis of differentially expressed genes in the muscle-less humerus and associated joints in two respects:

1. To identify any associations of DE genes with specific signalling pathways, using literature to manually annotate genes. This was then used to gauge the level of disturbance of known developmentally important signalling pathways.

2. To use gene expression analysis to establish if differentially expressed genes are disturbed in particular cell populations within the developing rudiment, giving an indication of the developmental processes disturbed. *In situ* hybridisation was used to assess the spatial distribution of expressing cells while Laser Capture Microdissection coupled with quantitative RT-PCR gave added information on relative levels of expression and was tested as a more high-throughput means of analysis.

4.2 Methods

4.2.1 Bioinformatic analysis of associations with cell signaling pathways

Gene Ontology (GO) annotations for each individual signalling pathways allowed some differentially expressed genes to be grouped according to pathway, retrieved using GOstat (http://gostat.wehi.edu.au/) and Database for Annotation, Visualisation and Integrated Discovery (DAVID) (http://david.abcc.ncifcrf.gov/). The GO terms used included GO:0030509 (BMP signalling), GO:0008543 (FGF signalling), GO:0016055 (Wnt signalling), GO:0035329 (Hippo signalling), GO:0007219 (Notch signalling) and GO:0007224 (Smoothened signalling). However GO annotations that assign genes to individual pathways are not complete (as judged by examining individual genes known to be associated with a pathway) so DE genes were also manually assigned to pathways based on literature and available databases such as the Wnt homepage, available at http://web.stanford.edu/group/nusselab/cgi-bin/wnt/; a repository of data on components and targets of Wnt signalling pathways. Preliminary information on cell signalling component gene expression was obtained using publically available databases including Mouse Genome Informatics (MGI), available at http://www.informatics.jax.org/; and the transcriptome-wide mouse atlas database Eurexpress, available at http://www.eurexpress.org/ee/.

4.2.2 Tissue Preparation

All tissue came from timed matings of heterozygous C57BL/Pax3^{Spd} mice to produce homozygous *Pax3*$^{Spd/Spd}$ mutant embryos, as per section 2.1. All embryos were staged and genotyped using PCR amplification to confirm homozygote mutants and distinguish heterozygote and homozygote controls, as described in section 2.2.

Vibratome and cryo-sectioning of forelimbs was carried out for in situ hybridisation as described in section 2.4.1 and 2.4.2.

4.2.3 In Situ Hybridisation

Probe preparation was performed as described in section 2.5.1, and details of the cDNA clones used to generate anti-sense or sense RNA in situ probes are given in Table 4:1. *In situ* hybridisation was carried out on vibratome sections and frozen sections as described in sections 2.5.2 and 2.5.3 respectively. Post hybridisation washing and antibody detection as described in section 2.5.4. Adaptations were made for the post-hybridisation wash durations for the cyrosections, comprising of one initial post-hybridisation wash to remove coverslips in 50%formamide/5x SSC, then two 30min washes in 50% formamide/2x SSC, three 10min washes in 2x SSC, three 10mins washes in 0.2x SSC, followed by TNT washes prior to blocking.

4.2.4 Immunohistochemistry

Immunohistochemistry was performed as described in section 2.10. Detection of the primary antibody Noggin[2], (polyclonal goat IgG, AF719 R&D Systems) (1:100) was performed using a donkey-anti-goat secondary antibody conjugated with horse radish peroxidise (1:200) and amplified using a tyramide kit. Detection of the primary antibody pSMAD1/5/8 (polyclonal rabbit IgG, #9511 Cell signalling Technology®) (1:100) was performed using a goat-anti rabbit alkaline phosphatase secondary antibody (1:200) and stained using NMT containing 167.5ug/ml 4-nito blue tetrazolium chloride (NBT; Roche) and 175ug/ml 5-bromo-4-chloro-3-indolyl-phosphate (BCIP; Roche). Mounting of fluorescent samples was performed using DAPI counter-stain (DAPI Prolong Anti-fade Mounting Medium, P-36931, Invitrogen) and colourometrically stained samples with Aquapolymount (Polysciences Inc).

[2] Noggin Immunohistochemistry was performed by Pratik Singh, Indian Insitute of Technology, Kanpur on *Spd/Spd* tissue provided by me; for a collaborative project investigating the role of BMP signalling in mechanical regulation of articualr cartilage development.

Table 4:1: Details of cDNA clones used to generate RNA in situ probes.

Gene	Genebank Ref Sequence	Alignment on reference	Source
Barx2	NM_013800.2	Nucleotide 833 to 1560	I.M.A.G.E EST Library
Bmp2	NM_007553.2	Nucleotide 53 to 1215	Prof RE Hill
Bmp4	NM_007554.2	Nucleotide 6-1181	Prof. Si Jen Lee
Cd44	NM_00103915.1	Nucleotide 222 to 3020	I.M.A.G.E EST Library
Chrdl2	NM_133709	Nucleotide 36 to 1520	I.M.A.G.E EST Library
Cilp	NM_173385	Nucleotide 3353 to 4153	I.M.A.G.E EST Library
Col10a1	NM_009925.3	Nucleotide 915 to 2729	I.M.A.G.E EST clone
Col8a1	NM_007739.2	Nucleotide 1189 to 2468	I.M.A.G.E EST Library
Col20a1	NM_028518.1	Nucleotide 3389 to 3721	I.M.A.G.E EST Library
Col26a1	NM_024474.2	Nucleotide 1070 to 2705	I.M.A.G.E EST Library
Crapb1	NM_013496.2	Nucleotide 13 to 741	I.M.A.G.E EST Library
Dll1	NM_007865.3	Nucleotide 2664 to 3444	I.M.A.G.E EST Library
Enpp2	NM_001136077.1	Nucleotide 1 to 2745	I.M.A.G.E EST Library
Epha4	NM_007936.3	Nucleotide 2697 to 3622	I.M.A.G.E EST Library
Fgf8	See Ref: Mahmood *et al.*, 1995		Prof RE Hill
Fgf10	NM_008002.4	Nucleotide 686-1315	Dr. R. Kelly
Fgfr4	NM_008011.2	Nucleotide 2180 to 3127	I.M.A.G.E EST clone
Fzd10	NM_175284.3	Nucleotide 1829 to 2988	I.M.A.G.E EST clone
Gdf5	NM_008109.2	Nucleotide 304 to 2010	Dr. C. Tabin
Hhatl	NM_029095.2	Nucleotide 142 to 1314	I.M.A.G.E EST Library
Hhip	NM_020259.4	Nucleotide 2241 to 3050	I.M.A.G.E EST Library
Ihh	NM_010544.2	Nucleotide 663 to 2459	Prof RE Hill
Itgb1bp2	NM_013712.2	Nucleotide 1 to 1308	I.M.A.G.E EST Library
Lrrn1	NM_008516.4	Nucleotide 2115 to 3742	I.M.A.G.E EST Library
Noggin	NM_008711.2	Nucleotide 291 to 1285	Dr. Richard Harland
Parm1	NM_145562.2	Nucleotide 1 to 2100	I.M.A.G.E EST Library
Pcdh8	NM_001042726.3	Nucleotide 2882 to 3700	I.M.A.G.E EST Library
Pcdh10	NM_001098172.1	Nucleotide 3181 to 4658	I.M.A.G.E EST Library
Pdgfa	NM_008808.3	Nucleotide 1to 1019	I.M.A.G.E EST Library
Pdgfra	NM_001083316.1	Nucleotide 2602 to 4220	I.M.A.G.E EST Library
Prrx1	NM_175686.3	Nucleotide 4498 to 4983	I.M.A.G.E EST Library
Runx2	NM_009820.2	Nucleotide 262 to 3442	I.M.A.G.E EST clone
Scx	NM_198885.2	Nucleotide 657 to 1059	Prof RE Hill
Sfrp2	U88567.1	Nucleotide 82 to 852	Dr A. Rattner
Sox5	NM_0111444.3	Nucleotide 1757 to 2250	Dr. V. Lefebvre
Spp1	NM_001204201	Nucleotide 27 to 1472	I.M.A.G.E EST Library
Spry1	NM_011896.2	Nucleotide 1793 to 2488	I.M.A.G.E EST Library
Wnt2	NM_023653.4	Nucleotide 35-1510	Prof A. McMahon
Wnt2b	NM_009520.1	Nucleotide 1010 to 1215	Dr Lise Zakin
Wnt4	NM_009523.1	Nucleotide 639 to 1101	Prof A. McMahon
Wnt16	NM_053116.3	Nucleotide 537 to 1532	Generated by PCR

4.2.5 Laser-Capture Microdissection

Unfixed, frozen tissue sections were prepeared for LCM: Collection and dissection of fresh forelimb samples from homozygous *Pax3*$^{Spd/Spd}$ mutant embryos and littermate controls was performed as described in 2.1. Laser-capture microdissection was performed as described in

section 2.11. Territories sub-dissected in TS23 control and mutant forelimbs included the elbow joint (EJ), the humerus pre-hypertrophic zone (pre-hz) and the hypertrophic zone (HZ).

4.2.6 RNA preparation, amplification of laser capture micro-dissected tissue

Directly following micro-dissection the territories of interest were immediately processed. Optimisation of removal of the micro-dissected tissue from the thermoplastic film was performed using variations on previous descriptions (McGinley et al., 2010). In brief, the 0.5ml micro-centrifuge tubes containing the film on the cap, were inverted and placed in an inverted heating block at 42°C for 30mins, the tubes were then centrifuged to collect the cell extract in the RNA extraction buffer. Flushing of the film surface with the extraction agent and scraping of cells off of the thermoplastic film was also performed, to aid further cellular dissociation. Total cellular RNA was extracted using the SV Total RNA Isolation System (Promega) as per manufacturer's instructions. Total RNA quantity and integrity was assessed using a NanoDrop® ND-1000.

RNA yields were found to be as low as 118ng total, and this was not sufficient for screening of multiple genes from a single sample, by qRT-PCR, as planned. RNA was amplified using the TargetAmp™ 1-Round aRNA Amplification kit (Epicentre, Illumina), which is based on the linear T7 amplification that was originally developed in the Eberwine Lab in 1990 (Van Gelder et al., 1990). Step 1 comprises the reverse transcription and incorporation of a T7 RNA polymerase to a RNA sample to make cDNA. A second strand cDNA synthesis is then performed in step 2, following the fragmentation of the first cDNA: RNA hybrid produced in the initial reverse transcription, to yield cDNA containing the T7 transcription promoter. Step 3 involves *in vitro* transcription of aRNA (amplified RNA) utilising the double stranded cDNA in step 2. This aRNA was then quantified and total amplification on average increased the RNA yield by 5.8 fold, in comparison to the amplification of control RNA from Hela cells which was amplified 100 fold.

4.2.7 Reverse transcription and quantitative Real Time PCR of LCM aRNA

To quantify mRNA expression, 100ng of total aRNA was reverse transcribed into cDNA using iScript™ cDNA systhesis kit (BioRad) as per manufacturer's instructions. Quantitative real-time reverse transcription-polymerase chain reaction (qRT-PCR) was used to analyse the relative gene expression differences between RNA extracted from the three distinct territories in control samples, or to compare control and mutant gene expression levels in the same territory. Seven target genes were analysed including *Sfrp2*, *Sox5*, *Spp1*, *Dll1*, *Wnt4*, *Fgf10* and *Rxrg*. All expression was normalised to the endogenous ubiquitously expressed control gene *Gapdh*. All primers were designed using Primer Express Software®, version 3.0, under default settings for TaqMan® quantification and purchased through Sigma (Sigma-Aldrich, Ireland). Primer sequences for the gene analysed are listed in Table 3:1 Amplification was performed and analysed as described in section 2.7.

4.3 Results

4.3.1 Signalling pathway analysis of differentially expressed genes

Given the strong enrichment of genes associated with cell Signalling Pathways and Development and Differentiation functions, identified and described in chapter 3 (Table 3:6 and Table 3:7) I sorted the DE genes according to participation in major developmental regulatory pathways (Table 4:2 and Table 4:3). I did this by utilising the GO terms associated with each gene to construct a table showing how each of the different pathway components are affected by a reduction in mechanical stimulation. In addition, literature searches and utilisation of databases such as Array Express (http://www.ebi.ac.uk/arrayexpress/) were used to make additional functional links between DE genes and signalling pathways- manually annotating the genes. The indicated role of the gene product in the signalling pathway and the relevant literature supporting these associations are cited in Table 4:2 and Table 4:3.

The pathways identified include the BMP signalling pathway, the Hedgehog signalling pathway, the Fibroblast growth factor signalling pathway, the Hippo, the Notch signalling pathways (Table 4:2) and the Wnt signalling pathway (Table 4:3). The identification of these signalling pathways as potential mechanoregulators of bone and joint formation is of particular interest as these pathways were previously shown to be key regulators of bone formation and cartilage differentiation (section 1.3).

Table 4:2: Differentially Expressed genes associated with specific signalling pathways.

	Down-Regulated					
	Up-Regulated					
	Fold Change		**Gene Symbol**	**Gene Name**	**Role in Pathway**	**Reference**
	RNA seq	**Micro-array**				
Bone Morphogenetic Protein Signalling Pathway						
	87.94	50.88	Hfe2	hemochromatosis type 2	Negative regulator	(Babitt et al., 2006)
	5.25		Fgf8	fibroblast growth factor 8	T	(Heymer and Ruther, 1999)
	4.36	4.9	Grem2	Gremlin2	Ant	(Zuniga et al., 2011)
	2.44		Scx	scleraxis	T	(Blitz et al., 2009)
	2.17		Egr2	early growth response 2	T	(Leclerc et al., 2004)
	2.03		Bmp3	bone morphogenetic protein 3	L	(Yamaji et al., 1994)
Hedgehog Signalling Pathway						
	14.55	4.59	Hhatl	hedgehog acyltransferase-like	Negative regulator	(Abe et al., 2008)
	3.35		Glis3	GLIS family zinc finger 3	TF	(Kim et al., 2003)
	2.70		Ptchd1	patched domain containing 1	R	
	2.27		Hhip	hedgehog interacting protein	Ant + T	(Chuang and McMahon, 1999)
	2.14		Ptch1	patched 1	R + T	(Bellusci et al., 1997)
Fibroblast Growth Factor Signalling Pathway						
	#		Fgf4	fibroblast growth factor 4	L	
	#		Fgf6	fibroblast growth factor 5	L	
	5.25		Fgf8	fibroblast growth factor 8	L	
	5.10		Fgf5	fibroblast growth factor 5	L	
	4.54	3.23	Fgfr4	fibroblast growth factor receptor4	R	
	3.24		Spry1	sprouty homolog 1	Ant + T	(Gross et al., 2001)
	3.22		Spry4	sprouty homolog 4	Ant +T	
	2.75		Spry2	sprouty homolog 2	Ant + T	(Gross et al., 2001)
	2.39		Fgf2	fibroblast growth factor 2	L	
	2.134	2.48	Fgf10	fibroblast growth factor 10	L	
Hippo Signalling Pathway						
	98.29	49.05	Vgll2	vestigial like 2 homolog (Drosophila)	Co-TF	(Johnson et al., 2011)
	97.73	75.14	Ankrd1	Ankyrin repeat domain 1	T	(Dupont et al., 2011)
	3.86	4.38	Tead4	TEA domain family member 4	Co-TF	(Chen et al., 2010a)
	2.96		Fat4	Fat tumor suppressor homolog 4	R	(Katoh, 2012)
	2.43		Fat2	Fat tumor suppressor homolog 2	R	
Notch Signalling pathway						
	5.64		Dner	delta/notch-like EGF-related receptor	R	(Eiraku et al., 2005)
	3.16	2.21	Dll1	delta-like 1 (Drosophila)	L	(Shimizu et al., 2000)
	2.69		Hes6	hairy and enhancer of split 6	T	(Fior and Henrique, 2005)
	2.54		Dtx4	deltex homolog 4	T	
	2.09		Jag2	jagged 2	R	(Shimizu et al., 2000)
	3.25	2.87	Nrg1	neuregulin 1	T	(Zhang et al., 2012)
	2.36	2.09	Foxc2	forkhead box C2	Upstream-activator	(Kume et al., 2001)
	2.27	2.29	Cntn1	contactin 1	PL	(Bizzoca et al., 2012)

No numerical value for fold change as no transcripts detected in the Mutant

T -Target, L -Ligand, L-act- Ligand activator, R -Receptor, Ant -Antagonist, Co-TF- -Co-Transcription Factor, PL –Potential Ligand

Table 4:3: Differentially expressed Wnt signalling pathway genes

	Down-Regulated					
	Up-Regulated					
Fold Change		**Gene Symbol**	**Gene Name**	**Role in Pathway**	**Reference**	
RNA seq	**Micro -array**					
Wnt Signalling Pathway						
#	41.05	Fgf4	fibroblast growth factor 4	T	(Kratochwil et al., 2002)	
#		Snai3	snail homolog 3	PT	(ten Berge et al., 2008)	
90.87	32.06	Cacng1	calcium channel, voltage-dependent, gamma subunit 1	T	(Wisniewska et al., 2010)	
42.86	18.77	Pitx3	paired-like homeodomain transcription factor 3	PT	(Kioussi et al., 2002)	
37.43	17.22	Kremen2	kringle containing transmembrane protein2	Co-Ant	(Mao et al., 2002)	
29.52		Ccnb3	Cyclin B3	PT	(Shtutman et al., 1999)	
12.29	7.05	Rxrg	retinoid X receptor gamma	PT	(McGrew et al., 1999)	
5.95	5.20	Islr2	immunoglobulin superfamily containing leucine-rich repeat 2	PT	(Tice et al., 2002)	
4.87		Pitx2	paired-like homeodomain transcription factor 2	T	(Kioussi et al., 2002)	
3.58		Fzd10	frizzled homolog 10	R	(Kawakami et al., 2000)	
3.16	2.21	Dll1	Delta-like 1	T	(Hofmann et al., 2004)	
3.05		Prg4	Lubricin	T	(Koyama et al., 2008)	
2.81	2.57	Lrrn1	leucine rich repeat protein 1, neuronal	T	(Hasenpusch-Theil et al., 2012)	
2.52		Sall1	sal-like 1	PT	(Bohm et al., 2006)	
2.47		Tnik	TRAF2 and NCK interacting kinase	TF-act	(Mahmoudi et al., 2009)	
2.32		Tcf15	transcription factor 15	T		
2.32		Met	met proto-oncogene	T	(Boon et al., 2002)	
2.18	2.28	Cd44	CD44 antigen	T	(Wielenga et al., 1999)	
2.09		Jag2	Jagged2	PT	(Estrach et al., 2006)	
4.36	4.91	Grem2	Gremlin	T	(Im et al., 2007)	
3.96		Wnt2	wingless-related MMTV integration site 2	L		
3.50		Wnt2b	wingless-related MMTV integration site2b	L		
3.07		Wnt16	wingless-related MMTV integration site16	L		
2.85	2.90	Kcnd2	potassium voltage-gated channel, shal-related family, member 2	T	(Hasenpusch-Theil et al., 2012)	
2.73		Cldn1	claudin-1	T	(Miwa et al., 2001)	
2.44		Dkk2	Dickkopf	Ant	(Hasenpusch-Theil et al., 2012; Li et al., 2005)	
2.43	3.08	Rspo2	R-spondin 2	L/ T	(Abed et al., 2011; Hasenpusch-Theil et al., 2012; Nam et al., 2007)	
2.37		Epha4	Eph receptor A4	T	(Hasenpusch-Theil et al., 2012)	
2.11		Elavl2	ELAV (embryonic lethal, abnormal vision, Drosophila)-like 2	T	(Hasenpusch-Theil et al., 2012)	
2.10		Cpz	Carboxypeptidase Z	Co-act	(Wang et al., 2009)	
2.09	2.62	Sfrp2	secreted Frizzled related protein 2	Ant/ T	(Lescher et al., 1998)	
2.03		Wnt4	wingless-related MMTV integration site 4	L		
2.02		Rspo3	R-spondin 3	L/ T	(Hasenpusch-Theil et al., 2012; Nam et al., 2006)	
	2.41	E330013P04Rik	RIKEN cDNA E330013P04 gene	T	(Hasenpusch-Theil et al., 2012)	

No numerical value for fold change as no transcripts detected in the Mutant
T -Target, PT -Potential Target, R -Receptor, TF-act -Transcription factor activator, L -Ligand, Ant -Antagonist, Co-act -Co-activator

4.3.2 Expression analysis of signalling pathway component genes and proteins on tissue sections

Expression of each selected DE gene was analysed in normal control forelimb tissue at TS23 to establish if the ISH method can detect a localised gene expression pattern and if so, to establish the normal pattern, prior to analysis of muscle-less tissue. Gene expression databases were also used to search for detection of gene expression in the relevant tissues and stages. Genes were selected for analysis based on a number of criteria:

1. They show differential expression in the transcriptome screen and are associated with a developmentally important cell signalling pathway (Table 4:2 and Table 4:3); the BMP pathway (section 4.3.2.1, Figure 4.1, Figure 4.2), the HH signalling pathway (section 4.3.2.2, Figure 4.3) and the Wnt signalling pathway (section 4.3.2.3, Figure 4.5, Figure 4.6).

2. They were not found to be significantly differentially expressed by at least 2 fold, but they are key mediators of the pathway under analysis. This was undertaken since it is possible that the spatial pattern of expression might be altered in an informative way without the quantitative level being altered significantly, at least above the cut off criteria. This group also includes protein markers of pathway activity such as activated transcription factors or known pathway modulators.

3. Other selected genes that were identified to be differentially expressed and are known to be involved in bone or joint development but are not associated directly with specific signalling pathways (section 4.3.2.4).

Some of the genes were discontinued following the first level of analysis because a clear spatial pattern of expression was not revealed by ISH. This may be due to the expression level of the individual transcripts (reflected in the read count values from RNA seq analysis) being below the level of detection by ISH, or detection revealed expression only in the adjacent

muscle. These were not followed up in the muscle-less mutant and results are only shown in the Appendix Figure B.1: . The regions of most interest for detection include territories associated with ossification, termed the ossification site (OS), including the hypertrophic zone (HZ) or pre-hypertrophic zone (preHZ) and the adjacent perichondrium (PC)/ bone collar, in the mid-diaphysis of the humerus; the shoulder joint (SJ) encompassing the territory between the humerus and the scapula, and the elbow joint (EJ) defined by the territories between the humerus and the ulna and radius.

4.3.2.1 BMP signalling pathway

Six DE genes are known to be associated with the BMP signalling pathway (Table 4:2 and Schematic Figure 4.11). These include a gene encoding a BMP ligand (*Bmp3* 2.03; fold up) which, although encoding a ligand of the pathway, is implicated in repressesing osteogenic BMPs such as Bmp2, possibly through stimulating the TGFβ pathway (Bahamonde and Lyons, 2001). One known BMP antagonist *Grem2* (4.26 fold, up), which has previously been shown to block BMP activity in the patterning of the facial skeleton (Zuniga et al., 2011). Two known direct targets genes of BMP signalling are down-regulated (Egr2; 2.17 fold and Fgf8; 5.25 fold). The Scx transcription factor is not known to respond to BMP signalling but is positively regulated by TGFβ signalling (Maeda et al., 2011) and is reported to up-regulate expression of BMP4 (Blitz et al., 2009). The gene is down-regulated 2.4 fold in this study. Hfe2 is implicated more tangentially in the BMP pathway as it encodes a co-receptor of transferrin and has been shown to block BMP signalling (Babitt et al., 2006)

Nine genes associated with the BMP pathway were analysed in order to identify any alterations in spatial expression patterns in muscle-less tissue (Table 4:4, Figure 4.1). Of the 5 genes identified as differentially expressed by RNAseq, only Scx was analysed in muscle-less limbs by ISH. This was either because the expression level was too low (Fgf8, Egr2) or a probe was not available (Bmp3, Hfe2). However regionalised expression in the developing

skeletal rudiment, gleaned from the MGI database is noted in Table 4:4. Additional BMP ligand, antagonist and target genes known to be important in skeletal development were assayed; Bmp2 ligand, Noggin antagonist, Runx2 and Prrx1 target genes (Table 4:4). *Crabp1*, *Grem2*, *Lrrn1* and *Bmp4* were analysed but were not detected in the regions of interest, so were not followed up in the muscle-less mutant (Appendix Figure B.2).

Table 4:4: The BMP pathway components that were analysed by ISH

Bone Morphogenetic Protein Signalling Pathway					
Gene	**DE** (fold)	**Role in Pathway**	**Read count in Control**	**Spatial Expression**	
				Control	**Muscle-less mutant**
Ossification site					
Bmp2	**0.8**	Ligand	530 reads	HZ and PC (Figure 4.1a)	reduced HZ
Bmp3	**2.03**	Ligand- but negatively regulates osteogenic BMPs	385 reads	PC and hypertrophic chondrocytes (Minina et al., 2005)	NA
Egr2	**2.17**	Target gene	102 reads	Weak in HZ (Levi et al., 1996)	NA
Fgf8	**5.25**	Target gene	16 reads	Weak in Proliferating chondrocytes & hypertrophic chondrocytes (Minina et al., 2005)	NA
Nog	**0.95**	Antagonist	513 reads	preHZ (Figure 4.1g)	Reduced in preHZ
Runx2	**1.8**	Target and co-transcription factor	1285 reads	PC and preHZ (Figure 4.1k)	Reduced territory but More intense in PC
Prrx1	**2.32**	Potential Target	5621 reads	No localised expression detected	Up-regulated in the outer PC (Figure 4.1r)
Joint					
Bmp2	**0.8**	Ligand	530 reads	Joint line (Figure 4.1c, e)	Absent joint line, reduced HZ
Nog	**0.95**	Antagonist	513 reads	Joint line and periarticular	Not restricted in joint line
Scx	**2.44**	Upstream regulator	971 reads	Tendons. PC, condyles (Figure 4.1m-p)	Absent tendons No apparent change elsewhere
Gdf5	**1**	Ligand	727 reads	Joint line	Reduced in EJ, SJ & some carpal joints but digits normal
Emid2	**1.16**	Target	4871 reads	Flanking anterior and posterior to joint. Joint line	Down in joint line but normal in anterior and posterior of joint
Other					
Hfe2	**88**	Upstream regulator	1069 reads	Highly expressed in muscle (Schmidtmer and Engelkamp, 2004)	NA

NA; not applicable, PC; perichondrium, HZ; hypertrophic zone, preHZ; pre-hypertrophic zone, EJ; elbow joint, SJ; shoulder joint

Detection of *Bmp2* was noted in the control perichondrium and HZ of the humerus (Figure 4.1a) with a reduction shown in both territories in the mutant (Figure 4.1b). Expression of *Bmp2* was also detected in the joint line of the EJ (Figure 4.1c) and in the peripheral cells at the anterior and posterior margins of the SJ (Figure 4.1e), this expression was altered (Figure 4.1d) or absent (Figure 4.1f), as indicated by the white arrows for the comparable regions in the muscle-less mutants. Analysis of the transcript expression of the pathway antagonist Noggin revealed more widespread expression in the EJ territory in the mutant (Figure 4.1j) with continuous expression across the joint line, compared to the distinct restriction of expression shown in the proliferating chondrocytes/ the periarticular region at the distal end of the humerus and the distal end of the ulna (Figure 4.1i). Expression of noggin transcript was also detected in the pre-hypertrophic cells that are spreading in the mid-diaphyseal region of the humerus (Figure 4.1g), this pattern was absent in the mutant; rather low levels of expression were detected in the midline of the humerus (Figure 4.1h), consistent with delayed ossification. While the extent of the domain of expression of the target gene *Runx2* in the perichondrium and the HZ of the mutant (Figure 4.1l) was reduced, consistent with a reduced ossification site, expression within the perichondrium was elevated.

Expression of the potential upstream activator Scleraxis (*Scx*) was detected broadly in the perichondrium of the condyles, in the ligaments and tendons (Figure 4.1m-p) and while no change was seen in the perichondrium at the EJ or the SJ, no tendon expression was visible (Figure 4.1m-p). This is not surprising since tendons do not form in the muscle-less embryos. The expression of the potential target gene *Prrx1* (paired related homeobox 1) was not detected in a localised pattern in the control rudiment but an increased line of expression at the outer edge of the perichondrium surrounding the humerus was revealed in the mutant (Figure 4.1r). The expression of the ligand encoding gene *Gdf5* in the joint line was absent in the muscle-less elbow (Figure 4.1t) and shoulder joints (Figure 4.1v), and reduced in carpal joints but normal in digit joints (data not shown). The expression of the target gene *Emid2*

was reduced in the joint line in both the elbow joint (Figure 4.1x) but the anterior and posterior expression flanking both EJ and SJ remained. These findings are summarised and integrated with relevant data from RNAseq (Chapter 3) and expression data from the MGI database (Table 4:4; Figure 4.11).

An assimilation of the gene expression findings (Figure 4.11 schematic A&B) suggests that BMP pathway signalling is reduced in the joint line and in the ossification site, although perhaps elevated in the perichondrium. To test this model, protein localisation of two key components of the pathway were analysed to reveal pathway activity in the muscle-less mutant (Figure 4.2). Analysis of the antagonist Noggin at the protein level revealed a similar pattern to transcript detection. Within the humero-ulnar (Figure 4.2a-d) and humero-radial (Figure 4.2e-h) joints noggin protein was more widely localised through the terminal ends of the humerus (Figure 4.2c, g), ulna (Figure 4.2c) and radius (Figure 4.2g) and across the joint line in the muscle-less mutant, indicating a more widespread territory of antagonism of the BMP pathway in these cells close to the joint. In control humeri, Noggin was detected within the hypertrophic zone (Figure 4.2i) but detected outside this region extending into the prehypertrophic zone in the mutant (Figure 4.2k). However detection of Noggin in the control perichondium was apparently unaltered in the mutant. An overall expansion of the noggin expression domain in the cells of the rudiment was seen in the muscle-less mutant (Figure 4.2k).

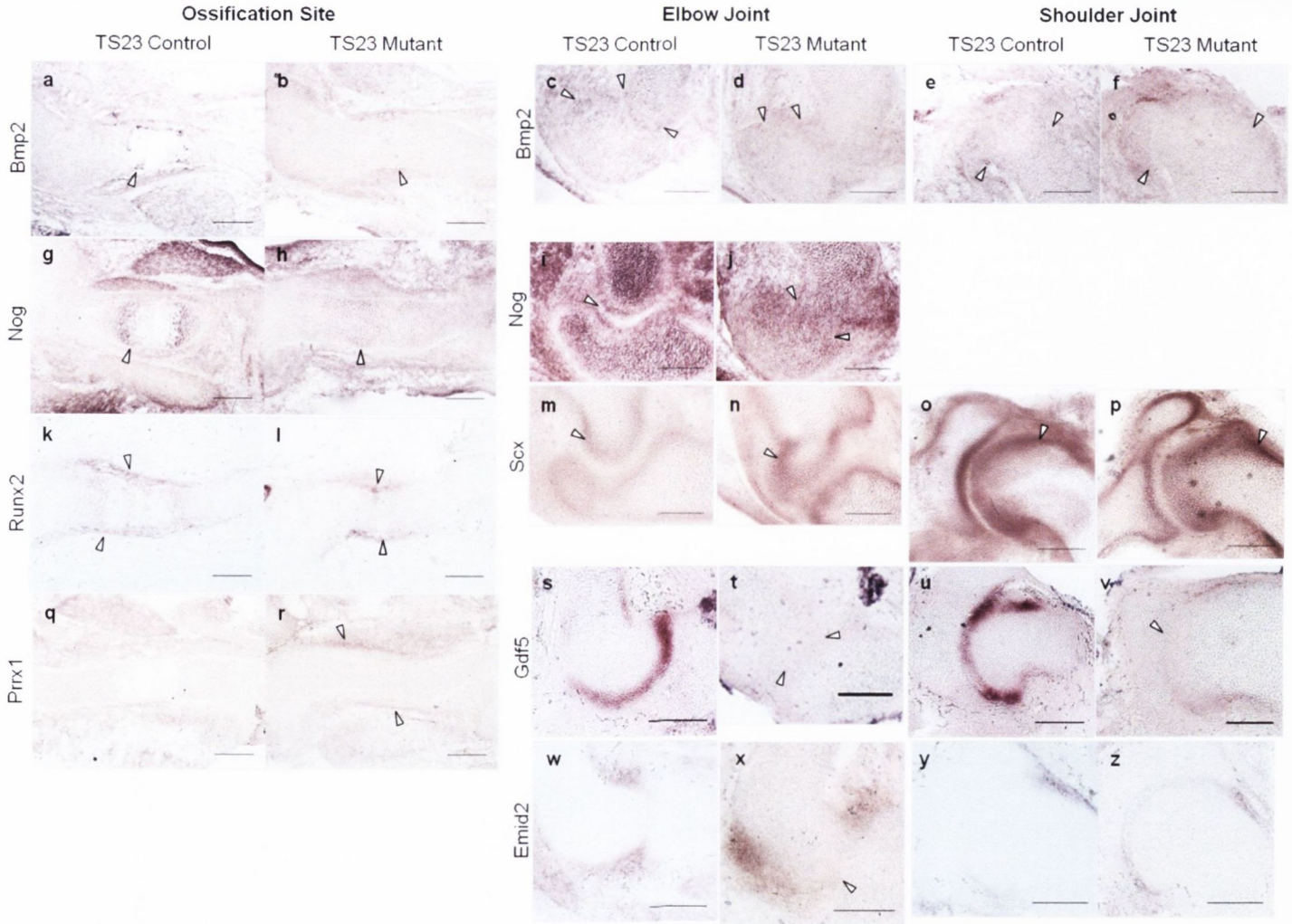

Figure 4.1: BMP cell signalling pathway genes, showing altered expression patterns in the ossification site (**a-b, g-h, k-l, q-r**) and the elbow (**c-d, i-j, m-n, s-t, w-x**) and shoulder joints (**e-f, o-p, u-v-, y-z**) of TS23 control (a, **c, e, g, i, k, m, o, q, s, u, w, y**) and muscle-less mutant forelimbs (**b, d, f, h, j, l, n, p, r, t, v, x, z**). White arrows indicate regions described in the text. All scale bars are 100μm.

Antibody detection of the downstream effectors of canonical BMP signalling, the phosphorylated versions of SMAD proteins 1, 5 and 8, referred to as pSMAD1/5/8 protein, is a standard means of assessing BMP pathway activation. pSMAD1/5/8 was detected in the proliferating chondrocytes at the distal end of the humerus and the proximal end of the ulna (Figure 4.2m-p) and in the hypertrophic zone (Figure 4.2q, r) of control and muscle-less mutant tissue. An increase in the extentof pSMAD1/5/8 positive cells in the terminal end of the ulna in the mutant (Figure 4.2p) can be seen compared to control (Figure 4.2n), while a similar distribution of positive cells in the humerus was shown. pSMAD1/5/8 was detected in cells throughout the ossification site and in the perichondium at the mid-diaphysis in the control (Figure 4.2q), there was a reduction in the number of positive cells in the mid-diaphysis in the mutant, yet there was still a level of detection in the cells that have not yet undergone hypertrophy, and dramatic reduction in the extent in the perichondium (Figure 4.2r).

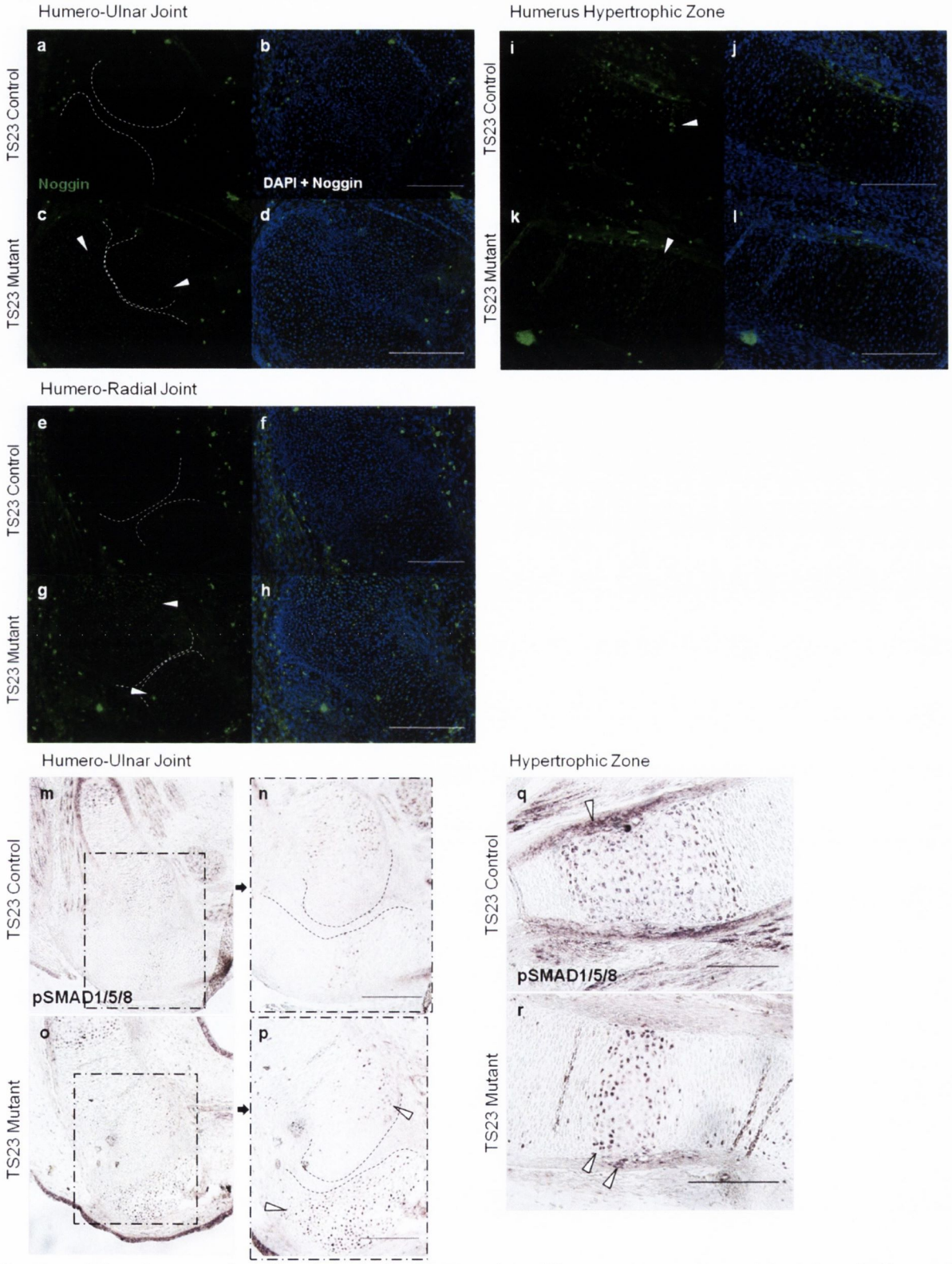

Figure 4.2: Immunolocalisation of BMP signalling components Noggin (**a-l**) and pSMAD1/5/8 (**m-r**) in TS23 control (**a-b, e-f, i-j, m-n, q**) and TS23 mutant forelimb tissue (**c-d, k-l, o-p, r**). Detection was compared in the humero-ulnar joint (**a-d, m-p**), the humero-radial joint (**e-h**) and the humerus hypertrophic zone (**i-l, q-r**). White dotted lines indicate the distal end of the humerus and white arrows indicate regions described in the text. All scale bars are 100μm.

4.3.2.2 Hedgehog signalling pathway

Five components of the Hedgehog signalling pathway (GO:0007224 smoothened signalling pathway) were identified as differentially expressed. *Hhatl* (Hedgehog acetyltransferase like; 14.55 fold down) is a poorly studied gene related to Hhat which influences the pathway by post-translationally activating the ligand. However, a study suggests that the Hhatl gene product negatively regulates Hedgehog activity (Abe et al., 2008). One transcription factor that is closely related to the Gli Kruppel-like zine finger proteins that act downstream in Hh signalling, *Glis3* (GLIS zinc finger protein 3; 3.25 fold up), which has previously been reported to be expressed in the developing limb, specifically in the inter-digital region and to cross-talk with Hh-Gli activation (Kim et al., 2003). The three remaining genes are targets or potential targets of the pathway but also encodes pathway components *Hhip* (2.3 fold up) encodes an antagonist of Hedgehog signalling (Chuang and McMahon, 1999). *Ptch1* (2 fold up) product also acts as a receptor and a feedback negative regulator, *Ptchd1* 2.7 fold up is related to Ptch1 and 2 and appears to also act as a receptor (Noor et al., 2010). No other DE genes have known association with the Hedgehog pathway.

Three components of the hedgehog signalling pathway were analysed by ISH; *Hhip*, *Hhatl*, both shown to be differentially expressed by RNAseq (Table 4:2) and *Ihh*. Although *Ihh* did not show differential expression by RNAseq, its expression was previously shown to be disturbed in immobilised chick embryos (Nowlan et al., 2008b). Similarly, analysis of *Ihh* in the muscle-less mutant reveals that expression detected in the control in two bands of pre-hypertrophic/ hypertrophic chondrocytes is reduced to a single band in the mutant (Figure 4.3 f, h). *Hhip* is a target of the pathway and also encodes an antagonist (Chuang and McMahon, 1999). Expression in control tissue was detected in muscle, perichondrium and extensively throughout the humerus, elevated in the pre-hypertrophic chondrocytes (Figure 4.3 a, c), with expression more extensive in the mutant in the cells in the mid-diaphysis of the humerus (Figure 4.3 d). *Hhatl* expression was not detectable by ISH in control limbs (Appendix Figure

B.2 (B)) so was not further analysed. This is not surprising since the transcriptome read count was 84.13 in the control humerus and 5.78 in the mutant. Overall the hedgehog pathway appears to be activated in the mutant limb compared to control; however the 3 target genes up regulated each encode negative regulators of the pathway.

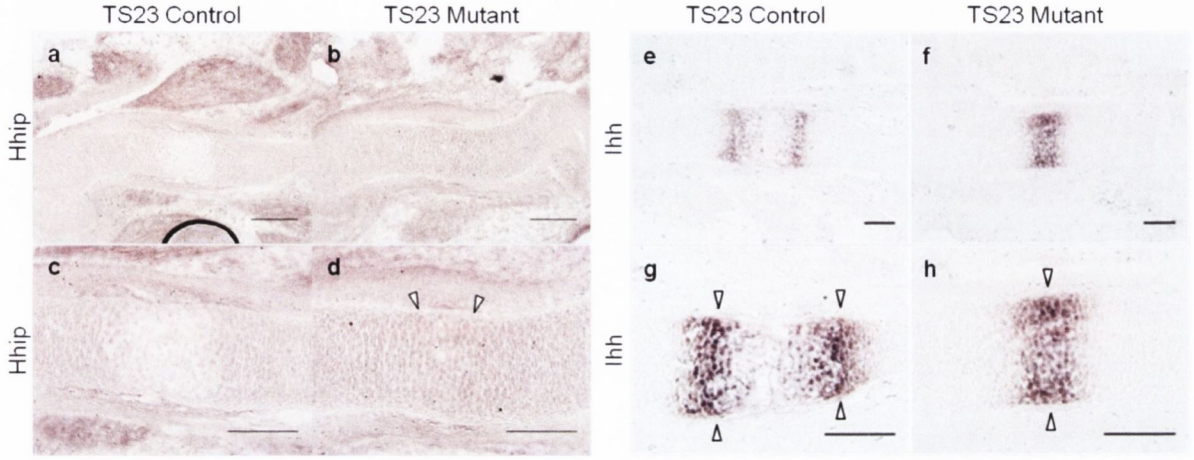

Figure 4.3: Analysis of the Hedgehog signalling pathway components *Hhip* and *Ihh* in the TS23 control (**a, c, e, g**) and TS23 muscle-less humeri (**b, d, f, h**). White arrows indicate regions described in the text. All scale bars are 100μm.

4.3.2.3 Wnt Signalling pathway

By far the most strongly impacted cell communication pathway is Wnt signalling with 34 DE genes encoding signalling molecules, receptors, pathway antagonists, known targets or potential targets of the pathway (Figure 4.4, Table 4:3). From the diagrammatic representation of pathway components shown in Figure 4.4, it is apparent that the encoded products of DE genes act either at the cell surface in Wnt signal generation/ modulation/ interpretation or are targets of the pathway. The genes listed in Table 4:3 include known targets of the pathway and seven potential target genes (not verified), included here due to their similarity to known targets; for example *Sall1*is included because the orthologous gene *Sall4* is a known direct target of the pathway (Bohm et al., 2006). Thus *Sall1* is proposed to be a potential target; its orthologue is expressed in the mouse limb and Sall genes function in a co-operative manner in organogenesis (Kawakami et al., 2009), so are potentially regulated in a similar manner. In

general, genes encoding cell surface components of the pathway are up-regulated, including signalling ligands and agonists (*Wnt2*, *Wnt2b*, *Wnt4*, *Wnt16*, *Rspo2* and Rspo3), and extracellular antagonists (*Dkk2*, *Sfrp2*), while down-regulated genes identified are more commonly targets of the pathway (e.g. *Fgf4*, *Cacng1*, *Pitx2*, *Dll1*, *Prg4*, *Lrrn1*, *Met*, and *Cd44*). Interestingly nine known Wnt target genes are up-regulated, including *Dkk2*, *Rspo2*, *Rspo3*, *Cldn1*, *Grem2*, *Kcnd1*, *Epha4* and *Sfrp2*, but all encode membrane associated proteins, some of which regulate the Wnt pathway (*Dkk2*, *Sfrp2*, *Rspo2*, *Rspo3*).

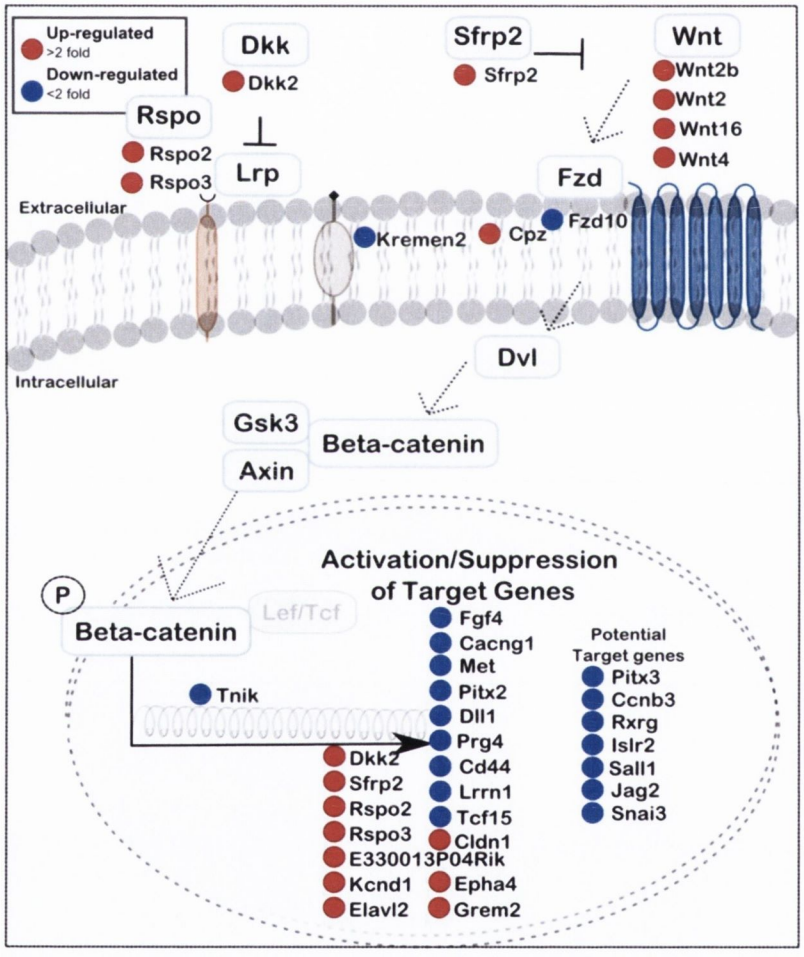

Figure 4.4: Visual representation of Wnt signalling pathway components, showing altered expression in developing muscle-less humeri. Blue circles indicate down-regulated genes red are up-regulated genes (Fold change ≥2, p≤0.05, genes and details listed in Table 4:3).

As the Wnt pathway was revealed to be the most affected, more genes in this category were analysed for spatial expression patterns. Of the 34 DE genes associated with the Wnt

pathway, 16 were selected for ISH analysis. Genes which showed a relatively high read count, indicating a possibility of detecting expression on tissue sections, or were of particularly high interest (e.g. ligand encoding) were prioritised. Table 4:5 details the Wnt pathway component genes that were analysed; colours indicate regulation status from quantitative transcriptomic analysis, with blue indicating down- and red up-regulation. Spatial expression analysis of selected genes is shown in Figure 4.5 and Figure 4.6.

Table 4:5: The Wnt pathway components that were analysed by ISH. A lists the components of the pathway and B lists targets and potential targets of the pathway that were screened

Gene	Regulation Status (fold)	Control Read count	Mutant Read count	Localised Expression			
				Joint		Ossification Site	
				Control	Mutant	Control	Mutant
(A) Components of Wnt signalling pathway							
Fzd10	3.58	94	26	Undetectable	Undetectable	Extensive in preHZ and growth plate	Undetectable
Wnt16	3.07	19	59	Future joint site: 2nd digit	Increase at future joint site:2nd digit	Undetectable	Undetectable
Wnt2	3.96	42	167	Undetectable		Undetectable	
Wnt4	2.03	135	274	Ventral surface of EJ and SJ	Up-regualted in joint line of EJ and SJ	preHZ two separated bands	Reduced separation but level normal
Sfrp2	2.09	2888	6041	Low level in joint interzone and periphery of joint	Up-regulated in joint and periphery		
Wnt2b	3.50	53	184	Undetectable			
Rspo2	2.43	331	802	Undetectable			clavicle
Rspo3	2.02	784	1586	Undetectable		clavicle	
(B) Targets/ Potential Targets of the Wnt signalling pathway							
Fgfr4	41.1	1459	321	Undetectable	Undetectable	muscle	Undetectable
Dll1	3.16	262	83			HZ & PC	Reduced in both
Cd44	2.18	2273	1041	Joint interzone in EJ & SJ	Absence in both	Undetectable	Undetectable
Epha4	2.37	1545	3657	Tendon, digit		PC	
Lrrn1	2.81	2234	794			muscle	
Grem2	4.36	117	509			rudiment	
Rxrg	12.3	455	37	Interdigital (Visel et al., 2004)	Too low to detect	Limb musculature (Dolle, 2009)	Too low to detect
Pitx2	4.9	320	66		Too low to detect	Possible tendon and PC (Diez-Roux et al., 2011)	Too low to detect

EJ; elbow joint, SJ; shoulder joint, preHZ; pre-hypertrophic zone, HZ; hypertrophic zone, PC; perichondrium

Figure 4.5 presents expression and expression alterations in the joint region. This shows most strikingly that the Wnt ligand encoding gene *Wnt4* is dramatically up-regulated in a wide domain spanning the entire joint region (Figure 4.5 g-l). In the wild type, *Wnt4* is only detectable at the peripheral edges of the joint. Wnt16 is up-regulated at the site of future digit joints (Figure 4.5ag-ah) but is not clearly detected in mutant or control proximal joints; it is possible that the level of expression at proximal joints is below detection by this method. The *Sfrp2* gene which encodes a Wnt signalling pathway modulator (can bind Wnt extra-cellularly) is also up-regulated in the joint interzone and the periphery, particularly on the ventral side (Figure 4.5 n, p, r). Higher levels of expression were detected in the more distal joints including the carpal region (Figure 4.5 u) and the digit joints (Figure 4.5 w), with no distinct difference in mutant joints (Figure 4.5 v, x respectively). The receptor-encoding *Fzd10* is normally expressed widely, at a low level throughout the rudiment termini with reduced expression within the joint (Figure 4.5 s). This expression is entirely undetectable in the mutant. Cd44 encodes membrane bound protein that acts as a receptor for hyaluronan, required during cavitation (reviewed in Archer et al., 2003; Pitsillides and Ashhurst, 2008), and is a target gene of Wnt signalling (Wielenga et al., 1999). Cd44 expression is entirely lost in the humero-ulnar (Figure 4.5 z), the humero-radial (Figure 4.5 ab), and the shoulder joint (Figure 4.5 ad) compared to clear joint line restricted expression in controls (Figure 4.5 y, aa, ac). Another Wnt target gene is *Dll1*, encoding a Notch signalling receptor. Dll1 is widely expressed with particularly elevated expression in a wide peri-articular band within the humerus in controls (Figure 4.5 ae). In the mutant, expression is down-regulated throughout the rudiment termini and the peri-articular band is not distinct (Figure 4.5 af). The joint line is clearly reduced.

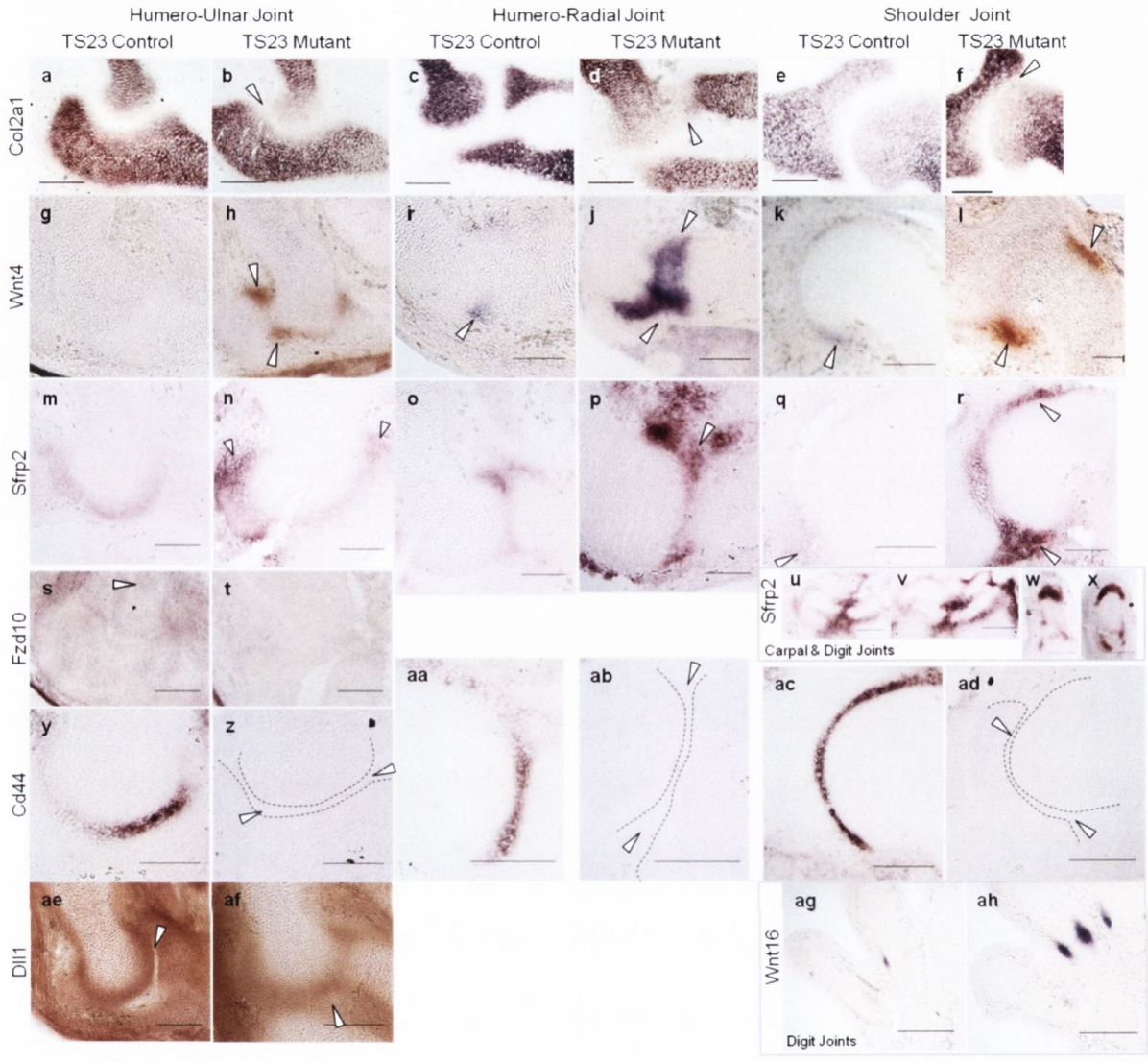

Figure 4.5: Spatial analysis of Wnt signalling genes in the developing joints. Joints shown include the humero-ulnar joint (**a-b, g-h, m-n, s-t, y-z, ae-af**), the humero-radial joint (**c-d, i-j, o-p, aa-ab**), the shoulder joint (**e-f, k-l, q-r, ac-ad**), the carpal joint (**u-v**) and the digit joints (**w-x, ag-ah**). Expression of gene *Col2a1* is shown (**a-f**) to demonstrate the phenotypic differences seen in the muscle-less joints. Expression of signalling ligands *Wnt4* (**g-l**), *Wnt16* (**ag-ah**), the antagonist *Sfrp2* (**m-r, u-x**), the receptor *Fzd10* (**s-t**), a target gene *Cd44* (**y-ad**), and a potential target gene *Dll1* (**ae-af**) are shown. White arrows indicate regions described in the text. All scale bars are 100μm.

Some Wnt pathway component genes were also found to be expressed through the humerus including the ossification zones under development, and showed altered patterns in the mutant (Figure 4.6). *Col2a1*, *Spp1* and *Col10a1* demonstrate the altered ossification phenotype in the muscle-less mutant, as shown by absent separation of *Col2a1* (Figure 4.6 b, d), an absence of *Spp1* expression in the HZ (Figure 4.6 f, h) and a reduction in *Col10a1* expression in the

ossification site (Figure 4.6 j, l) compared to normal control expression. *Fzd10* is expressed at a low level through most of the rudiment with elevated expression in the pre-hypertrophic chondrocytes and growth plates, and reduced expression in the hypertrophic zone, in the control (Figure 4.6 m). In the mutant there is a clear reduction of expression throughout and there is no longer a distinction between the hypertrophic and pre-hypertrophic chondrocytes (Figure 4.6 n). In addition to expression in the joint, *Wnt4* is expressed at the boundary between hypertrophic and pre-hypertrophic chondrocytes in two stripes (Figure 4.6 o, q). This pattern and intensity is unaltered in the mutant, except that the stripes are now closer together, consistent with reduced ossification (Figure 4.6 p, r). The expression of the target gene *Dll1* is dramatically down-regulated in the chondrocytes throughout the rudiment (Figure 4.6 t). In the control, there is elevated expression in the hypertrophic chondrocytes and this is reduced in the mutant (Figure 4.6 t, v).

The gene encoding a receptor of FGF signalling *Fgfr4* is a target of Wnt signalling and as such a particularly interesting gene to examine. However, while it showed high levels of expression in muscle in the control, there was no detectable expression in the rudiment and joint (Figure 4.6x). Several other genes were analysed but either showed no detectable expression by ISH (*Wnt2*, *Wnt2b*, *Wnt16*, *Rspo2*, *Rspo3*, *Lrrn1*, *Rxrg*, *Pitx2*) or no discernible alteration in the mutant (Appendix Figure B.2 (C)).

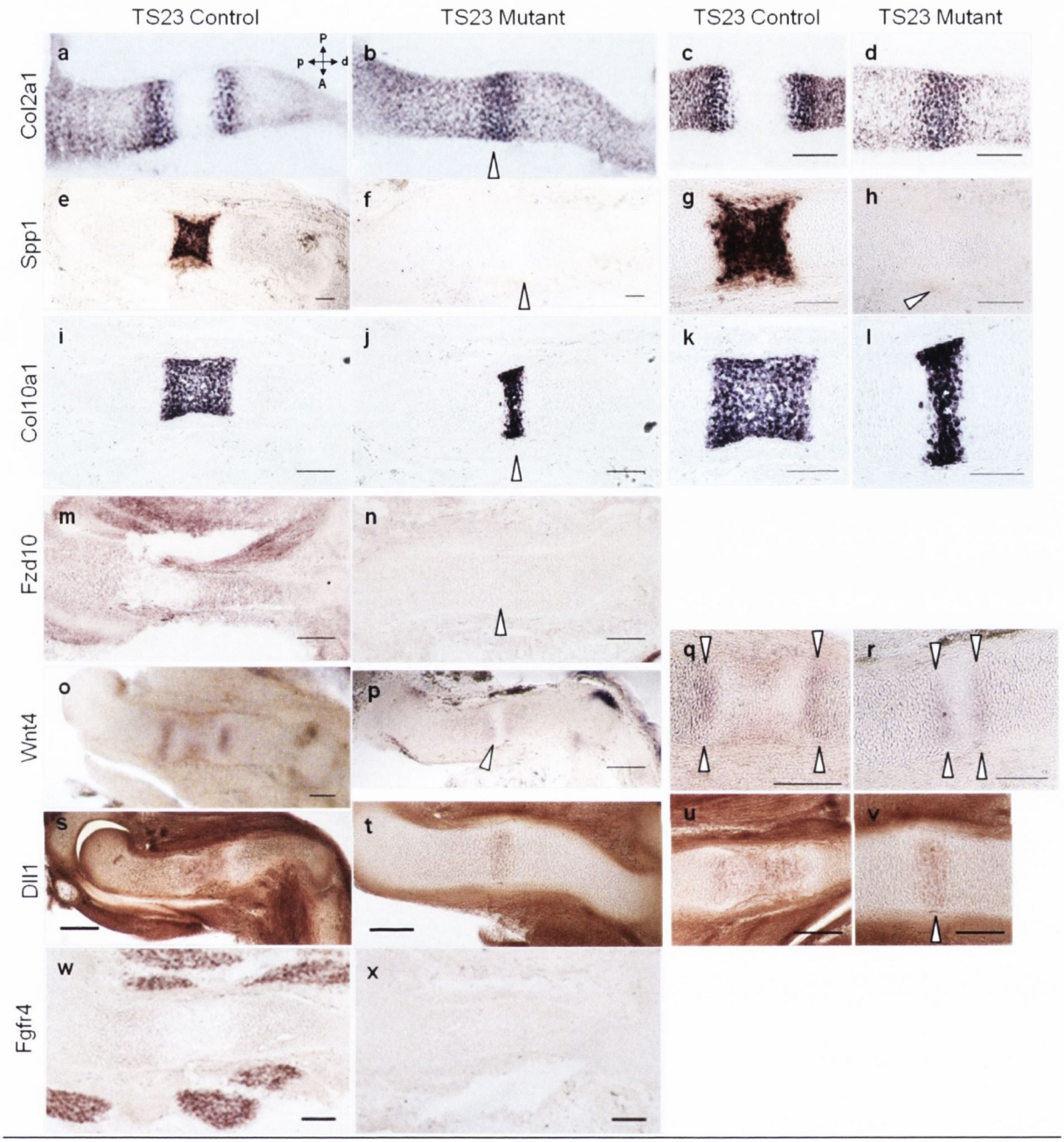

Figure 4.6: Spatial analysis of Wnt signalling genes in the Ossification site. Expression is shown in the whole humerus (**a-b, e-f, i-j, m-p, s-t, w-x**) and associated ossification sites (**c-d, g-h, k-l, q-r, u-v**). Expression of *Col2a1* (**a-d**), *Spp1* (**e-h**) and *Col10a1* (**i-l**) are shown to demonstrate the phenotypic reduction in the muscle-less ossification site. Expression of the receptor *Fzd10* (**m-n**), signalling ligand *Wnt4* (**o-r**), and target genes *Dll1* (**s-v**) and *Fgfr4* (**w-x**) are shown. White arrows indicate regions described in the text. A; anterior, P; posterior, d; distal, p; proximal. All scale bars are 100μm.

4.3.2.4 Other Signalling pathways identified as differentially expressed.

Ten components of the fibroblast growth factor signalling pathway (GO:0008543) were identified to be differentially expressed; 6 ligand-encoding genes (*Fgf4, Fgf6, Fgf8, Fgf5, Fgf2* and *Fgf10)*, one FGF receptor gene (*Fgfr4*) and 3 potential antagonists of the pathway (*Spry1, Spry4* and *Spry2*) as differentially expressed. Eight of the identified genes were down-regulated and two were up-regulated (*Fgf2, Fgf10*). Spatial expression of four members (*Fgf8, Fgf10, Fgfr4* and *Spry1*) of this pathway were tested. In conjunction with the previously reported expression in the developing muscle for the signalling ligand *Fgfr4* (Figure 4.6), similar expression patterns were seen for *Fgf8* and *Spry1*, (Appendix Figure B.2 (D)) and detection of *Fgf10* was only found in the distal regions of the digits (Appendix Figure B.2). No further analysis was done on the FGF pathway for these reasons.

Five genes associated with the Hippo signalling pathway were identified to be differentially expressed; two transcription factors that were down-regulated (*Vgll2, Tead4)*, two cadherins that act as receptors for the pathway that were up-regulated (*Fat2, Fat4*) and one target gene of YAP/TAZ activity *Ankrd1*(Table 4:2). Components involved in the hippo pathway have been shown to respond to the mechanical environment through YAP/TAZ activity responding to ECM stiffness (Dupont et al., 2011). Genes annotated to be involved in the Notch signalling pathway (GO:0007219) were also identified to be DE, these included 6 signalling molecules (*Dner, Dll1, Dtx4, Jag2, Nrg1* and *Cntn1*) and 2 transcription factors (*Hes6, Foxc2*), of these 5 were down-regulated (*Dner, Dll1, Hes6, Dtx4* and *Jag2)* and 3 were up-regulated (*Nrg1, Foxc2, Cntn1*).

4.3.3 Distinguishing expression in the joint region and ossification site: exploring the use of Laser Capture Microdissection (LCM)

While ISH is a valuable technique for revealing localised expression in specific cells and spatial domains, it is limited to relatively highly expressed genes and is time consuming and expensive. It was uninformative for a number of the genes analysed in the preceding section. To uncover if genes are specifically expressed in the joint or the ossification site, and if they are specifically differentially regulated in muscle-less mutants in one site or the other, an alternative approach would be to micro-dissect the territories from control and muscle-less limbs. To this end I used LCM followed by quantitative analysis of extracted mRNA. If successful, this method would allow a high-throughput screen of the DE genes in distinct territories. To test this, distinct territories in the TS23 control humerus, including the elbow joint (EJ), the pre-hypertrophic zone (pre-hz) and the hypertrophic zone (HZ) were dissected using LCM and RNA extracted.(Figure 4.7a). Relative expression analysis for each sub-region was performed (n=1) in triplicate, expression of each gene in each sample was normalised to the endogenous control gene *Gapdh* and compared to expression in the elbow joint (Figure 4.7c).

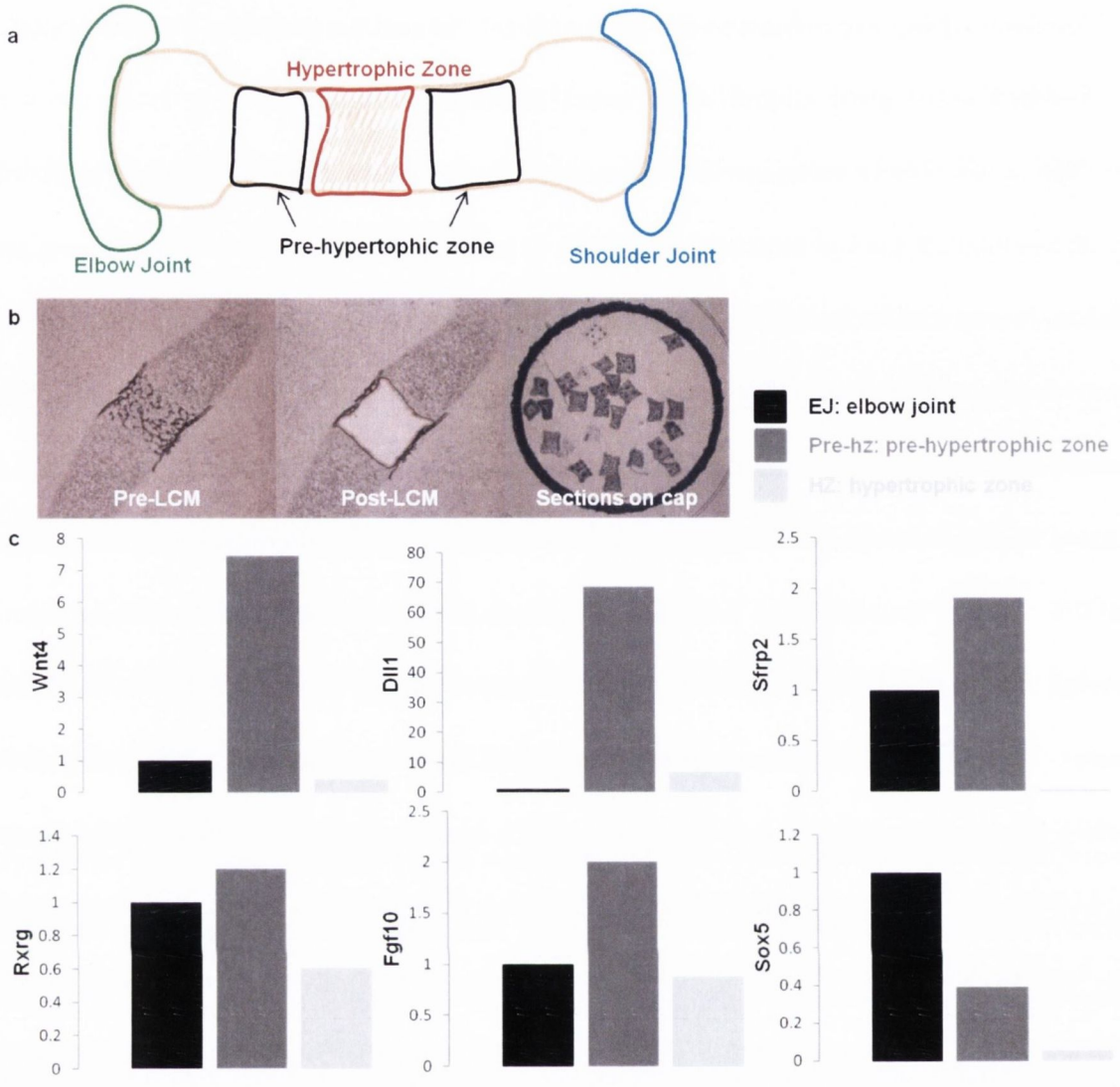

Figure 4.7: Laser-capture micro-dissection of the normal expression of mechanically regulated genes in distinct territories of the developing humerus. (**a**) A schematic of the micro-dissection approach, (**b**) three images depicting the stages of the approach for micro-dissection of the HZ, pre-LCM, post-LCM and the sections transferred onto the cap. (**c**) Histograms representing the expression of *Wnt4*, *Dll1*, *Sfrp2*, *Rxrg*, *Fgf10* and *Sox5* across the sub-dissected territories, relative to expression in the elbow joint. EJ (Elbow Joint), pre-hz (pre-hypertrophic zone), HZ (hypertrophic zone). Black bar (EJ), Dark grey (pre-hz), light grey (HZ). n=1 for each territory.

Expression of *Wnt4* in the control humerus showed 7.5 fold higher expression in the pre-hz and lower expression level in the HZ (2.5 fold) relative to the elbow joint, this is in agreement with the spatial expression analysis shown in Figure 4.7. A similar pattern of expression was seen for the Wnt target gene *Dll1* in the pre-hz relative to the EJ, but with a distinctly greater expression of 68.6 fold. An increase in expression of 6.4 fold was observed in the HZ

compared to the EJ (Figure 4.7c) for *Dll1*, again, entirely consistent with the *in situ* hybridisation findings (Figure 4.6c). Analysis of *Sfrp2* showed a slightly higher transcript expression in the pre-hz (1.9 fold) relative to the EJ, however a distinct reduction was observed in the HZ (105 fold) relative to the EJ. While this is not obviously consistent with the *in situ* data where expression is detectable only in the joint at this stage, it could be explained by more cells expressing less per cell in the PHZ. Similar expression levels were observed in all three regions for the Wnt potential target gene *Rxrg*, Retinoid X receptor gamma. An increase in expression was detected in the pre-hz relative to the EJ for the FGF signalling ligand *Fgf10*, and no difference was observed in the HZ relative to the EJ. All of these genes thus potentially have roles within the rudiment, either within the pre-hz or the HZ to regulate differentiation.

One of the genes analysed, *Sox5*, SRY-box 5, showed a reduction in the expression levels in the cells of the rudiment, pre-hz (2.6 fold) and HZ (20.8 fold) comparative to EJ expression, this is one of the master chondrogenic transcription factors that have previously been implicated in joint morphogenesis (Dy et al., 2010). Visualisation of these spatial differences in *Sox5* expression levels are demonstrated in Figure 4.9, with a higher level of detection found in the elbow joints (Figure 4.9c, e), and also in the shoulder and carpal joints (Figure 4.9g and i, k, respectively) compared to the pre-hypertrophic and the hypertrophic zones of the control humerus (Figure 4.9a, indicated by white arrows for HZ, EJ and SJ, and brackets for pre-hz).

4.3.4 Differential expression in muscle-less humeri assayed by LCM

Using LCM technology it was possible to compare expression of individual genes in the sub-dissected territories, comparing control and muscle-less tissue (Figure 4.8). The three distinct regions described in Figure 4.7 were compared, the Elbow joint (Figure 4.8a) (n=1 biological replicate), the pre-hypertrophic zone (Figure 4.8c) (n=1 biological replicate) and the

hypertrophic zone (Figure 4.8b) (n=2 biological replicates). The LCM q-PCR approach showed a down-regulation of *Spp1* in the elbow joint and a 3 fold ($p \leq 0.05$, paired t-test) down-regulation in the hypertrophic zone, consistent with RNA-seq and ISH findings, with no reduction in the pre-hypertrophic site (Figure 4.8 a-c). *Sox5* was shown to be up-regulated in all zones (Figure 4.8 d-f), but is more highly expressed in the elbow joint (Figure 4.7), this was corroborated by *in situ* hybridisation findings, showing a higher level of expression in all territories of the muscle-less mutant (Figure 4.9). Up-regulation in the humero-radial and humero-ulnar joints (Figure 4.9d and f), the shoulder joint (Figure 4.9h) and the carpal and digit joints (Figure 4.9j and l) were observed in comparison to control expression. Expression in the muscle-less joints illustrate an extension to a wider domain across the joint, in comparison to restricted joint line expression in the control (Figure 4.9, comparing regions indicated by white arrows in c-d, e-f and g-h). An up-regulation of *Wnt4* was observed in both the EJ (1.7 fold) and the HZ (2.7fold) (g-h), while an up-regulation of *Sfrp2* (6.7 fold) was observed only in the elbow joint and no quantitative difference observed in the muscle-less HZ compared to control (Figure 4.8 i-j). Consistent with RNA-seq levels, the potential Wnt target genes *Rxrg* (9.6 fold) and *Dll1* (2.1 fold) were down-regulated, specifically in the Elbow joint and Hypertrophic zone respectively, consistent to what was observed previously for *Dll1* (Figure 4.8 k & l, Figure 4.6 s-v).

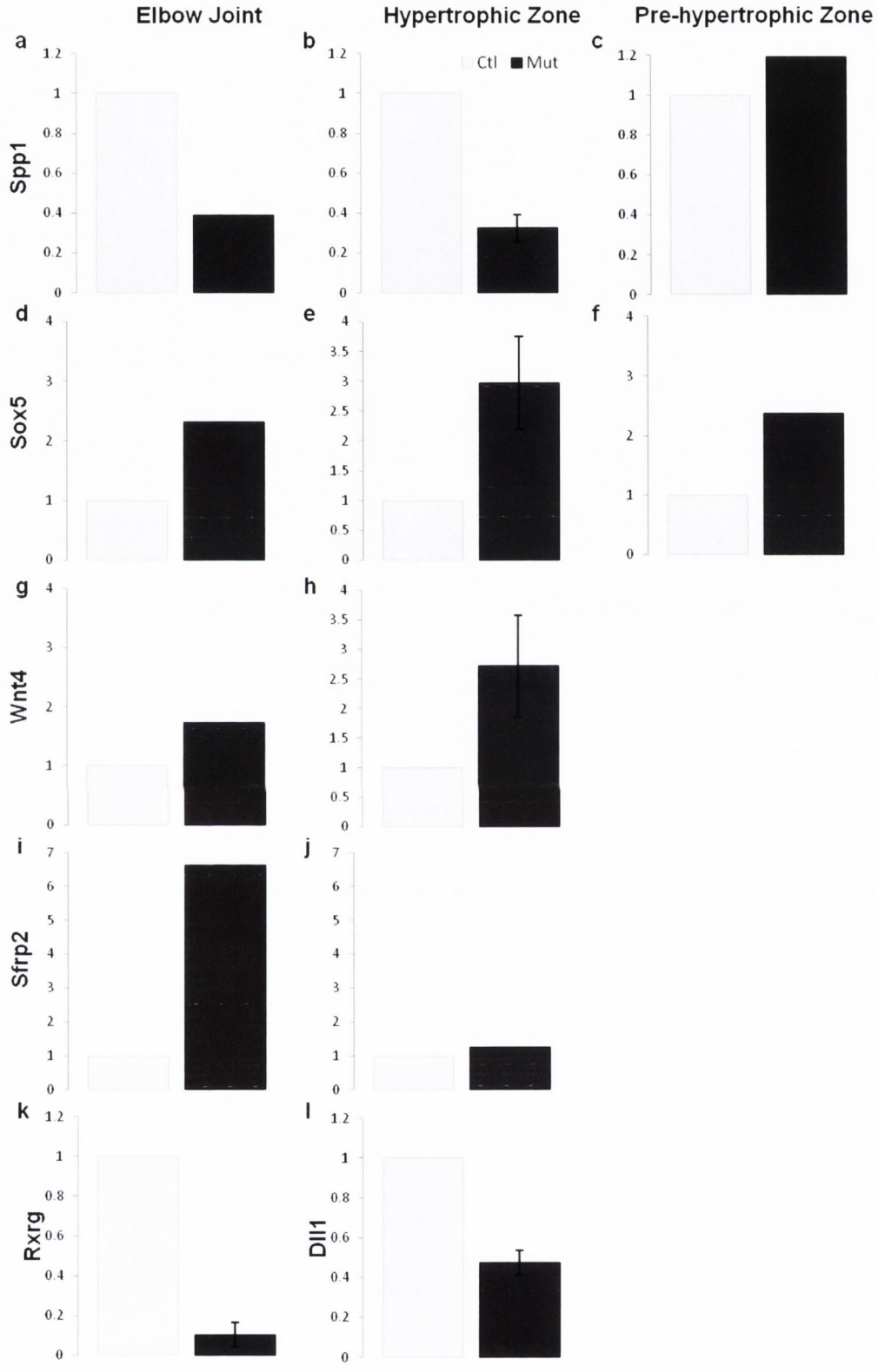

Figure 4.8: Quantitative analysis of differentially expressed genes from Laser-capture Micro-dissection of distinct territories of the developing TS23 control and mutant humerus. The territories analysed include the Elbow Joint (EJ) (**a**, **d**, **g**, **i**, **k**) (n=1), the Hypertrophic zone (HZ) (**b**, **e**, **h**, **j**, **l**) (n=2) and the pre-hypertrophic zone (preHZ) (**c**, **f**) (n=1). Relative expression is shown for *Spp1* (**a-c**), *Sox5* (**d-f**), *Wnt4* (**g-h**), *Sfrp2* (**i-j**), *Rxrg* (**k**) and *Dll1* (**l**). Error bars show Standard deviation. Grey bar is control, Black bar is mutant.

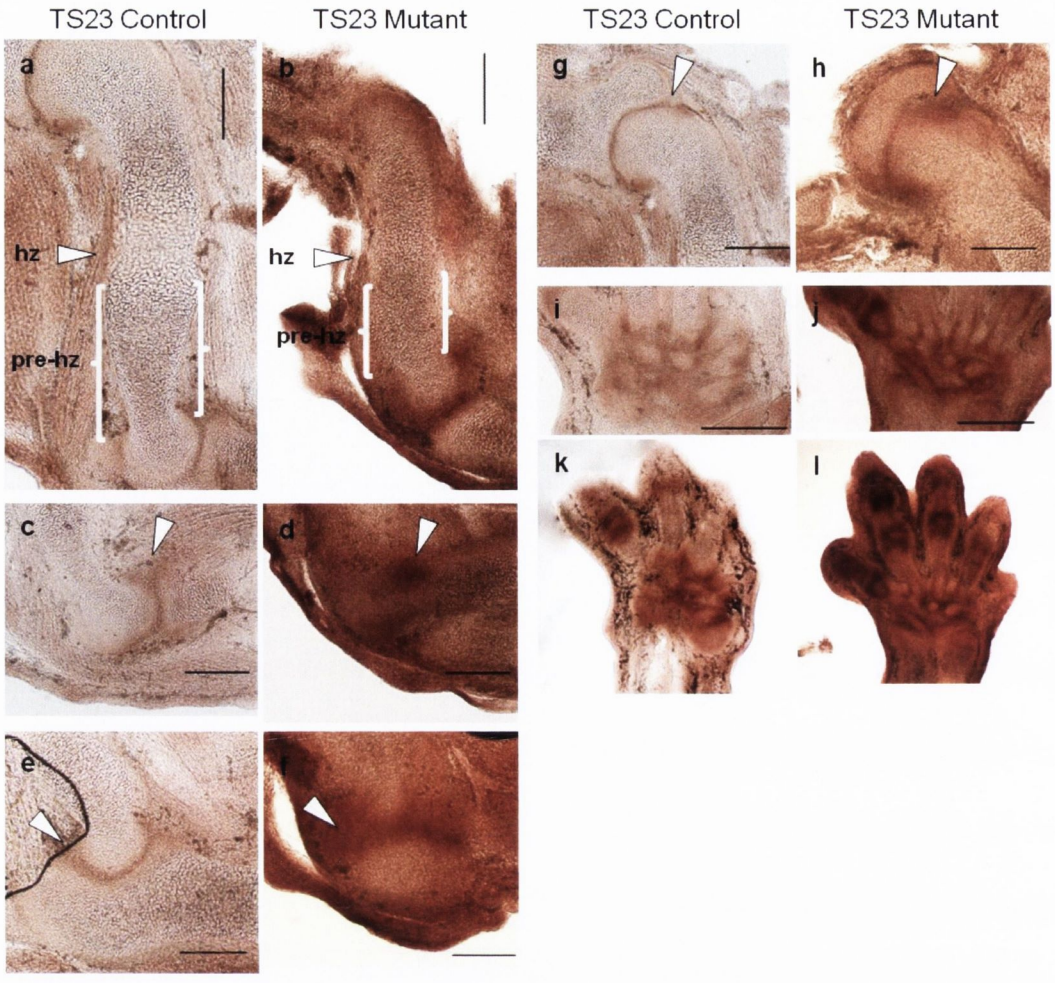

Figure 4.9: Spatial analysis of *Sox5* in the control (**a, c, e, g, i, k**) and muscle-less (**b, d, f, h, j, l**) TS23 humerus and associated joints. Expression is shown in the whole humerus (**a-b**), humero-radial joint (**c-d**), humero-ulnar joint (**e-f**), shoulder joint (**g-h**), carpal joints (**i-j**) and in the hand-plate (**k-l**). White arrows indicate regions described in the text. hz; hypertrophic zone, pre-hz; pre-hypertrophic zone. All scale bars are 100μm

4.4 Discussion

Establishing precisely which pathways are disturbed and to what extent, potentially helps to reveal the mechanistic basis of mechanical control of skeletal development. Focusing to begin with on the three pathways that were disturbed, BMP, Hedgehog and Wnt signalling; pathway analysis was used to determine the level of disturbance of each of these pathways in order to reveal which precise cell populations are altered in the mutant, helping to link these components and pathways to the alterations in the biological processes that are occurring in the developing skeletal system at this time in development.

This analysis has revealed that the pathways are disturbed during both ossification and joint development and has given insights into how the pathways are implicated. Proposed models of pathway alterations for Hedgehog, BMP and Wnt signalling in the muscle-less mutant are described. These pathways are known to co-ordinately regulate bone and joint development, with Wnt and BMP signalling being shown to be most disturbed.

In addition, to explore the quantitative levels of differentially expressed genes in distinct territories an alternative experimental approach was utilised that attempted to provide a high through-put screen. A method to micro-dissect tissue territories called Laser capture micro-dissection was used to harvest sub-populations of distinct cell types with a higher level of sensitivity to distinguish control and mutant humeri expression. This corroborated previous findings and indicated some new aspects but had some limitations, as discussed below.

4.4.1 Hedgehog pathway activation in muscle-less mutants

Integrating the observed alterations to Hedgehog signalling pathway genes in muscle-less mutants suggests that the pathway is activated in the mutant limb compared to the control with the up-regulation of several target genes (Figure 4.10), for example *Hhip* in the mid-diaphysis (Figure 4.3). However since this and several of the target genes also encode negative regulators of the pathway it also suggests that the pathway feeds back negatively.

Over-expression of *Hhip* results in severe skeletal detects, including shortened limbs with a reduction in the zones of undifferentiated chondrocytes (Chuang and McMahon, 1999). The identification of the *Glis3* transcription factor also being up-regulated supports this model of activation. Glis3 has previously been identified to be highly expressed in human osteoblasts and shown to promote differentiation into an osteoblast lineage in synergy with Bmp2 (Beak et al., 2007). As Bmp2 was shown to be down-regulated in the perichondrium and hypertrophic chondrocytes (Figure 4.6), the up-regulation of *Glis3* in the mutant might be occurring as a feedback mechanism to the BMP pathway to promote hypertrophy that is absent in the mutant. The down-regulation of the negative regulator of the pathway *Hhatl*, further supports this model; however no expression data is available, to directly link a particular region in the developing limb to its regulation. The genes *Ptch1* and *Ptchd1* encode necessary co-receptors but are also targets of the pathway, and feedback negatively indicating complex regulation; *Ptch1* is expressed in the perichondrium and digit joints, and *Ptchd1* only in the perichondium (Diez-Roux et al., 2011). Up-regulation of these genes also support the suggestion of activation of the pathway including negative feedback in reduced mechanical stimulation

Recent work using LCM technology identified both *Hhip* (hedgehog-interacting protein) and *Ptch1* (patched homolog 1) to be expressed at higher levels in the outer cartilage layer of the developing knee joint, on the surface of the rudiment, than the intermediate inner layer of the interzone (Jenner et al., 2014). This identification suggests that HH signalling might also be occurring within the joint region. This is in agreement with the expression of Glis3 (Kim et al., 2003) and Hhip described in the digit joints (Chuang and McMahon, 1999) and the joint phenotype in Ihh mutants (St-Jacques et al., 1999) A major signalling ligand of the pathway, Ihh, was previously shown to have altered expression following *in ovo* immobilisation (Nowlan et al., 2008b), indicating the pathways potential role in mechanotransduction.

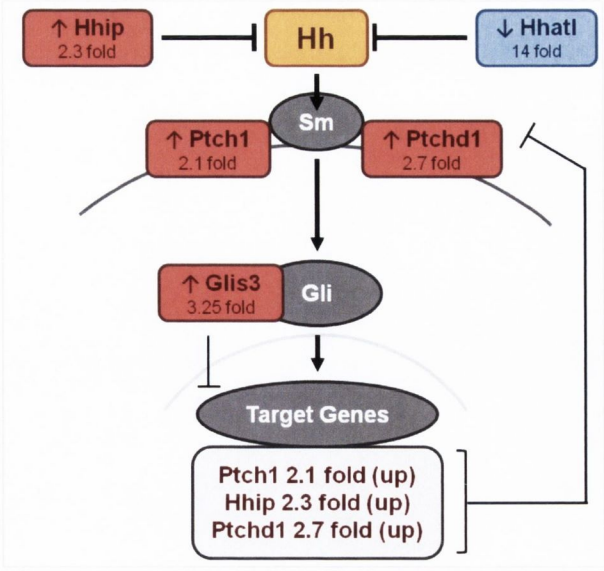

Figure 4.10: Schematic of the Hedgehog pathway including components showing differential expression in the muscle-less embryos, revealed by transcriptomic analysis. Red box indicates up-regulation, blue box down-regulation and grey and yellow boxes pathway components.

4.4.2 Reduced BMP signalling in the Joint line and Ossification Site

Six BMP pathway components were identified to be DE. Following spatial screening of these components in conjunction with data from the literature a model is proposed that suggests that BMP signalling is reduced in the joint line and in the ossification site of muscle-less mutants (Figure 4.11). Two BMP extracellular associated components were identified to be up-regulated, *Grem2* an antagonist of the BMP pathway, and *Bmp3* a pathway ligand but with a previously reported negative effect on the pathway. The BMP antagonist *Grem2* has previously been shown to block BMP activity during the patterning of the facial skeleton (Zuniga et al., 2011). Bmp3, although a ligand does not have osteoinductive potential (Bahamonde and Lyons, 2001; Daluiski et al., 2001) and is unable to activate receptor regulated SMADS, with a net result to decrease BMP and/ or activin signalling (Gamer et al., 2005). In the mammalian skeleton BMP3 has been shown to reduce BMP activity as mice lacking BMP3 exhibit increase bone mass, and those over-expressing BMP3 in bone show delayed endochondral ossification (Daluiski et al., 2001; Gamer et al., 2005).

Bmp3 has been shown to be localised to the developing perichondrium in the developing chick limb, with mis-expression reducing BMP signalling and enhancing chondrocyte proliferation prior to hypertrophic differentiation thus widening skeletal elements and producing joint fusions (Gamer et al., 2008). In parallel to the observed down-regulation of *Bmp2* expression in the perichondrium and the hypertropic chondrocytes (Figure 4.6, schematic Figure 4.11B) we propose that an up-regulation of Bmp3 is occurring at these sites thus resulting in decreased overall SMAD mediated BMP signalling resulting in the down-regulation of target genes *Erg2* in the hypertrophic chondrocytes, *Fgf8* in the hypertrophic chondrocytes and proliferating chondrocytes. A down-regulation of BMP in the ossification site agrees with the phenotypic disturbances seen in the mutant, displaying reduced hypertrophic chondrocytes evident through down-regulation of *Col10a1* and *Spp1* expression (Figure 4.6) and an absent proximal distal separation of *Col2a1* (Figure 4.6).

Alteration in the balance of BMP signalling is also evident in the muscle-less mutant joints, as shown by a down-regulation of *Bmp2* and *Gdf5* and an up-regulation at both the transcript and protein level of the antagonist Noggin (Figure 4.1 and Figure 4.2, illustrated in schematic in Figure 4.11C). Increased activity of the pathway is however occurring at the proximal end of the ulna in the mutant, potentially increasing a proliferating pool of chondrocytes.

Two BMP pathway components identified to be DE have previously been reported to be differentially expressed following alterations of the mechanical environment. Application of dynamic compression on primary chondrocytes *in vitro* resulted in an up-regulation of the transcription factor *Egr2*, early growth response 2 (Bougault et al., 2012), in agreement with the results of a down-regulation following removal of mechanical stimulation. The BMP ligand *Bmp3* was also shown to be differentially regulated in response to an alteration in the mechanical environment with an up-regulation of gene expression in response to removal of mechanical stimulation in a microgravity environment (Patel et al., 2007). A similar up-

regulation was seen in a bone chamber study that applied loading to induce cartilage formation; after 1 week of loading BMP3 was strongly expressed in the unloaded controls compared to the loaded cartilage; implying that with loading the down-regulation of the inhibiting BMP3 enables the induction of cartilage (Aspenberg et al., 2000).

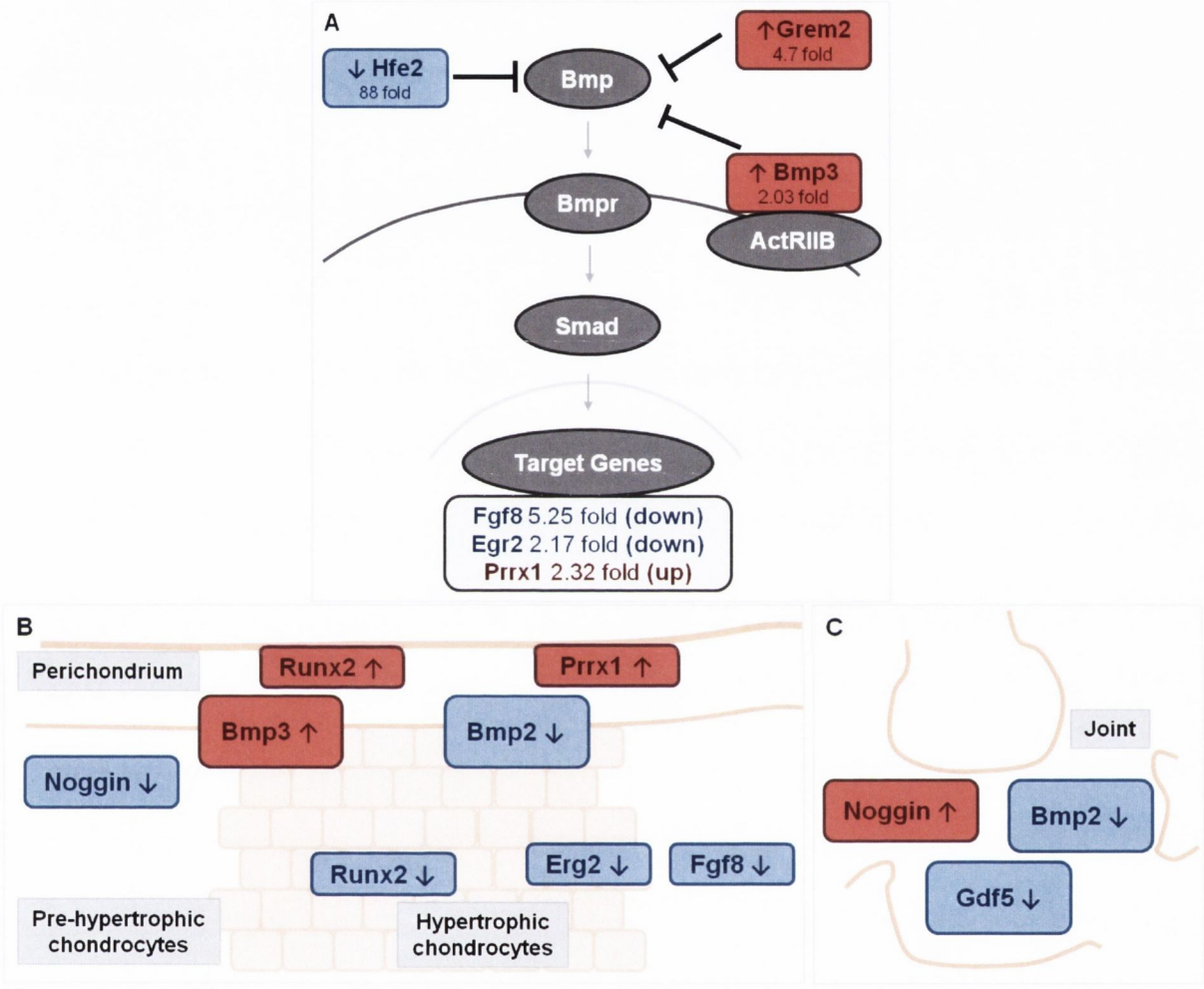

Figure 4.11: Schematic of BMP pathway including components showing differential expression in the muscle-less embryos, revealed by transcriptomic analysis, (**A**). Changes in localised expression of BMP pathway components in the ossification site (**B**) and joint (**C**). Red box indicates up-regulation, blue box down-regulation and grey boxes pathway components.

Overall the BMP pathway appears to be suppressed in the mutant limb compared to control, with down-regulation evident in the hypertrophic zone, resulting in a reduced hypertrophy, and suppression in the joint, in parallel to the evident up-regulation of the antagonist noggin repressing BMP signalling.

4.4.3 Complex cross interactions of Wnt signalling in the Joint and Ossification Site

Thirty four components of the Wnt signalling pathway were identified to be altered in the reduced mechanical environment (Figure 4.4). Canonical Wnt signalling has been reported to be involved in the regulation of mesenchymal condensations (section 1.3.3.1), regulation of chondrocyte hypertrophy (section 1.3.3.2) and maintenance of joint integrity (section 1.3.3.3), and reported to be disturbed in the joints of muscle-less mouse embryos (Kahn et al., 2009). This suggests that Wnt signalling may be a main mediator of mechanoregulation, contributing to abnormal ossification and joints seen the muscle-less embryos. Previous indications that the Wnt pathway is responsive to mechanical stimulation was reported in mesenchymal stem cells (Haudenschild et al., 2009), in mature bone in vivo (Robling et al., 2008) and in response to injury of articular cartilage (Dell'Accio et al., 2006).

The alteration of Wnt signalling occurs predominantly at two levels; extra-cellularly through the alteration of Wnt ligands, agonists and antagonists, and at the nuclear level through the down and up-regulation of pathway target genes (Figure 4.4, red circles show up-regulated and blue down-regulated genes). Genes encoding four Wnt ligands are up-regulated in muscle-less embryos and in the case of *Wnt4* I show specific up-regulation in the elbow and shoulder joint region (Figure 4.5). The wnt antagonist *Sfrp2* is also up-regulated, as specifically shown in the elbow and shoulder joint regions (Figure 4.5). The identification of positive and negative regulation of the pathway within the joint is suggestive of negative feedback in this territory; as the pathway regulates itself to control cellular proliferation and differentiation, depicted in the schematic in Figure 4.12.

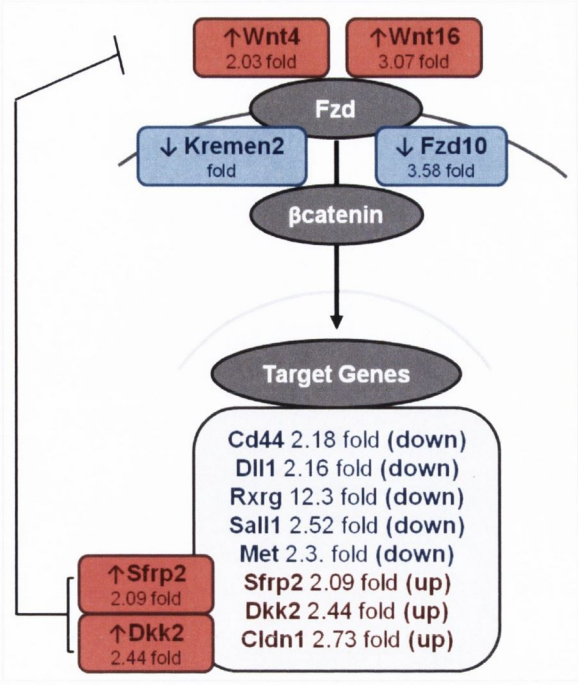

Figure 4.12: Schematic of Wnt pathway regulation in the developing joints, including components showing differential expression in the muscle-less embryos, revealed by transcriptomic analysis. Red box indicates up-regulation, blue box down-regulation and grey boxes pathway components.

The upregulation of *Wnt4* and *Wnt16* in the joint would suggest activation of the pathway; however this simplistic proposal is not consistent with the status of regulation of many of the target genes, thus suggestive of multiple levels of regulation of the pathway being affected. The majority of the Wnt target genes are down-regulated (Figure 4.4), this perhaps is due to increase expression of the negative regulators *Sfrp2* and *Dkk2* and down-regulation of the *Fzd10* and *Kremen2* receptors. The down-regulation in target gene expression in particular; *Cd44* and *Dll1* specifically in the joint, support that negative regulation hypothesis of Wnt signalling in the muscle-less joint.

The expression of the ligand-encoding gene *Wnt4* was still present in two distinct territories in the mid-diaphysis of the rudiment, yet the proximal to distal extent of expression was reduced compared to control expression (Figure 4.6). The expression of *Dll1* in hypertrophic chondrocytes was previously suggested to regulate hypertrophic differentiation (Crowe et al.,

1999; Watanabe et al., 2003), and expression of this gene is down-regulated in muscle-less humeri, in agreement with the reduction in hypertrophy demonstrated.

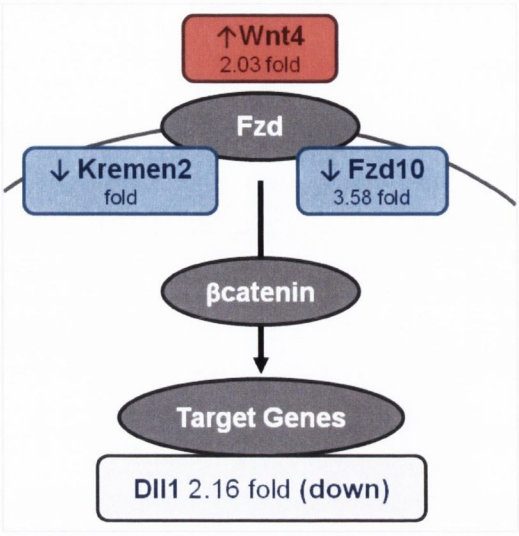

Figure 4.13: Schematic of Wnt pathway regulation in the developing ossification site, including components showing differential expression in the muscle-less embryos, revealed by transcriptomic analysis. Red box indicates up-regulation, blue box down-regulation and grey boxes pathway components.

Overall the Wnt pathway appears to be the most affected signalling pathway following removal of mechanical stimulation, yet the complexity of this deregulation is difficult to assess due to the up-regulation of pathway agonists and antagonists and the variable regulation status of down-stream pathway targets. Pathway response is complicated by the up-regulation of both positive and negative regulators of the pathway and may include feedback loops in response to deregulation. Negative feedback of the pathway in the joint region may help to explain the down-regulation of wnt target genes, but due to the complex nature of the pathway and the involvement of target genes in other pathways, it may be the case that regulation is through different means. A maintained but reduced extent of wnt signalling is suggested in the ossification site, but once again this may be due to the complex cross interaction with other signalling pathways.

4.4.4 Cd44 plays an important role in joint formation through interaction with Hyaluronic acid; Hyaluronan biosynthesis is also deregulated in muscle-less mutants.

Cd44 has been reported to be a target gene of Wnt signalling, its absence in muscle-less mutants may be due to the negative regulation of Wnt signalling following the up-regulation of antagonists of the pathway. Cd44 encodes a single-pass membrane glycoprotein that binds proteoglycan and hyaluronan (HA) to produce a pericellular matrix surrounding chondrocytes (reviewed in Knudson and Loeser, 2002), and has been implicated in joint cavitation through interaction with HA (Dowthwaite et al., 1998). The loss of expression of the Cd44 gene in the interzone of the forming knee joints has previously been shown following immobilisation of the chick (Roddy et al., 2011b). Upon further inspection, other HA synthesising encoding genes were identified to be DE in the muscle-less mutant.

HA is synthesised via hyaluronan synthesising enzymes, hyaluronan synthases (*Has*) (Weigel et al., 1997), as shown in schematic in Figure 4.14 and listed in Table 4:6. There were three hyaluronan synthase enzymes identified, *Has1, Has2* and *Has3*, and they function to synthesise HA from precursors uridine diphospho-sugars (UDP). *Has1* is down-regulated (2.36 fold) in the microarray comparing control and muscle-less humeri. Embryonic expression of *Has* encoding genes are variable, with *Has2* and *Has3* being reported in articular cartilage, but variable expression of *Has1* has been reported in cultured chondrocytes. The most highly expressed hyaluronan synthase in the control transcriptome was *Has2* (Table 4:6). A number of cytokines and signalling molecules have been reported to induce HA biosynthesis through *Has* up-regulation, these include Platelet derived growth factor (PDFA) (Heldin et al., 1989; Jacobson et al., 2000), FGF2 (Shimabukuro et al., 2011), Epidermal growth factor (Pienimaki et al., 2001) and Interleukin 1β (Oguchi and Ishiguro, 2004), members of which have also been reported to be differentially expressed.

During normal joint development subsequent to accumulation of HA in the intercellular region (Figure 4.14 A(b)), HA binds to the Hyaluronan receptor Cd44 (Figure 4.14 A(c)). Interaction of HA with Cd44 receptors have been shown to directly activate intracellular signalling pathways (reviewed in Turley et al., 2002); and it was suggested that changes in hyaluronan-cell interactions with Cd44 may serve as means to modulate cellular responsiveness to BMP (Peterson et al., 2004).

Hyaluronidases are another type of enzyme responsible for regulating the levels of intercellular HA in the extracellular matrix. Three of the six hyaluronidase encoding enzymes were expressed in control trancriptome tissue, Hyal1 (hyaluronoglucosaminidase 1), Hyal2, Hyal3 (Table 4:6). Embryonic expression was reported in the central and peripheral nervous system for *Hyal3* (Visel et al., 2004), low levels of *Hyal2* detected in the limb (Diez-Roux et al., 2011), and no regional embryonic expression of *Hyal1* (Visel et al., 2004). However, homozygous *Hyal1* null mice display progressive Osteoarthritis associated with bony outgrowths and early loss of articular cartilage proteogylcans and an accumulation of HA in the cartilage of knee joints (Martin et al., 2008). Expression of *Hyal1* was up-regulated in muscle-less mutants (2.25 fold), and this could potentially be due to an up-regulation of HA degradation, as there is a down-regulation of Cd44 reception, and thus no cavity formation occurring in the muscle-less mutants (Figure 4.14B), as has been displayed in TS22 and TS23 elbow and shoulder joints (Figure 3.2).

An alteration in HA biosynthesis has previously been associated with defects in cavity formation in developing joints. Distinct cavities were not present in *Has2*-deficient limbs of E16.5 autopods, with the joint regions wider than normal and filled with closely packed cells. The elbow and shoulder joints were also reported to be considerable smaller and less extensive than normal (Matsumoto et al., 2009). In agreement with previous suggestions that cavitation occurs due to the local accumulation of HA and its surface receptor Cd44

(reviewed in Archer et al., 2003; Pitsillides and Ashhurst, 2008), the suggested down-regulation of the HA receptor Cd44, down-regulation of *Has1* and up-regulation of *Hyal1*, degrading any HA that has accumulated in the intercellular space due to activity of *Has3* and more likely *Has2* (due to expression levels, 889 reads in mutant) co-corroborates the reduced cavitation phenotype observed in muscle-less embryos.

Table 4:6: Hyaluronan biosynthesis associated genes identified to be expressed and differentially expressed upon removal of mechanical stimulation.

Gene	Name and Role		Fold change	Ctl Read	Spatial Expression
Has1	hyaluronan synthase1	Synthesises HA	2.36*	11	No expression shown (Visel et al., 2004). Low regional expression in hindlimb rudiment (Diez-Roux et al., 2011). Variable expression in cultured chondrocytes
Has2	hyaluronan synthase2		0.78	1132	Joint, chondrogenous layer in chick knee joint (Roddy et al., 2011b). Articular cartilage expression
Has3	hyaluronan synthase3		0.74	52	Articular chondocytes and hypertrophic chondrocytes
Hyal1	hyaluronoglucosaminidase 1: HA degradation enzyme, role to remove HA from intercellualr space		2.25	79	No regional expression shown (Visel et al., 2004) Homozygous null mice display a progressive OA associated with bony outgrowths, early loss of articular cartilage proteoglycans and accumulation of HA in the cartilage of knee joints.
Hyal2	hyaluronogluc osaminidase 2	HA degradation	0.98	1268	Low levels in limb (Diez-Roux et al., 2011)
Hyal3	hyaluronogluc osaminidase 3:		1.69	1	CNS and PNS (Visel et al., 2004)
Cd44	Cd44 antigen: Hyaluronan receptor, involved in binding HA to decrease intercellular HA content		2.18	2273	Joint line that is absent in muscle-less mutants

Application of mechanical strain has been shown to up-regulate HA production and CD44 expression in articular fibrocartilage cells from chick tibotarsal joints (Dowthwaite et al., 2003; Dowthwaite et al., 1999). Conversely, removal of mechanical stimulation through immobilisation resulted in the loss of *Cd44* and *Has2* gene expression from the intermediate layer of immobilised joints (Roddy et al., 2011b), indicating that HA biosynthesis is disrupted, in agreement with the proposal suggested for the muscle-less joint (Figure 4.14B).

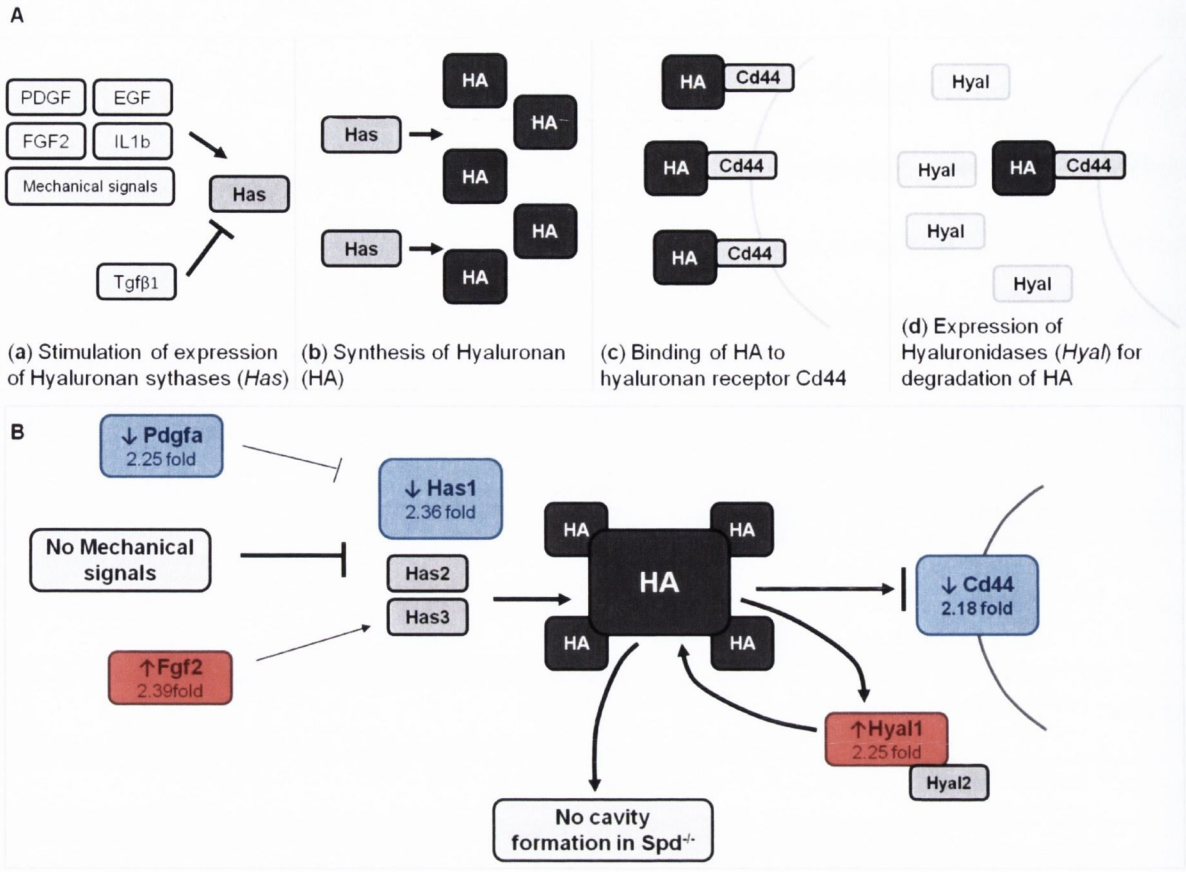

Figure 4.14: Process of Hyaluronan (HA) Biosynthesis for the regulation of cavitation in the developing joint. (**A**) (**a-d**). Schematic of deregulation in HA biosynthesis in muscle-less embryos; including components showing differential expression revealed by transcriptomic analysis (**B**). Red box indicates up-regulation, blue box down-regulation and grey boxes pathway components.

4.4.5 Quantitative spatial detection of differentially expressed genes.

Laser capture Micro-dissection was utilised in the exploration of differentially expressed genes within the developing skeletal rudiment, in an attempt to identity in which specific territory expression was present, and then specifically where it was disturbed in the muscle-less mutant. LCM has been used to analyse the molecular profiles of multiple tissue types, accordingly the objective of its use in this study was as a high-throughput method to examine multiple DE genes to assess spatial expression. During this study multiple technical considerations were addressed with respect to obtaining pure RNA from micro-dissected tissue for downstream amplification analysis. However, a major limitation was low yields of

RNA obtained from distinct territories, deeming the high through-put screen of multiple DE genes not possible. Attempts were made to increase the screening capacity, firstly by increasing the number of micro-dissected samples on a cap for extraction, secondly by adapting/ optimising the RNA extracting methods used to increase yields, and thirdly through the use of RNA amplification technologies to increase the yield of RNA for amplification.

Nevertheless LCM provided valuable data on cell territories for the genes analysed. The territories screened included the elbow joint, the hypertrophic zone and the pre-hypertrophic zone, confirming the results of ISH showing restricted patterns of certain genes. For example the down-regulation of *Spp1 (*Figure 4.8b) and *Dll1* (Figure 4.8l) in the muscle-less hypertrophic zone; and the up-regulation of *Sfrp2* (Figure 4.8i) in the muscle-less elbow joint is consistent with previous findings. The use of LCM technology added quantitative spatial information about genes in the muscle-less mutant, for example the analysis of *Sox5* revealed a higher level of expression in the control elbow joint relative to the pre-hypertrophic and hypertrophic regions of the humerus, and this expression was consistently elevated in all muscle-less territories examined (Figure 4.7c, Figure 4.8 d-f), corroborating spatial *in situ* hybridisation detection (Figure 4.9). This is consistent with the identification that *Sox5* in conjunction with *Sox6,* is required for promoting growth plate and chondrocyte differentiation during synovial joint morphogenesis (Dy et al., 2010).

4.5 Conclusions

Given the importance of appropriate mechanical stimulation generated by embryo movement on skeletal development I identified that an absence of movement results in deregulation of multiple signalling pathway components that are known to be essential for normal skeletal development. This chapter reports analysis of differentially expressed genes in the HH, BMP and Wnt signalling pathways. Through the identification that the Wnt signalling pathway is most strongly affected by a reduction in mechanical stimulation. It is now important to functionally test the mechanisms linking mechanical stimulation with Wnt signalling. This work provides sets of candidate genes to use in functional assays to excavate this important link. Understanding how mechanical stimuli influence the Wnt signalling pathway would be a major step forward in understanding how mechanical cues work together with classical molecular positional information to guide spatially appropriate tissue differentiation and provide indications of how conditions can be effectively recreated *in vitro* to guide stem cell differentiation.

Chapter 5:

5. Functional analysis of Wnt signalling: investigating a role in skeletal patterning

5.1 Introduction

Canonical Wnt signalling is a critical mediator of multiple cell-cell signalling events during vertebrate development. It is known to be pivotal in the regulation of mesenchymal condensations during the initiation of chondrogenesis (section 1.3.3.1), for the regulation of hypertrophy (section 1.3.3.2) and for joint formation (section 1.3.3.3) with very elegant gain of function experiments showing that it is required in particular to maintain the joint once it is specified (Guo et al., 2004; Spater et al., 2006). The key intracellular mediator of canonical Wnt signalling, β-catenin (*Ctnnb1*) is the most highly expressed Wnt signalling component in the TS23 humerus and associated joint transcriptome (28,608 read count; Figure 3.6). Wnt signalling was also shown to be the most strongly impacted signalling pathway in the muscle-less mutant developing limb, indicating that it is an important point of integration of mechanical and biochemical positional information. In chapter 4, analysis of Wnt pathway component gene expression showed restricted expression within the developing humerus and joints with altered expression of specific components in different territories in muscle-less mutants.

Further indications of Wnt signalling being responsive to mechanical stimulation have been demonstrated in mesenchymal stem cells (Haudenschild et al., 2009), in osteoblasts subjected to microgravity (Patel et al., 2007), in mature bone *in vivo* (Robling et al., 2008) and in response to articular cartilage injury (Dell'Accio et al., 2006). A reduction of β-catenin activity was reported in joint forming cells in *Spd* mutants, and therefore suggested to be regulated by muscle contraction (Kahn et al., 2009).

In the differential screen presented in chapter 3, 34 genes encoding Wnt signalling pathway components were identified to be altered in the reduced mechanical environment. Four Wnt ligands were up-regulated in muscle-less embryos, *Wnt4* specifically in the joint and the wnt antagonist *Sfrp2* specifically in the elbow and shoulder joint regions (Figure 4.5). The

majority of Wnt target genes identified were down-regulated (Figure 4.4), perhaps due to increased expression of the negative regulators *Sfrp2* and *Dkk2* and down-regulation of the *Fzd10* and *Kremen2* receptors. As ligands and agonists *Rspo2* and *Rspo3* of the pathway are up-regulated, as are some target genes, this indicates that multiple levels of regulation of the pathway must be affected, including possible feedback mechanisms that attempt to re-stabilise the system. It is interesting to note that a number of the up-regulated target genes encode negative regulators of the pathway, for example *Dkk2* and *Sfrp2*.

Understanding how mechanical stimuli influence the Wnt signalling pathway would be a major step forward in understanding how mechanical cues work together with classical molecular positional information to guide spatially appropriate tissue differentiation. However, evidence to date suggests a complex balance of signalling via multiple Wnts, through multiple pathways that vary in different cell populations within the forming skeleton. This makes it difficult to test specific aspects of Wnt pathway function and integration with biophysical signals in a targeted way. A first step in functional testing, explored in this chapter, is therefore to generally up regulate or repress Wnt signalling and observe the effects on skeletal development. It can then be asked if altering Wnt signalling directly produces phenotypic effects that overlap with the effects of altering the mechanical environment.

A powerful approach for unravelling the molecular mechanisms involved in developmental processes is to ectopically express a gene or signalling pathway of interest and examine the effect. The avian embryo offers many advantages for developmental studies over mammalian embryos, due to the ease of access for *in ovo* manipulations. Different types of manipulations can be performed *in ovo* including surgical manipulations and as previously discussed, chemically induced immobilisation (Kavanagh et al., 2006; Nowlan et al., 2008b; Roddy et al., 2011b). Retroviral transmission has been used very successfully to deliver genes into tissue locations in chick embryos (reviewed in Gordon et al., 2009). Retroviral independent

gene transfer can be achieved in chick embryos using *in ovo* electroporation, a more successful technique for targeting specific embryonic tissues/cells compared to microparticle bombardment and lipofection, offering a positive alternative to broad retroviral infection (Muramatsu et al., 1997; Muramatsu T., 1996).

The basis of the electroporation technique relies on the transient generation of pores in the plasma membrane, to allow macromolecules to penetrate the cytoplasm and DNA to enter due to its negative charge (Potter et al., 1984). Gain- and loss- of function electroporation studies involving DNA, RNAi, morpholinos and virus constructs are now widely used in molecular studies involving chick embryos (reviewed in Nakamura et al., 2004; Sauka-Spengler and Barembaum, 2008). Electroporation following microinjection of the DNA construct of interest into the targeted tissue was selected as the method of choice in this study as it is minimally invasive and allows for continued development *in vivo.* Variations of the electroporation method have been reported in order to try to improve precision and efficiency of DNA site specific uptake (Momose et al., 1999), as the viability of electroporated embryos was reported to be low because of the toxicity of high electric currents on the embryo. Traditionally electroporation was used to transfer DNA into cells in suspension using high voltages and short durations of electrical stimulation (Potter et al., 1984), however for *in ovo* electroporation in chick embryos lower voltages and longer durations are used to achieve DNA delivery into the cells with minimal damage (Muramatsu et al., 1997). Multiple electroporation systems have been described with respect to targeting different tissues in the developing chick, for example the neural tube (Miller-Delaney et al., 2011), the somites (Krull, 2004; Scaal et al., 2004), and the eye (Durand et al., 2010; Islam et al., 2012). Although the developing limb has been successfully targeted, this is restricted to early stages of development; Hamburger and Hamilton (HH) (Hamburger and Hamilton, 1992) stage 7-12

(Takeuchi et al., 1999), HH13/14 (Yamamoto and Kuroiwa, 2003) and HH11-22 have been reported (Durand et al., 2010; Sabherwal et al., 2007).

In general, *in ovo* electroporation has been most commonly applied to chick embryos at early stages of development, younger than Hamburger and Hamilton stage 20 (HH20/ ~E3.5) (reviewed in Krull, 2004), and has been successfully used to target the hindbrain in our research group (Miller-Delaney et al. 2011). At later stages of development problems arise associated with tearing of the membranes and vasculature. In the research reported here, early attempts to target the limb bud after HH20 revealed an extra difficulty of accessing the limb since embryos move and turn and submerge their flanks in the yolk. An alternative to carrying out the DNA transfer *in ovo* for older embryos is to use shell-less culture techniques (Datar and Bhonde, 2005; El-Ghali et al., 2010; Krull, 2004; Luo and Redies, 2005; Luo et al., 2012; Schomann et al., 2013; Yalcin et al., 2010). Such *ex ovo* methods have been described using petri dishes (El-Ghali et al., 2010; Krull, 2004; Luo and Redies, 2005; Luo et al., 2012), plastic cups (Yalcin et al., 2010), glass bowls (Datar and Bhonde, 2005) and drinking glasses (Schomann et al., 2013). In order to manipulate the developing forelimb from the onset of elbow joint formation (approx HH24-HH25/ ~E4.5) we decided to utilise the drinking glass and hammock cling film system, as recently described (Schomann et al., 2013), in order to gain appropriate accessibility to the limb and to prevent damage associated with the tearing of membranes and vasculature during manipulation through a small window in the shell.

Given the importance of Wnt signalling during embryonic skeletal development, I postulated that altering the balance of Wnt signalling in the developing limb would impact chondrogenesis and/or joint formation. The response to canonical Wnt signalling involves accumulation of stabilised β-catenin through inhibition of phosphorylation at sites toward the COOH end of β-catenin, binding of β-catenin to TCF/Lef transcription factors in the nucleus which in turn bind to the regulatory regions of target genes via the TCF/Lef DNA binding

domain. Regulation of gene expression is achieved through the activation domain of β-catenin. Constitutive up-regulation of the canonical pathway was achieved by expressing a β-catenin-Tcf fusion protein which lacks β-catenin phosphorylation sites so is constitutively stabilised, and provides the DNA binding domain and activation domain in one fusion protein (Figure 5.1a).

Suppression of canonical signalling was performed by expressing the Wnt extracellular antagonist; Sfrp3 (Figure 5.1b). The CRD domains of Sfrp proteins share sequence homology with the extracellular Wnt binding portion of the Wnt receptor Frizzled (FZ), so can bind specifically to Wnt. Since Sfrps are secreted proteins they are widely considered to antagonise Wnt-receptor interaction (Kawano and Kypta, 2003).

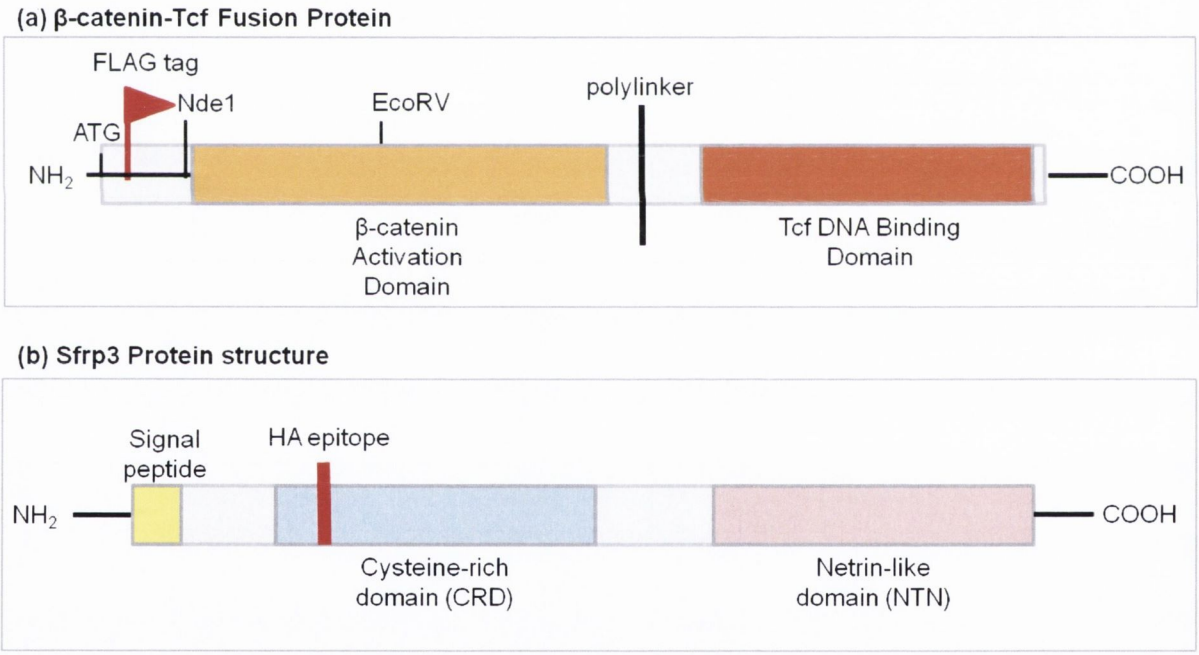

Figure 5.1: Diagram of the proteins encoded in the constructs. used to activate (**a**) or block (**b**) Wnt signalling. (**a**) β-catenin-Tcf fusion protein incorporating the FLAG tag and fusing the β-catenin activation domain and the Tcf DNA binding domain. (**b**) The Sfrp3 protein is secreted (signal peptide) and consists of a cysteine-rich domain (CRD) that binds Wnt ligands, thus preventing pathway activation. NH2; N-terminal of protein, COOH; C-terminal of protein.

This chapter reports analysis of skeletal development following the activation and blocking of the Wnt signalling pathway in the developing chick forelimb. The aims of this work were:

1. To establish an *ex-ovo* cultivation regime that allowed for the manipulation of the limb bud in chick embryos *in vivo,* especially at later stages of development.

2. To optimise an electroporation regime using the *ex ovo* cultivation system; with the main objective to sustain the viability of specimens at least 24 hours post electroporation, in a manner that was easily reproducible across experiments.

3. To investigate the phenotypic effects of expressing a constitutively active form of β-catenin in the limb bud during skeletal formation, mimicking activation of the canonical Wnt pathway.

4. To examine the effects of over-expression of a Wnt pathway antagonist, Sfrp3, blocking Wnt signalling.

The overall objective was to assess whether manipulation of the Wnt pathway could mimic aspects of the skeletal phenotype in muscle-less mutant embryos, testing the hypothesis that disturbances to Wnt signalling contribute to the effects of when the mechanical environment is altered.

5.2 Methods

5.2.1 *Ex ovo* cultivation setup

Fertilised chick embryos, supplied by Enfield Broiler breeders Ltd (breed: Ross 503), were pre-incubated (Naturform® UT350N Hatchery) at 37.5°C in a humidified chamber for a period of 72hrs prior to *ex ovo* cultivation. The *ex ovo* cultivation system, (adapted from Schomann et al., 2013) consisted of a sterilised glass (GODIS, Art-nr: 800.921.09, IKEA 7 3/4oz. 23cl) filled with 160ml sterilised water. A cling film hammock support was carefully lowered until an area of approx 4-5cm was in contact with the water, and secured with an elastic band. The lid of a sterile 9cm petri dish was placed on top of the glass, as shown in Figure 5.2. Eggshells were sterilised by wiping with 70% ethanol prior to opening. Without changing egg orientation, the bases of eggs were cracked against the glass edge, both sides of the shell were then pulled apart using thumbs in a smooth action, to open and empty the contents onto the cling film support. Five ml of culture medium (DMEM), 50µl of Antibiotic-Antimycotic (100X: Gibco 15240096) and a pinch of ground eggshell were added to each egg, not covering the embryo directly. The *ex ovo* cultivation setup was further incubated at 37.5°C in a humidified chamber.

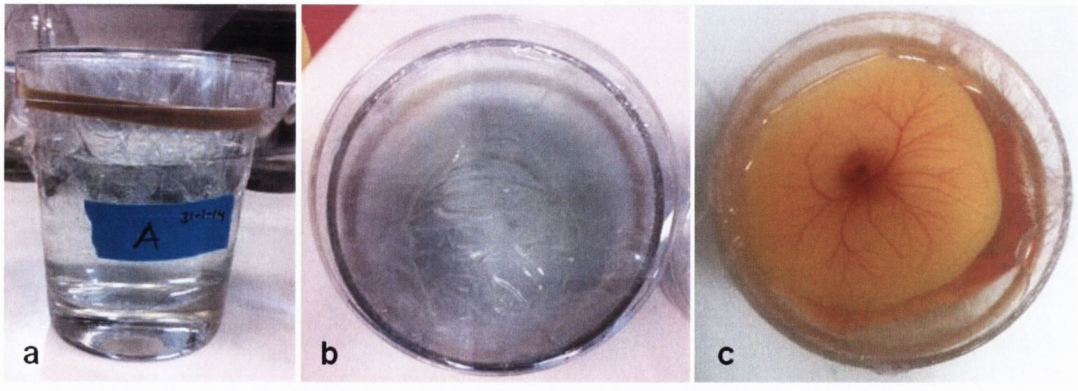

Figure 5.2: *Ex Ovo* cultivation setup. (**a**) Side view of glass support filled with water with a cling film hammock supported with an elastic band and covered with a petri dish lid. (**b**) Surface view of cling film support setup, (**c**) specimen on cling film support within cultivation setup.

5.2.2 Alcian Blue staining of whole chick embryos

Whole chick embryos were fixed in 95% ethanol for at least 3 days. Whole embryos were stained using 0.1% Alcian Blue in 95% ethanol for 8 to 24 hours at room temperature (RT), duration dependant on the stage of the embryo. Embryos were then washed twice in 95% ethanol and cleared using 1% potassium hydroxide at RT for 2-5hours, or until the tissue was sufficiently cleared and background stain removed and then fixed in 4% PFA in PBS overnight.

5.2.3 *Ex Ovo* electroporation Experimental Design

An overview of the methodological approach to the introduction and analysis of foreign DNA into the developing chick forelimb is shown in Figure 5.3. Each step in the process involved a number of phases that are described in detail in following sections. The construct of interest was microinjected together with a GFP expression vector, into the limb bud, followed by electroporation (Figure 5.3A). Following 24hours post electroporation incubation, GFP expression was assessed by whole embryo photography under a fluorescent dissecting microscope (Figure 5.3B). Expression of the targeted gene constructs was assayed by *in situ* hybridisation and immunohistochemistry of fusion protein tags (FLAG tag on the β-catenin fusion protein and HA epitope tag on the Sfrp3 construct) (Figure 5.3C). Resulting phenotypes in skeletal elements were assessed via *Col2a1* expression (marker of the skeletal rudiments) by whole-mount in situ hybridisation (ISH) and Optical Projection Tomography (OPT) 3D scanning (Sharpe et al 2002; Summerhurst et al 2008) to compare electroporated (EP) and non-electroporated (non-EP) limbs (Figure 5.3D). Downstream effects were further assessed by analysis of the known Wnt target gene *Sfrp2* (Lescher et al., 1998) using wholemount ISH, as this gene was previously shown to be joint specific and up-regulated following the removal of mechanical stimulation (Figure 4.5).

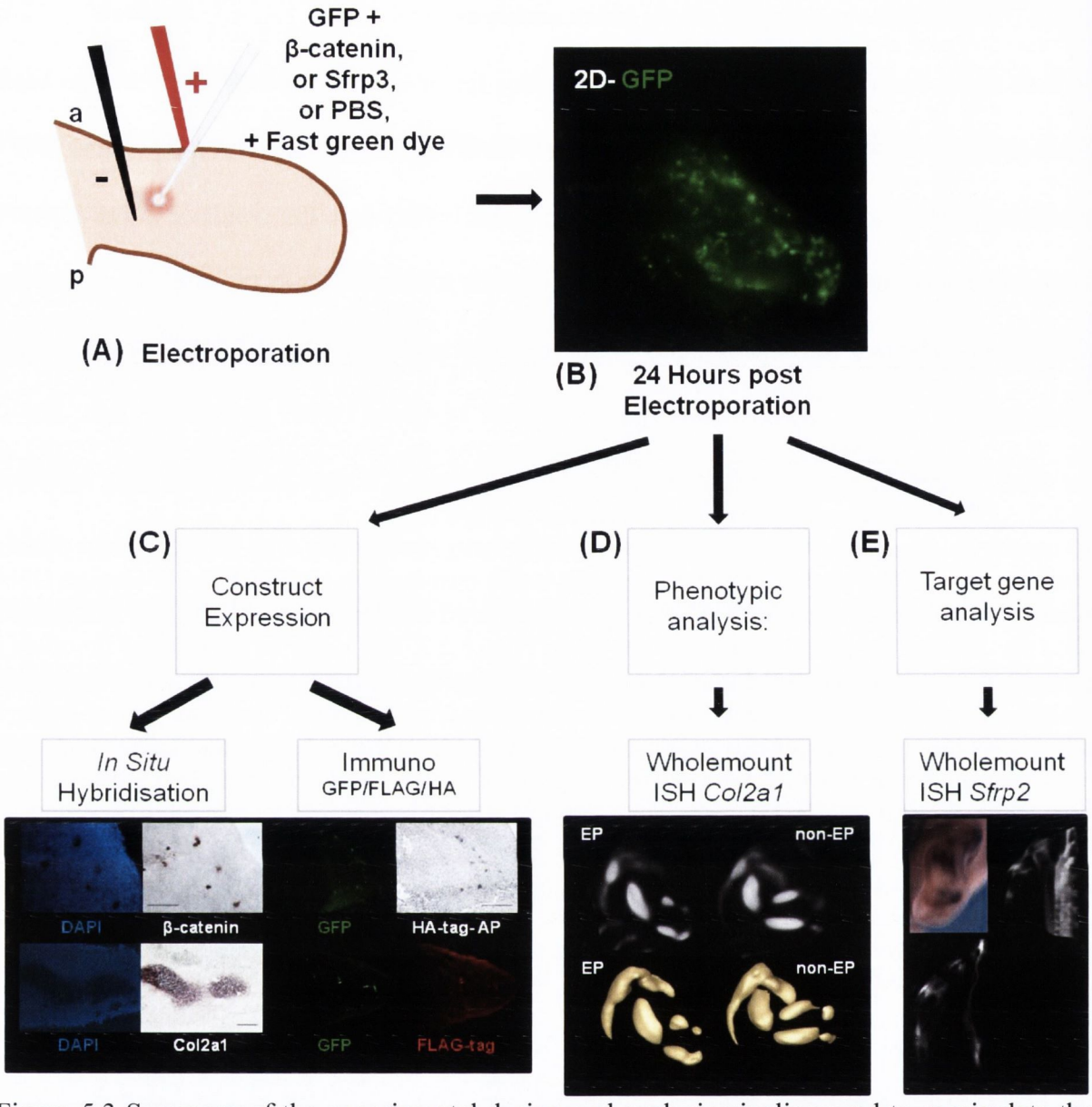

Figure 5.3 Summary of the experimental design and analysis pipeline used to manipulate the Wnt signalling pathway in the developing chick forelimb. (**A**) Electroporation setup with positive (+) and negative (-) electrodes placed on the ventral and dorsal side of the limb. a; anterior, p; posterior. (**B**) Whole embryo GFP analysis 24hrs post-electroporation. (**C**) Construct transgene expression analysis of electroporated limbs using *In situ* hybridisation and Immunohistochemistry to detect transcript and fusion protein tags (FLAG and HA). (**D**) Phenotyoic analysis of skeletal elements using *Col2a1* wholemount ISH and 3D imaging by OPT of electroporated (EP) and non-electroporated (non-EP) limbs. (**E**) *Sfrp2* target gene analysis of EP and non-EP limbs.

5.2.3.1 *Ex Ovo* electroporation

Ex ovo electroporation was carried out on the forelimb of day 4-4.5, HH24-HH26 embryos.

The vitelline membrane was carefully opened above the visible forelimb to allow access to

the embryo. Parallel electrodes were positioned on either side of the limb, ensuring not to touch the tissue, approximately 3-4mm apart.

DNA for electroporation was prepared by Qiagen plasmid extraction kit at a concentration of at least 1μg/ml (good purity and high concentration are important requirements). DNA was sequence verified and mixtures of plasmid DNA were prepared as follows: (1) GFP (pEGFP-C1 map in Appendix Figure C.3) (1μg/μl) 1μl volume + 0.5μl of 0.05% fast-green dye, (2) β-catenin (pCDNA3.1-βcatΔTcf, map in Appendix Figure C.1) (1μg/μl), 1ul + 1μl GFP (0.5-1μg/μl) + 0.5μl of 0.05% dye, (3) Sfrp3 (pCS2mFRZB-HA, map in Appendix Figure C.2) (1μg/μl), 1ul + 1μl GFP (0.5-1μg/μl) + 0.5μl of 0.05% dye. Plasmids were injected, via a mouth-pipette. The targeted site of injection was midway along the proximal/distal and anterior/posterior axes, approximately at the site of the of the prospective elbow joint region, as indicated in Figure 5.3A, however there was inevitable variation from embryo to embryo. Immediately following injection, embryos were electroporated using an Electro Square Porator™ ECM (Genetronics Inc.). Multiple parameters were tested for electroporation optimisation including varying the voltage, the number of pulses applied and volume of construct injected. The parameters optimised for electroporation consisted of six 60ms pulses of 25Volts (V), at an interval of 100ms. 5ml of fresh DMEM culture medium, 50μl of Antibiotic-Antimycotic and ground eggshell were added. Specimens were re-incubated and harvested 24hours post electroporation. Viability of the embryo and stage of development were assessed for the embryo and for each limb (electroporated and contra-lateral non-electroporated limb) using Hamburger and Hamilton criteria (Hamburger and Hamilton, 1992). Specimens were either fixed in 95% ethanol (for alcian blue staining), or 4% DEPC treated 4% PFA in PBS overnight.

5.2.3.2 Expression Vectors

Details of each expression vector used can be found in Table 5:1. Sham electroporation was also performed on limbs using PBS, GFP and dye, to act a technical control.

The β-catenin-Tcf fusion protein encoding plasmid (pCDNA3.1-βcatΔTcf) contained a FLAG tag that has the specific protein sequence (MDYKDDDDK), and the Sfrp3/Frzb (pCS2mFRZB-HA) sequence was altered to encode the epitope Hemagglutinin (HA) tag that has the protein sequence (YPYDVPDYA) within the encoded protein (plasmid maps are shown in Appendix C).

Table 5:1: Details of Plasmid Expression vectors used in Electroporation.

Construct	**Backbone**	**Protein encoded**	**Special features within Vector**	**Function of expression vector**
pCDNA3.1-βcatΔTcf	pCDNA3.1(+)	Tcf3- binding domain, Ctnnb1- Activation (β-catenin-Tcf domain)	FLAG Tag	Constitutively activate canonical Wnt signalling
pCS2mFRZB-HA	pCS2 (6.36kb)	Sfrp3/ FRZB	Hemagglutinin tag (HA)	Block canonical Wnt signalling
pEGFP-C1	pECFP-C1 (4.7kb)	GFP		N/A

5.2.3.3 Analysis of transgenic embryos

Using an Olympus SZX12 microscope with UV lamp and an appropriate GFP filter. Green Fluorescent Protein (GFP) expression was analysed and imaged in whole embryos following immediate harvesting of each specimen. Visualisation of GFP expression indicated the cells that had taken up and expressed DNA (the plasmid mix) during electroporation.

5.2.3.4 Sectioning of electroporated specimens

Electroporated and contra-lateral non-electroporated limbs were processed for cryosectioning and wax sectioning (section 2.4.2, 2.4.3). 10μm longitudinal sections were obtained for immunohistochemistry and *in situ* hybridisation analysis.

5.2.3.5 Immunohistochemistry

Details of the primary and secondary antibodies used are listed in Table 5:2. Frozen sections were thawed at RT (at least 30mins) and washed in PBS; paraffin sections were de-waxed and re-hydrated prior to blocking. Slides were blocked in 5% goat serum in PBTT (PBS +0.1% Triton +0.1% Tween) for 1 hour in a humid chamber at RT then incubated in Primary Antibody (Ab) (αGFP (1:500), αFLAG (1:200), αHA (1:200)) in 5% goat serum in PBTT in a humid chamber overnight at 4°C. Post antibody washes were performed in PBS, 3 times for 15mins on a rocker at RT. Incubation with secondary Ab was performed at 1:200 and 1:500 for 1hour at RT in the dark. Post secondary antibody washes were carried out 3 times in PBS and counterstained with DAPI mounting medium to stain the nuclei. Colourimetric staining involved 3 washes in NMT and staining with half strength NBT/BCIP staining solution (as previously described in section 2.5.4).

Table 5:2 Summary of Antibodies used.

Antibody name	Supplier Cat #	Species	Dilution	Secondary Antibody	Excitation/ Emission
αFLAG	Sigma-Aldrich F4042	Mouse, M5-monoclonal	1:200	Donkey anti-mouse AlexaFluor 568 (1:200)	578/603nm
αHA.11	BioLegend® mms-101bp	Mouse, monoclonal	1:200	Donkey anti-mouse AlexaFluor 568 (1:200)	578/603nm
				Goat anti-mouse IgG-AP (1:300)	colourometric
αGFP	Molecular Probes® A-11122	Rabbit, polyclonal	1:500	Goat anti-rabbit AlexaFluor 488 (1:500) A-11008	488/519nm

5.2.3.6 In Situ Hybridisation

Digoxigenin (dig) labelled antisense RNA probes for chick *Col2a1* and *Sfrp2* were produced from cEST clones, detailed in Table 5:3, as previously described (section 2.5.1), with the following adaptations for working with chick embryos: Proteinase K treatment 20μg/ml for 1min per HH stage. Post hybridisation whole-mount washes consisted of 2xSSC, 2xSSC/0.1% CHAPS, 0.2X SSC/0.1%, CHAPS. Anti-DIG antibody was used a 1:1000. mRNA for mouse β-catenin and Sfrp3, encoded in the electroporated mouse DNA, were detected using ISH on

sections (as previously described; section 2.5.3). Double ISH and Immunohistochemistry (IHC) was performed in some cases, with ISH performed up to the point of DIG detection first, then co-incubation with anti-DIG antibody and the primary antibody for IHC; in most cases to detect GFP using fluorescently labelled secondary antibody. ISH colourimetric staining was then performed in the dark.

Table 5:3: Summary of cDNA clones used to generate RNA in situ probes

Gene	Genebank Ref sequence	Alignment of cDNA on Ref sequence	Source
cCol2a1	NM_204426.1	Nucleotide to 3887-4689	ChEST 179115, BBSRC* ChickEST database
cSfrp2	AF2 18056	Nucleotide 520-1317	ChEST 296f13, BBSRC* ChickEST database
mβcatenin	NM_001165902.1	Nucleotide 2069-2496	Dr. U Borello
mSfrp3	NM_011356.4	Nucleotide 1866-2328	I.M.A.G.E clone 805986

*Biotechnology and Biological Sciences Research Council (BBSRC) ChickEST Database

5.2.3.7 Optical Projection Tomography

In situ hybridised embryos were prepared and processed for OPT as described in section 2.12.

5.3 Results

5.3.1 *Ex ovo*-cultivated chick embryos display normal morphological development and chondrogenesis

The development rate and morphology of *ex ovo*-cultivated embryos were compared to *in ovo* incubated embryos using morphological criteria as described by Hamburger and Hamilton (Hamburger and Hamilton, 1951). Embryos placed in *ex-ovo* culture at E3 were monitored over the following 5 days in culture (to E8) demonstrating normal development (Figure 5.4A). During incubation the yolk spread on the support hammock and the vasculature network spread smoothly over the yolk. With the exception of a number of embryos that were damaged during transfer (20.6%), 60.7% of embryos survive in *ex ovo* culture up to at least E8. To assess the rate of development over time, specimens cultured *ex ovo* and *in ovo* were sacrificed every 12 hrs from E4.5 to E6 and then every 24 hrs from E6 to E8. For all time points analysed no difference was observed in the stages of the embryos based on external morphological features (Figure 5.4B). A subset of embryos (n= 2 for each stage) were further stained with Alcian blue to assess the progress of chondrogenesis and stage match more precisely. At E5/ HH26 detection of cartilage was only visible in the developing vertebra (Data not shown), at E5.5/ HH28 individual cartilage elements were visible in the forelimbs (Figure 5.4D E5.5) and hindlimbs (data not shown). No visible differences were seen in the alcian blue staining pattern of the developing forelimb between *in ovo* and *ex ovo* specimens across E5.5, E6, E7 or E8 (Figure 5.4D). A clear region, in the mid-diaphysis of the humerus at E8/ HH34 in both the *in ovo and ex ovo* specimens represents the beginning of ossification, indicating that the *ex ovo* cultivation set-up is not restricting development up until endochondral ossification at least (Figure 5.4E).

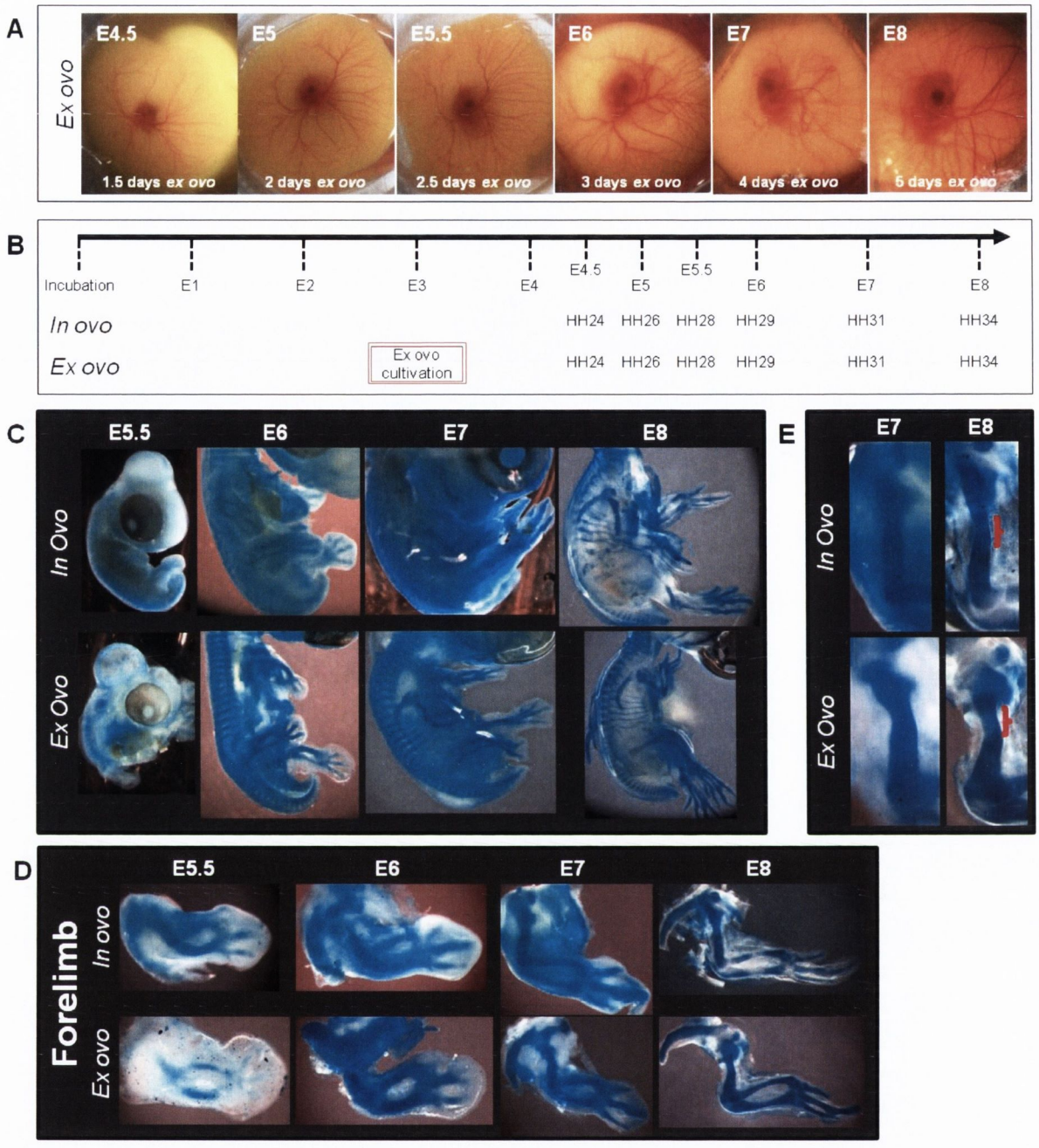

Figure 5.4: *Ex ovo* cultivated chick embryos show normal development over time. (**A**) Morphological development of the embryo shown *in situ* within the *ex ovo* cultivation set-up from E4.5 to E8. (**B**) Time-line of the stages identified at each time-point (E4.5-E8, n=1). (**C**) Whole embryo Alcian Blue cartilage staining (E5.5 to E8) shows the same pattern for *in ovo* and *ex ovo* cultivated specimens, with specific focus of the whole forelimb from E5.5 to E8 (**D**) and the humerus (**E**) at E7 and E8, red box indicates ossification site.

5.3.2 Viability of Electroporated chick embryos

Ex ovo chick embryos were electroporated (n=321) at various time-points between E4-E5, consisting of embryos at 6 independent stages: HH22 to HH27. Eighty-nine percent of the

embryos electroporated were at stages HH24, HH25 and HH26 (Table 5:4A). This window of development was chosen as it represents early stages of mesenchymal condensation that prefigures chondrogenesis of the humerus, radius and ulna of the forelimb (Wezeman, 1998), and as the Wnt signalling pathway has been previously shown to be critical for joint formation, it is within the window where the joint regions are being defined.

Table 5:4: Overview of survival and development rate following electroporation

(A) Number of specimens electroporated at each stage							Total # of specimens electroporated
Stage	**HH22**	**HH23**	**HH24**	**HH25**	**HH26**	**HH27**	
Embryo #	4	14	71	107	110	15	**321**
Numbers surviving and stages reached + 24 hours		2:HH25 4:HH28	1:HH25 4: HH26 11:HH27 6:HH28 1:HH29	1:HH26 4:HH27 32:HH28 4:HH29	2:HH27 32:HH28 8:HH29 6:HH30	1:HH28 3:HH29 2:HH30	
(B) Viable electroporated embryos: Stage and total numbers viable after 24 hours							Total # of viable electroporated embryos
Stage	**HH25**	**HH26**	**HH27**	**HH28**	**HH29**	**HH30**	
Embryo #	3	5	17	75	16	8	**124**

Across 24 experiments, 38.63% of electroporated embryos (124/321) were viable 24 hours later. Viable embryos had healthy vasculature and an obvious heartbeat. These embryos were analysed for the efficiency of electroporation via visualisation of GFP expression (section 5.3.3). In general embryos that were not alive 24 hours post electroporation had advanced in development by at least one or two stages suggesting that DNA uptake may have occurred so these embryos were also assessed for GFP expression, but none were used for further phenotypic analysis.

5.3.3 Tissue Distribution of electroporated cells assessed through GFP transgene expression

Co-electroporation with an expression construct for GFP was used as a convenient means to quickly assess successful uptake and expression of microinjected DNA. Of the 124 viable embryos 24 hours post-electroporation, (Table 5:4B), 96 (77.4%) showed GFP positive cells within limb bud mesenchyme across 6 stages (Table 5:5); others showed GFP expression restricted to ectoderm. The majority of the GFP positive embryos were at stage HH28

(63.5%), following electroporation at stages HH25 and HH26. In addition, of the 197 non-viable embryos harvested 24hours post-electroporation, 80 (40.6%) were also GFP positive in mesenchyme of the electroporated limb. The focal plane of GFP positive cells indicated whether they were within limb mesenchyme or restricted to surface ectoderm.

Table 5:5 Number and stage of viable embryos with GFP positive cells in limb bud mesenchyme 24 hours post-electroporation.

GFP expression in electroporated embryos							Total # of embyros GFP positive
Stage	**HH25**	**HH26**	**HH27**	**HH28**	**HH29**	**HH30**	
Embryo #	2	3	15	61	10	5	**96**

Location and intensity of GFP expression was analysed to determine consistency in the position and extent of DNA uptake (Figure 5.5). Figure 5.5 shows representative examples of the variations seen across electroporated embryos. An example of a viable limb that was termed GFP negative is shown in Figure 5.5a-a^{1}, since GFP is restricted to the anterior ectoderm. The specimen shown in Figure 5.5b-b^{1} similarly shows GFP expression on the anterior surface, but also within cells in the distal interior portion of the limb, indicated by the white arrow. Expression shown in specimens c-f and h indicates GFP positive cells throughout the whole limb, but variations in the extent and intensity of GFP. For example there is ectoderm expression in c, d and h, yet in e and f there is no surface expression. Some specimens showed GFP positive cells in an extensive territory along the proximo-distal axis (c, d, e, f and h), although positive cells in specimen h are restricted to the anterior limb. Specimens g, i and j show GFP restricted to more proximal territories, excluded from the distal handplate, whereas positive cells in specimen k are restricted to the handplate. The expression in i and j is more restricted to the region of the elbow joint. The wound site where the capillary pierced the surface ectoderm during microinjection of DNA is visible on some specimens (d^{1}, e^{1}, h^{1}, i^{1}, j^{1}, and k^{1}, all indicated by yellow arrows). Given the variation seen in the position and extent of GFP positive cells across specimens, the GFP pattern in each numbered specimen was recorded for later reference.

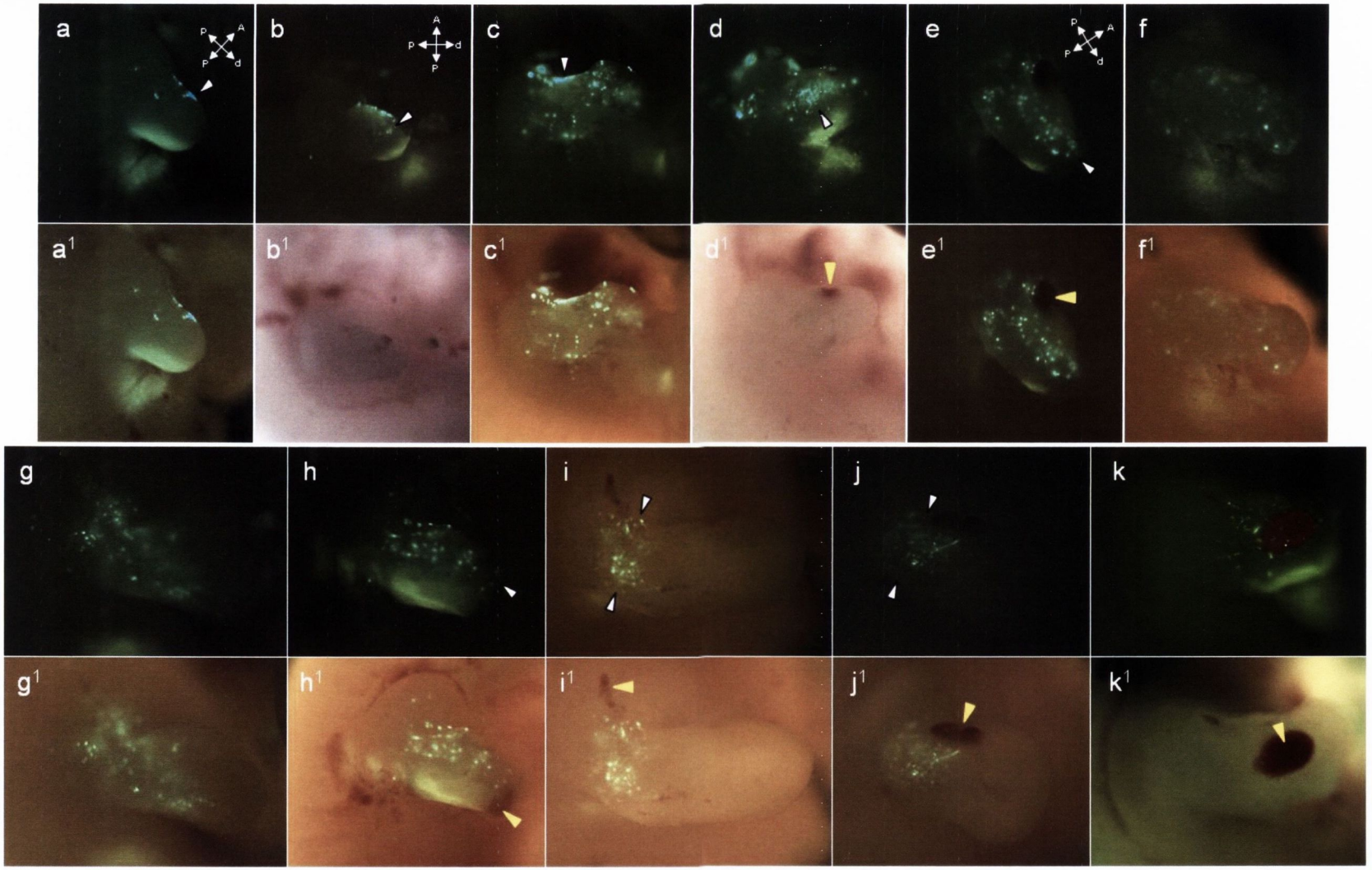

Figure 5.5: Variability in GFP expression (location and intensity) in forelimbs 24 hours post-electroporation. (a-k) GFP expression in dark field views, (a1, c1, e1- j1) GFP merged with bright field images, (b1, d1, k1) show bright field alone. White arrows indicate GFP expression; Yellow arrows indicate capillary insertion point. Orientation is the same for b-d and f-k. A; anterior, P; posterior, p; proximal, d; distal.

5.3.4 The developing Cartilaginous Skeleton

In order to assess any phenotypic changes following transgene activity, *Col2a1* gene expression was chosen as a good marker for chondrogenesis, using 3D imaging to assess any alterations in the pattern of forming rudiments. In order to facilitate this, a detailed data set for normal patterning was required. The development of cartilaginous elements in the avian embryo were observed and recorded in 3D using OPT across stages HH26-HH30 following detection of *Col2a1* expression by *in situ* hybridisation (Figure 5.6). The whole cartilaginous structure develops substantially over the five stages analysed, corresponding to a window of 2 embryonic days. At HH26, the expression of *Col2a1* is strong in the developing vertebral column, with proximal rudiments visible in both fore- and hindlimbs. The 3D data can be visualised as external views following either "volume rendition" (Figure 5.6 upper panel; expressing tissues shown in white/grey (a-e, k-o)) or "surface rendition" (lower panel; expressing tissues shown in yellow (f-k, p-t). Because this is true 3D data, it can also be viewed by cutting virtual sections in any plane through the specimen (as demonstrated later).

The limb cartilaginous elements appear in a proximal to distal order. At HH26 expression of *Col2a1* is present in the future scapula (s) and humerus (h), with very faint expression in the future ulna (u) (Figure 5.6k, p). At HH27 the scapula and ulna have increased in size, and the future radius (r) is now clearly visible (Figure 5.6l, q), but note that it is distinctly shorter than the ulna at this stage. By HH28 *Col2a1* expression in the carpal (c) elements is beginning to appear as sites of expression distal to both the radius and ulna, but the carpal joints are not yet apparent. The expression territories in the future humerus, radius and ulna have all increased in length with the radius and ulna now more similar in length (Figure 5.6m, r). At HH29 the expression of *Col2a1* in the humerus is visibly reduced at the mid-diaphysis, corresponding to hypertrophy/ the beginning of ossification; red arrows show continued expression at the ends of the rudiment. A clearing in the centre of the ulna is also visible (Figure 5.6n), suggesting the onset of chondrocyte hypertrophy is also occurring here. The expression of *Col2a1* in the

future metacarpals (mc) can also be seen at this stage, with a demarcation of the carpal joint also occurring (Figure 5.6n, s). At HH30 the scapula loses *Col2a* expression mid rudiment (blue arrows indicating persistent expression at the rudiment termini (Figure 5.6o, t). Future phalanges (p) are evident at HH30 (Figure 5.6o, t).

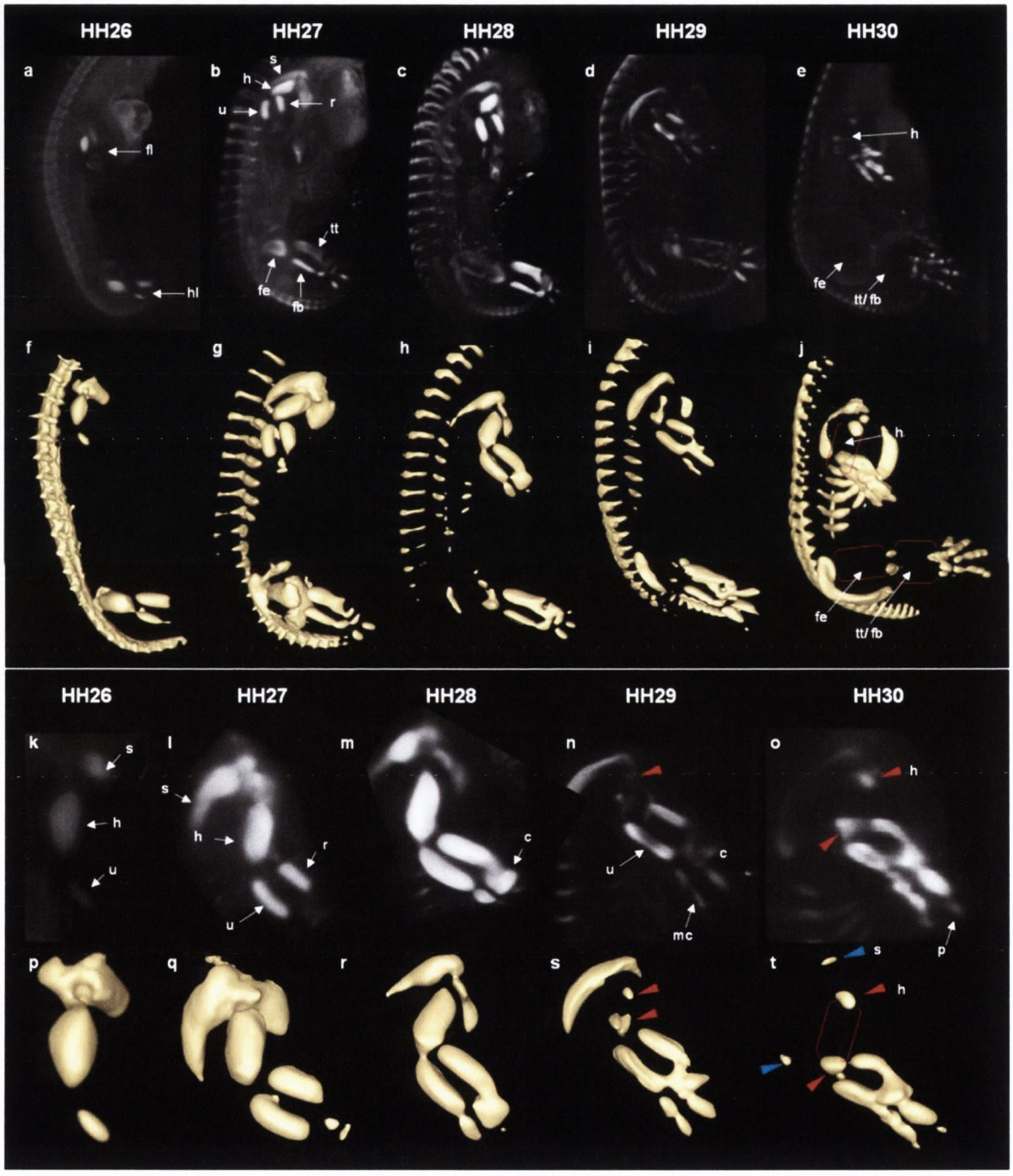

Figure 5.6: The developing cartilaginous skeleton. 3D analysis of the expression pattern of *Col2a1* in whole chick embryos (**a-e**) and in the developing forelimb (**k-o**) across stages HH26-HH30, Lateral views of volume rendered 3D reconstructions of the data following OPT scanning (expressing tissues appear white/grey). (**f-j**, **p-t**) Matching lateral views of surface rendered data (expression shown in yellow). Red brackets show separation of *Col2a1* expression in the mid-diaphysis of the rudiment at HH30. fl; forelimb, hl; hindlimb, s; scapula, h; humerus, u; ulna, r; radius, tt; tibiotarsus, fe; femur, fb; fibula.

5.3.5 Constitutive activation of Wnt signalling in the developing limb

5.3.5.1 Detection of Tcf-β-catenin fusion protein expression in electroporated limbs

Nineteen experiments were carried out to express constitutively active β-catenin in cells of the developing limb bud, producing 63 transgenic embryos. Two methods of detection of the encoded transgene product were used; (1) visualising the Tcf-β-catenin fusion protein through immune detection of an incorporated FLAG tag epitope (Figure 5.1and Appendix Figure C.1); (2) through detecting the RNA transcript using a mouse β-catenin antisense probe (specific to transgene expression). Co-localisation of GFP positive cells using anti-GFP antibodies was used to co-detect both expressed proteins in the same section. Detection of the FLAG tag can be seen in the same cells that express GFP (Figure 5.7 a^1, a^2, a^3, c^1, c^2 (white arrows)), but where GFP is detected throughout the cell, the fusion protein is always nuclear (e.g. a^3 distal). But not all GFP positive cells are also clearly positive for the FLAG tag (Figure 5.7b^1- b^3).

Analysis of transgene expression at the transcript level using ISH with anti-sense mouse β-catenin probe, also showed co-localisation with GFP (c^1 and c^3). When GFP, FLAG and β-catenin RNA detection was performed on the same sections, co-expression can be seen for the three elements, but with apparently different levels of expression (c^1, c^2 and c^3). Note very low levels of FLAG detection in a cell strongly labelled for β-catenin transcription (c^2 and c^3, yellow arrow) and GFP. This might indicate less sensitive detection with the FLAG antibody or may be due to different sub-cellular localisation of the GFP and fusion proteins, or the dampening of fluorescence by the colourimetric staining. Sections shown in Figure 5.7d represent the non-electroporated contra-lateral forelimb of the same specimen shown in c, no GFP, FLAG or β-catenin was detected.

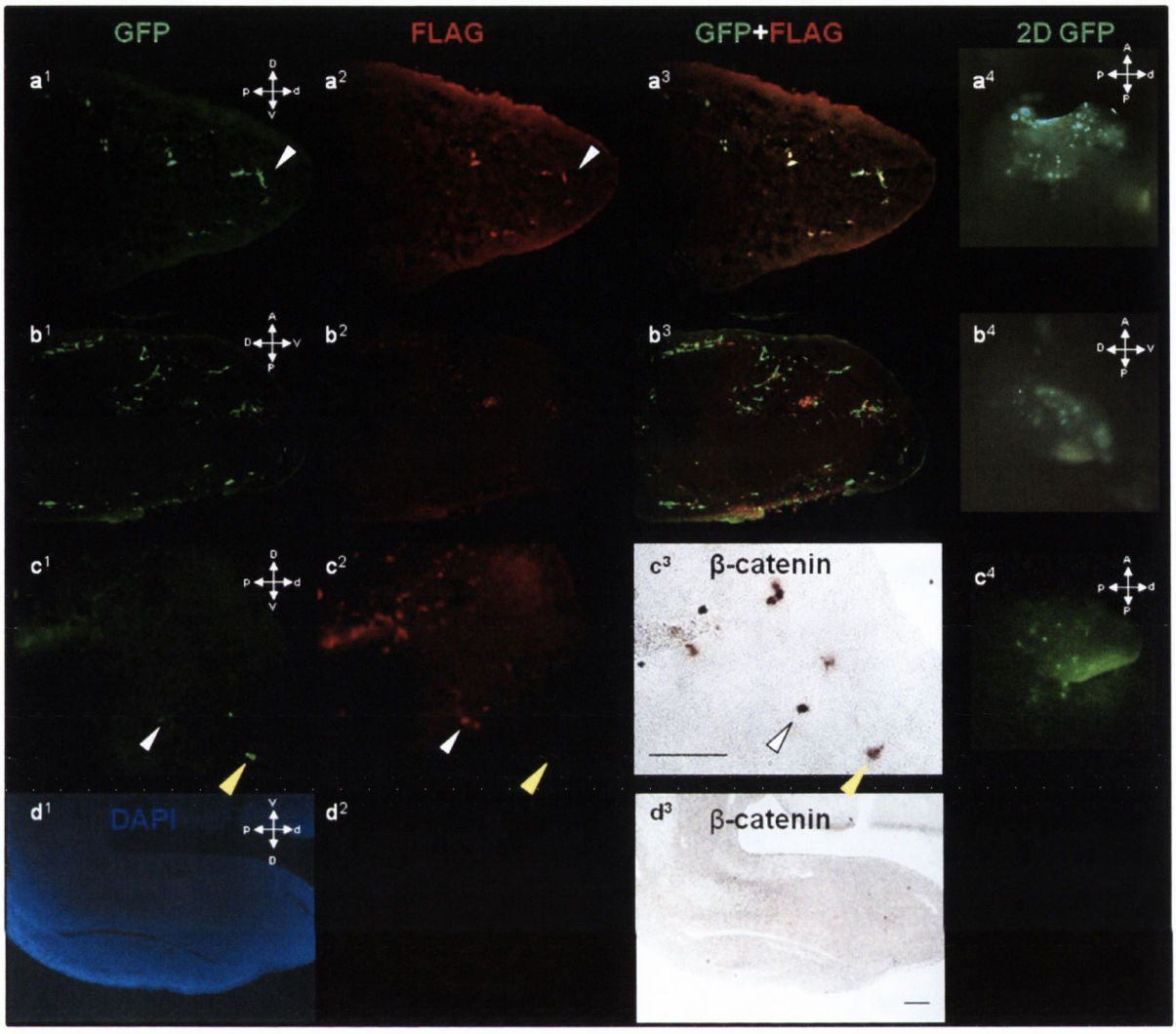

Figure 5.7: Detection of transgene expression in electroporated limbs (**a-c**), compared to a non-electroporated controlateral limb (**d**; same embryo as c). Columns 1-3 show sections through the whole limbs shown in column 4. Immunolocalisation of GFP (**a**[1], **b**[1], **c**[1]) the FLAG-tag (**a**[2], **b**[2], **c**[2], **d**[2]) and *in situ* hybridisation of β-catenin RNA (**c**[3], **d**[3]), merge of GFP and FLAG (**a**[3],**b**[3]),. Embryos **a** and **c** are stage HH28 and **b** is HH29. All scale bars 100μm. A; Anterior, P; Posterior, V: Ventral, D; Dorsal, p: proximal, d; distal.

5.3.5.2 Phenotypic Effects of activating the canonical Wnt pathway on skeletal development

To assess the phenotypic effects of forced expression of stabilised β-catenin on skeletal patterning, experimental limbs were compared to (a) the contra-lateral non-electroporated limb of the same specimen and (b) to sham electroporated embryos where only the GFP expressing vector was transferred, using an identical procedure. Seven Tcf-β-catenin fusion protein electroporated specimens and 5 sham electroporated specimens were analysed in detail using *Col2a1* expression to accurately stage the progression of skeletal development

and assess any alterations in morphogenesis of the skeletal rudiments. All specimens were electroporated between stages HH24-26 (Table 5:6).

Table 5:6: Stages of electroporated (EP) and non-electroporated (non-EP) forelimbs

Sham Electroporated			
Specimen	Stage when electroporated	**Stage of EP limb**	**Stage of non-EP limb**
		Based on *Col2a1* expression pattern	
1	HH25	HH26	HH26
2	HH24	HH26/27	HH27
3	HH26	HH27	HH27
4	HH25	HH27/28	HH28
5	HH26	HH28/29	HH29
Tcf-β-catenin Electroporated			
1	HH26	<HH26?	HH27
2	HH25	HH27	HH28
3	HH26	HH27	HH28
4	HH24	HH27	HH28
5	HH26	HH27	HH28
6	HH24	HH27	HH28
7	HH26	HH26/27?	HH29/30

The effect of electroporation on the rate of development was assessed by comparing the *Col2a1* expression patterns in the electroporated limb (sham and activated β-catenin) to the contra-lateral limb in that specimen (Table 5:6; Figure 5.8 and Figure 5.9). For sham electroporated embryos, the stage of the electroporated limb was similar to the non-electroporated limb; for two specimens, the electroporated limb appeared to be slightly less advanced, but by less than 1 stage (Figure 5.8; Table 5:6; specimens 2 and 4) while the remaining 3 showed no difference. Note that GFP expressing cells are widely distributed in the sham electroporated limbs with no correspondence between extent of expression observed and slight delay (Figure 5.8a-e). In Tcf-β-catenin electroporated limbs there was a consistent delay of at least 1 stage (Figure 5.9 and Table 5:6), in fact all EP limbs were at most HH27. The electroporated limb in specimen 7 was three stages younger (EP; HH26/27 compared to non-EP; HH29/30, Table 5:6).

In terms of morphogenesis of the skeletal rudiments, analyses of *Col2a1* expression revealed no alterations, or minimal alterations, in Sham electroporated embryos. The youngest specimen analysed was specimen 1, with *Col2a1* expression in both limbs indicating stage HH26 (Figure 5.8f, k). No differences in the *Col2a1* pattern were observed in specimens 1, 2 and 3 (Figure 5.8f-h compared to k-m respectively), despite GFP expression, particularly widespread for specimen 3 (Figure 5.8c). Specimens 4 and 5 showed some differences in *Col2a1* expression in the future carpal regions (Figure 5.8i - n and j - o). In the EP limb of specimen 4, there was a distal truncation of the pattern, (Figure 5.8i, indicated by red arrows). Similarly in the EP limb of specimen 5, although there is some *Col2a1* expression distal to the radius and ulna, no distinct carpals or phalanges are discernible (Figure 5.8j and o, indicated by circle). While the alterations to the specimen 4 pattern are consistent to a delay (comparable to HH27 in Figure 5.6), the pattern in specimen 5 is not obviously similar to an earlier stage. It is possible that the electroporation process has affected differentiation in the distal tip of the limb in specimen 5.

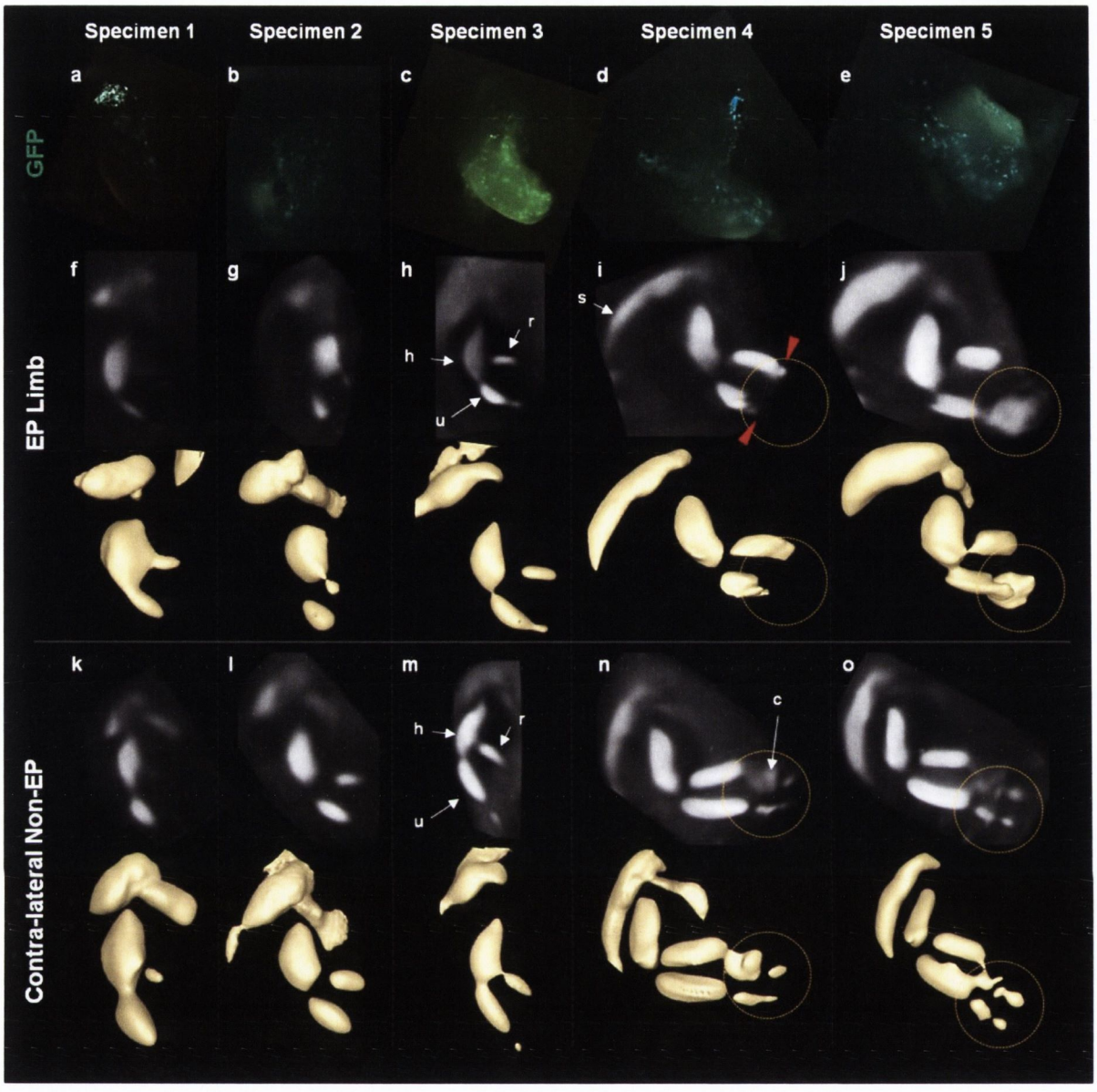

Figure 5.8: Three dimensional analysis of *Col2a1* expression in Sham electroporated (EP) forelimbs. (**a-j**) compared to contra-lateral non-electroporated (non-EP) limbs (**k-o**). Whole limb images of GFP expression in sham-EP limbs (**a-e**), lateral views of 3D reconstructions of the volume rendered data following OPT scanning (expressing tissue appears white/grey) and surface representations of *Col2a1* of the patterns (below), are shown. Orange circles indicate alteration in *Col2a1* expression. Red arrows indicate regions described in text; scapula, h; humerus, u; ulna, r; radius, c; carpal.

In contrast to the minimal effects seen in sham electroporated embryos, expression of the Tcf-β-catenin fusion protein had more dramatic effects on the pattern of *Col2a1* expression in the forming skeletal rudiments. Each specimen was thoroughly analysed using both 3D external views of the pattern and transverse and medial virtual sections through the 3D reconstructions (an example of virtual section analysis is shown for specimen 4 in Figure 5.10: full analysis of

remaining specimens is shown in Appendix Figure C.5). Each limb was visibly reduced in size compared to the contra-lateral limb (Appendix Figure C.4; 3D views of *Col2a1* expression, specimens 1-7).

In **specimen 1**, there was a complete absence of the ulna and radius in the EP limb compared to the contra-lateral non-EP limb (Figure 5.9g, n). In addition the ventral posterior portion of the scapula was reduced in size (red arrow heads in g compared to n), while no difference was seen in the shape or size of the humerus. Therefore there are effects on a proximal structure (scapula) and more distal rudiments.

In **specimen 2** the scapula, humerus and radius were visibly shorter in the EP limb compared to the non-EP limb (Figure 5.9h and o). Like specimen 1 the scapula has reduced *Col2a1* expression in the ventral portion, as indicated by the red arrow on the surface representation (Figure 5.9h). A more dramatic effect is seen in the region of the radius where *Col2a1* expression is divided into two territories proximally and distally. This appears to be a break or interruption in the radius territory based on (1) the relative position (green arrowhead) of the break, measured through serial sections of the 3D reconstructions and (2) although carpal *Col2a1* expression normally appears distal to the radius, this occurs after carpal expression distal to the ulna and at a more distal position. Carpal region expression is present distal to the ulna and not the radius on the contra-lateral limb, indicated by the orange circle. This supports the hypothesis that chondrogenesis in the region of the radius is interrupted in this experimental limb. The humerus in the EP limb in specimen 2 is shorter and displays an abnormal shape (Appendix Figure C.5 (2b)). The EP limb was deduced to be one stage behind the non-EP, however the phenotypic abnormalities cannot be explained by a delay and indicate an impact of abnormal canonical Wnt activation on skeletogenesis.

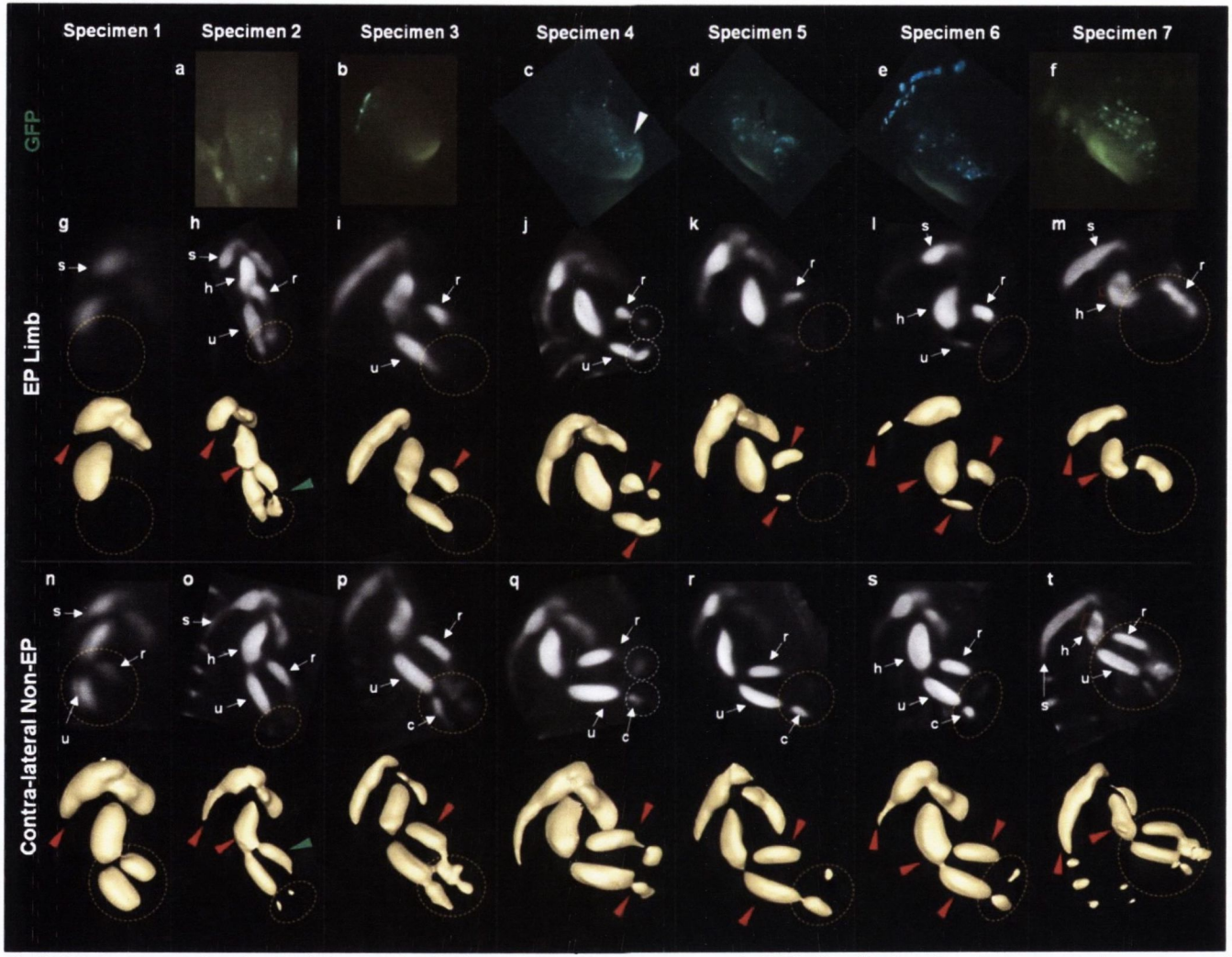

Figure 5.9: 3D analysis of *Col2a1* expression in Tcf-β-catenin fusion protein electroporated (EP) forelimbs (a-m) compared to contra-lateral non-electroporated (non-EP) limbs (n-t). Whole limb images of GFP expression in EP limbs (a-e), Lateral views of 3D reconstructions of the volume rendered data following OPT scanning (expressing tissue appears white/grey in the reconstructions) and surface representation of Col2a1 expression for 7 specimens (yellow denotes expression territory). Orange circles indicate absence of element expression. Red arrows indicate alterations described. Red brackets indicate hypertrophy. s; scapula, h; humerus, u; ulna, r; radius, c; carpal, p; phalanges.

Specimen 3 shows largely distal transgene expression and the *Col2a1* expression is compatible with a distal truncation in development (i, orange circle, Figure 5.9), corresponding to the carpal and metacarpal expression displayed in the non-EP limb (p, orange circle). There is less *Col2a1* expression in the radius and the ulna (Figure 5.9i and p, red arrow head), supported by transverse sections (Appendix Figure C.5 (3b) i-ii). The shape of the humerus appears abnormal in the EP limb, with a higher intensity of *Col2a1* expression in a ridge on the surface towards the upper portion of the element ((3b) iv compared to (3a) iv in non-EP).

Specimen 4 had a similar defect to specimen 2 with an interruption in the *Col2a1* radius expression territory (Figure 5.9j, green arrow head in surface view of limb). Transverse sections through the distal portion of the EP limb show a high level of expression of *Col2a1* in the region of the distal ulna (Figure 5.10 (4b) i), with a shape change visible from the posterior (+90degrees) angle view of the limb (Figure 5.10(4b) white arrow). This indicates either interrupted expression within the radius and ulna or the distal most expression represents carpel territories. If the latter is correct, this suggests severe shortening of the ulna and radius elements. The territory of transgene expression in this specimen was captured in the UV channel (Figure 5.10 (4b) right, pseudocoloured green) showing spatial correlation between transgene expression and localised alterations to the skeletal pattern in the radius (green arrows;Figure 5.10).

Specimen 5 showed severe alterations in the distal elements. A complete absence of carpal elements (Figure 5.9k, orange circle) was observed in the EP compared to non-EP limb (r). A significant decrease in the amount of *Col2a1* expression was observed in the ulna of the EP limb, and this was visualised with the surface representative expression comparing EP (k, red arrow) to non-EP (r, red arrow), and further analysed with transverse and medial sections through the rudiment (Appendix Figure C.5 (5b) i, iv). Transgene expression is localised anterior and posterior to where the defects occur in the radius and ulna (Appendix Figure C.5 (5b) i-ii, iv-v). The absence of carpal expression correlates with GFP/ transgene expression in

the distal portion of the EP limb as indicated by the green arrows in Appendix Figure C.5 (5b)(v).

Specimens 6 and 7 show severe cartilaginous defects in the EP limb (Figure 5.9l and m). These include a shortening and separation in the scapula, a reduction in the length of the humerus and the radius (Figure 5.9l, m compared to s, t), a reduction in the length and diameter of the ulna (l) and a complete absence of the ulna in specimen 7 (m; all defects indicated by red arrows, comparing EP (l, m) to the non-EP limb (s, t). An absence of carpal elements is common to both specimen 6 and 7 (l, m). Transgene expression in the EP limb in specimen 6 can be visualised in Appendix Figure C.5 (6b) (i, ii, v-viii) with the green arrows. The defects in the radius, ulna and carpals correlate with the level of, visible GFP ((6b) i, ii, v-viii). In specimen 6 there is a visible curvature of the humerus, seen in detail in the medial section ((6b) vii), compared to the non-EP humerus ((6a)iv). In specimen 7 the non-EP limb has lower intensity *Col2a1* expression in the central portion of the humerus, (Figure 5.9t red brackets, Appendix Figure C.5 (7b)iv), this suggests that hypertrophy is occurring in the centre of the element; a lighter expression can also be viewed in the central portion of the EP humerus (Figure 5.9m) suggesting that the element is proceeding to ossify in the mid diaphysis even though the extent of *Col2a1* is not normal. This was confirmed by transverse and medial sections of the EP humerus, with the lighter stain in the centre of the element ((7b) iii, vi) compared to the non-EP limb ((7a) iv, vi). It is difficult to assign a stage of development to the EP limb in specimen 7 due to the cartilaginous defects displayed.

Taking the observations of all seven activated β-catenin expressing transgenic embryos together, suggests that it is not a matter of simply delayed development but that activation of the canonical wnt pathway led to alterations including absence of skeletal territories.

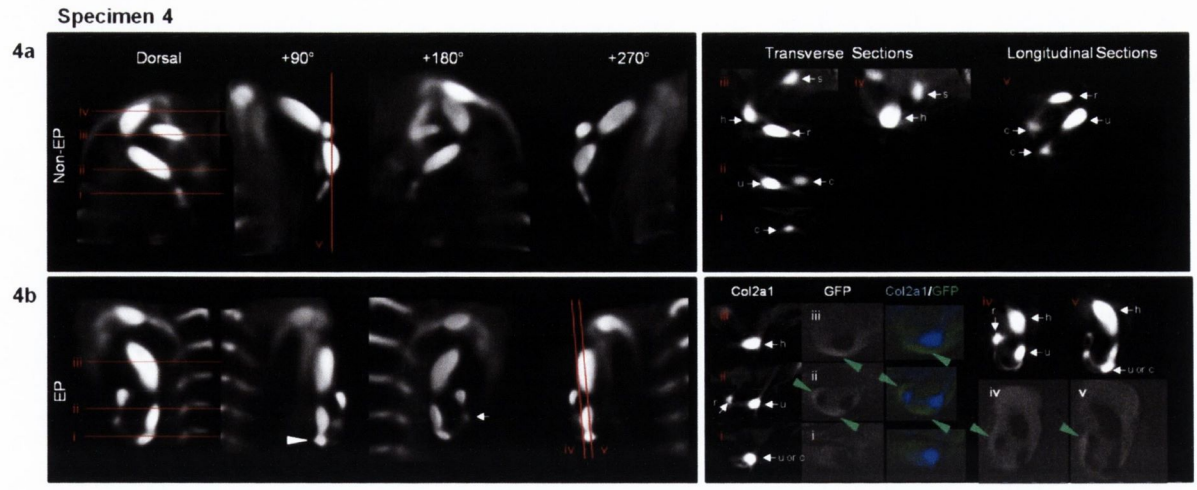

Figure 5.10: Analysis of *Col2a1* and GFP expression in β-catenin electroporated Specimen 4. EP limb (**4b**) compared to contra-lateral non-electroporated (non-EP) limb (**4a**). External views of volume representation of the same limb following OPT scanning of *Col2a1* expression is shown for each specimen, with rotations every 90°. Transverse and longitudinal sections were taken through the 3D reconstructions as indicated by red lines, showing *Col2a1* and *GFP* expression. Expressing tissue appears as white/light grey. **4a** (non-EP) (i-iv, transverse sections; v longitudinal section) **4b** (EP) (i-iii, transverse sections; iv-v longitudinal sections, *Col2a1* (blue)/GFP (green) pseudocoloured merge shown). Green arrows indicate GFP expression. s; scapula, h; humerus, u; ulna, r; radius, c; carpals.

5.3.5.3 Wnt target gene analysis following activation of Wnt signalling

To further assess the impact of expressing Tcf-β-catenin in the developing limb, the expression of a known canonical Wnt pathway target gene; Sfrp2 (Lescher et al., 1998) which also encodes an antagonist of the pathway, was performed on two further Tcf-β-catenin EP specimens (called specimens 8 and 9). Sfrp2 is expressed early in development in the limb mesenchyme surrounding cartilage condensations and then later becomes regionally restricted to regions of all synovial joints in the limb (as previous data in the lab, Ikegawa et al., 2008; Witte et al., 2009). In addition, this pathway component was identified to be up-regulated in the elbow and shoulder joints following the removal of mechanical stimulation (Figure 4.5). Analysis of the down-regulated Wnt target Cd44 was also attempted using wholemount *in situ* hybridisation in combination with 3D scanning technology, however due to the low levels of expression at the stages of development analysed, this analysis was uninformative and was not further pursued.

Normal *Sfrp2* expression in the developing limb at HH27 can be seen in Figure 5.11a dorsal view of a forelimb in (a) and (b) shows a high level of intense staining in the proximal portion of the limb including the future shoulder joint (SJ) and the future elbow joint (EJ) regions. Volume rendered 3D reconstruction of the pattern following OPT scanning are shown in Figure 5.11e. A longitudinal section cut through the dorsal plane reveals the two restricted regions of expression in the elbow joint region and the shoulder joint region (Figure 5.11f i).

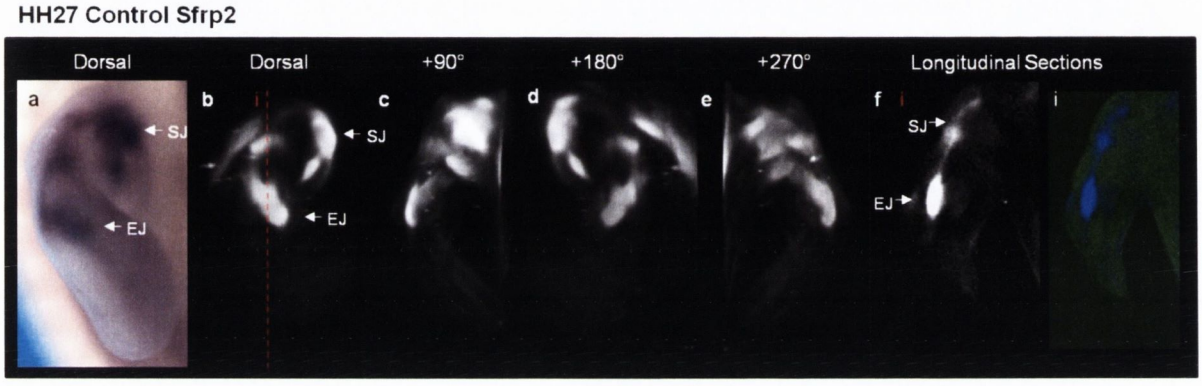

Figure 5.11: Analysis of *Sfrp2* expression in the developing chick limb at HH27. Dorsal view of *Sfrp2* expression in the forelimb prior to scanning (**a**), External views of volume rendered 3D reconstructions of the same limb following OPT scanning, with views from different angles (**b** same dorsal view as in **a**), **c** (rotated +90°), **d** (rotated +180°) and **e** (rotated +270°). Red line indicates the plane of a virtual longitudinal section shown in f and i; *Sfrp2* expression is pseudocoloured blue in **i**. EJ; elbow joint region, SJ; shoulder joint region.

The 2 Tcf-β-catenin electroporated limbs analysed here were shorter than the contra-lateral limbs, as previously depicted; specimen 8 was at stage HH27 and specimen 9 at stage HH28. In specimen 8 an increase in the extent and intensity of expression of *Sfrp2* was evident in both the elbow (EJ) and shoulder joint (SJ) regions, as shown by longitudinal virtual sections through the limb (Figure 5.12l compared to f), and is also much more extensive in the region of the elbow joint. A reduction in the separation of expression between the elbow region and the future carpal joint (CJ) region was evident in the EP limb (Figure 5.12 l (CJ) compared to f (CJ)). The *Sfrp2* expression pattern in specimen 9 shows an extended expression in the distal region of both limbs, with a distinct increase in expression in the carpal joint region (Figure 5.12 m and s respectively, CJ). An increase in dorsal expression is evident in the EJ region of

the EP limb in comparison to the non-EP limb (Figure 5.12x compared to r). Expression is more regionally restricted in the joint regions of specimen 9 (HH28) than in the control and specimen 8 (both HH27); this may be related to the difference in stage.

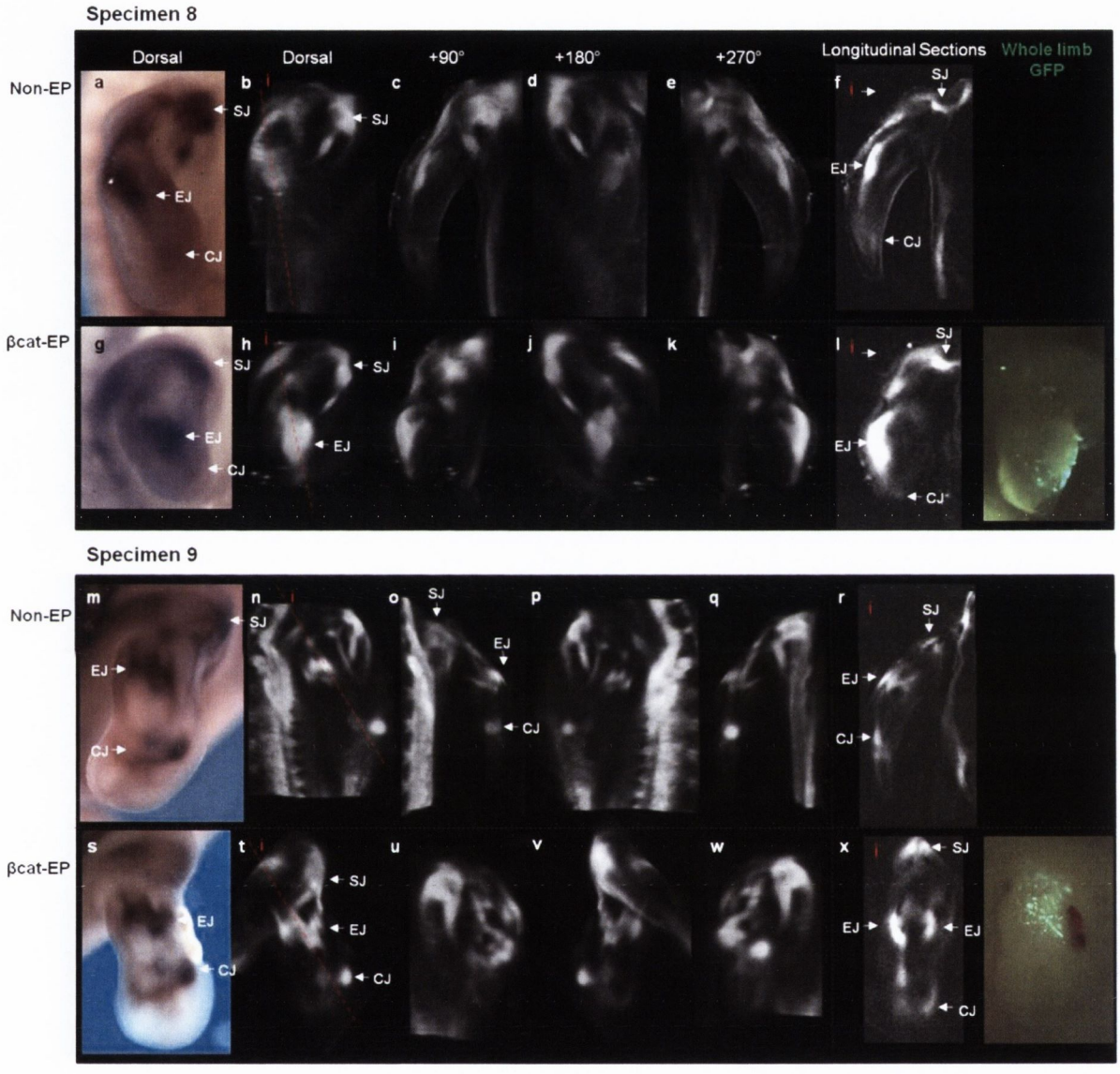

Figure 5.12: Analysis of *Sfrp2* expression in Tcf-β-catenin electroporated forelimbs. Dorsal views of *Sfrp2* expression in whole forelimb prior to scanning (**a, q, m, s).** Specimen 8 (HH27) non-EP limb (**a-f**), EP limb (**q-l**), Specimen 9 (HH28) non-EP (**m-r**), EP (**a-x**). External views of volume representation of the same limb following OPT scanning and reconstruction are shown in (**b, h, n, t),** rotated +90° (**c, i, o, u**), rotated +180° (**d, i, p, v**) and rotated +270° (**e, k, q, w**). Red line indicated the plane of a virtual longitudinal (**i**) section for each limb (**f, l, r, x**). Whole limb GFP is shown for EP limbs. Expressing tissue appears as white/light grey. SJ; shoulder joint region, EJ; elbow joint region, CJ; carpal joint region.

5.3.6 The effect of overexpression of the Wnt antagonist Sfrp3 in the developing limb

5.3.6.1 Localisation of the electroporated Sfrp3 transgene expression

The mouse Sfrp3 full length cDNA sequence was altered to encode a Haemoglutinin (HA) epitope tag fused to the protein product, encoded in the expression vector used in electroporations (Appendix Figure C.2). The HA tag could therefore be used to detect transgene expression on sections of electroporated limbs using a HA specific antibody. Co-expression of HA and GFP was identified in the same cells, as shown for 3 independent specimens in Figure 5.13 (red arrow heads a-a^{1}, b-b^{1}, c-c^{1}). No detection of GFP or HA was observed in the non-electroporated contra-lateral limbs (Figure 5.13d^{1}). Similarly no HA detection was demonstrated in Sham electroporated limbs (Data not shown).

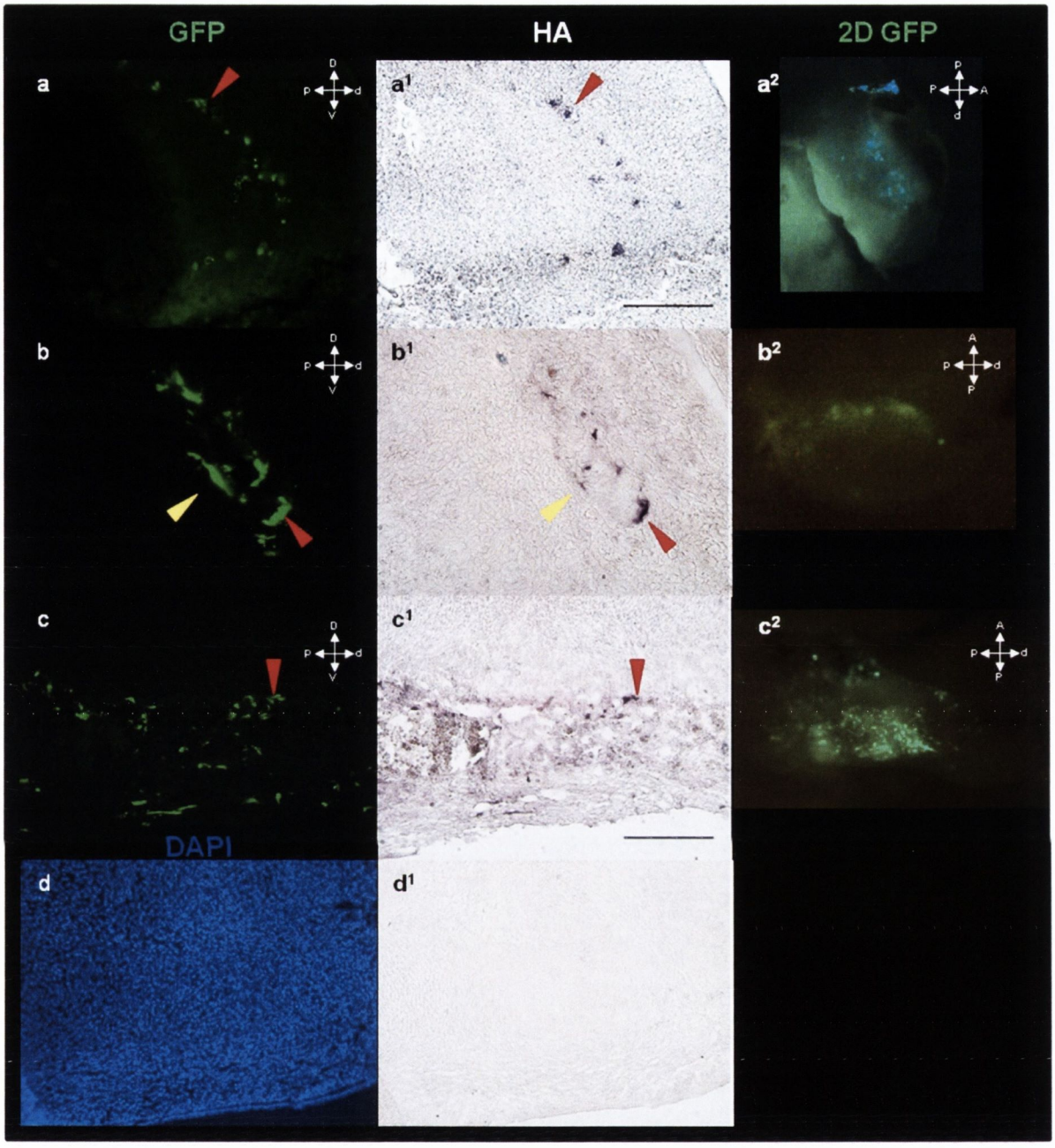

Figure 5.13: Detection of transgene expression in chick limbs electroporated with GFP and Sfrp3 expression vectors in 3 independent specimens (**a-c**) and in the non-electroporated contra-lateral limb of specimen c (**d**). GFP (**a,b,c**), HA-tag on the Sfrp3 protein ($\mathbf{a^1}$, $\mathbf{b^1}$, $\mathbf{c^1}$) expression were detected by immunolocalisation on wax sections. Embryo **a** is HH27, **b** and **c** are HH28. Images of whole limb GFP expression for the individual electroporated limbs ($\mathbf{a^2}$, $\mathbf{b^2}$, $\mathbf{c^2}$). All scale bars 100μm. A; Anterior, P; Posterior, V: Ventral, D; Dorsal, p: proximal, d; distal.

5.3.6.2 Phenotypic effect of Sfrp3 ectopic expression on skeletal development

A total of 6 Sfrp3 EP embryos were analysed for phenotypic changes in *Col2a1* cartilaginous expression. In all cases the electroporated limb was the right forelimb, and, as previously (Section 5.3.5.2) compared to the contra-lateral non-EP limb and to sham electroporated

limbs. Through the use of the normal *Col2a1* expression pattern (Figure 5.6), the Sfrp3 electroporated specimens were staged (Table 5:7). In 5/6 Sfrp3 electroporated specimens development was delayed by 1 stage or less compared to contra-lateral controls. This compares to a slight delay in 2/5 specimens for sham controls.

Table 5:7: Stages of electroporated (EP) and non-electroporated (non-EP) forelimbs

Sham Electroporated			
Specimen	Stage when electroporated	**Stage of EP limb**	**Stage of non-EP limb**
		Based on *Col2a1* expression pattern	
1	HH25	HH26	HH26
2	HH24	HH26/27	HH27
3	HH26	HH27	HH27
4	HH25	HH27/28	HH28
5	HH26	HH28/29	HH29
Sfrp3 Electroporated			
1	HH24	HH27	HH27
2	HH24	HH26	HH27
3	HH26	HH27	HH27/28
4	HH26	HH26	HH28
5	HH25	HH26	HH27
6	HH25	HH28	HH29

Each EP limb was altered in size compared to the contra-lateral limb, shown in Appendix Figure C.6: with variability in the severity of effect; described in more detail below, for each specimen.

Specimen 1: A visible reduction in the intensity of expression of *Col2a1* was apparent in the whole EP limb compared to the contra-lateral limb (Figure 5.14g and m). Specifically in he humerus (Figure 5.14red arrow) but this may be a consequence of lower level of *Col2a1* expression. There is a complete absence of expression in the radius (orange circles). The separation of expression between the humerus and ulna was greater in the EP limb compared to the non-EP limb; this could be due to an increase in the joint region, or due to a reduction in the extent of *Col2a1* expression in each element. The whole limb GFP image in Figure 5.14a, indicates that the localisation of GFP expression and the phenotypic alterations occur at the same position.

Specimen 2: A severe alteration in the size and shape of all the cartilage elements was observed in the electroporated limb in Specimen 2 (Figure 5.14h). A restricted extent of expression in the humerus, and ulna was observed (Figure 5.14h compared to n, red arrows) and in virtual longitudinal sections through these elements (Appendix Figure C.7 (2b)iii-iv). A complete absence of expression in the future radius was observed (indicated by the orange circles in Figure 5.14h and n), and the absence of detection in transverse and longitudinal sections in Appendix Figure C.7 (2b) (i-iv). The shape of the humerus and ulna appear more 'rounded' in comparison to the normal cylindrical shape displayed in the stage matched control limbs and the contra-lateral limb. Longitudinal sections confirm this variation in shape (Appendix Figure C.7 (2b)). GFP was detected on the lateral surface of the limb, adjacent to the elements that display alterations in morphology.

Specimen 3: The only observable phenotypic alteration was an apparent absence of carpal elements in the EP limb (Figure 5.14i). However analysis of transverse and longitudinal virtual sections through the EP limb revealed faint expression distal to the ulna (Appendix Figure C.7). The whole limb view shows GFP expression is restricted to the base of the limb (Figure 5.14c) and no GFP was detected in virtual sections of the EP limb (data not shown), supporting the minimal disturbances observed.

Specimens 4 and 5: Severe alterations in the pattern of *Col2a1* expression was observed in the electroporated limbs in specimens 4 and 5. For both of these EP limbs GFP detection indicates transgene expression throughout the proximal-distal axis of the limb (Figure 5.14 white arrow in d, and in e). A reduction in the extent of *Col2a1* expression in the ulna and radius for both specimens was observed (Figure 5.14j & k, red arrows). Similarly to specimens 1 and 2, the localisation of GFP detected in the transverse and longitudinal sections, was adjacent to where the alterations in *Col2a1* expression were observed, in the distal portion of the limb (Appendix Figure C.7 (4b) i, ii, v). There was also an absence of carpal elements in specimen 4 (orange circle in Figure 5.14j).

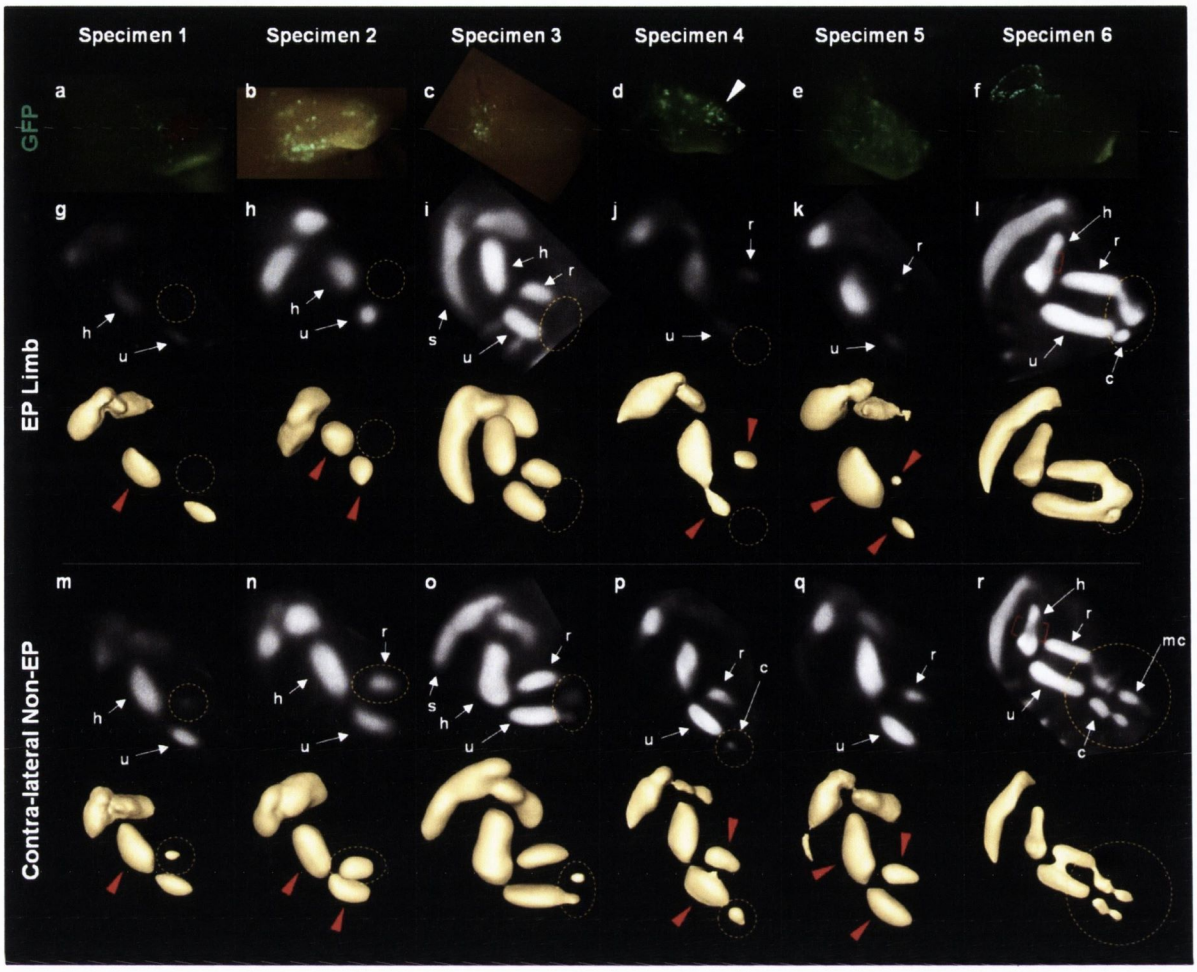

Figure 5.14: 3D analysis of *Col2a1* expression in Sfrp3 electroporated (EP) forelimbs (a-l), compared to contra-lateral non-electroporated (non-EP) limbs (m-r). Whole limb views of GFP expression in the corresponding EP limbs (a-f), Lateral views of 3D reconstructions of the expression data following OPT scanning (expressing tissue appears white/grey) and surface representation of Col2a1 expression is shown for 6 specimens (yellow images of surface expression). Orange circles indicate absence of element expression. Red arrows indicate alterations described. Red brackets indicate hypertrophy. s; scapula, h; humerus, u; ulna, r; radius, c; carpal, mc; metacarpals

Similar to specimens 1 and 2, the humerus of specimen 5 has a more 'rounded' morphology. GFP was detected on the distal and anterior surface of the EP limb, again in the vicinity of the effects supporting a proposal that the signalling antagonist is affecting the differentiation of adjacent cells and thus altering the pattern of *Col2a1* expression in developing cartilage.

Specimen 6 was the most developed Sfrp3 electroporated specimen analysed; at HH29 according to the *Col2a1* expression pattern in the non-EP limb (Figure 5.6). The expression of GFP was detected only at the proximal base of the limb and at the distal tip of the limb (Figure 5.14f). The only observable phenotypic alteration in the EP limb was at the distal end,

with reduced expression of carpal elements and a reduced separation of *Col2a1* expression between the radius and the carpal (Figure 5.14l). In both EP and non-EP control limbs, *Col2a1* expression in the humerus has started to fade at the mid-diaphysis, indicative of the initiation of hypertrophy (red brackets in Figure 5.14l). This suggests that hypertrophy and ossification of the humerus is not affected in this EP limb and the only effect is restricted to the distal extremity where transgene expression is localised.

To summarise, analysis of Sfrp3 electroporated embryos revealed that severe alterations were observed in 4 out of the 6 specimens analysed, and the severity of alterations corresponded to the extent and approximate location of GFP expression, and thus potential suppression of Wnt signalling. The two specimens that displayed minimal alterations (specimen 3 and 6) had the lowest quantity of visible GFP in the limb 24hours post electroporation (Figure 5.14c and f). The absence and alteration of elements in the most severely affected limbs suggests that it is not a delay in development as Table 5:7 might suggest, but it is hypothesised that the alterations are due to the alteration in Wnt signalling within these differentiating cells, thus affecting cartilage differentiation.

5.3.6.3 Analysis of Wnt target gene expression following Sfrp3 ectopic expression

Two Sfrp3 electroporated specimens were analysed for expression of the canonical Wnt target gene *Sfrp2*. One of the specimens showed no difference in expression in the EP limb compared to the non-EP limb. The intensity and extent of expression was very low in both limbs, with the highest level of expression detected in the mesenchyme adjacent to the developing vertebral column, indicating a HH26 embryo (Data not shown). The second Sfrp3 electroporated specimen, specimen 8, showed a general increase in *Sfrp2* expression in the EP limb compared to the contra-lateral limb. External views of volume representation through 360degrees of the same limb following OPT scanning and reconstruction and serial coronal sections through the whole specimen illustrate this increase in expression (Figure 5.15a-c). The difference in expression intensity in the shoulder joint (SJ) region is indicated in section

(c ii) comparing the non-EP to the EP limb. An increase in *Sfrp2* expression is evident in the ventral and dorsal regions of the shoulder in the EP limb, with high level of expression in section (c ii) (ventral) and (c vii) and (c viii) (dorsal). An increase in intensity of *Sfrp2* expression is also visible in the elbow joint (EJ) region of the EP limb (c iii) and (c iv). However, a restriction in the extent of expression is detected in the EP limb, expression in the non-EP limb is first detected in section (iii) and extents to section (viii), compared to the higher intensity of expression in the EP limb from section (ii) to (v) (Figure 5.15).

No difference in *Sfrp2* expression was observed in the limbs of the Sham electroporated specimens (n=2). A low level of *Sfrp2* was detected in one specimen, correlating to stage HH26 (specimen 6), the other specimen showed no difference in expression pattern between the EP and non-EP limbs (specimen 7) (Data shown in Appendix Figure C.8).

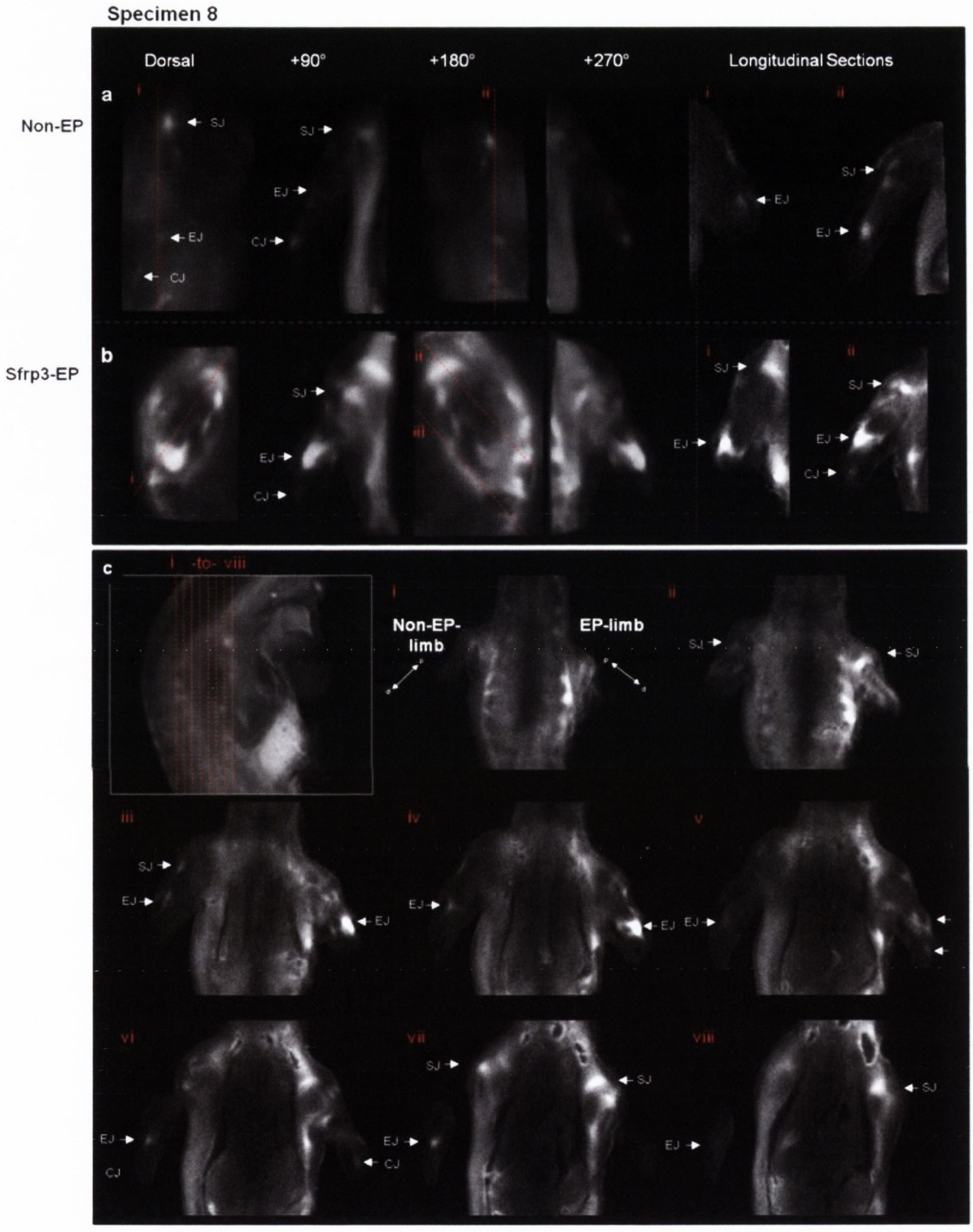

Figure 5.15: Analysis of *Sfrp2* expression in specimen 8 electroporated with Sfrp3. External views of volume representation of the same limb following OPT scanning and reconstruction are shown in **(a-b),** rotated +90°, rotated +180° and rotated +270°, (**a**) non-EP limb and (**b**) EP limb. Red lines indicate the plane of a virtual longitudinal (**i**) section for each limb (**c**). Coronal sections of *Sfrp2* expression through the whole specimen (i-viii). Expressing tissue appears as white/light grey. SJ; shoulder joint, EJ; elbow joint, CJ; carpal joint. p; proximal, d; distal.

5.4 Discussion

This study developed an approach to ectopically express transgenes in the developing limb during early chondrogenesis, designed to either activate or block Wnt signalling. Expression of both a canonical Wnt pathway activator and antagonist led to alterations in the pattern of chondrogenesis of the emerging skeletal rudiments, including alterations and absences of skeletal territories, as summarised in Table 5:8. This work set out to compare the effects of altering the Wnt pathway during limb skeletal development to the effects of reduced embryo movement to test the hypothesis that the alterations to Wnt signalling is a major component of the effects of reduced movement. While some similarities were noted, the comparisons that can be made are limited because of (a) limitations in the ability to target ectopic expression spatially in a precise manner and (b) a limited period of development following electroporation resulting in differences in timing of the observations and developmental events examined.

5.4.1 The challenge of targeting ectopic expression to the developing limb during skeletogenesis

To access and manipulate developing limbs at older stages a novel technique was established. *In ovo* electroporation of older chick specimens highlighted multiple difficulties including; poor visibility of embryos, lack of accessibility of limb tissue for manipulation, increased movement of older embryos limiting control of orientation and low viability of embryos. Comparative analysis of *in ovo* and *ex ovo* cultivation revealed no differences in the development of specimens but provides better access to the embryo. The basis of *ex ovo* cultivation consists of pouring the entire egg into a suitable container and taking precautions against excessive evaporation or bacterial infection. Shell-less culture systems have been described to investigate various developmental events, providing multiple advantages including access to the embryo, increased visibility for observations of morphogenesis and growth, and application of different exogenous agents (Datar and Bhonde, 2005). This proved to be a successful cultivation strategy that increased the survival of embryos and allowed for

direct targeting of the developing limb; however, the extent of cells expressing the transgenes and precise spatial control of targeted cells was limited.

A comparative technique to the one utilised in this study is the use of retroviral transmission to incorporate a particular gene product into cells. In theory once a cell becomes infected by a virus, every descendent of that cell maintains expression of the virus and inserted genes. However integration is limited to the mitotic phase of the cell cycle; consequently infection generally occurs in chicks at early developmental stages, resulting in a larger proportion of the embryo being infected. Use of retroviral transmission directly into the lateral plate mesoderm has allowed the study of early axis patterning of the chick limb (Logan and Tabin, 1999). Misexpression through viral injection into the lateral plate mesoderm at HH10-12 can have adverse effects on survival and analysis of later skeletal development, due to the widespread infection of the virus. Targeted viral injection approach at HH21-23 prior to chondrogenic condensations has been used to study later skeletal events; for example viral driven Ihh expression in the chick limb has been invaluable in the understanding of chondrocyte biology (Vortkamp et al., 1996). Viral infection techniques are very effective but can have broader effects than those required, so electroporation was chosen as a means of potentially targeting tissues more precisely, temporally and spatially.

While *in ovo* electroporation has been used widely to mis-express genes in various territories; including the eye, the neural tube and the somites (Islam et al., 2012; Krull, 2004; Miller-Delaney et al., 2011), studies targeting the developing limb are limited. All studies targeting the developing limb by electroporation have been performed *in ovo* and at stages earlier to this study. The first report of limb electroporation was performed at HH10-12 with very low voltage regimes (12-16V, 1-3times with a 90ms duration) (Takeuchi et al., 1999). A study of muscle development performed electroporation on HH13/14 limbs using a higher voltage (25V) once for 30ms (Yamamoto and Kuroiwa, 2003). The latest study of limb targeting described used HH19-22, significantly earlier than stages of interest here, using a higher

voltage regime (45V, once for 50ms duration) (Durand et al., 2010; Sabherwal et al., 2007). Multiple variations exist for the voltage regimes (15-70V) reported to be applied to different developing tissues types (neural tube, limb bud mesencyhme, spinal cord, diencephalon), across various stages (HH10-22), for multiple durations (30-90ms) and repetitions (1-7) (Croteau and Kania, 2011; Krull, 2004; Martinelli and Fan, 2007; Miller-Delaney et al., 2011; Misra et al., 2012; Sabherwal et al., 2007; Sharp and Fromherz, 2011; Winning and Krull, 2011). Following optimisation, the regime found to be most successful included 6 repetitions of 25V for 60ms with 100ms separation.

In this study early attempts to use *in ovo* electroporation revealed some of the issues of targeting the limb due to poor visibility of older embryos, the shell reducing accessibility and the increase movement displayed by older embryos. The use of the *ex-ovo* system overcame several of these limitations and was reported to support a high viability of normal development with 60.7% of *ex ovo* cultivated embryos surviving until at least E8; and 38.63% of electroporated embryos surviving 24 later. The method thus allows improved access to target the limb and this offers a great advantage for manipulation and analysis of later skeletal development.

5.4.1.1 Tissue distribution of electroporated cells

Following optimisation of the cultivation method some issues remained that limited control over the site and extent of targeted cells. Co-electroporation of the GFP construct with our Wnt pathway modulator was a valuable resource that aided further analysis of individual specimens. In this study the co-electroporation involved the combination to two constructs with a visible green dye that was used to monitor the transfer of solution from the capillary into the limb. To assess the tissue distribution of electroporated constructs, the first method was to examine the extent of DNA uptake and expression by viewing GFP expression in whole limbs. These superficial views indicated variation in the localisation of GFP within the limb, with some limbs showing proximal restriction, some showing distal restriction and

others with GFP throughout the whole limb, from anterior to posterior and ventral to dorsal. The localisation of GFP was secondly examined in tissue sections of EP limbs through secondary detection. GFP was assessed and in general was found to be located in the mesenchyme and ectoderm surrounding areas where *Col2a1*expression was disturbed.

To directly identify the electroporated cells that were expressing the Wnt modulator construct, two methods were employed, the first examining the RNA transcript for the transgene, and secondly through immunolocalisation of a tag epitope fused to the encoded protein within the expression vector. Detection of the constitutively active β-catenin was identified through both methods, but the RNA transcript detection was more sensitive in demonstrating positive cells indicating that the FLAG tag has reduced sensitivity although it was faintly visible in the nuclei of ISH positive cells. Detection of the FLAG tag however gave the important advantage of confirming that the protein product is produced, not just the transcript, and is localised to the nucleus. Detection of the pathway antagonist construct product Sfrp3 was successful through immunolocalisation of the incorporated HA tag, but this protein product is not restricted localised to the nucleus. Similarly to β-catenin detection, individual cells were visible through this method, and the parallel detection of GFP corresponded to co-expression of both electroporated constructs in most cases, with some exceptions. Variations in the extent of expression of co-electroporated vectors has previously been reported, with the extent of detected GFP expression being more widespread, for example in the developing neural tube (Miller-Delaney et al., 2011). Similar but non-identical patterns of co-electroporated GFP and RFP (red fluorescent protein) constructs were also reported in electroporated chick limb buds (Sabherwal et al., 2007). This could be due to differences in the efficiency of marker detection.

5.4.2 Altering Wnt signalling in the developing limb has profound effects on chondrogenesis

Expression of both a canonical Wnt pathway activator and general antagonist led to phenotypic alterations in the pattern of chondrogenesis in the emerging skeletal rudiments, including alterations, reductions and absences of skeletal territories, as summarised in Table 5:8.

Table 5:8: Summary of effects on limb skeletal development following Tcf-β-catenin and Sfrp3 ectopic expression.

Tcf-β-catenin ectopic expression				**Sfrp3 ectopic expression**			
Effect on chondrogenic pattern			**Transgene expression**	**Effect on chondrogenic pattern**			**Transgene expression**
Reduction or absence in	*Region*	*Specimen*	Localised to the affected region	Reduction or absence in	*Region*	*Specimen*	Localised to the affected region
	scapula	1, 2, 6, 7			humerus	2	
	humerus	2, 3, 6			ulna	2, 4, 5	
	ulna	1, 4, 5, 6,7			radius	2, 4, 5	
	radius	1, 2, 5, 6, 7			carpal	3, 4, 6	
	carpal	2, 3, 5, 6, 7		Shortened and Rounded	humerus	2, 5	
Interruption of chondrogenesis within the radius		2,4			ulna	2	
Up-regulation of *Sfrp2* target gene at shoulder and elbow joint		8, 9		Reduced *Col2a1* expression		1	Throughout limb

5.4.2.1 Electroporation alone causes no changes in *Col2a1* or *Sfrp2* expression

Results from sham electroporated embryos are an important component of this work for the correct interpretation of the phenotypic changes as a result of Wnt pathway modulation. All sham electroporated specimens analysed (n=7) had expression patterns corresponding to the same stages in the EP limb as in the non-EP contra-lateral limb. However a slight delay was noted in some cases indicating that the manipulation of the limb involved, may result in a slight delay in the development, reflected in the distal-most elements only.

5.4.2.2 Activation of canonical Wnt signalling inhibits chondrogenesis

Forced expression of stabilised β-catenin resulted in multiple malformations (n=9), with commonalities including reductions or absence of *Col2a1* expression in skeletal elements and interruptions in expression pattern in the radius (n=2). For 5/7 specimens analysed reductions

in expression were reported in the ulna, radius and carpals, 4/7 specimens displayed reduced expression in the scapula and 3/7 in the humerus (Table 5:8). A range of phenotypic alterations were displayed in individual specimens, with specimens 5, 6 and 7 showing the most sever phenotypes, and specimen 3 showing mild alterations. This variability in effect may be due to the localisation of the transgene as indicated by GFP in the whole limb; this supports the mild alteration shown in specimen 3 corresponding to low GFP levels.

It is important to note that the impact of expression of activated β-catenin would result in the direct alteration of canonical Wnt pathway target gene transcription and is cell autonomous in its direct effect. However it can also have indirect effects through altering the signalling capacity of that cell. The observed up-regulation of expression of the Wnt target gene *Sfrp2* (n=2) suggests that the stabilisation of β-catenin is resulting in target gene transcription. *Sfrp2* is expressed early in development in the limb mesenchyme surrounding cartilage condensations and then later becomes regionally restricted to be expressed within all synovial joints in the limb (Ikegawa et al., 2008; Witte et al., 2009). An increase in intensity of expression was seen in the elbow joint regions of both specimens analysed, and this is suggested to be due to the up-regulation of wnt signalling in these areas. Direct up-regulation of the pathway, can then feedback to cause further alteration of Wnt signalling and on other signalling pathways, so also having effects on neighbouring cells indirectly. This indirect mechanism of pathway activation may perhaps be having a broader effect on cells surrounding those expressing the transgene.

The forced expression of β-catenin in prechondrogenic cells in chick limbs was previously shown through viral infection, leading to shortened or missing skeletal elements due to an acceleration of chondrogenesis, as shown in Figure 5.16B (Hartmann and Tabin, 2000). This could explain the reduction and absence of cartilage gene expression observed here. The formation of mesenchymal condensation is reported to begin to occur in the developing chick limb at HH22 (Ahrens et al., 1977). The condensation of the mesenchyme is a very important

phase of skeletal development, as it acts as the future template for chondrogenesis that becomes segmented into individual skeletal elements later in development. The negative regulation of wnt signalling has been shown to be important during the condensation of mesenchyme, as an inhibition of chondrogenesis has been observed following the ectopic over-expression of wnt ligands; *Wnt1*, *Wnt7a*, *Wnt5a* and *Wnt14* (Hartmann and Tabin, 2001; Kawakami et al., 1999; Rudnicki and Brown, 1997). The observed reduction in size of the ulna and radius in all of the specimens electroporated with β-catenin, is in correspondence with phenotypic observations found following the ectopic over-expression of the Wnt ligand *Wnt5a*, which resulted in a profound reduction in the length of the radius and the ulna (Kawakami et al., 1999).

Variability in transgene and GFP uptake and the potential low density of cells expressing the construct has to be taken into account when interpreting the phenotypic changes in *Col2a1* expression. Detection of GFP in longitudinal sections of EP limbs indicated that uptake and expression of the construct was occurring more in marginal cells of the limb and less within core condensations. In light of this, a report that describes the removal of the Wnt6 expressing dorsal ectoderm resulted in the up-regulation of early chondrogenic genes *Sox9* and *Col2a1*; supporting our results that disturbances of Wnt signalling can have major effects on chondrogenesis at a distance (Geetha-Loganathan et al., 2010).

To understand Wnt signalling during correct skeletal development, multiple studies have used sophisticated mouse models to remove and over-express wnt signalling components in particular cell types to understand in more detail the role of the pathway. Activation of β-catenin through mice that carry a conditional β-catenin allele, upon Cre recombination produces a stabilised form of β-catenin (Harada et al., 1999). Embryos expressing stabilised β-catenin (*β-cat*Δex3$^{Prx/+}$) in the limb mesenchyme displayed limbs with an extreme effect, that contained only tiny remnants of skeletal elements (Hill et al., 2005) (Figure 5.16C). Activation of β-catenin in *Col2a1* expressing cells (β-*catenin*$^{+/flox(ex3)}$; *Col2a1-Cre*) show

severe skeletal malformations, including reductions in the size of the limbs, specifically the size of the ulna (Akiyama et al., 2004) (Figure 5.16D). The phenotypes observed following over expression of β-catenin support the proposal that the up-regulation of canonical wnt signalling in the limb at this stage of development, negatively affects skeletogeneisis, limiting mesenchymal cells from differentiating into skeletal precursors.

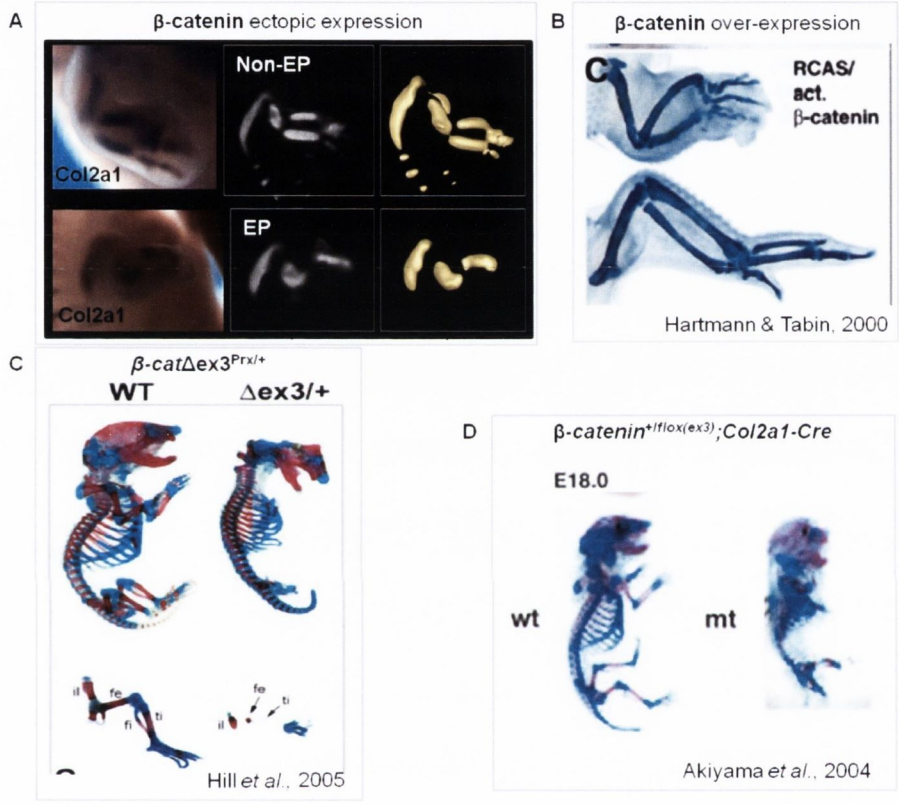

Figure 5.16: Similarities in skeletal phenotypes demonstrated in Chick and Mouse studies that have over expressed β-catenin directly or through ectopic expression. (**A**) Dorsal *Col2a1* expression of non-EP and EP limb (specimen 7) (**B**). Retroviral over-expression of β-catenin, Alcian Blue staining at E9.5, Viral injected right wing on top of the uninjected contra-lateral control left wing, β-catenin infected limbs show a severe shortening of the ulna (Hartmann and Tabin, 2000). (**C**) Alizarin red and alcian blue stained skeletal preparations of wild-type and β-catΔex3Prx/+ mutant embryos at P0, magnification of hindlimb (Hill et al., 2005). (**D**) Severe, generalized chondrodysplasia in β-catenin+/flox(ex3);Col2a1-Cre embryos. Skeletons of E18.0 embryos stained by alcian blue followed by alizarin red (Akiyama et al., 2004). All images are adapted from references.

5.4.2.3 Suppression of Wnt signalling interferes with normal rudiment size and shape

Suppression of Wnt signalling demonstrated malformations in the *Col2a1* expression patterns. A reduction or absence of *Col2a1* expression was seen in 4/6 specimens, while 2 specimens

showed shortening and rounded humeri and ulna (specimen 2 and 5). One specimen showed an overall reduction in the intensity of expression, which was not seen in any other specimen analysed (Table 5:8). To note, over-expression of the pathway antagonist Sfrp3 operates at the extracellular level, the effect of incorporation of this construct into few cells in the limb could thus have a more widespread effect on multiple surrounding cells; as well have direct effects on the cells that express it.

The shape change in the humerus and ulna of specimen 2 and 5 to a shortening and less elongated pattern of expression is similar to that previously described in a study that over-expressed Sfrp3 using viral infection in chick limbs. Infected rudiments displayed a shortening and widening of the radius, accompanied by bending of the ulna, and no sign of endochondral ossification (Enomoto-Iwamoto et al., 2002). Conditional inactivation of β-catenin has been studied in various cells within the developing limb including the ectoderm, chondrocyte (*Col2a1*) expressing cells and in mesenchymal progenitor cells. Overall analysis of these inactivation models demonstrate multiple limb specific skeletal abnormalities indicating the importance of β-catenin mediated Wnt signalling for both joint and bone development.

Restricted removal of β-catenin in limb ectodermal cells (*Brn4Cre:βcatenin*$^{flox/flox}$) resulted in variable hindlimb deformations, including truncations of the proximal femur, digenesis' of the tibia and fibia and loss of digits 1-4 (Soshnikova et al., 2003). Inactivation of β-catenin in *Col2a1* expressing tissues resulted in variable joint loss and fusions, with more severe joint absence found in the distal joints of the ankle and tarsals (Guo et al., 2004). Guo and colleagues suggested that the timing of *Cre* expression in the *Catnby*$^{c/c}$*;Col2a1-Cre* model was the reason for this, as the *Col2a1* promoter is inactivated in the interzone that forms soon after chondrocyte differentiation, so the joint interzone cells only briefly express *Cre* in the *Col2a1-Cre* mice, but this might not be enough to inactivate β-catenin to stop joint formation early. But as the ankle and tarsal joints form later (at E15.5) it may be enough time to remove

β-catenin to disrupt their formation (Guo et al., 2004). To inactivate β-catenin earlier the use of another Cre system has been used; *Catnby$^{c/c}$;Dermo1-Cre* inactivating β-catenin in mesenchymal progenitor cells, resulted in synovial joint fusions (Guo et al., 2004) and long bones that were shorter, thicker and bowed due to abnormal osteoblast and chondrocyte differentiation (Day et al., 2005). This shorter and thicker description of the cartilage elements is similar to what was observed in the humerus and ulna of specimen 2 and 5 in the EP limbs. Inactivation of β-catenin in *Col2a1* expressing chondrogenic cells similarly resulted in long bones that were shorter, thicker and bowed (Day et al., 2005). In these shorter limbs, it was found that many areas of chondrocyte specific staining was lost including in the ulna, radius and humerus; and it was suggested that chondrocytes had lost their characteristic cellular phenotypes and may have adopted other cell fates (Guo et al., 2004). Early inactivation of β-catenin in the Prx1-Cre line (*β-cat*$^{\Delta Prx/-}$) showed complete removal of β-catenin in forelimb mesenchyme at E10.5 and hindlimb at E11 (Hill et al., 2005). Appendicular long bones were shortened, partially fused and lacked distal structures, with the forelimb more dramatically affected than the hindlimb (Hill et al., 2005), corresponding to the onset of Prx1-Cre activity (Logan et al., 2002) .

The up-regulation of the Sfrp2 target gene in the EP limb that contains the extracellular antagonist cannot be clearly interpreted, as it is data from one specimen. This analysis of the target gene needs to be expanded using more specimens as to be able to interpret the results seen here in more clearly.

5.4.3 Insight into Mechanoregulation of Skeletogenesis

This study aimed to test the hypothesis that disturbances to Wnt signalling contribute to the effects seen when the mechanical environment is altered. To draw conclusions from the work presented in this chapter, when the pathway is ectopically activated and when it was suppressed, we compared the phenotypic disturbances seen in these two scenarios (Table 5:8)

to the disturbances seen when the mechanical environment is altered. The most prominent disturbances seen when the mechanical environment is altered includes alterations in the correct patterning of territories in the developing joint and in the correct pattern of ossification. Both phenotypic disturbances demonstrate changes in the molecular landscape, as indicated by the identification of genes that are differentially expressed in these distinct territories (chapter 3/ chapter 4). Disturbances in the *Col2a1* and *Sfrp2* expression pattern have been demonstrated in both contexts; however showing different effects. The alteration in the *Col2a1* pattern in the TS23muscle-less mutant humerus and associated joints shows no reduction in expression, but the pattern is altered compared to control expression, supporting the phenotypic disturbances seen. The 3D pattern of *Col2a1* seen following ectopic over-expression and suppression of canonical wnt signalling does not match those seen in the altered mechanical environment, as reductions, complete absence, interruptions and shape changes were associated with the phenotypic disturbances seen in these cases.

A similarity in both contexts is the expression pattern of the wnt target gene, *Sfrp2*. An up-regulation of this gene was shown in the elbow and shoulder joints in the muscle-less mutant, and in both contexts when canonical wnt signalling was mis-expressed through electroporation. The spatial up-regulation of wnt signalling in the developing joint of muscle-less mutants was demonstrated through the up-regulation of the wnt ligand, Wnt4, and the alteration of target genes (Sfrp2 and Cd44). The preliminary down-stream analysis of wnt targets following electroporation is reported in this chapter, however further analysis of these and other targets are required to understand in more detail whether activation or suppression of the pathway is affecting the same tissue territories as those in the reduced mechanical environment.

It is difficult to draw any conclusions about the relationship of wnt signalling to the mechanical environment at this time of analysis, with future work needed on more specimens for down-stream target genes and at latter time stages of development. Two concerns that

need to be addressed following this study are that (1) due to the nature of the approach, limited control over where and how many cells expressed the construct became apparent during analysis, and (2) the duration of incubation for further development post EP was too short (24hrs); in order to see if alteration of the pathway has any effects on hypertrophy and ossification, as seen in the muscle-less mutant, post-EP time periods must be extended. Further refinement of the approach established here, in term of generation of transgenic embryos in site specific regions and the systemic analysis of them using 3D imaging is required to interpret the how Wnt signalling contributes to the effects seen when the mechanical environment is altered.

5.5 Conclusion

This study has established an *in vivo* approach to show that alterations of Wnt signalling in the developing limb has gross phenotypic effects on the development of the cartilaginous skeleton. This work has established a basis for future work that is required to target the transgenic introduction into the joint and/or the rudiment separately.Future work should attempt to increase the numbers of transgenic cells in these regions, and then maintain these specimens and observe their development over longer periods of time. This *ex ovo* approach has the potential to be utilised to alter Wnt signalling in conjunction with altering the mechanical environment, through chemically induced immobilisation. This combined study could identify if alterations seen with immobilisation could be potentially rescued by mis-expression of Wnt signalling; and this could help to directly specify the point of integration between mechanical stimuli and molecular regulation for correct skeletal development.

Chapter 6:

6. The influence of mechanical stimulation on chondrogenic differentiation from adult* and embryonic cell sources

* Work with porcine derived adult cells described in the chapter was published in Vinardell T., Rolfe R.A., Buckley C.T., Meyer E.G., Ahearne M., Murphy P., Kelly D.J.: Hydrostatic pressure acts to Stabilise a chondrogeneic phenotype in porcine joint tissue derived stem cells. *Journal of European Cells and Materials,* Vol 23; 2012; 23: pages 121-134

Statement of Contribution

I would like to acknowledge other members of my research group who were involved in specific components of the work presented in this chapter. Mouse embryonic limb bud micromass optimisation and application of Hydrostatic Pressure on micromass cultures was done in collaboration with Anurati Saha. Mouse adult derived progenitor cell work optimisation was performed in collaboration with Claire Shea. Porcine adult derived progenitor cell work was performed in collaboration with Dr. Tatiana Vinardell. Figure 6.3 and Figure 6.5 produced by Dr. Tatiana Vinardell.

6.1 Introduction

The work described in previous chapters focuses on the molecular programmes that control skeletogenesis in the embryo and how they are modulated by mechanical stimulation from embryo movement. This chapter aims to address whether knowledge gained from the developing embryo can be applied to improve *in vitro* differentiation regimes to engineer phenotypically stable cartilage, appropriate for repairing articular cartilage, using stem cells.

Articular cartilage is the tissue that lines the ends of bones within synovial joints and allows for low friction movement. Overtime, repeated trauma to or disease of the articular cartilage can lead to the clinical syndrome Osteoarthritis (OA) (reviewed in Martin and Buckwalter, 2002). Due to its avascular and aneural nature, articular cartilage has a limited ability to regenerate and repair itself. Clinical features of OA include the breakdown of cartilage matrix, the erosion of the cartilage surface and inflammation within the synovial cavity. Therapies for OA aim to relive the symptoms associated with the disease including pain and inflammation; with the goal to optimise biomechanics in affected joints. If the conditions deteriorate and little or no cartilage remains, the bones can rub against one another causing immense pain; and at this stage joint replacement is often the only therapeutic option. Investigation into the development of techniques for regenerating articular cartilage as a more sustainable and less invasive solution to joint replacement are currently being pursued.

Tissue engineering applies the principles from biology and engineering for the development of functionally viable tissues; in the case of articular cartilage damage, to restore normal biomechanical function. Numerous aspects have been investigated including the type of cells, the biomaterial scaffolds and the environmental factors that can be utilised to engineer functional cartilage (reviewed in Kelly and Jacobs, 2010). The use of progenitor cells derived from adult tissues, e.g. Mesenchymal Stem Cells (MSCs), for repair of cartilage damage is very attractive given their potential for proliferation and differentiation (Pittenger et al., 1999). Bone marrow derived cells are most commonly studied, however cells isolated from

synovial joint tissues such as the synovial membrane (Pei et al., 2008) and the infrapatellar fat pad (IFP) (Khan et al., 2008) are of particular interest given their location. A major issue in attempts to use MSCs, for regeneration of articular cartilage, is that the cartilage formed has a tendency to undergo hypertrophy and endochondral ossification (Dickhut et al., 2009; Pelttari et al., 2006; Richter, 2009), resembling the differentiation of chondrocytes within the skeletal rudiment of the embryo which lay the template for invading osteoblasts, self-destructing to be replaced by bone, rather than the stable maintenance of chondrocytes at the future articular sites. The maturation to hypertrophy is marked by the activation of the Ihh gene and a switch from predominant expression of Collagen type II (*Col2a1* gene) to Collagen type X (*Col10a1* gene).

It is therefore critical that the mechanisms that distinguish permanent articular cartilage and transient pre-ossification cartilage differentiation are understood in order to be able to control differentiation. It is clear that different regulatory systems act on embryonic cells within the skeletal rudiment where cartilage undergoes hypertrophy and is replaced by bone, and at the joint site where stable cartilage persists (section 1.2). Our research group has shown that the maintenance and further differentiation of cell territories in the embryo that will go on to form the articular cartilage depends on mechanical stimulation from movement; these cells are mis-specified in immobilised embryos (Nowlan et al., 2010a; Roddy et al., 2011b). The work reported in chapters 3 and 4 characterising the molecular response to movement, clearly show differential responses in ossifying rudiments and at joint sites.

One of the main aims of the work described in this chapter was to examine the effect of mechanical stimulation in the form of hydrostatic pressure (HP) on chondrogenesis in embryonic and adult derived stem cells. Previous computational modeling of the mechanical environment generated by muscle contractions demonstrated that dynamic, spatially organised patterns of HP and fluid flow are experienced by the cells of the interzone as the joint in forming (Roddy et al., 2011a). Hydrostatic forces play an important role in many biological

systems, transducing forces in hydrated or fluid filled tissues such as bone, cartilage and joint synovium generated by dynamic changes in pressure. HP has been implicated as a key regulator of MSC differentiation and numerous studies have demonstrated that cyclic HP leads to chondrogenic gene expression and proteoglycan and collagen synthesis (Angele et al., 2003; Elder et al., 2005; Meyer et al., 2011; Miyanishi et al., 2006a; Miyanishi et al., 2006b; Steward et al., 2012; Wagner et al., 2008). Recently, application of cyclic intermittent HP on chick limb bud micromass cultures similarly resulted in an increase in cartilage matrix production and an increase in expression of chondrogenic specific transcription factors (Juhasz et al., 2014).

The use of progenitor cells isolated from adult tissue is evidently an attractive source of cells for regenerative strategies; however it has not yet been established if cells derived from adult tissues respond in a similar way to embryonic cells during joint development. For that reason another aim of the work described in this chapter was to compare the response of embryonic and adult derived progenitor cells. Micromass culture is a common assay used to examine chondrogenic differentiation in embryonic cells (reviewed in Handschel et al., 2007); Micromass culture of mouse limb bud cells is used here to examine the effect of HP on the stability of chondrogenic differentiation.

The pig is a common source of adult progenitor cells for tissue engineering strategies to differentiate bone and cartilage (Bernstein et al., 2009; Buckley et al., 2010; Choi et al., 2010; Kumar et al., 2007; Thorpe et al., 2008). The number and accessibility of cells available from porcine adult joint sources far outweigh the numbers obtained from the mouse. Therefore porcine joints were utilised in parallel in order to compare embryonic responses to chondrogenic differentiation with an established chondrogenic culture regime. The availability and distinct territories of tissue within the porcine adult joint also allowed for sub-selection of different regions of progenitor derived cells to be compared to embryonic limb bud differentiation. *In vitro* Chondrogenesis has previously been reported to be dependent on

the concentration of supplemented TGFβ (Johnstone et al., 1998), however the interaction of mechanical stimulation and TGFβ supplementation for the initiation and maintenance of chondrogenesis remains poorly understood.

In this chapter I test the hypothesis that mechanical stimulation in the form of hydrostatic pressure can contribute to the differentiation of stable cartilage. The specific aims were:

1. To establish the chondrogenic differentiation profile of adult derived and embryo derived cells, including examining the effect of TGFβ on the differentiation of adult derived cells from different sources

2. To examine and compare, through quantitative gene expression changes, the effect of HP on hypertrophic maturation of chondrogenically differentiated cells from embryonic limb buds and adult derived progenitor cells.

In addition, mouse MSCs were derived and characterised in order to carry out similar comparisons on cells from the same species, in the future. I propose that the correct combination of mechanical and biochemical signalling is required to direct appropriate differentiation and maintenance of stable cartilage, preventing maturation and hypertrophy.

6.2 Methods

6.2.1 Isolation of embryonic mouse progenitor cells: Micromass and pellet culture

Embryonic forelimbs and hindlimbs were aseptically dissected from E11.5 mouse embryos. Limb buds were dissociated in 0.1% Tripsin EDTA for 30 minutes at 37°C. The reaction was stopped with addition of an equal volume of FBS (Foetal bovine serum) and the resultant cell suspension was triturated with a flame polished glass pipette, passing the cells through 15 times, then passed through a 70μm pore-size cell sieve. The cells were centrifuged at less than 1000rpm for 2 minutes and re-suspended in Growth medium (GM; Dulbecco's Eagle Medium F-12 Ham (DMEM/F12), 2Mm L-Glutamine, 100U Penicillin, 100μg/ml Streptomycin, 50μg/ml of Ascorbic acid and 10% FBS). For micromass cultures, spots were either plated directly on plastic multiwall dishes or on individual cover-slips at a density of 0.5-1 $x10^5$ cells per 10μl spot. Coverslips were previously treated with poly-Lysine or polyDLOrnithine. Medium was replaced ever second day.

Embryonic pellet cultures were formed by placing 250,000 cells in a 1.5ml conical microtube (Eppendorf) and centrifuged at 650G for 5 minutes. The pellets were cultured in a chemically defined chondrogenic medium (CDM): DMEM-F12 supplemented with 100U/ml penicillin/streptomycin, 100μg/ml sodium pyruvate, 40μg/ml L-proline, 50μg/ml L-ascorbic acid-2-phosphate, 4.7μg/ml linoleic acid, 1.5mg/ml BSA, 1×insulin–transferrin–selenium, 100nM dexamethasone (all from Sigma-Aldrich, Ireland). The pellets were cultured in conical microtubes with different concentrations of human TGF-β3 (Prospec, Israel) 0, 1 and 10ng/ml. Medium was exchanged every 3 or 4 days.

6.2.2 Cell isolation and Expansion of Adult derived Mouse progenitor cells

CD1 and C57BL6 adult mice (8-10week old) were used for harvesting joint derived progenitor cells. Hindlimbs were dissected at the pelvis, briefly dipped in 70% ethanol and the skin was pulled towards the foot and cut at the anklebone. This eliminated further contact with the animal's fur, to reduce contamination. Limbs were washed in sterile DMEM

supplemented with 100U/ml penicillin/streptomycin. All muscle and connective tissue was dissected from the femur and tibia prior to the dissection of the articular cartilage from the knee joint. Using a fine scalpel cartilage was sliced off and collected from multiple knees for dissociation. Slicing of cartilage was performed in a petri-dish prior to chemical digestion. Digestion of articular cartilage was performed for 16-18 hours under constant rotation at 37°C with 350U/ml collagenase (Gibco, #17104-019) in DMEM. Digestion was then stopped with 10% FBS, the resulting cell suspension filtered through a 40μm pore-size cell sieve (Falcon Ltd, Sarstedt, Ireland) and the filtrate centrifuged and rinsed with PBS twice. Articular cartilage derived stem cells were seeded at a density of 5×10^3 cells/cm^2 in a humidified atmosphere at 37°C and 5% CO_2. Medium for expansion contained DMEM-GlutaMAX supplemented with 100U/ml penicillin/streptomycin and 10% FBS and was changed every third day. The morphology and proliferation of the cells was monitored over time.

To harvest the bone marrow, both ends of the femur were cut just below the end of the marrow cavity. Using a 21 or 27-gauge needle, 1ml of growth medium (DMEM-GlutaMAX supplemented with 100U/ml penicillin/streptomycin and 15% FBS) was flushed through the spongy bone and collected. A 16-gauge needle was used to triturate the cells. The cell suspension was filtered through a 70μm cell sieve, cells counted and plated at a density of $2x10^6$ cells/cm^2; cells were incubated in a humidified atmosphere at 37°C and 5% CO_2. After 3-5hours the non-adherent cells were removed and medium was replaced. The following day the non-adherent cells were removed and the medium was changed. Medium was changed every 3-4 days. The morphology and proliferation of the cells was monitored over time.

6.2.3 Cell isolation and Expansion of Adult derived porcine progenitor cells

Chondrocytes (CC) and joint tissue derived stem cells were aseptically harvested from four month old pigs (two donors). Chondrocytes (CC), Infrapatellar Fat Pad (IFP) and Synovial Membrane (SM) of the femoropatellar joint were isolated. Cartilage was incubated with DMEM/F12 containing collagenase type II (125U/mg) (all from Sigma–Aldrich, Ireland) for

16-18 hours under constant rotation at 37°C. The resulting cell suspension was then filtered through a 40μm pore-size cell sieve (Falcon Ltd, Sarstedt, Ireland) and the filtrate centrifuged and rinsed with PBS twice. SM and FP tissues were harvested, sliced and rinsed with PBS (Sigma–Aldrich, Ireland) containing penicillin/streptomycin (200U/ml) (GIBCO, Biosciences, Ireland) and amphotericin B (2.5μg/ml) (Sigma–Aldrich, Ireland). SM and FP pieces were incubated with DMEM GlutaMAX (GIBCO, Biosciences, Ireland) containing collagenase type II (315U/mg) (Worthington, Langanbach Services, Ireland) for 3-4 hours under constant rotation at 37°C. The resulting cell suspension was then filtered through a 40μm pore-size cell sieve (Falcon Ltd, Sarstedt, Ireland) and the filtrate centrifuged and rinsed with PBS twice. CC, SM stem cells and FP stem cells were seeded at a density of 5×10^3 cells/cm^2 in 175 cm^2 T-flasks and expanded to passage one in a humidified atmosphere at 37°C and 5% CO_2. Viable cells were counted using a hemacytometer and 0.4% trypan blue staining. Isolated cells from different tissues were maintained in DMEM GlutaMAX supplemented with 10% FBS (GIBCO, Biosciences, Ireland) and 100U/ml penicillin/streptomycin during the expansion phase with 5ng/ml of human FGF-2 (Prospec, Israel).

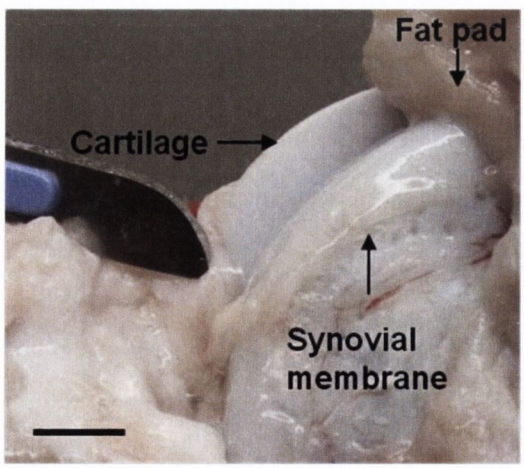

Figure 6.1: Picture of a porcine knee joint showing different structures of the joint used for cell extraction. Scale bar 2cm.

CC, SM and FP were all grown in pellet cultures. 250,000 cells were placed in 1.5 ml conical microtubes and centrifuged at 650G for 5minutes to form pellets. The pellets were cultured in

a chemically defined chondrogenic medium (CDM) (as section 6.2.1). The pellets were cultured with different concentrations of human TGF-β 3 (Prospec, Israel) 0, 1 and 10ng/ml. Medium was exchanged every 3 or 4 days.

6.2.4 Tripotentiality differentiation assay of adult mouse derived MSCs

Pellet cultures of 250,000 cells per pellet were grown in chondrogenic conditions as described in section 6.2.1. Pellet cultures were grown for 21 days and medium changed twice a week. Following the culture period the pellets were fixed in 4% PFA, paraffin wax embedded, sectioned and stained with 1% Alcian Blue (as section 6.2.6).

Adipogenic differentiation was performed in 2D cultures and cells were plated at a density of $1x10^3$ cells/cm^2. Adipogenic differentiation was started when cells were ~80% confluent and differentiated for 21 days. Culture medium included DMEM-GlutaMAX supplemented with 100U/ml penicillin/streptomycin, 10% FBS, 100nM dexamethasone, 0.5mM isobutyl-1-methyl xanthine (IBMX) and 50μM indomethacin. Media was changed every 2-3 days. Following 21days in culture, plates were fixed in 4% PFA and stained in 1% Oil Red-O solution for 30mins, positive differentiation is indicated by over 30% of the surface stained red.

Osteogenic differentiation was performed in 2D cultures with cells were plated at a density of $1x10^3$ cells/cm^2. Osteogenic differentiation was started when cells were ~80% confluent and differentiated for 21 days. Culture medium included DMEM-GlutaMAX supplemented with 100U/ml penicillin/streptomycin, 10% FBS, 100 nM Dexamethasone, 10mM betaGlycerol Phosphate and 0.05mM Ascorbic Acid. Media was changed every 2-3 days. Following 21days in culture, plates were fixed in 4% PFA and stained in 1% Alizarin Red for 30secs-2mins. Calcium deposits are stained orange-red.

6.2.5 Application of Hydrostatic pressure

For application of HP to micromass cultures, cover-slips containing a single micromass spot were placed onto a 6% agarose mould and covered with 1.8% Low melting point agarose to hold the coverslips in place. Moulds containing 5-6 coverslips were placed into heat-sealable, gas permeable, sterile bags (EVO120, Quest Biomedical, UK). Bags were heat sealed, air removed and filled with 6ml of medium. Medium was replaced every day. The constructs undergoing HP were placed into a pressure vessel (Figure 6.2) immersed in water and the free swelling (FS) controls immersed in water at 37°C during the loading period. Loading was applied at 1MPa of HP at a frequency of 1Hz for 4hr per day, for 8 consecutive days. A stainless steel pressure chamber (Parr instruments company, Moline, IL, USA), connected to a piston (phd Inc., Irish Pneumatics, Ireland), driven by an Instron 8801 materials testing machine was used to generate the required levels of HP.

For application of HP to pellet cultures, pellets (10 or 12 per group) were sealed in sterile plastic bags with 4 ml of chondrogenic medium with different concentrations of TGF-β3. The pellets were assigned to receive either mechanical stimulation (HP group), or were left unloaded (Free swelling: FS group). The loaded group was exposed to 10MPa of HP at a frequency of 1 Hz for 4 h per day, for 14 days, while the unloaded controls were kept in bags in an incubator immersed in water at 37°C during the loading period. After loading all pellets were returned to microtubes.



Figure 6.2: Setup of Hydrostatic pressure loading, Heat sealed gas permeable sterile bags containing constructs were placed into the pressure vessel (HP loading (left)) or into the water filled beaker (FS control (right)).

6.2.6 Histology

Proteoglycan synthesis of cultured cells was evaluated by alcian blue. Micromass cultures were fixed in 4% PFA for 45mins and then stained in 1 % Alcian blue (pH1) (8GX, A5268, Sigma) in water for 10-30mins at RT and washed in PBS. The alcian blue-stained cartilage nodules were photographed and counted. The area covered in a field of view (x20 magnification, 2 images) for the FS and HP conditions were compared and displayed as percentage of area.

Pellets were sectioned following paraffin embedding; 5μm sections were cut and mounted on to Superfrost slides. Slides were re-hydrated through a series of ethanol washes and then stained with 1% Alcian blue (pH1) or 0.1% Picro-sirius red (265548, Sigma) in water. Alcian Blue stains sulphated mucins blue and Picro-sirius red stains collagen red.

6.2.7 RNA Extraction

Quantitative real-time reverse transcription-polymerase chain reaction (RT-PCR) was used to determine the relative gene expression changes in chondrogenic specific genes over time and subsequent to the application of loading.

Micromass: RNA was extracted from E11.5 limbs buds following dissection as time 0. For total RNA extraction from micromass cultures, pooling of coverslips was performed to increase yield of RNA (n=4 coverslips per condition). Physical homogenisation using a motor driven pestle and mortar system (Sigma-Aldrich, Ireland) in 1ml of TRIZOL reagent (Invitrogen) was followed by a chloroform (Sigma-Aldrich, Ireland) extraction and RNA was purified with PureLink™ RNA Mini kit (Invitrogen) as per manufacturer's instructions. RNA was re-suspended in RNase free water and quantified using a NanoDrop® (ND-1000).

Porcine: Total RNA was extracted from SM, FP and CC pellet constructs following culture for 14 days and the application of HP. Day zero groups were harvested following centrifugation and formation of cellular pellets. Loaded and unloaded groups were harvested directly after the application of loading at day 14. Pellet construct pooling was performed for all groups, with a total of 4-5 pellets per group. Total cellular RNA was extracted from each pellet group by physical homogenisation using a motor driven pestle and mortar system (Sigma-Aldrich, Ireland), followed by a chloroform extraction and purification of RNA with PureLink™ RNA Mini kit (Invitrogen) as above.

6.2.8 Quantitative Real-Time Polymerase Chain Reaction

To quantify mRNA expression, 100ng of total RNA was reverse transcribed into cDNA using iScript™ cDNA systhesis kit (BioRad) as per manufacturer's instructions. TaqMan® gene expression Assay's (for all primer details refer to each individual code below from Applied Biosystems) which contain forward and reverse primers, and a FAM-labelled TaqMan probe were utilised for porcine pellet cultures (*Sus Scrofa*) *Sox9* (Ss03392406m1), *Acan* (Ss03374822m1), *Col1a1* (Ss03373340m1), *Col2a1* (Ss03373344g1), *Col10a1* (Ss03391766m1), *Ihh* (Ss03373541m1) and *GAPDH* (Ss03373286u1) in this study. Each assay was designed based on the amplicon spanning an exon junction. For the mouse micromass analysis all primers were designed as described previously (section 2.6) as shown in Table 6:1.A SYBR Green amplification master mix was utilised for these primer pairs.

Real-time PCR was performed using an ABI 7500 Sequence Detection system (Applied Biosystems), and analysed using relative quantification, as described previously (section 2.6). Triplicate values were averaged.

Table 6:1: Primer sequences for mouse qRT-PCR analysis.

Gene	Ref Sequence	Fwd	Rv
Col2a1	NM_0332263.3	AAGTCACTGAACAACCAGATTGAGA	AAGTGCGAGCAGGGTTCTTG
Sox9	NM_011448.4	CGGCTCCAGCAAGAACAAG	TGCGCCCACACCATGA
Col10a1	NM_009925.4	TGCAATCATGGAGCTCACAGA	CAGAGGAGTAGAGGCCGTTTGA
Ihh	NM_010544.2	CCACCTTCAGTGATGTGCTTATTT	CGATGACCTGGAAAGCTCTCA

6.2.9 Statistical Analysis

For the micromass culture conditions subjected to HP and FS, n=3 (HP) and n=5 (FS) experimental replicates were analysed. For each of these replicates, 4 samples were pooled for qRT-PCR. All samples assayed in triplicate and averaged. The data for all replicates were compared, each FS sample (n=5) to each HP sample (n=3), totalling 15 comparisons. All experimental comparisons were then used for subsequent statistical analysis. Differences in gene expression, with application of mechanical stimulation and/or time-in-culture were determined by paired t-tests.

For each porcine cell source, at least two study replicates were performed. For each of these replicates, 5 pellets were pooled for qRT-PCR. The data from all replicates was then pooled for subsequent statistical analysis. Differences in gene expression, with cell type and/or time-in-culture were determined by t-tests and by analysis of variance (ANOVA) with time or loading as independent factors, followed by Tukey's post-hoc test (95% confidence Interval). All data are expressed in the form of mean ± standard error of the mean (SEM). Statistical significance was declared at $p \leq 0.05$.

6.3 Results

6.3.1 Adult stem cells

6.3.1.1 Chondrogenic differentiation of porcine derived adult stems cells

Following 14 days in culture, porcine derived adult cell pellets were mostly spherical and stained positive for Alcian Blue (staining GAG) and picro-sirius-red (collagen) deposition when supplemented with TGFβ3, while minimum staining was observed in the non-supplemented groups (Figure 6.3). In general an increase in matrix staining was observed for infrapatellar fat pad (FP) stem cells and synovial membrane (SM) stem cells when supplemented with higher concentrations of TGFβ3.

Synovial membrane stem cells responded to the addition of 10ng/ml of TGFβ3 with a greater than 19-fold increase in *Sox9* expression, 2,400-fold increase in *Aggrecan* expression and a 140,000-fold increase in *Col2a1* expression following 14 days in culture compared to day 0 control levels (Figure 6.4a, b, c). The addition of 1ng/ml of TGFβ3 resulted in a 1,200-fold (Day14 FS: 1202.7 (±858.6) v_s Day0 FS: 0.92 (±0.04), $p \leq 0.0001$) increase in *Aggrecan* relative gene expression compared to day 0 control levels (Figure 6.4b). No significant difference was observed for *Col1a1* with and without TGFβ3 supplementation following 14 days in culture (Figure 6.4d). *Collagen type 10* and *Indian Hedgehog* were not expressed at day 0. By day 14, the expression of *Col10a1* and *Ihh* was 100 fold and 5 fold higher respectively in pellets supplemented with 10ng/ml compared to 1ng/ml of TGFβ3 (Data not shown).

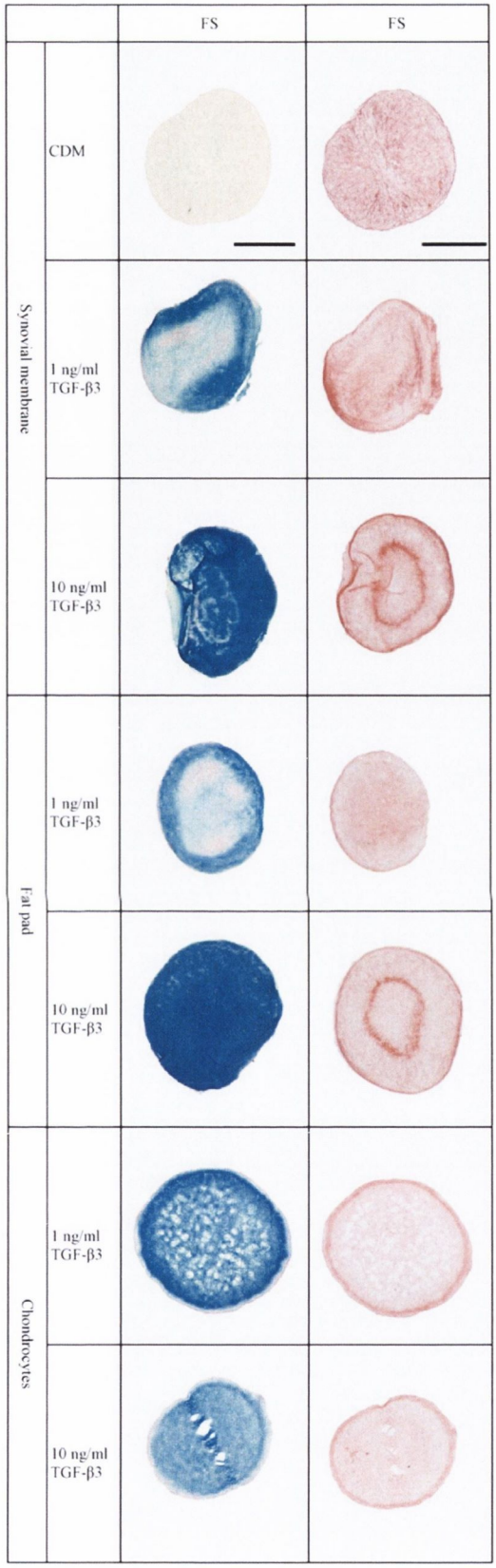

Figure 6.3: Histological sections of Synovial membrane, Fat pad and Chondrocytes derived cell pellets grown in Free swelling (FS) conditions for 14 days of culture. Pellets were stained with Alcian blue (stains GAG, right column) and Picro-sirius red (stains collagen, left column); scale bar 500μm.

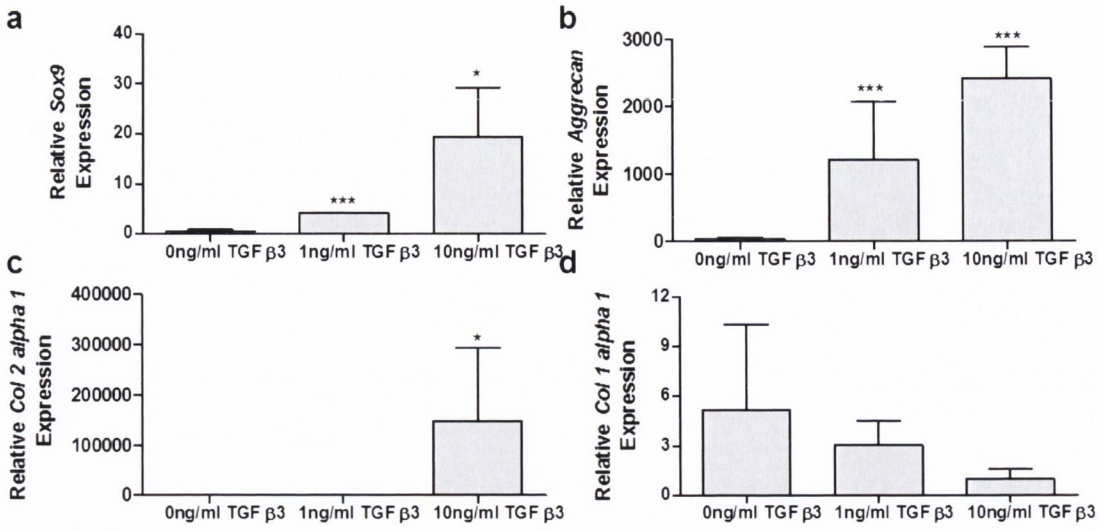

Figure 6.4: Chondrogenic marker gene expression in synovial membrane derived cell pellet cultures with 0, 1, or 10ng/ml TGFβ3 over 14days. Calibration performed according to expression of the endogenous control gene GAPDH and normalised to day 0 pellets. *Sox9* (**a**), Aggrecan (**b**), Collagen type II alpha 1 (**c**) and Collagen type I alpha 1 (**d**) expression. Data is expressed as relative expression per group and represented as mean ±SEM. n=3 samples per group, assayed in triplicate. *:$p<0.05$, ***:$p<0.0001$ v_s gene expression at day 0.

6.3.1.2 The effect of HP on adult derived cell pellet cultures

HP appeared to influence the organisation of the neo-tissue, as evident by the appearance of a core region in the FS pellets compared to more homogeneous distribution of extracellular matrix in the HP group (Figure 6.5). Chondrocyte (CC) derived pellets supplemented with 1ng/ml of TGFβ3 presented some evidence of cell clustering, with more intense staining observed in the FS group in comparison with pellets subjected to HP (Data not shown).

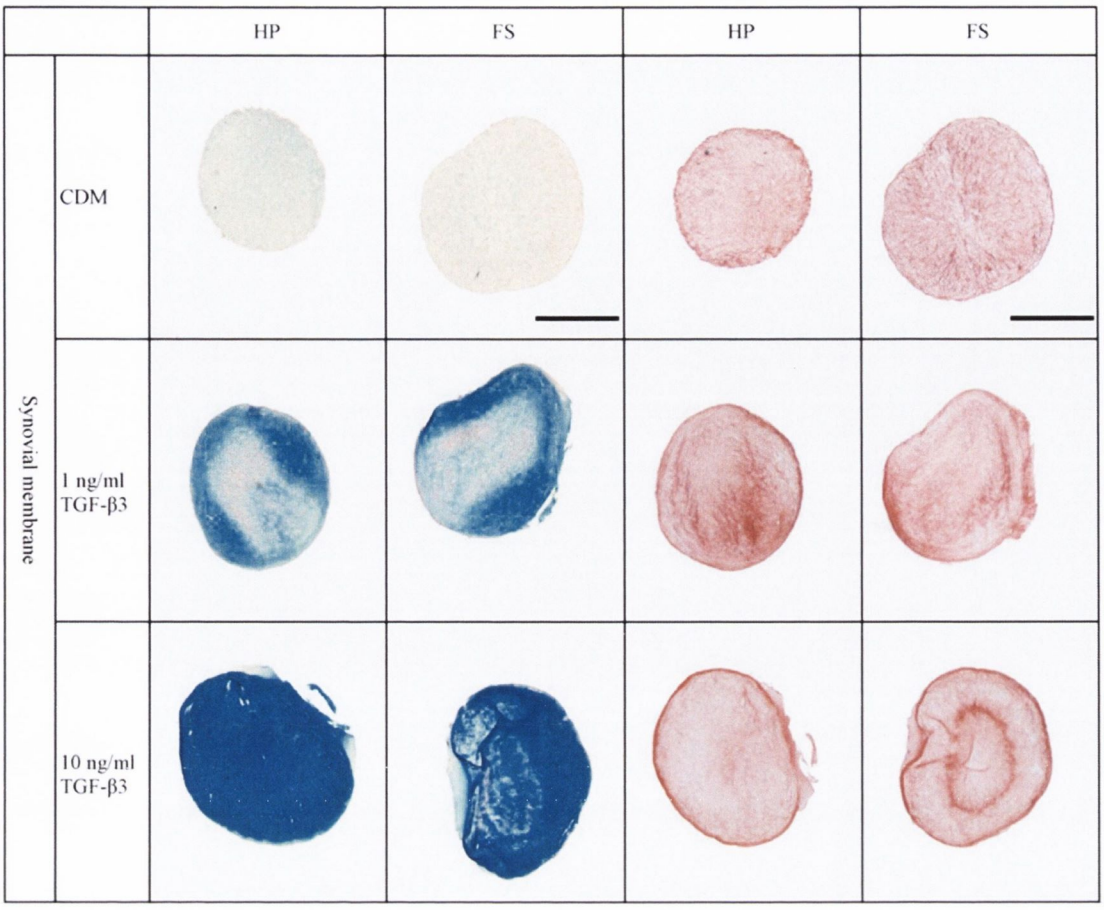

Figure 6.5: Histological sections of Synovial membrane derived cell pellet grown in Free swelling (FS) conditions or exposed to hydrostatic pressure (HP) following 14 days of culture. Pellets were stained with Alcian blue (stains GAG, right columns) and Picro-sirius red (stains collagen, left columns); scale bar 500μm.

6.3.1.3 Gene expression changes following HP and TGF-β3 supplementation on adult-derived pellets

Synovial Membrane: The application of HP had no significant effect on the expression of *Sox9, Aggrecan* and *Col2a1* in the absence of growth factor supplementation at day 14 but did lead to significant decrease in *Col1a1* gene expression (HP: 7.31 fold, $p \leq 0.01$) (data not shown). Applying HP in the presence of 1ng/ml of TGFβ3 resulted in a 3-fold increase in the mRNA levels of *Sox9* (HP: 3.19 fold, $p \leq 0.05$) in comparison to FS controls (Figure 6.6a). No significant difference was observed for the extracellular matrix specific genes *Aggrecan*, *Col2a1* and *Col1a1* following the application of HP combined with either 1 or 10ng/ml TGFβ3 (Figure 6.6b, c, d). Applying HP to SM pellets in the presence of TGFβ3 at 1 and

10ng/ml also lead to decreases in the mRNA levels of the hypertrophic marker *Col10a1* and the pre-hypertrophic marker *Indian Hedgehog (Ihh)* (Figure 6.6e, f). HP application resulted in decreases in *TGFβ3* and *TGFβrec3* (trend) expression in both 1ng/ml and 10ng/ml TGFβ3 supplementation (Figure 6.6g, h).

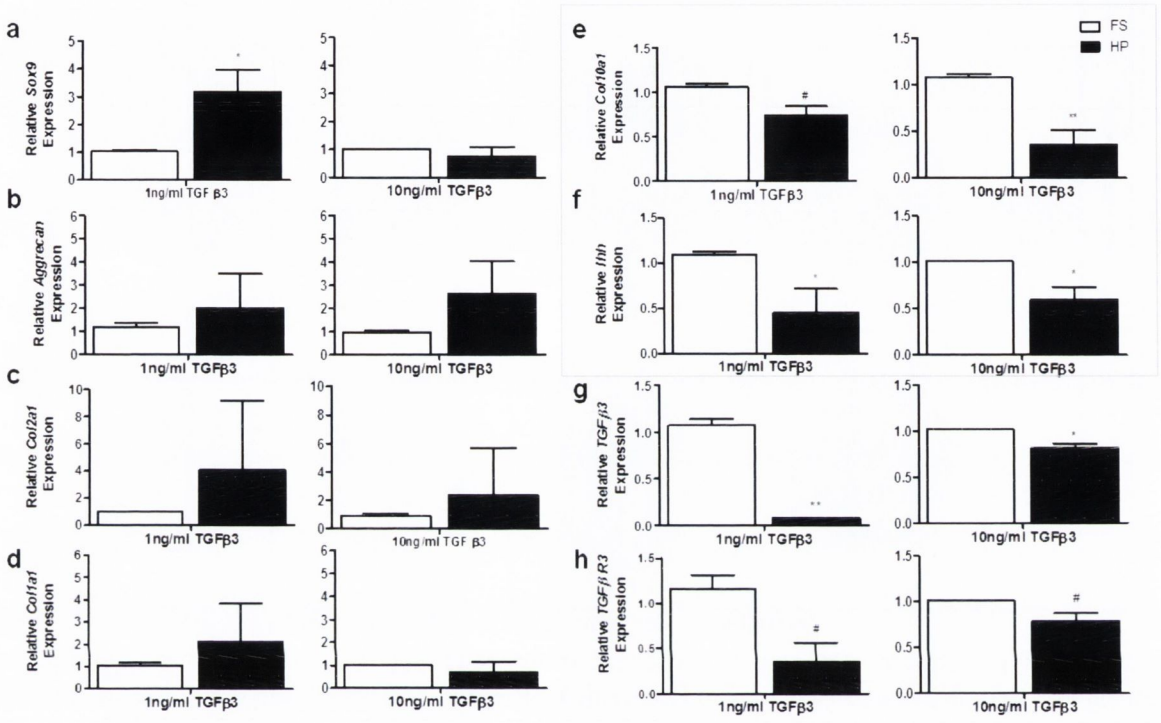

Figure 6.6:The influence of hydrostatic pressure on gene expression in Porcine adult-derived synovial membrane (SM) pellets at day 14 cultured in free swelling (FS) and hydrostatic pressure (HP) conditions with 1 or 10ng/ml TGFβ3. Calibration of each gene to GAPDH expression levels and normalised to free swelling controls. *Sox9* (**a**), *Aggrecan* (**b**), Collagen type II alpha 1 (*Col2a1*) (**c**), Collagen type I alpha 1 (*Col1a1*) (**d**), Collagen type X alpha 1 (*Col10a1*) (**e**) and Indian Hedgehog (*Ihh*) (**f**), *TGFβ3* (**g**), *TGFβrec3* (**h**) expression. Data is expressed as relative expression per group and represent mean ±SEM. n=3 per group. #:$p<0.1$, *:$p<0.05$, **:$p<0.01$. v_s gene expression at day 14 for FS control.

Analysis of fat pad derived stem cells showed a similar result following the application of HP and 1ng/ml of TGFβ3 supplementation with a 3.5-fold increase in *Sox9* (HP: 3.53 fold, $p\leq0.1$) relative gene expression in comparison to FS controls (Figure 6.7a). No significant differences were observed for the mRNA expression levels of *Aggrecan*, *Col2a1*, *Col1a1* and *Col10a1* comparing HP to FS samples (Data not shown).

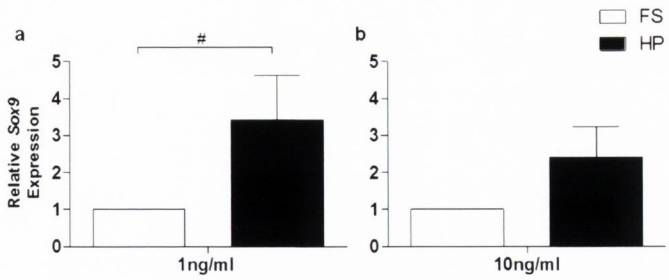

Figure 6.7: The influence of hydrostatic pressure on gene expression in Porcine adult-derived fat pad (FP) pellets at day 14 cultured in free swelling (FS) and hydrostatic pressure (HP) conditions with 1 or 10ng/ml TGFβ3. Calibration of each gene to GAPDH expression levels and normalised to free swelling controls. *Sox9* (**a-b**), Data is expressed as relative expression per group and represent mean ±SEM. n=2 per group. #: $p<0.1$ v_s gene expression at day 14 for FS control.

Analysis of articular cartilage derived chondrocytes following the application of HP and 1ng/ml of TGFβ3 stimulation showed a decrease in mRNA expression of *Aggrecan* (HP: 1.74 fold, $p<0.05$) and *Col2a1* (HP: 1.98 fold, $p<0.01$) relative gene expression in comparison to FS controls (Figure 6.8b, c), but no differences in the mRNA expression levels of *Sox9* and *Col1a1* comparing HP to FS samples. No detection of *Col10a1* was found in either FS of HP cultures supplemented with 1ng/ml TGFβ3.

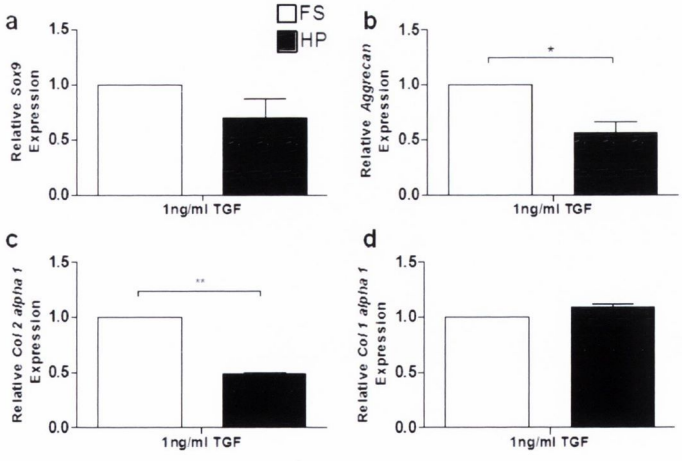

Figure 6.8: The influence of hydrostatic pressure on gene expression in articular cartilage derived chondrocyte pellets at day 14 cultured in free swelling (FS) and hydrostatic pressure (HP) conditions with 1 ng/ml TGFβ3. Calibration of each gene to GAPDH expression levels and normalised to free swelling controls. *Sox9* (**a**) *Aggrecan* (**b**), *Col2a1* (**c**), *Col1a1* (**d**), Data is expressed as relative expression per group and represent mean ±SEM. n=2 for 1ng/ml TGFβ3 group. *: $p<0.05$, **: $p<0.01$ vs gene expression at day 14 for FS control.

6.3.2 Embryonic limb bud derived cells

6.3.2.1 Chondrogenic differentiation of mouse embryonic limb bud cells in pellet culture

To test the ability of embryonic limb bud cells to differentiate chondrogenically in pellet cultures, pellets were cultured for 7 and 14 days with (1 and 10ng/ml) and without supplementation of TGF-β3. Pellet constructs were analysed histologically following paraffin sectioning and revealed light alcian blue staining in all cultures (Figure 6.9). An increase in intensity of alcian blue staining can be seen following 7 days of culture with 1ng/ml TGF-β3 (Figure 6.9b) and day 14 with 10ng/ml TGF-β3 (Figure 6.9f). Overall, the level of staining is very low in all cultures, suggesting that the cell pellet conditions that promote chondrogenesis in adult derived MSCs are not as effective on embryonic limb bud cells. A difference in the internal morphology of pellets can be seen in the sections with TGFβ supplementation, with large vacuoles appearing after 7 and 14 days. Differences in the surface morphology and colour of pellet cultures following 14 days *in vitro*, was seen comparing the 10ng/ml TGFβ3 and no supplementation groups. The TGFβ3 supplementation group had a more "rounded" smooth surface (Figure 6.9j-l), compared to the group with no supplementation, that had a less compact structure (Figure 6.9g-i).

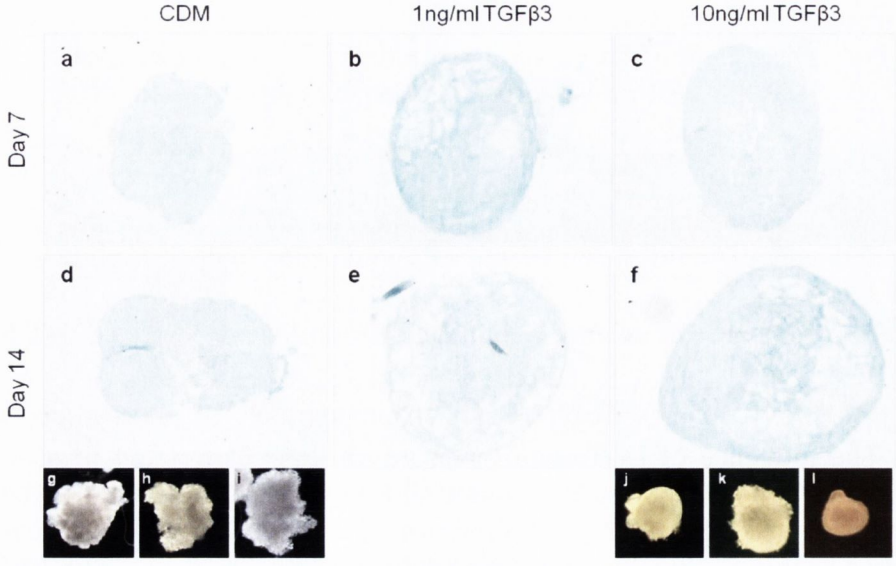

Figure 6.9: Alcian Blue staining of sections of embryonic limb bud cell pellets cultured for 7 days (**a-c**) and 14 days (**d-f**). Pellets were cultured in no TGFβ3 (**a, d**) 1ng/ml TGFβ3 (**b, e**) and 10ng/ml TGFβ3 (**c, f**). Surface morphology of pellets at day 14 with no supplementation (**g-i**) and with 10ng/ml TGFβ3 (**j-l**) (n=3).

6.3.3 Chondrogenic differentiation of mouse embryonic limb bud cells in micromass culture.

Micromass cultures were prepared from E11.5 embryo limb buds, at the initial stages of mesenchymal condensation prior to chondrogenesis (Wezeman, 1998). With further development *in vivo* cells in the mesenchymal condensations endergo chondrogenesis marked by activation of the *Col2a1* gene throughout the skeletal rudiments (E12.5 in the proximal limb), followed by initiation of *Ihh* expression in the pre-hypertrophic zone and *Col10a1* as the chondrogenic cells mature to hypertrophy at E14.5 (Figure 6.10).

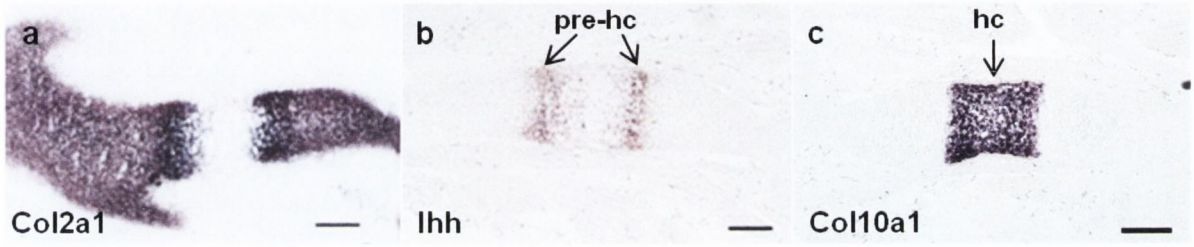

Figure 6.10: Spatial expression of hypertrophic specific genes *Ihh* (**b**) and *Col10a1* (**c**) in the developing E14.5 humerus. *Col2a1*(**a**) demonstrated expression in proliferating chondrocytes. Pre-hc; pre-hypertrophic chondrocytes, hc; hypertrophic chondrocytes. Scale bar 100μm.

Chondrogenic differentiation was assessed histologically by alcian blue staining of cartilaginous nodules in two sets of micromass cultures over 11/12 days in culture, n=4 per time point. In both sets of experiments the cartilaginous alcian blue positive nodules had formed by day 4/5 and increased in size and intensity of staining over time; no nodules were present at day 1 (Figure 6.11A). There was no difference in the number of nodules between day 4, day 8 and day 12 in experiment 1, or between day 5, day 9 and day 11 in experiment 2 (Data not shown). As the size of the nodules increased, union of nodules was seen at day 8 and day 9 in each experimental culture, with an increased coverage of Alcian blue staining as shown at day11 across the whole micromass (Figure 6.12A).

Quantitative real-time PCR analysis was used to assess changes in the expression of chondrogenic specific genes over time. Expression levels were normalised to E11.5 limb bud cells (time point zero). All data shown are from micromass cultures plated at a density of 1

$x10^5$ cells per micromass. Expression levels of the hypertrophic marker *Col10a1* showed dramatic increased levels over time in micromass cultures, with a continued increase in expression to day 11 (Figure 6.11B). An up-regulation of *Col2a1, Sox9 and Ihh* was identified at Day 1, as expected following initial plating of cells. Maintenance of *Col2a1* expression was evident at day 5 and day 9, with peak in expression at day 11. A down-regulation of *Sox9* was not surprising as cells progress to full differentiation. *Ihh* expression would have been expected to increase similarly to Col10a1 (in trend if not level) as cells mature to hypertrophy so the overall decrease in Ihh expression relative to E11.5 limb buds, over the time points analysed, is surprising.

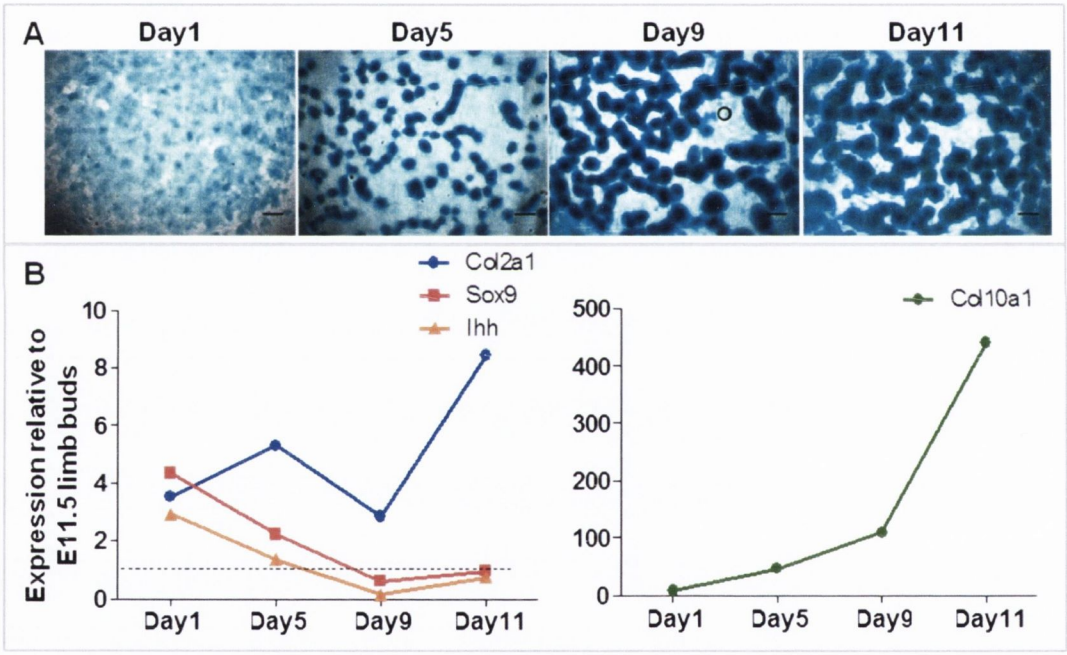

Figure 6.11: Chondrogenic differentiation of embryonic limb bud cells cultured in micromass conditions. (**A**) Alcian Blue staining of cartilage nodules, analysed over time; Scale bars 100μm. (**B**) Chondrogenic marker gene expression in embryonic limb bud micromass cultures relative to E11.5 limb bud (time point 0) expression. Calibration performed according to expression of the endogenous control gene GAPDH. *Col2a1* (blue), *Sox9* (red) *Ihh* (Orange) and *Col10a1* (green) expression is represented over time. All assays performed in triplicate.

6.3.3.1 Influence of HP on morphology of cartilage nodules in embryonic micromass culture

Following 9 days in culture, micromass constructs subjected to FS and HP conditions both contained Alcian Blue positive nodules (FS: a-d, HP: e-h). There was no significant difference in the number of nodules in the HP (245 ± 10) compared to the FS conditions (176.5 ± 21.5, p=0.106 (ns)) (Figure 6.12i). However the surface area covered by nodules was larger in the HP cultures compared to FS conditions. Using the highest magnification images shown in d and h, the percentage area containing nodules were compared for the FS and the HP cultures. The percentage area covered by nodules in the HP cultures (42.4%) was significantly higher than the FS conditions (14.6%, **p≤0.01) (Figure 6.12j).

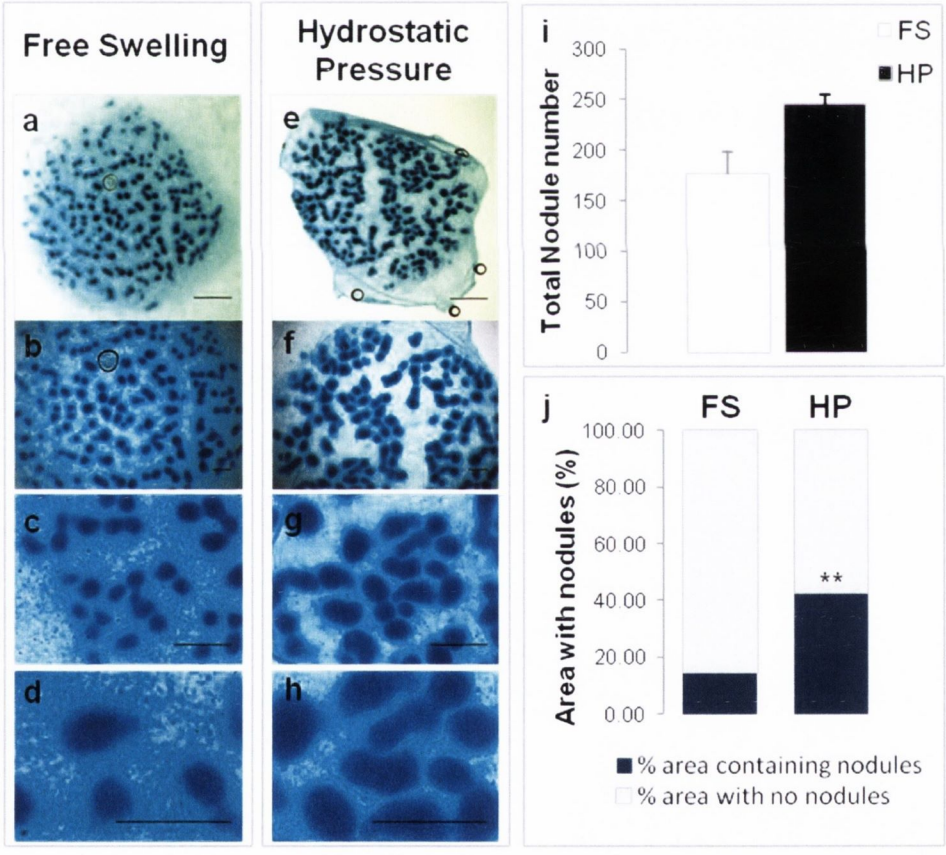

Figure 6.12: Alcian Blue staining of micromass cultures kept in Free swelling (FS, **a-d**) or exposed to hydrostatic pressure (HP, **e-f**) following 9 days of culture. Micromass cultures were stained with Alcian blue (stains GAG, **a-h**), higher magnifications for each micromass culture show the morphology of the stained modules; Scale bar in **a** and **e** 1000μm, scale bar in **b-d**, **f-g** 100μm. (**i**) Total nodule number was compared for FS (white bar) and HP (black bar). (**j**) The percentage area covered by nodule staining was compared for the highest magnification images (n=2) for FS and HP (**d** and **h**), with HP showing a higher percentage coverage (42.4%) compared to FS (14.6%, **p≤0.01).

6.3.3.2 Gene expression changes following HP on embryonic micromass cultures

The application of HP to embryonic limb bud micromass cultures plated at a density of 1 x10^5 cells per micromass for 9 days, showed no difference in mRNA expression levels of *Col2a1*, but a 2.19 ±0.182 fold (±SEM) increase in *Sox9* expression following HP compared to FS controls ($p \leq 0.05$) (Figure 6.13b). Application of HP resulted in a decrease in the mRNA levels of the hypertrophic marker *Col10a1* (HP: 2.9 ± 0.086 fold ±SEM, $p \leq 0.05$) and the developmental regulatory gene and pre-hypertrophic marker *Ihh* (HP: 17.3 ±0.012 fold ±SEM, $p \leq 0.001$) in comparison to FS controls (Figure 6.13c & d, respectively).

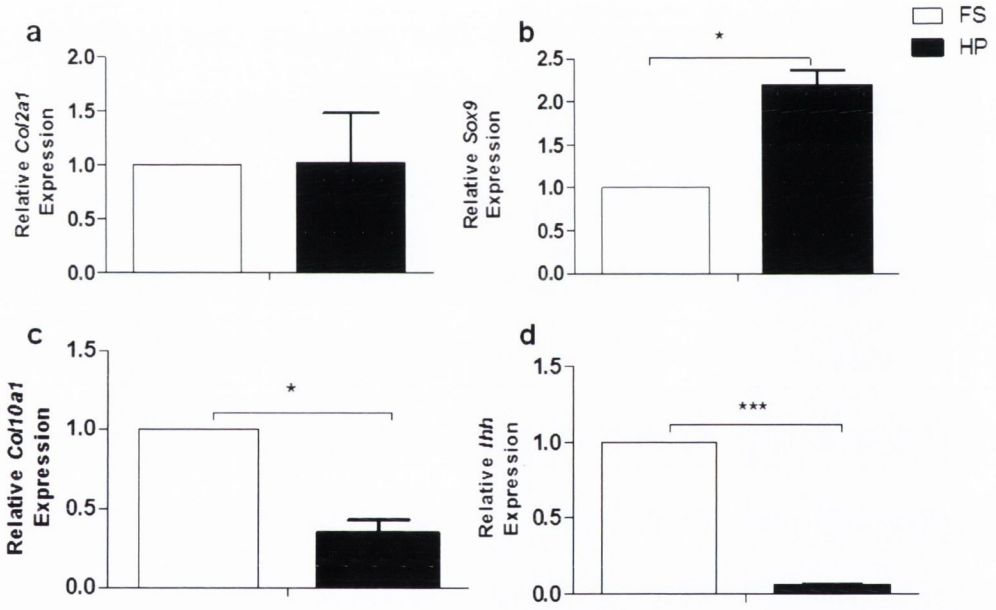

Figure 6.13: The influence of hydrostatic pressure (HP) on gene expression in embryonic limb bud micromass cultures at day 9 grown in free swelling (FS) and hydrostatic pressure (HP) conditions. Calibration of each gene to GAPDH expression levels and normalised to free swelling (FS) controls. *Col2a1* (**a**), *Sox9* (**b**), *Col10a1* (**c**), *Ihh* (**d**) expression. Data is expressed as relative expression per group and represent mean ±SEM. n=3. *$p<0.05$, **:$p<0.01$, ***: $p<0.001$. v_s. gene expression at day 9 for FS controls.

6.3.4 Initial characterisation of cells derived from adult mouse cartilage and bone marrow

It was possible to culture and proliferate both articular cartilage derived cells from the adult mouse knee joint and bone marrow derived cells, as can seen by the increased density of cells in individual colonies over time (Figure 6.14). Cells were monitored for morphology changes

and proliferated to approximately 70-80% confluence, and then passaged. Variations occurred in the rate and success of proliferation from independent experiments (AC: n=6, BM: n=3), making it difficult to replicate and assess the success of the isolation and proliferation method. Cultures were passaged between 2-3 times for the BM and once for AC, with proliferation maintained at each passage.

These cells were subjected to tripotentiality tests to investigate whether they were true MSCs capable of forming fat, bone and cartilage. Due to the low cell numbers for the bone marrow derived cells, results of the articular cartilage derived differentiation assay could only be interpreted. Alcian blue staining to detect mineralised matrix and cartilage was strong in chondrogenically primed pellet cultures (Figure 6.14c), Low levels of oil-O red staining for adipose tissue and alizarin red staining for mineralised matrix were observed (Figure 6.14a, b). Reduced adipogenic and osteogenic potential may indicate that these cells are chondrocytes rather than MSCs although the finding might also be due to lower than optimum cell density during the differentiation assay. Although cells could be harvested from these tissues, they were not further used to test the effect of HP due to the relatively small yields of cells and the variability in their proliferation and differentiation.

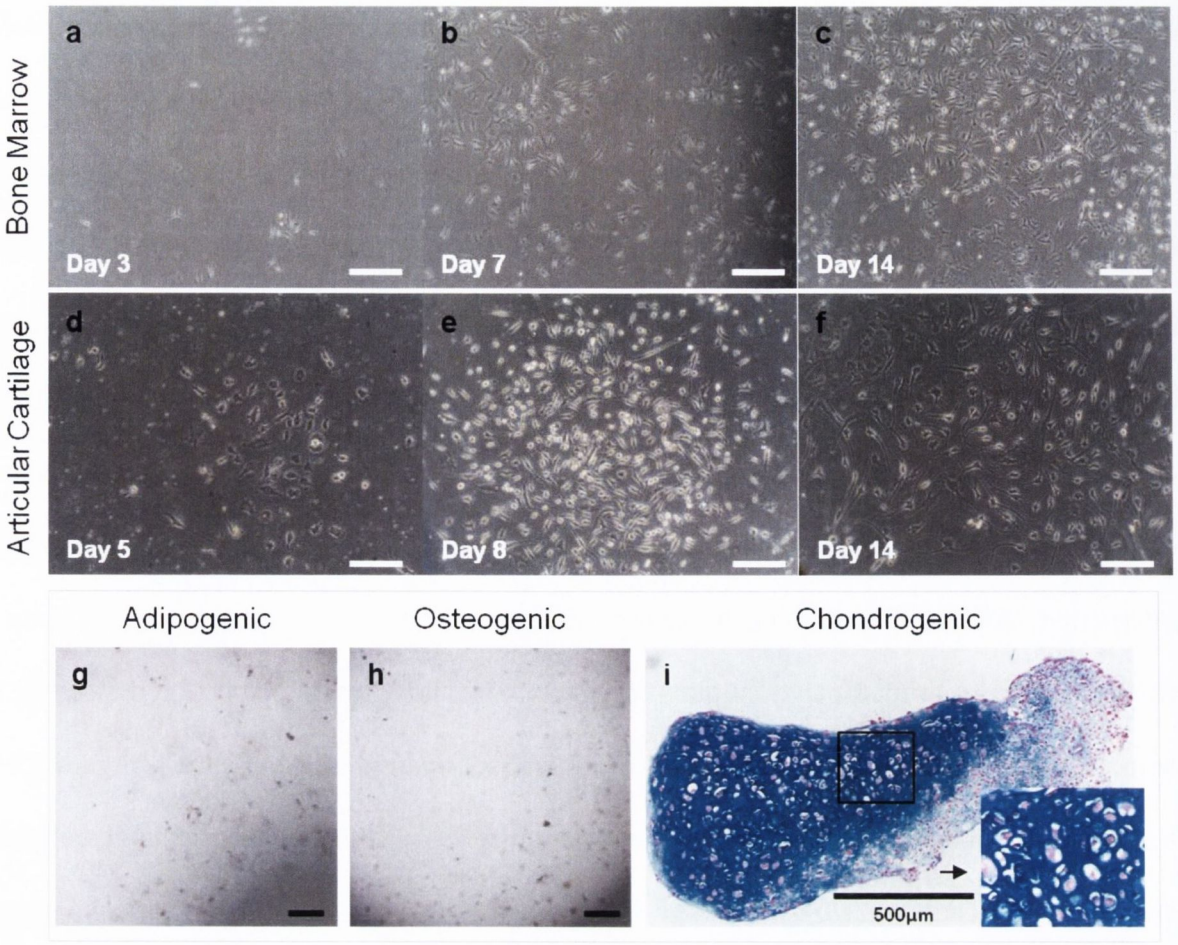

Figure 6.14: Isolation of possible Mesenchymal stem cells from adult mouse tissue. Bone marrow (**a-c**) and articular cartilage (**d-f**) were harvested from adult mouse hindlimbs and cultured for several months. Differentiation assays of adult mouse articular cartilage derived cells (**g-i**). To test the ability of 2D cell cultures to form adipose tissue stained with Oil-O Red (**h**), bone stained with Alizarin red (**h**) and cartilage in pellet cultures stained with Alcian blue (**i**). All scale bars 100µm, unless otherwise stated.

6.4 Discussion

Here I demonstrate the effect of application of dynamic hydrostatic pressure on the differentiation of embryonic limb bud derived cells and MSCs of adult origin. Both embryonic cells and adult derived MSCs showed reduced expression of hypertrophic markers with the addition of HP. Since dynamic HP stimulation is predicted to be experienced by cells in the future joint region and loss of movement derived stimulation leads to loss of articular cartilage territories, the postulation is that dynamic HP stimulation contributes to the stable differentiation of articular cartilage during normal development.

6.4.1 Response of progenitor cells to Hydrostatic pressure

Experimentally applied loading regimes are designed to mimic normal loading, for example joint loading results in the direct compression of chondrocytes, followed by a build up of hydrostatic pressure (HP). HP is one of the main mechanical stimuli exerted on articular cartilage and understanding its effects on progenitor cell differentiation is a central challenge in the field of articular cartilage tissue engineering and regeneration (Elder and Athanasiou, 2009). According to finite element models HP has been shown to promote cartilage formation and potentially suppress endochondral ossification (Carter et al., 1998; Carter and Wong, 2003; Loboa et al., 2001), and experimentally applied cyclic HP has been found to enhance chondrogenesis of MSCs (Angele et al., 2003; Miyanishi et al., 2006b) with no induction of osteogenesis (Wagner et al., 2008). The loading regime chosen here for the adult derived progenitor cells was based on previous reports demonstrating that 10MPa of HP applied for 4h daily at a frequency of 1 Hz enhanced chondrogenesis (Angele et al., 2003; Ikenoue et al., 2003; Miyanishi et al., 2006a). The loading regime on the micromass cultures was 10 fold lower than on pellet cultures, due to the technical limitation of the micromass being held on to glass coverslips, and at this pressure the coverslips were found to withstand the loading regime. In previous studies application of 1MPa was shown to induce chondrogenesis in human marrow cells (Wagner et al., 2008); and the application of much lower pressure, 600Pa

(0.0006MPa), to micromass cultures of chick limb bud cells was found to stimulate chondrogenesis (Juhasz et al., 2014). These results indicated that 1MPa might be a reasonable level to test for influence on limb bud micromass cultures.

An up-regulation of *Sox9* in the adult derived SM and FP pellet cultures and the micromass limb bud cultures suggests general enhancement of chondrogenic differentiation in response to HP, as *Sox9* is expressed in all cartilage primordia and is responsible for the maintenance of proliferating chondrocytes during development (Akiyama et al., 2002) prior to the expression of the extracellular matrix gene *Col2a1*. Previous studies have reported similar increases in *Sox9* (Miyanishi et al., 2006b) gene expression and protein production in SM derived cells (Sakao et al., 2008). Increases in Sox9 expression have been reported in human, rat and porcine bone marrow cells subjected to HP regimes (Li et al., 2009; Miyanishi et al., 2006b; Steward et al., 2012). Reports of no changes in aggrecan and *Col2a1* expression following HP are in agreement with the observations reported here, and it was previously suggested this was due to the 14day duration of loading not being sufficient (Finger et al., 2007). Recent work investigating the response of chick limb bud cells in micromass culture to mechanical stimulation showed a similar increase in *Sox9* mRNA and protein expression compared to un-stimulated controls (Juhasz et al., 2014).

The significant decrease in mRNA levels of *Col10a1* and *Ihh* in the SM adult derived and embryonic micromass culture systems following the application of HP, suggests that cells show reduced progression into pre-hypertrophy or hypertrophy. Following 9 days in culture without HP, the expression levels of *Col10a1* were shown to increase over 100 times higher in micromass cultures than in E11.5 limb bubs; and in SM derived cells no detection of either *Col10a1* or *Ihh* was quantifiable at day zero, in opposition to detectable levels with time, indicating an up-regulation of both hypertrophic markers. The decrease in expression of the hypertrophic markers *Col10a1* and *Ihh* following HP in the embryonic and adult derived cells, suggest that applying HP is reducing the cells from differentiating along the endochondral

route, for bone formation. The transcript changes in *Ihh* in the micromass cultures over time show no peak in expression profile compared to E11.5 expression levels (Figure 6.11B). This is in opposition to a peak in *Ihh* expression detected in mouse E11.5 micromass cultures following 10 days of culture (Taipaleenmaki et al., 2012). However, in this study a significant decrease in expression levels of Ihh was shown following HP, potentially suggesting that the time points analysed were not thorough enough to demonstrate the peak in expression representing pre-hypertrophy.

As in the developing bone, chondrogenically primed bone marrow MSCs proceed to terminal differentiation by expressing collagen type 10 (Winter et al., 2003) and alkaline phosphatase (Pelttari et al., 2006), indicative of a hypertrophic phenotype (Dickhut et al., 2009). The down-regulation in expression of hypertrophic genes in both culture systems described here, suggest that HP is playing a key role in the formation of a permanent or stable chondrocyte phenotype. Support for such a hypothesis can be found in the results of previous studies; HP has been shown to increase chondrogenic gene expression, while having no effect on osteogenic genes (Wagner et al., 2008). A down-regulation in the expression of *MMP-13* (matrix-metallopeptidase 13), a proteolytic enzyme in hypertrophic cartilage required for vascularisation of calcified cartilage was also found following HP (Wong et al., 2003). Supporting these results, HP on bone marrow-derived MSCs has been shown to reduce alkaline phosphatase activity (Steward et al., 2012) and to decrease calcification in long-term agarose cultures (Carroll et al., 2014).

6.4.2 The effect of TGFβ on priming chondrogenic differentiation of adult derived stem cells

Embryonic limb bud cells spontaneously differentiate to chondrocytes and form cartilage in micromass culture. E11.5 derived cells were shown to have the greatest potential for chondrogenic differentiation in micromass cultures compared to other stages (Anurati Saha, unpublished data in our group). In fact they spontaneously self organise into nodules that

resemble skeletal rudiments (e.g. Figure 6.12h). Previous optimisation of embryonic limb bud micromass cultures showed that cartilaginous nodule formation was best in growth media (DMEM plus 10% serum) containing no cytokine supplementation (A. Saha). Adult derived stem cells require chondrogenic priming and TGFβ has been shown to enhance chondrogenic differentiation (Johnstone et al., 1998). Here two levels of TGFβ were tested for their ability to prime differentiation and to potentially influence a response to HP.

Varying concentrations of TGFβ3 (0, 1 and 10ng/ml) were applied to the adult derived porcine cultures. Chondrocytes (CC) and joint tissue derived (SM and FP) stem cells were found to differentially respond to altered TGFβ3 concentrations. Johnstone *et al.* evaluated the effect of different concentrations of TGFβ3 (0.5 to 10ng/ml) on bone marrow derived MSCs, concluding that lowering the TGFβ concentration decreased their chondrogenic response (Johnstone et al., 1998). FP stem cells and SM stem cells responded similarly to TGFβ3 stimulation, corresponding to previous reports where these two stem cell sources demonstrate a comparable level of chondrogenesis in response to cytokine stimulation (Marsano et al., 2007; Mochizuki et al., 2006).

HP in the absence of TGFβ3 did not appear to induce chondrogenesis of synovium derived stem cells (Data not shown). HP was shown to act synergistically with low concentrations of TGFβ3 to enhance chondrogenesis of synovium and fat pad derived MSCs, as evidenced by a 3-fold increase in *Sox9* expression and enhanced GAG synthesis. In agreement with previous studies (Zeiter et al., 2009), we also observed that HP had no beneficial effect on cartilage-specific matrix expression when stem cells were supplemented with 1ng/ml or 10ng/ml of TGFβ3. In contrast, a number of other studies have reported a synergistic effect for bone marrow MSCs supplemented with 10ng/ml of TGFβ3 (Miyanishi et al., 2006b; Wagner et al., 2008). Previous studies have demonstrated that mechanical loading influences chondrogenesis of human bone marrow MSCs through the TGF pathway by up-regulating TGF gene

expression and protein synthesis (Li et al., 2010b). In this study we further analysed the expression levels of *TGFβ3* and *TGFβr3* (receptor) in SM progenitor cells to identify whether HP exerts its influence on differentiation through TGFβ signalling. HP did not up-regulate the expression of TGFβ3 or TGFβr3 in 1ng/ml or 10ng/ml supplemented cultures, but conversely resulted in a down-regulation of the cytokine and a trend down-regulation of the TGFβ receptor 3 (Figure 6.6g, h), further supporting TGFβ signalling as a chondrogenic primer in adult derived cells; and potentially suggesting that an alternative signalling pathway is regulating the differentiation of joint derived cells under mechanical stimulation.

6.4.3 MSCs derived from adult mouse

The embryonic cells used in this study were derived from mouse whereas the adult derived cells were porcine. It is not ideal to make such comparisons across species but the pig is not an established model for developmental study while porcine adult MSCs have been derived and well characterised by our research group (the Kelly lab). Although mouse MSCs have been successfully derived by many groups (Gosset et al., 2008; Salvat et al., 2005; Soleimani and Nadri, 2009), this study was the first attempt to generate mouse MSCs in our hands. While proliferative cells that show a morphology consistent with MSCs were isolated, there were some inconsistencies in behaviour between different experiments and they did not behave convincingly as MSCs in terms of tripartide differentiation potential (Figure 6.14). The mouse joint derived cells showed good differentiation to cartilage in pellet cultures but very limited capacity to differentiate to bone or adipose tissue. This might indicate that these are in fact largely chondrocytes rather than MSCs. Because of the much smaller size of the juvenile knee joint of the mouse it was difficult to specifically dissect the fat pad, synovium and the articular cartilages separately; therefore the whole joint region including all of these tissues was used to derive cells and could therefore include specified chondrocytes. Because of the doubts surrounding the characterisation of these cells they were not used in further analysis of the effect of HP. Preliminary comparisons were therefore made between porcine

adult cells and murine embryonic cells, two well characterised populations. Future work will require procurement of mouse MSCs to compare behaviour within a single species. The overall comparisons, even though not species equivalent can however help to inform the molecular response of progenitor cells to mechanical stimulation.

Long term sub-culturing of articular cartilage derived progenitor cells was not possible (section 6.3.4). The main problem associated with culturing of primary chondrocytes, is that cultured chondrocytes tend to dedifferentiate into fibroblasts, this can be detected by molecular analysis showing a switch from collagen type 2 or type 10 expression to collagen type 1 or 3 expression, switching from high-molecular weight to low-molecular weight proteoglycans. To minimise this fibroblastic conversion sub-culturing of immature murine (5-6 day old mice) articular cartilage was shown to be successful (Gosset et al., 2008; Salvat et al., 2005), so this may need to be addressed for future studies. A recent study described a successful protocol that dissects and uses adult mouse synovium and infrapatellar fat pad derived mesenchymal stem cells, however inflammation of the knee was induced in adults prior to harvesting of cells (Matsukura et al., 2014), indicating the difficulties in the approach of obtaining cells for mouse tissue. To extend and refine the analysis presented here, adult MSCs derived from mouse will be required for comparison with mouse embryonic limb bud cells; well characterised cells should be procured for this purpose from an external source, for example a specialist laboratory.

6.5 Conclusion

In conclusion, this study demonstrates that HP and TGFβ3 interact to regulate chondrogenesis of adult joint tissue derived stem cells. The data demonstrates that HP can act synergistically with low concentrations of TGFβ3 to up-regulate *Sox9* expression and the synthesis of cartilage-specific matrix molecules. Comparing the response of adult derived MSCs to embryo derived chondrogenic progenitors, it established that embryonic chondrocytes also respond to dynamic HP, stabilising the chondrogenic state. In particular, in both adult and embryonic cells, HP acts to down-regulate the expression of genes associated with pre-hypertrophy and terminal differentiation (*Indian hedgehog* and *collagen type ten*). This supports the evidence from the developing embryo indicating that dynamic mechanical stimulation is required for correct establishment of tissue types in the joint, specifically showing the effect on stable cartilage differentiation of embryonic chondrocytes. In the context of stem cell based therapies for articular cartilage repair, the results of this study demonstrate the importance of considering how both biochemical and biophysical joint specific environmental factors might interact to regulate not only the initiation of chondrogenesis, but also the development of a stable cartilage repair tissue.

Chapter 7:

7. General Discussion

The work presented in this thesis demonstrates how mechanical stimuli influence skeletal tissue patterning and cell differentiation through altering the activity of gene expression. The gene groups identified to be affected by a reduction in mechanical stimuli include the molecular machinery required for sensing and integrating this information for correct cell differentiation and patterning. This work provides an early step towards unravelling the mechanistic basis of biophysical regulation of skeletal development; the following objectives were met:

- A genome wide analysis of expression differences in developing skeletal rudiments from muscle-less compared to control littermate mouse embryos revealed 1,132 independent genes that are differentially expressed.

- Multiple developmentally important signalling pathways were identified to be impacted in response to an alteration in the mechanical environment. The expression of selected genes that encode key components of these pathways were screened to examine changes in spatial expression patterns in order to (a) build a picture of how the pathway is affected and (b) distinguish effects on the developmental processes of ossification and joint development which are occurring concurrently in the rudiment.

- The identification that the Wnt signalling pathway was most strongly affected by a reduction in mechanical stimulation led to the establishment of a whole embryo culture regime, which allows manipulation of older chick embryos, in order to devise a

novel approach to altering Wnt signalling in specific territories of the developing skeletal rudiment. The phenotypic effects following alteration of the pathway were analysed, demonstrating that both activation of canonical Wnt signalling and modulation of the signalling environment impact the pattern of chondrogenesis. Although the spatial and temporal targeting of transgene expression in this system requires improvement, this has established a basis for future work to disturb Wnt signalling in the joint and/or the rudiment separately.

- Initial comparisons of adult stem cell and embryonic cell cultures exposed to hydrostatic pressure, reveal that such mechanical stimulation of both progenitor cell types results in similar responses in gene expression, indicative of maintenance of a stable cartilage phenotype, with reduced maturation and hypertrophy, similar to that displayed in joint articular cartilage.

7.1 The developmental significance of the findings

7.1.1 Identification of mechanically regulated genes

A step towards gaining further understanding into the mechanistic basis for how developing cells interpret and respond to biophysical stimuli was the central objective for this thesis. Using a comparative transcriptome profiling approach from tissue that develops in the absence of muscle induced mechanical stimulation (*Spd/Spd* mutant), 1,132 independent differentially expressed genes (FC ≥2, p≤0.05) were identified. The transcriptomic screens presented in chapter 3 revealed specific categories of genes, grouped according to the biological processes they are involved in, to be highly enriched among DE genes. The differentially regulated genes identified, particularly those associated with cytoskeletal changes and signalling pathways represent a valuable focus for dissecting integrated regulation by biochemical and mechanical signals.

Preceding this work, gene expression profiling had been performed on *in vitro* culture systems to identify genome wide changes under altered mechanical environments (Bougault et al., 2012; Patel et al., 2007; Sironen et al., 2002). Using embryonic models, *in vivo* analysis was restricted to examining alterations in specific candidate genes to reveal any insights into the molecular response following alterations in biophysical stimuli (Kavanagh et al., 2006; Nowlan et al., 2012; Nowlan et al., 2008b; Roddy et al., 2011b). However, this study was the first to apply an *in vivo* genome-wide approach to investigate the role of biophysical stimuli on cell differentiation and patterning of the developing skeletal system; identifying multiple disturbances at a gene regulation level and implicating multiple biological processes eliciting a mechanoresponse. Data extracted from the studies referred to above, integrated with the present study, show overlap of genes identified in different contexts of mechanomodulation (Table 7:1). This corroborates the mechano relevance of several of the genes, including genes related to major signalling pathways (Chapter 4). The direction of modulation (e.g. up regulated or down regulated in reduced mechanical stimulation and the opposite in increased mechanical stimulation) is also generally consistent across studies.

Results from this work extends our knowledge considerably into the potential molecular mechanisms impacted by the removal of mechanical cues, thus providing insight into the type and groups of genes that are involved in transduction of biophysical stimuli into a molecular response. Multiple aspects critical to eliciting a mechanoresponse were identified to be altered including; (1) genes involved in sensing mechanical signals; ion channels G-protein coupled receptors and integrin complexes (Cell membrane components) (reviewed in Robling, 2012), (2) genes involved in relaying mechanical signals within cells; cytoskeletal networks and cell signalling pathway components, and (3) transcription factors and target genes indicating a transcriptional response affecting cell proliferation and differentiation.

Table 7:1: Integration of data on mechanosensitive genes identified in the current work (Column 1) and corroborated in other mechanomodulatory contexts or studies (Columns 2 and 3).

		(red=up-regulated) (blue=down-regulated)
Gene/Protein	**Method**	**Reference**
Egr2, *Fzd10*	*In vitro*: primary mouse chondrocytes in hydrogels subjected to short-term dynamic compression	(Bougault et al., 2012)
Cd44	*In ovo* immobilisation of chick knee joint	(Roddy et al., 2011b)
	In vitro: application of mechanical strain to chick fibrocartilage	(Dowthwaite et al., 1999)
Pdgfa, *Cdkn1a*, *F2rl1*, *Scn3b*	*In vivo* genome-wide microarray study using mouse endothelial RNAs isolated arterial regions exposed to disturbed flow, characterised by low or oscillatory shear stress, mimicking atherosclerosis conditions	(Ni et al., 2010)
Il1rl1, *Col8a1*, *Klf12*, *Krt15*, *Lamc3*, *Hyal1*	*In vitro*: hMSCs exposed to dynamic tension showed regulation of fibroblastic and osteogenic genes and compressive loading up-regulated genes associated with chondrogenesis.	(Haudenschild et al., 2009)
Sfrp2, *Bmp3*, *Trp63*, *Tuba4a*, *Enpep*, *Abca1*, *Hspb1*	*In vitro*: 2T3 murine osteoblast precursor cells were subjected to rotating wall vessel to stimulate a real microgravity environment.	(Patel et al., 2007)
Fgfr4	*In vitro*: Four point bending to create fluid shear and strain forces in an osteoblast cell line	(Jackson et al., 2006)
Pdgfa, *Fgf6*, *Cldn3*, *Tnxb*, *Abca1*, *Elavl2*	*In vitro* steady fluid shear stimulation of C3H and B6 murine osteoblasts	(Lau et al., 2006)
Fgf2	In ovo immobilisation of chick, knee joint	(Kavanagh et al., 2006)
Pdgfra, *Igf1*, *Itgb1bp2*, *Itga4*	*In vitro* applied microgravity to pre-osteoblasts using a random positioning machine	(Pardo et al., 2005)
Igf1	*In vitro* steady fluid shear stimulation of C3H and B6 murine osteoblasts	(Lau et al., 2006)
	In vitro mechanical cyclic tensile stretch on human osteoblast-like cells	(Cillo et al., 2000)
	In vivo: Four point bending of rat tibia	(Raab-Cullen et al., 1994)
Cdkn1a, *Hbegf*, *Sod3*	*In vitro*: chondrocyte cell line under continuous hydrostatic pressure	(Sironen et al., 2002)
Spp1	*In vitro*: intermittent hydrostatic pressure enhanced *Opn* (*Spp1*) expression in a ostoblast-like cell line. A loss of *Opn* expression in primary bone cells without mechanical stimulation	(Ishijima et al., 2002)
	In vitro: suggested that mechanotransduction acts through *Spp1* and the cytoskeleton in osteoblasts	(Toma et al., 1997)
	Ex vivo: Cyclic compression of whole rabbit femoral condyle explant	(Sundaramurthy and Mao, 2006)
	In vivo: Four point bending of rat tibia	(Raab-Cullen et al., 1994)
Fold change values for the genes named here are described in Appendix Table A.3		

7.1.2 Potential mechanisims of mechanotransduction

7.1.2.1 Cell membrane components responsible for sensing mechanical stimuli

Multiple potential mechanosensing machineries were implicated by altered expression of genes including the transient receptor potential (Trp) cation channel encoding genes (*Trpc5*, *Trpv1*) and the calcium channel voltage dependent encoding genes (*Cacna2d3*, *Cacna1s*, *Cacng1* and *Cacng6)*. The Trpv4 receptor has previously been shown to modulate the response to mechanical disuse (Mizoguchi et al., 2008) and be sensitive to shear stress (Gao et al., 2003). Eight G-protein coupled receptors (GPCRs) were found to be differentially expressed, and it was previously recognised that GPCRs serve as mechanosensors to fluid shear stress (Makino et al., 2006), thus highlighting potential for these genes to respond to an altered mechanical environment in our screen.

The identification of calcium channel voltage dependent encoding genes being down-regulated in muscle-less mutants, is supported by the identification that calcium signalling is implicated in mechanotransductive pathways (McMahon et al., 2008a; Riddle et al., 2006; Shakibaei and Mobasheri, 2003; Steward et al., 2014; Valhmu and Raia, 2002). Blocking of voltage gated calcium channels (VGCCs) was identified to abrogate chondrogenesis and impair cell proliferation in high-density MSC cultures (Fodor et al., 2013), further supporting their role for chondrogenesis *in vivo*. Recent work reports that the chondrogenic response of MSCs subjected to HP is reliant on the activity of VGCCs (Steward et al., 2014). VGCCs were previously reported to be involved in mechanotransduction following fluid flow and compression (Riddle et al., 2006; Shakibaei and Mobasheri, 2003; Valhmu and Raia, 2002), further corroborating the finding of VGCC encoded genes being down-regulated following removal of mechanical stimulation.

Integrin complexes are another group of genes that are implicated in transduction of biophysical stimuli to elicit cellular responses. Integrins are cell-surface receptors that connect the ECM to the actin cytoskeleton and transmit chemical and mechanical signals into cells

(reviewed in Docheva et al., 2014). Articular chondrocytes have been shown to express both integrin and non-integrin ECM receptors (Knudson et al., 1996; Woods et al., 1994). Under physical loading, integrins are activated on the surface of chondrocytes and have been shown to enhance cell proliferation (Chowdhury et al., 2004). Removal of loading in this system has resulted in the down-regulation of cell-adhesion associated integrins and cadherins, supporting the suggestion that they are involved in surface reception of mechanical stimuli.

7.1.2.2 Transmission of mechanical stimuli: The role of the Cytoskeleton

The cytoskeleton controls cell shape, organelle transport, cell motility and division, and connects the extracellular matrix to internal cell processes (reviewed in Alenghat and Ingber, 2002). It maintains the mechanical integrity of cells and has been implicated in relaying mechanical signals to downstream biochemical responses (Mammoto et al., 2012; Wang et al., 1993). This was observed in the embryonic lung where cytoskeletal network inhibitors resulted in altered tissue morphogenesis and conversely when cytoskeletal tension was activated, lung development was accelerated (reviewed in Ingber, 2006), indicating the dynamic role the cytoskeleton has in morphogenesis. The cytoskeleton has been demonstrated to be involved in the mechanotransduction of many different mechanical stimuli and has also been associated with Calcium signalling (Shakibaei and Mobasheri, 2003; Steward et al., 2014). Multiple genes associated with the cytoskeleton were identified to be DE; these include genes associated with microfilaments, microtubules and intermediate filaments. The most highly affected group, the filamentous-actin cytoskeleton, have previously been shown to be involved in articular cartilage chondrocyte mechanotransduction, converting mechanical stimuli into a biochemical response (Guilak, 1995; Knight et al., 2006; Parkkinen et al., 1995; Wang et al., 1993). In chondrocytes the actin microfilaments are predominantly located at the periphery of the cytoplasm (Idowu et al., 2000), tubulin microtubules are uniformly distributed throughout the cytoplasm (Jortikka et al., 2000) as are intermediate filaments,

connecting the nuclear membrane with the cell periphery (Blain et al., 2006), as shown in the schematic in Figure 7.1 with the names of the DE cytoskeletal associated genes listed.

The involvement of the actin cytoskeleton in cartilage chondrocyte mechanotransduction via manipulation of the actin accessory proteins has previously been uncovered (Campbell et al., 2007; Knight et al., 2006), but there are few reports on the effects of mechanical stimulation on microtubule and intermediate filaments (Steward et al., 2013). Recent work examining the influence of integrin-cytoskeletal mediated responses to mechanical stimuli, showed an alteration in the cytoskeletal organisation of the intermediate filament vimentin in response to HP (Steward et al., 2013). Alteration of the cytoskeleton has been shown to impact cell signalling, and thus could be the means that results in the alteration of transcription as demonstrated by alterations in cell signalling pathway components and downstream target genes.

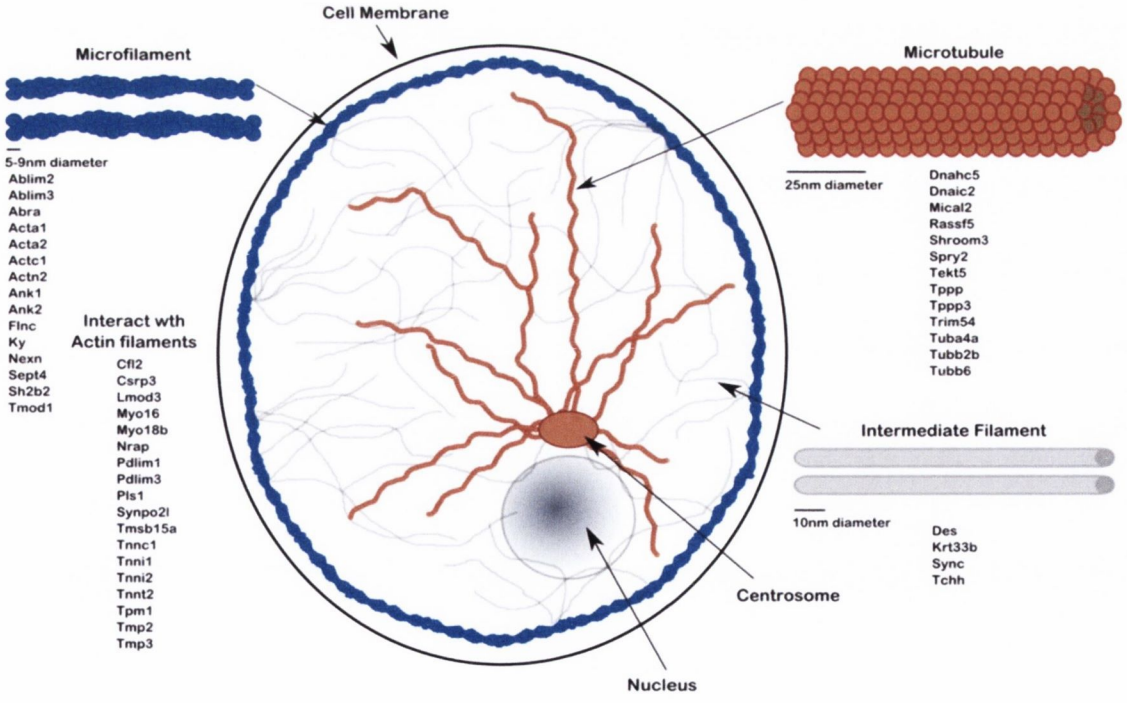

Figure 7.1: Visual representation of DE genes associated with cytoskeletal components.

Functional studies to test whether individual elements of the cytoskeleton alone can induce cellular responses from biophysical stimuli are required to understand in more detail the mechanisms of joint and bone development. An understanding of the role of individual cytoskeleton elements in cartilage biology is first required; to help to interpret responses that are altered with mechanical stimulation is applied in conjunction with an agent blocking one element of cytoskeletal function. Disruption of each cytoskeletal element was investigated in rabbit knee chondrocytes, with results showing that disruption of the micro-tubulin and intermediate filaments induced chondrocyte apoptosis and decreased *aggrecan* and *Col2a1* expression in cultures, suggesting that these elements of the cytoskeleton are involved in the synthesis of cartilage matrix by rabbit knee chondrocytes (Duan et al., 2014). The chondrogenic limb bud micromass culture system described in chapter 6 could be utilised to understand in more detail the embryonic cytoskeletal structure and function, prior to and after the application of mechanical stimuli. Blocking of individual elements of the cytoskeleton, for example the actin-polymerisation with Cytochalasin-D could subsequently be administered in parallel with mechanical stimuli, to identify whether mechanotransduction is occurring through this element of the cytoskeleton alone.

7.1.3 Molecular signalling is altered in the muscle-less mutant

Subsequent to the identification that multiple cell signalling pathway components that guide cell differentiation and tissue organisation were disturbed by an altered mechanical environment, three of the pathways most affected, Wnt, BMP and HH, were investigated in more detail. This approach also set out to separate potential molecular processes impacted by mechanical stimuli during distinct developmental events in the developing limb, with a particular focus on two main disturbances seen at the phenotypic level; ossification and joint definition.

Results from this differential screen agree with previously reported work seeking to identify molecular responses to mechanical stimulation. Previous mechanosensitive gene analysis

identified multiple components of signalling pathway to be altered, including *Sfrp2, Bmp3* (Patel et al., 2007), *Fzd10* (Bougault et al., 2012), *Bmp2, Pthlp* (Roddy et al., 2011b), *Fgfr1*, *Fgfr3*, *Fgfr4*, *Fgf1* (Jackson et al., 2006), *Fgf6* (Lau et al., 2006), *Fgf2* (Cillo et al., 2000; Kavanagh et al., 2006; Roddy et al., 2011b), and *Ihh* (Nowlan et al., 2008b), as detailed in Table 7:1 and Table 1:1. However the data created in this study adds extensively to previous reports and indicates a greater number of genes and pathways to be responsive to mechanical stimuli.

Expression analysis led to the suggestion that the Hedgehog pathway is abnormally activated in the ossification site of the muscle-less mutant, but that it feeds-back negatively (Figure 4.10). This suggestion builds on previous findings that this pathway is involved in the mechanotransduction of biophysical stimuli (Nowlan et al., 2012; Nowlan et al., 2008b). Overall analysis of BMP signalling revealed that BMP-mediated signalling is suppressed at the joint-line and in the ossification site of muscle-less mutants compared to control (Figure 4.11).

The BMP ligand *Bmp3* was previously shown to be differentially regulated in response to an alteration in the mechanical environment (Aspenberg et al., 2000; Patel et al., 2007). BMP signalling componenets have been shown to be regulated by muscle-induced movement during palate development, thus altering correct development (Rot and Kablar, 2013). The Wnt pathway appeared to be the most affected signalling pathway following removal of mechanical stimulation, yet the complexity of this deregulation was difficult to assess due to the up-regulation of pathway agonists and antagonists and the variable regulation status of down-stream pathway targets. This indicates that a tightly controlled balance of Wnt signalling might be fine tuned by mechanical signals and that Wnt signalling may be a main mediator of mechanoregulation, contributing to abnormal ossification and joints seen in muscle-less embryos.

7.1.4 The role of Wnt signalling in mechanotransduction

Wnt signalling was identified to be the most altered pathway in the reduced mechanical environment. Wnt signalling has previously been reported to be altered in mechanostimulatory experiments (Bougault et al., 2012; Case et al., 2008; Dell'Accio et al., 2006; Haudenschild et al., 2009; Hens et al., 2005; Kahn et al., 2009; Patel et al., 2007; Robinson et al., 2006; Robling et al., 2008), however this work greatly extends the pathway components identified to be responsive to mechanical stimulation. Differentially expressed wnt signalling components were identified to show spatially restricted patterns in both the developing joint and in the ossification site, corresponding to the sites of the two most affected phenotypic disturbances in the muscle-less mutant. This points towards wnt signalling being a key point of integration for mechanical cues to guide correct tissue patterning and differentiation.

Due to the alteration of wnt pathway components occurring predominately at two levels; extracellular (Wnt ligands, agonists and antagonists) and at the nuclear level (pathway target genes), it was obvious that complex cross interactions of wnt signalling must be occurring in the joint and ossification site of muscle-less mutants. Due to these observations and the identification that both a pathway ligand (*Wnt4*) and pathway antagonist (*Sfrp2*) were up-regulated in the developing joint it was hard at this point, to simplify the expression status of the pathway in the regions analysed, but these finding are suggestive of multiple levels of regulation of the pathway being affected. Sfrp2 has previously been identified to be a target of Wnt4 mediated pathway activation in the developing kidney (Lescher et al., 1998), and this could be why both are up-regulated in the muscle-less mutant in the same territories.

As wnt signalling was identified to be highly affected upon removal of mechanical stimulation, we set out to assess whether manipulation of wnt signalling phenocopies what is seen following the removal of mechanical stimulation. *Ex ovo* electroporation targeting the developing limb allowed for the modulation of wnt signalling in two ways. Firstly ectopic

over-activation of the pathway was performed by introducing the constitutively active β-catenin-Tcf fusion protein, and secondly ectopic over-expression of the pathway antagonist Sfrp3, was designed to suppress the pathway. Altering Wnt signalling was shown to have profound effects on chondrogenesis, in agreement with previous reports that modulated Wnt signalling in the chick and in the mutant mouse models (Akiyama et al., 2004; Day et al., 2005; Enomoto-Iwamoto et al., 2002; Geetha-Loganathan et al., 2010; Guo et al., 2004; Hartmann and Tabin, 2000; Hill et al., 2005; Rudnicki and Brown, 1997; Soshnikova et al., 2003). Although at a superficial level, both β-catenin activation and antagonist expression appeared to have similar effects, more careful analysis showed important distinctions; while activation caused gaps in chondrogenesis close to ectopically expressing cells, antagonist expression led to shortened, misshapen rudiments.

The techniques described in this work, specifically the optimisation of *ex ovo* electroporation, has added value by extending the techniques used to manipulate the developing chick. However further work is required to refine this manipulation in order to target specific regions of the developing limb, for example the elbow joint or within the rudiment, in order to identify whether manipulation of the pathway mimics what is seen when mechanical stimulation is removed. This technical advancement can potentially allow for future combined manipulation of the mechanical and the signalling environment.

Successful immobilisation is induced by *in ovo* treatment with a neuromuscular blocking agent (reviewed in section 1.5.1). I suggest that this treatment be administered using *ex ovo* cultivation, thus allowing the mechanical environment to be tested in conjunction with the administration of Wnt pathway modulators. This would assess whether Wnt modulation influences or rescues the phenotypic effects observed in the joint and ossification site following immobilisation. This would potentially be a major step forward in understanding how mechanical cues work together with classical molecular positional information to guide spatially appropriate tissue differentiation.

7.2 The Influence of mechanical stimulation on chondrogenesis

To assess how cells in culture respond to the application of mechanical stimulation, chapter 6 reports the comparison of the response of adult derived MSCs to embryo derived chondrogenic progenitors. This work established that embryonic chondrocytes and adult derived joint cells both respond to dynamic HP, by stabilising the chondrogenic state; HP acted to down-regulate the expression of genes associated with pre-hypertrophy and terminal differentiation (*Indian hedgehog* and *collagen type ten*) in both cell types, thus maintaining a stable cartilage phenotype, preventing maturation and hypertrophy.

Building on work described in chapter 6, future work should attempt to compare the chondrogenic response to mechanical stimulation by embryonic and adult cells from the same species. Due to the technical issues surrounding the derivation of adult mouse stem cells described in this thesis (chapter 6), murine MSCs should be procured from an external source, for example a specialist laboratory, to be used in future studies for comparison with embryonic limb bud cells. While murine adult articular cartilage derived cells demonstrated a morphology consistent with MSCs, there were inconsistencies and issuses with the purity of the cell population isolated. Future work isolating and proliferating adult derived murine cells should use a fluorescence-activated cell sorting (FACS) technique with established stem cell surface antibodies, for example Cd44 as previously established for synovium and bone marrow derived murine cells (Futami et al., 2012; Shen et al., 2011).

To extend the comparison further it would be valuable to try to recapitulate aspects of bone and joint development *in vitro*. For example a bioreactor system could be designed to mimic the embryonic mechanical environment and embryonic movement. Such a system could be used to compare the responses of adult derived stem cells and embryonic primary limb bud cells to specific stimuli in more detail. A system that exerted cycles of compression and strain on the surface of a 3D scaffold construct during bending would mimick the action of the contracting musculature in the developing limb. The stresses and strains generated within the

construct could be modelled using Finite Element analysis and could be compared to previously established models of contacting musculature (Roddy et al., 2011a). Monitoring the response to mechanical stimulation through expression of mechanosensitive genes and differentiation markers in 2D and 3D should be assessed. 3D imaging will be particularly important in this context since differential patterns of stimuli across the scaffold may lead to spatially organised differentiation.

7.3 Other future Directions highlighted from this work

7.3.1 What is the role of Hippo signalling in mechanotransduction?

The Hippo signalling pathway co-ordinates cell proliferation, apoptosis and differentiation for the regulation of organ development, with its perturbation resulting in tissue overgrowth and enlarged organ size (reviewed in Hiemer and Varelas, 2013). The pathway's role has been studied in various stem cell populations and has been shown to influence cell fate (reviewed in Hiemer and Varelas, 2013). Assessment of hippo pathway activity commonly relies on the localisation of the transcriptional regulators YAP/TAZ (Yorkie in Drosophila); if the pathway is activated YAP/TAZ are phosphorylated and cytoplasmic levels are increased, resulting in decreased YAP/TAZ transcriptional activity. If the pathway is not activated, nuclear localisation of YAP/TAZ occurs thus enhancing transcriptional activation (reviewed in Hiemer and Varelas, 2013). The localisation of YAP/TAZ has been shown to be sensitive to external factors including cell morphology (Wada et al., 2011), cell density and substrate stiffness (Aragona et al., 2013). YAP/TAZ has been shown to be required for the differentiation of mesenchymal stem cells induced by mechanical stimuli (Dupont et al., 2011), and further interesting associations linking the hippo pathway with actin cytoskeletal changes (Dupont et al., 2011; Wada et al., 2011; Zhao et al., 2012) highlights the potential importance of the pathway to sense and respond to mechanical stimulation.

The identification of 5 members of the hippo signalling pathway being differentially expressed following removal of mechanical stimulation in the *Spd* mutant model further highlights this pathway and its interaction with the cytoskeleton controlling chondrocyte cell fate as an area that requires further investigation. Interestingly two transmembrane proteins, *Fat2* and *Fat4* protocadherins that act as receptors for the pathway were found to be up-regulated and two co-transcription factors (*Tead4*, *Vgll2*) and one target gene was down-regulated following the removal of mechanical stimuli, suggesting that the pathway is activated and no nuclear localisation is occurring thus affecting cell proliferation. Future work analysing the localisation of YAP/TAZ in muscle-less mutants would address whether the pathway is activated or not in the regions showing phenotypic alterations. Mutations in the Fat4 gene have been associated with defects in the sternum, and abnormal patterns of ossification (Mao et al., 2011). To understand whether hippo signalling is involved in skeletal development analysis of hippo components should be screened in skeletal elements during development, to identify embryonic expression, and also in muscle-less embryos to identify whether they are spatially affected.

The hippo signalling pathway has also been demonstrated to negatively regulate Wnt signalling (Heallen et al., 2011; Varelas et al., 2010), thus further investigation into these two pathways during chondrogenesis for joint development and during endochondral ossification, might help to identify their role in the mechanical regulation of skeletal development.

7.3.2 Potetinal role of microRNAs in mechanotransduction?

Another level of gene regulation that could be involved in the integration of biophysical stimulation to elicit molecular responses is through the action of microRNAs (miRNAs). In fact 8 miRNAs were found to be down-regulated in the muscle-less mutant humeri (Appendix Table A.3). MiRNAs are non-coding regulatory RNAs of 19-22nucleotides in length that, play an important role in the post-transcriptional regulation of target mRNA or the translational repression of target proteins (reviewed in Papaioannou et al., 2014). Multiple

miRNAs have been reported to be expressed in developing bone (reviewed in Papaioannou et al., 2014).

Of the eight miRNAs identified to be differentially expressed two (mir17hg, mir133a) have been reported to be associated with skeletal development. The mir17hg locus encodes the miR17-92 cluster, which has been shown to be essential for mammalian development. Mice with deletions for a single allele of miR17-92 have severe shortening of the limbs, with an absence of the mesophalanx of the fifth digit (de Pontual et al., 2011). Haploinsufficiency of the miR17-92 cluster impairs osteoblast proliferation and differentiation (Zhou et al., 2014), and germ-line deletions of the cluster in humans are seen with brachydactyly and other anomalies in the hands and feet (de Pontual et al., 2011). MiRNA 133a was identified to be expressed in mouse pre-osteoblastic cells, and suggested to have an inverse correlation with osterix expression in the mouse skull (Chen et al., 2013).

Another miRNA demonstrated to be DE, mir23b, has been reported to induce differentiation of hMSCs into chondrocytes (Ham et al., 2012). This miRNA has been shown to be up-regulated following pulsatile shear flow in endothelial cells; and revealed to play a significant role in mediating the flow-induced suppression of gene expression (Wang et al., 2010). The mir17-92 was also demonstrated to be differentially expressed in response to shear flow (Wang et al., 2010). In parallel to the results of this study these miRNAs represent examples of the potential roles of miRNAs in mechanotransduction, and therefore could be of keen interest to understand more about the mechanisms of mechanostransduction. The transcriptomic analysis described in this thesis was not designed to capture small miRNAs specifically and some may have escaped detection because of their small size. Therefore an analysis focusing specifically on detecting miRNAs, such as use of a miRNA specific microarray chip, might produce more data on disturbances at this level.

7.3.3 Investigation into the regulatory mechanisms impacted by mechanical stimulation?

Work to date has clearly shown that mechanical stimulation generated by muscle contractions is required for normal ossification and the definition of constituent tissue patterning in the joint. However, as previously noted, until now we knew nothing of the molecular mechanisms that mediate the effects. Elucidating aspects of these as yet unknown molecular mechanisms hold potential for a truly novel insight into gene regulation. The regulation of gene expression involves a diverse regulatory system. Chapter 3 described the identification of mechanoresponsive genes, including both direct and indirect genes. Chapter 4 shows the spatial expression of signalling pathway genes, which can be used to more closely predict their part in specific developmental processes and their response to an altered mechanical environment. Each gene contains a unique combination of regulatory sequence elements in the genomic regions surrounding the coding sequence of the gene, most often but not exclusively at the 5' end, that determines its temporal and spatial expression. The development of different cell types is governed ultimately by molecular interactions at these regulatory regions that influence gene activity (note that gene expression during embryonic development is often predominantly controlled at the level of transcription). This involves the binding of Transcriptions Factors (TFs) to these regulatory elements (Transcription-Factor Binding Sites; TFBS). Interactions between bound TFs and cofactors stabilise the transcription-initiation machinery to enable gene expression (Wasserman and Sandelin, 2004). If mechanical cues somehow influence the binding of TFs to TFBSs, identifying potential regulatory regions containing such TFBSs would be possible through the comparison and identification of common regulatory regions in mechanoresponsive genes.

Utilising a bioinformatics approach to analyse putative regulatory regions of candidate genes could be performed to identify any common control sites. Following the identification of these control regions for individual genes or groups of genes, these could be analysed using phylogenetic foot-printing for cross species sequence conservation, which is an indicator of

functionally important (therefore conserved) regulatory elements. Chick-mouse comparisons would be of particular importance because we know that the responses to mechanical stimulation are similar across birds and mammals and the chick presents a more compact genome, decreasing the possibility of noise in the analysis (ChickGenome, 2004). Appropriate tools for the identification of predicted upstream regulators can be used including, Ingenuity pathway analysis (http://www.ingenuity.com/), and oPOSSUM (http://opossum.cisreg.ca/oPOSSUM3/). Both are powerful tools for biologists seeking insight into gene regulatory networks (Kwon et al., 2012).

I carried out preliminary oPOSSUM analysis of the DE genes identified in this study and found that *Hoxa5* and *Klf4* were the transcription factors identified to be most commonly associated with the up-regulated and down-regulated genes respectively (Data not shown). Opossum single site analysis (SSA) is a tool for identification of over-represented transcription factor binding sites (TFBS) in the promoters of co-expressed genes. The oPOSSUM system for identifying over-represented TFBSs in sets of co-expressed genes is built upon a database of conserved TFBSs for human-mouse orthologs, derived from an analysis pipeline that combines phylogenetic footprinting with TFBS identification using the JASPER (Sandelin et al., 2004) library of PSSMs (position specific scoring matrices). Given a set of human or mouse genes, the pipeline retrieves the genomic DNA sequence for the human and mouse genes plus 5000bp of the upstream/downstream sequence, it performs an alignment of the orthologous sequences and extracts non-coding DNA subsequences that are conserved above a predefined threshold. The software then searches the sub-sequences for matches to TFBS profiles contained in JASPER and stores the results in the oPOSSUM database. Upon querying the web based interface with a list of co-expressed genes the software retrieves the TFBS counts for each gene in the list and computes two statistics (Z-score, Fischer exact test) to measure over-representation of TFBSs in the set relative to a background comprising all genes in the oPOSSUM database.

Hoxa5 is a homeobox gene that was found in the 5000bp region upstream or downstream of 411 out of 452 of the up-regulated genes from the RNA-seq dataset. Hoxa5 binds to the motif 5'-CYYNATTA[TG]Y-3'. The Hoxa5 gene is expressed widely in cartilaginous tissues at E14.5 (Diez-Roux et al., 2011), and the knockout mutant displays abnormalities in skeletal structures of the cervical and thoracic regions (described in Jeannotte et al., 1993). Kruppel-like factor 4 (*Klf4*) is a zinc finger type of transcription factor highly expressed in the skin, intestine, testis, lung and bone. Klf4 was identified in the 5000bp region upstream or downstream of 519 out of 680 down-regulated DE genes. In the long bones expression of *Klf4* is reported to be restricted to the pre-hypertrophic chondrocytes, perichondrium and osteoblasts (Michikami et al., 2012). Klf4 transgenic mice, where Klf4 is ectopically expressed under the collagen type 1 regulatory sequence, show skeletal deformities, including a reduction in the length and mineralised content of long bones (Michikami et al., 2012). Klf4 can act as an activator and repressor and binds to a 5'-CACCC-3' core sequence. Neither Hoxa5 or Klf4 are differentially expressed ($FC \geq 2$, $p \leq 0.05$) in the screen described here. These two transcription factors are two examples of regulators of some of the DE genes identified, whose activity is potentially impacted when the mechanical environment is altered. This analysis also has the potential of indicating regulatory regions that are responsive to mechanical stimuli. This analysis needs to be extended and tested more rigorously but it holds the potential of indicating regulatory regions that are responsive to mechanical stimuli. This could be built on in future work to design cell culture assays to test the mechnoresponsiveness of specific control elements.

7.4 Broader implications of understanding embryonic mechanobiology

Much progress has been made over recent years towards understanding the role that mechanical stimulation has on the development of tissues and the impact it has to guide cell differentiation. The response that cells make following the application of external mechanical stimulation has been demonstrated to be critical for the correct differentiation and formation

of skeletal tissues. However until recently the mechanisms by which cells respond to biophysical stimuli remained poorly understood. Developmental research provides a great deal of knowledge about the molecular mechanisms that guide normal development; therefore through the alteration of the mechanical environment during the development of skeletal structures it has been possible to gain insights into the mechanisms that sense and respond to mechanical cues, and to study the impact that it has on the skeleton.

Understanding how the mechanical environment impacts cellular differentiation has tremendous impact to other research fields. For example tissue engineers apply principles from biology and engineering to try to develop functionally viable tissues. This strategy uses stem cells in combination with biomaterial scaffolds, and alterations in the mechanical environment to attempt to create functionally viable tissue. Information from the developing embryo about the mechanistic response to alterations in the mechanical environment could inform new strategies in tissue engineering for regenerative approaches for diseased or damaged skeletal conditions, such as osteoarthritis. For example, results from this thesis suggest that potential modulation of the signalling environment (with focus on the wnt pathway) experienced by the cell could, in conjunction with application of mechanical stimulation be an important regulator of chondrogenesis for articular cartilage differentiation. Uncovering the molecular outcomes of the integrated signalling environment provides the possibility of designing a strategy that potentially incorporates spatially localised biochemical signals with mechanical stimulation; either by transfecting cells, or localised delivery of genes/proteins in a 3D scaffold. First more work is required to understand precisely which source of cells respond to particular signals and then asses which aspects of the environment in normal development need to be re-capitulated and which can be stimulated more conveniently to guide differentiation.

References

Abe, Y., Kita, Y., Niikura, T., 2008. Mammalian Gup1, a homolog of Saccharomyces cerevisiae glycerol uptake/transporter 1, acts as a negative regulator for N-terminal palmitoylation of Sonic hedgehog. FEBS J. 275, 318-31.

Abed, E., Chan, T. F., Delalandre, A., Martel-Pelletier, J., Pelletier, J. P., Lajeunesse, D., 2011. R-spondins are newly recognized players in osteoarthritis that regulate Wnt signaling in osteoblasts. Arthritis Rheum. 63, 3865-75.

Adamo, L., Naveiras, O., Wenzel, P. L., McKinney-Freeman, S., Mack, P. J., Gracia-Sancho, J., Suchy-Dicey, A., Yoshimoto, M., Lensch, M. W., Yoder, M. C., Garcia-Cardena, G., Daley, G. Q., 2009. Biomechanical forces promote embryonic haematopoiesis. Nature. 459, 1131-5.

Ahrens, P. B., Solursh, M., Reiter, R. S., 1977. Stage-related capacity for limb chondrogenesis in cell culture. Dev Biol. 60, 69-82.

Aigner, T., Stove, J., 2003. Collagens--major component of the physiological cartilage matrix, major target of cartilage degeneration, major tool in cartilage repair. Adv Drug Deliv Rev. 55, 1569-93.

Aigouy, B., Farhadifar, R., Staple, D. B., Sagner, A., Roper, J. C., Julicher, F., Eaton, S., 2010. Cell flow reorients the axis of planar polarity in the wing epithelium of Drosophila. Cell. 142, 773-86.

Akavia, U. D., Socher, R., Benayahu, D., 2012. Tracking the molecular signature of developing skeletal tissues. Front Biosci (Elite Ed). 4, 1941-50.

Akiyama, H., Chaboissier, M. C., Martin, J. F., Schedl, A., de Crombrugghe, B., 2002. The transcription factor Sox9 has essential roles in successive steps of the chondrocyte differentiation pathway and is required for expression of Sox5 and Sox6. Genes Dev. 16, 2813-28.

Akiyama, H., Lyons, J. P., Mori-Akiyama, Y., Yang, X., Zhang, R., Zhang, Z., Deng, J. M., Taketo, M. M., Nakamura, T., Behringer, R. R., McCrea, P. D., de Crombrugghe, B., 2004. Interactions between Sox9 and beta-catenin control chondrocyte differentiation. Genes Dev. 18, 1072-87.

Alenghat, F. J., Ingber, D. E., 2002. Mechanotransduction: all signals point to cytoskeleton, matrix, and integrins. Sci STKE. 2002, pe6.

Amizuka, N., Warshawsky, H., Henderson, J. E., Goltzman, D., Karaplis, A. C., 1994. Parathyroid hormone-related peptide-depleted mice show abnormal epiphyseal cartilage development and altered endochondral bone formation. J Cell Biol. 126, 1611-23.

Angele, P., Schumann, D., Angele, M., Kinner, B., Englert, C., Hente, R., Fuchtmeier, B., Nerlich, M., Neumann, C., Kujat, R., 2004. Cyclic, mechanical compression enhances chondrogenesis of mesenchymal progenitor cells in tissue engineering scaffolds. Biorheology. 41, 335-46.

Angele, P., Yoo, J. U., Smith, C., Mansour, J., Jepsen, K. J., Nerlich, M., Johnstone, B., 2003. Cyclic hydrostatic pressure enhances the chondrogenic phenotype of human mesenchymal progenitor cells differentiated in vitro. J Orthop Res. 21, 451-7.

Aragona, M., Panciera, T., Manfrin, A., Giulitti, S., Michielin, F., Elvassore, N., Dupont, S., Piccolo, S., 2013. A mechanical checkpoint controls multicellular growth through YAP/TAZ regulation by actin-processing factors. Cell. 154, 1047-59.

Archer, C. W., Dowthwaite, G. P., Francis-West, P., 2003. Development of synovial joints. Birth Defects Res C Embryo Today. 69, 144-55.

Arnsdorf, E. J., Tummala, P., Jacobs, C. R., 2009a. Non-canonical Wnt signaling and N-cadherin related beta-catenin signaling play a role in mechanically induced osteogenic cell fate. PLoS One. 4, e5388.

Arnsdorf, E. J., Tummala, P., Kwon, R. Y., Jacobs, C. R., 2009b. Mechanically induced osteogenic differentiation--the role of RhoA, ROCKII and cytoskeletal dynamics. J Cell Sci. 122, 546-53.

Asharani, P. V., Keupp, K., Semler, O., Wang, W., Li, Y., Thiele, H., Yigit, G., Pohl, E., Becker, J., Frommolt, P., Sonntag, C., Altmuller, J., Zimmermann, K., Greenspan, D. S., Akarsu, N. A., Netzer, C., Schonau, E., Wirth, R., Hammerschmidt, M., Nurnberg, P., Wollnik, B., Carney, T. J., 2012. Attenuated BMP1 function compromises osteogenesis, leading to bone fragility in humans and zebrafish. Am J Hum Genet. 90, 661-74.

Aspenberg, P., Basic, N., Tagil, M., Vukicevic, S., 2000. Reduced expression of BMP-3 due to mechanical loading: a link between mechanical stimuli and tissue differentiation. Acta Orthop Scand. 71, 558-62.

Babitt, J. L., Huang, F. W., Wrighting, D. M., Xia, Y., Sidis, Y., Samad, T. A., Campagna, J. A., Chung, R. T., Schneyer, A. L., Woolf, C. J., Andrews, N. C., Lin, H. Y., 2006. Bone morphogenetic protein signaling by hemojuvelin regulates hepcidin expression. Nat Genet. 38, 531-9.

Bahamonde, M. E., Lyons, K. M., 2001. BMP3: to be or not to be a BMP. J Bone Joint Surg Am. 83-A Suppl 1, S56-62.

Baldridge, D., Shchelochkov, O., Kelley, B., Lee, B., 2010. Signaling pathways in human skeletal dysplasias. Annu Rev Genomics Hum Genet. 11, 189-217.

Bandyopadhyay, A., Tsuji, K., Cox, K., Harfe, B. D., Rosen, V., Tabin, C. J., 2006. Genetic analysis of the roles of BMP2, BMP4, and BMP7 in limb patterning and skeletogenesis. PLoS Genet. 2, e216.

Banziger, C., Soldini, D., Schutt, C., Zipperlen, P., Hausmann, G., Basler, K., 2006. Wntless, a conserved membrane protein dedicated to the secretion of Wnt proteins from signaling cells. Cell. 125, 509-22.

Barros, A., Teixeira, F., Camacho, M. C., Alves, C., 2011. Campomelic dysplasia and malignant hyperthermia. BMJ Case Rep. 2011.

Beak, J. Y., Kang, H. S., Kim, Y. S., Jetten, A. M., 2007. Kruppel-like zinc finger protein Glis3 promotes osteoblast differentiation by regulating FGF18 expression. J Bone Miner Res. 22, 1234-44.

Beissbarth, T., Speed, T. P., 2004. GOstat: find statistically overrepresented Gene Ontologies within a group of genes. Bioinformatics. 20, 1464-5.

Bell, D. M., Leung, K. K., Wheatley, S. C., Ng, L. J., Zhou, S., Ling, K. W., Sham, M. H., Koopman, P., Tam, P. P., Cheah, K. S., 1997. SOX9 directly regulates the type-II collagen gene. Nat Genet. 16, 174-8.

Belluoccio, D., Bernardo, B. C., Rowley, L., Bateman, J. F., 2008. A microarray approach for comparative expression profiling of the discrete maturation zones of mouse growth plate cartilage. Biochim Biophys Acta. 1779, 330-40.

Bellusci, S., Furuta, Y., Rush, M. G., Henderson, R., Winnier, G., Hogan, B. L., 1997. Involvement of Sonic hedgehog (Shh) in mouse embryonic lung growth and morphogenesis. Development. 124, 53-63.

Benjamini Y., H. Y., 1995. Controlling the False Discovery Rate: a Practical and Powerful approach to Multiple testing. Journal of the Royal Statistical Society. Series B (Methodological). 57, 289-300.

Bernstein, P., Dong, M., Graupher, S., Corbeil, D., Gelinsky, M., Gunther, K. P., Fickert, S., 2009. Sox9 expression of alginate-encapsulated chondrocytes is stimulated by low cell density. J Biomed Mater Res A. 91, 910-8.

Bernstein, P., Sticht, C., Jacobi, A., Liebers, C., Manthey, S., Stiehler, M., 2010. Expression pattern differences between osteoarthritic chondrocytes and mesenchymal stem cells during chondrogenic differentiation. Osteoarthritis Cartilage.

Bi, W., Deng, J. M., Zhang, Z., Behringer, R. R., de Crombrugghe, B., 1999. Sox9 is required for cartilage formation. Nat Genet. 22, 85-9.

Bi, W., Huang, W., Whitworth, D. J., Deng, J. M., Zhang, Z., Behringer, R. R., de Crombrugghe, B., 2001. Haploinsufficiency of Sox9 results in defective cartilage primordia and premature skeletal mineralization. Proc Natl Acad Sci U S A. 98, 6698-703.

Bizzoca, A., Corsi, P., Polizzi, A., Pinto, M. F., Xenaki, D., Furley, A. J., Gennarini, G., 2012. F3/Contactin acts as a modulator of neurogenesis during cerebral cortex development. Dev Biol. 365, 133-51.

Blain, E. J., Gilbert, S. J., Hayes, A. J., Duance, V. C., 2006. Disassembly of the vimentin cytoskeleton disrupts articular cartilage chondrocyte homeostasis. Matrix Biol. 25, 398-408.

Blitz, E., Viukov, S., Sharir, A., Shwartz, Y., Galloway, J. L., Pryce, B. A., Johnson, R. L., Tabin, C. J., Schweitzer, R., Zelzer, E., 2009. Bone ridge patterning during musculoskeletal assembly is mediated through SCX regulation of Bmp4 at the tendon-skeleton junction. Dev Cell. 17, 861-73.

Bohm, J., Sustmann, C., Wilhelm, C., Kohlhase, J., 2006. SALL4 is directly activated by TCF/LEF in the canonical Wnt signaling pathway. Biochem Biophys Res Commun. 348, 898-907.

Bolstad, B. M., Irizarry, R. A., Astrand, M., Speed, T. P., 2003. A comparison of normalization methods for high density oligonucleotide array data based on variance and bias. Bioinformatics. 19, 185-93.

Boon, E. M., van der Neut, R., van de Wetering, M., Clevers, H., Pals, S. T., 2002. Wnt signaling regulates expression of the receptor tyrosine kinase met in colorectal cancer. Cancer Res. 62, 5126-8.

Bottomly, D., Walter, N. A., Hunter, J. E., Darakjian, P., Kawane, S., Buck, K. J., Searles, R. P., Mooney, M., McWeeney, S. K., Hitzemann, R., 2011. Evaluating gene expression in C57BL/6J and DBA/2J mouse striatum using RNA-Seq and microarrays. PLoS One. 6, e17820.

Bougault, C., Aubert-Foucher, E., Paumier, A., Perrier-Groult, E., Huot, L., Hot, D., Duterque-Coquillaud, M., Mallein-Gerin, F., 2012. Dynamic compression of chondrocyte-agarose constructs reveals new candidate mechanosensitive genes. PLoS One. 7, e36964.

Bougault, C., Paumier, A., Aubert-Foucher, E., Mallein-Gerin, F., 2008. Molecular analysis of chondrocytes cultured in agarose in response to dynamic compression. BMC Biotechnol. 8, 71.

Brunet, L. J., McMahon, J. A., McMahon, A. P., Harland, R. M., 1998. Noggin, cartilage morphogenesis, and joint formation in the mammalian skeleton. Science. 280, 1455-7.

Buckley, C. T., Vinardell, T., Thorpe, S. D., Haugh, M. G., Jones, E., McGonagle, D., Kelly, D. J., 2010. Functional properties of cartilaginous tissues engineered from infrapatellar fat pad-derived mesenchymal stem cells. J Biomech. 43, 920-6.

Buckwalter, J. A., Martin, J. A., 2006. Osteoarthritis. Adv Drug Deliv Rev. 58, 150-67.

Cameron, T. L., Belluoccio, D., Farlie, P. G., Brachvogel, B., Bateman, J. F., 2009. Global comparative transcriptome analysis of cartilage formation in vivo. BMC Dev Biol. 9, 20.

Campbell, J. J., Blain, E. J., Chowdhury, T. T., Knight, M. M., 2007. Loading alters actin dynamics and up-regulates cofilin gene expression in chondrocytes. Biochem Biophys Res Commun. 361, 329-34.

Cao, X., Chen, D., 2005. The BMP signaling and in vivo bone formation. Gene. 357, 1-8.

Carmeliet, G., Vico, L., Bouillon, R., 2001. Space flight: a challenge for normal bone homeostasis. Crit Rev Eukaryot Gene Expr. 11, 131-44.

Carroll, S. F., Buckley, C. T., Kelly, D. J., 2014. Cyclic hydrostatic pressure promotes a stable cartilage phenotype and enhances the functional development of cartilaginous grafts engineered using multipotent stromal cells isolated from bone marrow and infrapatellar fat pad. J Biomech. 47, 2115-21.

Carter, D. R., Beaupre, G. S., Giori, N. J., Helms, J. A., 1998. Mechanobiology of skeletal regeneration. Clin Orthop Relat Res. S41-55.

Carter, D. R., Beaupre, G. S., Wong, M., Smith, R. L., Andriacchi, T. P., Schurman, D. J., 2004. The mechanobiology of articular cartilage development and degeneration. Clin Orthop Relat Res. S69-77.

Carter, D. R., Wong, M., 2003. Modelling cartilage mechanobiology. Philos Trans R Soc Lond B Biol Sci. 358, 1461-71.

Case, N., Ma, M., Sen, B., Xie, Z., Gross, T. S., Rubin, J., 2008. Beta-catenin levels influence rapid mechanical responses in osteoblasts. J Biol Chem. 283, 29196-205.

Castagnola, P., Moro, G., Descalzi-Cancedda, F., Cancedda, R., 1986. Type X collagen synthesis during in vitro development of chick embryo tibial chondrocytes. J Cell Biol. 102, 2310-7.

Chen, J. H., Liu, C., You, L., Simmons, C. A., 2009. Boning up on Wolff's Law: mechanical regulation of the cells that make and maintain bone. J Biomech. 43, 108-18.

Chen, L., Chan, S. W., Zhang, X., Walsh, M., Lim, C. J., Hong, W., Song, H., 2010a. Structural basis of YAP recognition by TEAD4 in the hippo pathway. Genes Dev. 24, 290-300.

Chen, Q., Liu, W., Sinha, K. M., Yasuda, H., de Crombrugghe, B., 2013. Identification and characterization of microRNAs controlled by the osteoblast-specific transcription factor Osterix. PLoS One. 8, e58104.

Chen, W., Qing, H., He, Y., Wang, J., Zhu, Z., Wang, H., 2010b. Gene expression patterns of osteocyte-like MLO-Y4 cells in response to cyclic compressive force stimulation. Cell Biology International. 34, 425-432.

ChickGenome, 2004. Sequence and comparative analysis of the chicken genome provide unique perspectives on vertebrate evolution. Nature. 432, 695-716.

Choi, K. H., Choi, B. H., Park, S. R., Kim, B. J., Min, B. H., 2010. The chondrogenic differentiation of mesenchymal stem cells on an extracellular matrix scaffold derived from porcine chondrocytes. Biomaterials. 31, 5355-65.

Chow, G., Nietfeld, J. J., Knudson, C. B., Knudson, W., 1998. Antisense inhibition of chondrocyte CD44 expression leading to cartilage chondrolysis. Arthritis Rheum. 41, 1411-9.

Chowdhury, T. T., Salter, D. M., Bader, D. L., Lee, D. A., 2004. Integrin-mediated mechanotransduction processes in TGFbeta-stimulated monolayer-expanded chondrocytes. Biochem Biophys Res Commun. 318, 873-81.

Christiansen, J. H., Dennis, C. L., Wicking, C. A., Monkley, S. J., Wilkinson, D. G., Wainwright, B. J., 1995. Murine Wnt-11 and Wnt-12 have temporally and spatially restricted expression patterns during embryonic development. Mech Dev. 51, 341-50.

Chuang, P. T., McMahon, A. P., 1999. Vertebrate Hedgehog signalling modulated by induction of a Hedgehog-binding protein. Nature. 397, 617-21.

Church, V., Nohno, T., Linker, C., Marcelle, C., Francis-West, P., 2002. Wnt regulation of chondrocyte differentiation. J Cell Sci. 115, 4809-18.

Church, V. L., Francis-West, P., 2002. Wnt signalling during limb development. Int J Dev Biol. 46, 927-36.

Cillo, J. E., Jr., Gassner, R., Koepsel, R. R., Buckley, M. J., 2000. Growth factor and cytokine gene expression in mechanically strained human osteoblast-like cells: implications for distraction osteogenesis. Oral Surg Oral Med Oral Pathol Oral Radiol Endod. 90, 147-54.

Claes, L., Augat, P., Schorlemmer, S., Konrads, C., Ignatius, A., Ehrnthaller, C., 2008. Temporary distraction and compression of a diaphyseal osteotomy accelerates bone healing. J Orthop Res. 26, 772-7.

Connelly, J. T., Vanderploeg, E. J., Mouw, J. K., Wilson, C. G., Levenston, M. E., 2010. Tensile loading modulates bone marrow stromal cell differentiation and the development of engineered fibrocartilage constructs. Tissue Eng Part A. 16, 1913-23.

Croteau, L. P., Kania, A., 2011. Optimisation of in ovo electroporation of the chick neural tube. J Neurosci Methods. 201, 381-4.

Crowe, R., Zikherman, J., Niswander, L., 1999. Delta-1 negatively regulates the transition from prehypertrophic to hypertrophic chondrocytes during cartilage formation. Development. 126, 987-98.

Daluiski, A., Engstrand, T., Bahamonde, M. E., Gamer, L. W., Agius, E., Stevenson, S. L., Cox, K., Rosen, V., Lyons, K. M., 2001. Bone morphogenetic protein-3 is a negative regulator of bone density. Nat Genet. 27, 84-8.

Datar, S., Bhonde, R. R., 2005. Shell-less chick embryo culture as an alternative in vitro model to investigate glucose-induced malformations in mammalian embryos. Rev Diabet Stud. 2, 221-7.

Day, T. F., Guo, X., Garrett-Beal, L., Yang, Y., 2005. Wnt/beta-catenin signaling in mesenchymal progenitors controls osteoblast and chondrocyte differentiation during vertebrate skeletogenesis. Dev Cell. 8, 739-50.

De Bari, C., Dell'Accio, F., Tylzanowski, P., Luyten, F. P., 2001. Multipotent mesenchymal stem cells from adult human synovial membrane. Arthritis Rheum. 44, 1928-42.

de Pontual, L., Yao, E., Callier, P., Faivre, L., Drouin, V., Cariou, S., Van Haeringen, A., Genevieve, D., Goldenberg, A., Oufadem, M., Manouvrier, S., Munnich, A., Vidigal, J. A., Vekemans, M., Lyonnet, S., Henrion-Caude, A., Ventura, A., Amiel, J., 2011. Germline deletion of the miR-17 approximately 92 cluster causes skeletal and growth defects in humans. Nat Genet. 43, 1026-30.

Dell'Accio, F., De Bari, C., El Tawil, N. M., Barone, F., Mitsiadis, T. A., O'Dowd, J., Pitzalis, C., 2006. Activation of WNT and BMP signaling in adult human articular cartilage following mechanical injury. Arthritis Res Ther. 8, R139.

Deng, C., Wynshaw-Boris, A., Zhou, F., Kuo, A., Leder, P., 1996. Fibroblast growth factor receptor 3 is a negative regulator of bone growth. Cell. 84, 911-21.

Devlin, R. D., Du, Z., Pereira, R. C., Kimble, R. B., Economides, A. N., Jorgetti, V., Canalis, E., 2003. Skeletal overexpression of noggin results in osteopenia and reduced bone formation. Endocrinology. 144, 1972-8.

Dickhut, A., Pelttari, K., Janicki, P., Wagner, W., Eckstein, V., Egermann, M., Richter, W., 2009. Calcification or dedifferentiation: requirement to lock mesenchymal stem cells in a desired differentiation stage. J Cell Physiol. 219, 219-26.

Diez-Roux, G., Banfi, S., Sultan, M., Geffers, L., Anand, S., Rozado, D., Magen, A., Canidio, E., Pagani, M., Peluso, I., Lin-Marq, N., Koch, M., Bilio, M., Cantiello, I., Verde, R., De Masi, C., Bianchi, S. A., Cicchini, J., Perroud, E., Mehmeti, S., Dagand, E., Schrinner, S., Nurnberger, A., Schmidt, K., Metz, K., Zwingmann, C., Brieske, N., Springer, C., Hernandez, A. M., Herzog, S., Grabbe, F., Sieverding, C., Fischer, B., Schrader, K., Brockmeyer, M., Dettmer, S., Helbig, C., Alunni, V., Battaini, M. A., Mura, C., Henrichsen, C. N., Garcia-Lopez, R., Echevarria, D., Puelles, E., Garcia-Calero, E., Kruse, S., Uhr, M., Kauck, C., Feng, G., Milyaev, N., Ong, C. K., Kumar, L., Lam, M., Semple, C. A., Gyenesei, A., Mundlos, S., Radelof, U., Lehrach, H., Sarmientos, P., Reymond, A., Davidson, D. R., Dolle, P., Antonarakis, S. E., Yaspo, M. L., Martinez, S., Baldock, R. A., Eichele, G., Ballabio, A., 2011. A high-resolution anatomical atlas of the transcriptome in the mouse embryo. PLoS Biol. 9, e1000582.

Docheva, D., Popov, C., Alberton, P., Aszodi, A., 2014. Integrin signaling in skeletal development and function. Birth Defects Res C Embryo Today. 102, 13-36.

Dolle, P., 2009. Developmental expression of retinoic acid receptors (RARs). Nucl Recept Signal. 7, e006.

Dowthwaite, G. P., Edwards, J. C., Pitsillides, A. A., 1998. An essential role for the interaction between hyaluronan and hyaluronan binding proteins during joint development. J Histochem Cytochem. 46, 641-51.

Dowthwaite, G. P., Flannery, C. R., Flannelly, J., Lewthwaite, J. C., Archer, C. W., Pitsillides, A. A., 2003. A mechanism underlying the movement requirement for synovial joint cavitation. Matrix Biol. 22, 311-22.

Dowthwaite, G. P., Ward, A. C., Flannely, J., Suswillo, R. F., Flannery, C. R., Archer, C. W., Pitsillides, A. A., 1999. The effect of mechanical strain on hyaluronan metabolism in embryonic fibrocartilage cells. Matrix Biol. 18, 523-32.

Drachman, D. B. S., L., 1966. The role of movement in embryonic joint development. Developmental Biology. 14, 401-420.

Dragoo, J. L., Samimi, B., Zhu, M., Hame, S. L., Thomas, B. J., Lieberman, J. R., Hedrick, M. H., Benhaim, P., 2003. Tissue-engineered cartilage and bone using stem cells from human infrapatellar fat pads. J Bone Joint Surg Br. 85, 740-7.

Duan, W., Wei, L., Cao, X., Guo, H., Wang, L., Hao, Y., Wei, X., 2014. Effect of the disruption of three cytoskeleton components on chondrocyte metabolism in rabbit knee cartilage. Chin Med J (Engl). 127, 3764-70.

Dupont, S., Morsut, L., Aragona, M., Enzo, E., Giulitti, S., Cordenonsi, M., Zanconato, F., Le Digabel, J., Forcato, M., Bicciato, S., Elvassore, N., Piccolo, S., 2011. Role of YAP/TAZ in mechanotransduction. Nature. 474, 179-83.

Duprez, D., Bell, E. J., Richardson, M. K., Archer, C. W., Wolpert, L., Brickell, P. M., Francis-West, P. H., 1996. Overexpression of BMP-2 and BMP-4 alters the size and shape of developing skeletal elements in the chick limb. Mech Dev. 57, 145-57.

Durand, C., Bangs, F., Signolet, J., Decker, E., Tickle, C., Rappold, G., 2010. Enhancer elements upstream of the SHOX gene are active in the developing limb. Eur J Hum Genet. 18, 527-32.

Dy, P., Smits, P., Silvester, A., Penzo-Mendez, A., Dumitriu, B., Han, Y., de la Motte, C. A., Kingsley, D. M., Lefebvre, V., 2010. Synovial joint morphogenesis requires the chondrogenic action of Sox5 and Sox6 in growth plate and articular cartilage. Dev Biol. 341, 346-59.

Eiraku, M., Tohgo, A., Ono, K., Kaneko, M., Fujishima, K., Hirano, T., Kengaku, M., 2005. DNER acts as a neuron-specific Notch ligand during Bergmann glial development. Nat Neurosci. 8, 873-80.

El-Ghali, N., Rabadi, M., Ezin, A. M., De Bellard, M. E., 2010. New methods for chicken embryo manipulations. Microsc Res Tech. 73, 58-66.

Elder, B. D., Athanasiou, K. A., 2009. Hydrostatic pressure in articular cartilage tissue engineering: from chondrocytes to tissue regeneration. Tissue Eng Part B Rev. 15, 43-53.

Elder, S. H., Fulzele, K. S., McCulley, W. R., 2005. Cyclic hydrostatic compression stimulates chondroinduction of C3H/10T1/2 cells. Biomech Model Mechanobiol. 3, 141-6.

Enomoto-Iwamoto, M., Kitagaki, J., Koyama, E., Tamamura, Y., Wu, C., Kanatani, N., Koike, T., Okada, H., Komori, T., Yoneda, T., Church, V., Francis-West, P. H., Kurisu, K., Nohno, T., Pacifici, M., Iwamoto, M., 2002. The Wnt antagonist Frzb-1 regulates chondrocyte maturation and long bone development during limb skeletogenesis. Dev Biol. 251, 142-56.

Epstein, D. J., Vogan, K. J., Trasler, D. G., Gros, P., 1993. A mutation within intron 3 of the Pax-3 gene produces aberrantly spliced mRNA transcripts in the splotch (Sp) mouse mutant. Proc Natl Acad Sci U S A. 90, 532-6.

Espina, V., Wulfkuhle, J. D., Calvert, V. S., VanMeter, A., Zhou, W., Coukos, G., Geho, D. H., Petricoin, E. F., 3rd, Liotta, L. A., 2006. Laser-capture microdissection. Nat Protoc. 1, 586-603.

Estrach, S., Ambler, C. A., Lo Celso, C., Hozumi, K., Watt, F. M., 2006. Jagged 1 is a beta-catenin target gene required for ectopic hair follicle formation in adult epidermis. Development. 133, 4427-38.

Finger, A. R., Sargent, C. Y., Dulaney, K. O., Bernacki, S. H., Loboa, E. G., 2007. Differential effects on messenger ribonucleic acid expression by bone marrow-derived human mesenchymal stem cells seeded in agarose constructs due to ramped and steady applications of cyclic hydrostatic pressure. Tissue Eng. 13, 1151-8.

Fior, R., Henrique, D., 2005. A novel hes5/hes6 circuitry of negative regulation controls Notch activity during neurogenesis. Dev Biol. 281, 318-33.

Fodor, J., Matta, C., Olah, T., Juhasz, T., Takacs, R., Toth, A., Dienes, B., Csernoch, L., Zakany, R., 2013. Store-operated calcium entry and calcium influx via voltage-operated calcium channels regulate intracellular calcium oscillations in chondrogenic cells. Cell Calcium. 54, 1-16.

Francis-West, P. H., Parish, J., Lee, K., Archer, C. W., 1999. BMP/GDF-signalling interactions during synovial joint development. Cell Tissue Res. 296, 111-9.

Franz, T., 1993. The Splotch (Sp1H) and Splotch-delayed (Spd) alleles: differential phenotypic effects on neural crest and limb musculature. Anat Embryol (Berl). 187, 371-7.

Franz, T., Kothary, R., Surani, M. A., Halata, Z., Grim, M., 1993. The Splotch mutation interferes with muscle development in the limbs. Anat Embryol (Berl). 187, 153-60.

Friedenstein, A. J., Chailakhyan, R. K., Gerasimov, U. V., 1987. Bone marrow osteogenic stem cells: in vitro cultivation and transplantation in diffusion chambers. Cell Tissue Kinet. 20, 263-72.

Friedenstein, A. J., Deriglasova, U. F., Kulagina, N. N., Panasuk, A. F., Rudakowa, S. F., Luria, E. A., Ruadkow, I. A., 1974. Precursors for fibroblasts in different populations of hematopoietic cells as detected by the in vitro colony assay method. Exp Hematol. 2, 83-92.

Friedenstein, A. J., Piatetzky, S., II, Petrakova, K. V., 1966. Osteogenesis in transplants of bone marrow cells. J Embryol Exp Morphol. 16, 381-90.

Frost, H. M., 1987. Bone "mass" and the "mechanostat": a proposal. Anat Rec. 219, 1-9.

Frost, H. M., 2000. The Utah paradigm of skeletal physiology: an overview of its insights for bone, cartilage and collagenous tissue organs. J Bone Miner Metab. 18, 305-16.

Fukui, N., Ikeda, Y., Tanaka, N., 2011. The use of laser capture microdissection on adult human articular cartilage for gene expression analysis. Methods Mol Biol. 755, 449-59.

Futami, I., Ishijima, M., Kaneko, H., Tsuji, K., Ichikawa-Tomikawa, N., Sadatsuki, R., Muneta, T., Arikawa-Hirasawa, E., Sekiya, I., Kaneko, K., 2012. Isolation and characterization of multipotential mesenchymal cells from the mouse synovium. PLoS One. 7, e45517.

Gamer, L. W., Ho, V., Cox, K., Rosen, V., 2008. Expression and function of BMP3 during chick limb development. Dev Dyn. 237, 1691-8.

Gamer, L. W., Nove, J., Levin, M., Rosen, V., 2005. BMP-3 is a novel inhibitor of both activin and BMP-4 signaling in Xenopus embryos. Dev Biol. 285, 156-68.

Gao, B., Guo, J., She, C., Shu, A., Yang, M., Tan, Z., Yang, X., Guo, S., Feng, G., He, L., 2001. Mutations in IHH, encoding Indian hedgehog, cause brachydactyly type A-1. Nat Genet. 28, 386-8.

Gao, X., Wu, L., O'Neil, R. G., 2003. Temperature-modulated diversity of TRPV4 channel gating: activation by physical stresses and phorbol ester derivatives through protein kinase C-dependent and -independent pathways. J Biol Chem. 278, 27129-37.

Gao, Y., Lan, Y., Liu, H., Jiang, R., 2011. The zinc finger transcription factors Osr1 and Osr2 control synovial joint formation. Dev Biol. 352, 83-91.

Geetha-Loganathan, P., Nimmagadda, S., Christ, B., Huang, R., Scaal, M., 2010. Ectodermal Wnt6 is an early negative regulator of limb chondrogenesis in the chicken embryo. BMC Dev Biol. 10, 32.

Gerber, H. P., Ferrara, N., 2000. Angiogenesis and bone growth. Trends Cardiovasc Med. 10, 223-8.

Gomez, C., David, V., Peet, N. M., Vico, L., Chenu, C., Malaval, L., Skerry, T. M., 2007. Absence of mechanical loading in utero influences bone mass and architecture but not innervation in Myod-Myf5-deficient mice. J Anat. 210, 259-71.

Gordon, C. T., Rodda, F. A., Farlie, P. G., 2009. The RCAS retroviral expression system in the study of skeletal development. Dev Dyn. 238, 797-811.

Gosset, M., Berenbaum, F., Thirion, S., Jacques, C., 2008. Primary culture and phenotyping of murine chondrocytes. Nat Protoc. 3, 1253-60.

Grifone, R., Demignon, J., Houbron, C., Souil, E., Niro, C., Seller, M. J., Hamard, G., Maire, P., 2005. Six1 and Six4 homeoproteins are required for Pax3 and Mrf expression during myogenesis in the mouse embryo. Development. 132, 2235-49.

Gross, I., Bassit, B., Benezra, M., Licht, J. D., 2001. Mammalian sprouty proteins inhibit cell growth and differentiation by preventing ras activation. J Biol Chem. 276, 46460-8.

Guilak, F., 1995. Compression-induced changes in the shape and volume of the chondrocyte nucleus. J Biomech. 28, 1529-41.

Guo, X., Day, T. F., Jiang, X., Garrett-Beal, L., Topol, L., Yang, Y., 2004. Wnt/beta-catenin signaling is sufficient and necessary for synovial joint formation. Genes Dev. 18, 2404-17.

Guo, X., Mak, K. K., Taketo, M. M., Yang, Y., 2009. The Wnt/beta-catenin pathway interacts differentially with PTHrP signaling to control chondrocyte hypertrophy and final maturation. PLoS One. 4, e6067.

Gutierrez, J. A., Suzara, V. V., Dobbs, L. G., 2003. Continuous mechanical contraction modulates expression of alveolar epithelial cell phenotype. Am J Respir Cell Mol Biol. 29, 81-7.

Hall, B. K., Herring, S. W., 1990. Paralysis and growth of the musculoskeletal system in the embryonic chick. J Morphol. 206, 45-56.

Hall, B. K., Miyake, T., 2000. All for one and one for all: condensations and the initiation of skeletal development. Bioessays. 22, 138-47.

Ham, O., Song, B. W., Lee, S. Y., Choi, E., Cha, M. J., Lee, C. Y., Park, J. H., Kim, I. K., Chang, W., Lim, S., Lee, C. H., Kim, S., Jang, Y., Hwang, K. C., 2012. The role of microRNA-23b in the differentiation of MSC into chondrocyte by targeting protein kinase A signaling. Biomaterials. 33, 4500-7.

Hamburger, V., 1963. SOME ASPECTS OF THE EMBRYOLOGY OF BEHAVIOR. Q Rev Biol. 38, 342-65.

Hamburger, V., Hamilton, H. L., 1951. A series of normal stages in the development of the chick embryo. J Morphol. 88, 49-92.

Hamburger, V., Hamilton, H. L., 1992. A series of normal stages in the development of the chick embryo. 1951. Dev Dyn. 195, 231-72.

Hammond, C. L., Simbi, B. H., Stickland, N. C., 2007. In ovo temperature manipulation influences embryonic motility and growth of limb tissues in the chick (Gallus gallus). J Exp Biol. 210, 2667-75.

Han, Y., Lefebvre, V., 2008. L-Sox5 and Sox6 drive expression of the aggrecan gene in cartilage by securing binding of Sox9 to a far-upstream enhancer. Mol Cell Biol. 28, 4999-5013.

Handschel, J. G., Depprich, R. A., Kubler, N. R., Wiesmann, H. P., Ommerborn, M., Meyer, U., 2007. Prospects of micromass culture technology in tissue engineering. Head Face Med. 3, 4.

Harada, N., Tamai, Y., Ishikawa, T., Sauer, B., Takaku, K., Oshima, M., Taketo, M. M., 1999. Intestinal polyposis in mice with a dominant stable mutation of the beta-catenin gene. EMBO J. 18, 5931-42.

Hartmann, C., Tabin, C. J., 2000. Dual roles of Wnt signaling during chondrogenesis in the chicken limb. Development. 127, 3141-59.

Hartmann, C., Tabin, C. J., 2001. Wnt-14 plays a pivotal role in inducing synovial joint formation in the developing appendicular skeleton. Cell. 104, 341-51.

Hasenpusch-Theil, K., Magnani, D., Amaniti, E. M., Han, L., Armstrong, D., Theil, T., 2012. Transcriptional analysis of Gli3 mutants identifies Wnt target genes in the developing hippocampus. Cereb Cortex. 22, 2878-93.

Hatton, J. P., Pooran, M., Li, C. F., Luzzio, C., Hughes-Fulford, M., 2003. A short pulse of mechanical force induces gene expression and growth in MC3T3-E1 osteoblasts via an ERK 1/2 pathway. J Bone Miner Res. 18, 58-66.

Haudenschild, A. K., Hsieh, A. H., Kapila, S., Lotz, J. C., 2009. Pressure and distortion regulate human mesenchymal stem cell gene expression. Ann Biomed Eng. 37, 492-502.

Heallen, T., Zhang, M., Wang, J., Bonilla-Claudio, M., Klysik, E., Johnson, R. L., Martin, J. F., 2011. Hippo pathway inhibits Wnt signaling to restrain cardiomyocyte proliferation and heart size. Science. 332, 458-61.

Hecht, J., Seitz, V., Urban, M., Wagner, F., Robinson, P. N., Stiege, A., Dieterich, C., Kornak, U., Wilkening, U., Brieske, N., Zwingman, C., Kidess, A., Stricker, S., Mundlos, S., 2007. Detection of novel skeletogenesis target genes by comprehensive analysis of a Runx2(-/-) mouse model. Gene Expr Patterns. 7, 102-12.

Heldin, P., Laurent, T. C., Heldin, C. H., 1989. Effect of growth factors on hyaluronan synthesis in cultured human fibroblasts. Biochem J. 258, 919-22.

Hens, J. R., Wilson, K. M., Dann, P., Chen, X., Horowitz, M. C., Wysolmerski, J. J., 2005. TOPGAL mice show that the canonical Wnt signaling pathway is active during bone development and growth and is activated by mechanical loading in vitro. J Bone Miner Res. 20, 1103-13.

Heymer, J., Ruther, U., 1999. Syndactyly of Ft/+ mice correlates with an imbalance in bmp4 and fgf8 expression. Mech Dev. 88, 173-81.

Hiemer, S. E., Varelas, X., 2013. Stem cell regulation by the Hippo pathway. Biochim Biophys Acta. 1830, 2323-34.

Hill, T. P., Spater, D., Taketo, M. M., Birchmeier, W., Hartmann, C., 2005. Canonical Wnt/beta-catenin signaling prevents osteoblasts from differentiating into chondrocytes. Dev Cell. 8, 727-38.

Hilton, M. J., Tu, X., Cook, J., Hu, H., Long, F., 2005. Ihh controls cartilage development by antagonizing Gli3, but requires additional effectors to regulate osteoblast and vascular development. Development. 132, 4339-51.

Hindchliffe J.R., J. D. R., 1980. The development of the vertebrate limb: an approach through experiment, genetics and evolution. . Oxford University Press.

Hofmann, M., Schuster-Gossler, K., Watabe-Rudolph, M., Aulehla, A., Herrmann, B. G., Gossler, A., 2004. WNT signaling, in synergy with T/TBX6, controls Notch signaling by regulating Dll1 expression in the presomitic mesoderm of mouse embryos. Genes Dev. 18, 2712-7.

Holder, N., 1977. An experimental investigation into the early development of the chick elbow joint. J Embryol Exp Morphol. 39, 115-27.

Hosseini, A., Hogg, D. A., 1991a. The effects of paralysis on skeletal development in the chick embryo. I. General effects. J Anat. 177, 159-68.

Hosseini, A., Hogg, D. A., 1991b. The effects of paralysis on skeletal development in the chick embryo. II. Effects on histogenesis of the tibia. J Anat. 177, 169-78.

Huang, A. H., Farrell, M. J., Kim, M., Mauck, R. L., 2010. Long-term dynamic loading improves the mechanical properties of chondrogenic mesenchymal stem cell-laden hydrogel. Eur Cell Mater. 19, 72-85.

Huang da, W., Sherman, B. T., Lempicki, R. A., 2009. Systematic and integrative analysis of large gene lists using DAVID bioinformatics resources. Nat Protoc. 4, 44-57.

Idowu, B. D., Knight, M. M., Bader, D. L., Lee, D. A., 2000. Confocal analysis of cytoskeletal organisation within isolated chondrocyte sub-populations cultured in agarose. Histochem J. 32, 165-74.

Ikegawa, M., Han, H., Okamoto, A., Matsui, R., Tanaka, M., Omi, N., Miyamae, M., Toguchida, J., Tashiro, K., 2008. Syndactyly and preaxial synpolydactyly in the single Sfrp2 deleted mutant mice. Dev Dyn. 237, 2506-17.

Ikenoue, T., Trindade, M. C., Lee, M. S., Lin, E. Y., Schurman, D. J., Goodman, S. B., Smith, R. L., 2003. Mechanoregulation of human articular chondrocyte aggrecan and type II collagen expression by intermittent hydrostatic pressure in vitro. J Orthop Res. 21, 110-6.

Im, J., Kim, H., Kim, S., Jho, E. H., 2007. Wnt/beta-catenin signaling regulates expression of PRDC, an antagonist of the BMP-4 signaling pathway. Biochem Biophys Res Commun. 354, 296-301.

Imamura, T., Takase, M., Nishihara, A., Oeda, E., Hanai, J., Kawabata, M., Miyazono, K., 1997. Smad6 inhibits signalling by the TGF-beta superfamily. Nature. 389, 622-6.

Ingber, D. E., 2006. Mechanical control of tissue morphogenesis during embryological development. Int J Dev Biol. 50, 255-66.

Isaksson, H., Comas, O., van Donkelaar, C. C., Mediavilla, J., Wilson, W., Huiskes, R., Ito, K., 2007. Bone regeneration during distraction osteogenesis: mechano-regulation by shear strain and fluid velocity. J Biomech. 40, 2002-11.

Ishijima, M., Tsuji, K., Rittling, S. R., Yamashita, T., Kurosawa, H., Denhardt, D. T., Nifuji, A., Noda, M., 2002. Resistance to unloading-induced three-dimensional bone loss in osteopontin-deficient mice. J Bone Miner Res. 17, 661-7.

Islam, M. M., Doh, S. T., Cai, L., 2012. In ovo electroporation in embryonic chick retina. J Vis Exp.

Ito, M. M., Kida, M. Y., 2000. Morphological and biochemical re-evaluation of the process of cavitation in the rat knee joint: cellular and cell strata alterations in the interzone. J Anat. 197 Pt 4, 659-79.

Jackson, R. A., Kumarasuriyar, A., Nurcombe, V., Cool, S. M., 2006. Long-term loading inhibits ERK1/2 phosphorylation and increases FGFR3 expression in MC3T3-E1 osteoblast cells. J Cell Physiol. 209, 894-904.

Jacobson, A., Brinck, J., Briskin, M. J., Spicer, A. P., Heldin, P., 2000. Expression of human hyaluronan synthases in response to external stimuli. Biochem J. 348 Pt 1, 29-35.

James, C. G., Appleton, C. T., Ulici, V., Underhill, T. M., Beier, F., 2005. Microarray analyses of gene expression during chondrocyte differentiation identifies novel regulators of hypertrophy. Mol Biol Cell. 16, 5316-33.

Jeannotte, L., Lemieux, M., Charron, J., Poirier, F., Robertson, E. J., 1993. Specification of axial identity in the mouse: role of the Hoxa-5 (Hox1.3) gene. Genes Dev. 7, 2085-96.

Jenner, F., A, I. J., Cleary, M., Heijsman, D., Narcisi, R., van der Spek, P. J., Kremer, A., van Weeren, R., Brama, P., van Osch, G. J., 2014. Differential gene expression of the intermediate and outer interzone layers of developing articular cartilage in murine embryos. Stem Cells Dev. 23, 1883-98.

Johnson, C. W., Hernandez-Lagunas, L., Feng, W., Melvin, V. S., Williams, T., Artinger, K. B., 2011. Vgll2a is required for neural crest cell survival during zebrafish craniofacial development. Dev Biol. 357, 269-81.

Johnstone, B., Alini, M., Cucchiarini, M., Dodge, G. R., Eglin, D., Guilak, F., Madry, H., Mata, A., Mauck, R. L., Semino, C. E., Stoddart, M. J., 2013. Tissue engineering for articular cartilage repair--the state of the art. Eur Cell Mater. 25, 248-67.

Johnstone, B., Hering, T. M., Caplan, A. I., Goldberg, V. M., Yoo, J. U., 1998. In vitro chondrogenesis of bone marrow-derived mesenchymal progenitor cells. Exp Cell Res. 238, 265-72.

Jortikka, M. O., Parkkinen, J. J., Inkinen, R. I., Karner, J., Jarvelainen, H. T., Nelimarkka, L. O., Tammi, M. I., Lammi, M. J., 2000. The role of microtubules in the regulation of proteoglycan synthesis in chondrocytes under hydrostatic pressure. Arch Biochem Biophys. 374, 172-80.

Judex, M., Neumann, E., Gay, S., Muller-Ladner, U., 2004. Laser-mediated microdissection as a tool for molecular analysis in arthritis. Methods Mol Med. 101, 93-105.

Juhasz, T., Matta, C., Somogyi, C., Katona, E., Takacs, R., Soha, R. F., Szabo, I. A., Cserhati, C., Szody, R., Karacsonyi, Z., Bako, E., Gergely, P., Zakany, R., 2014. Mechanical loading stimulates chondrogenesis via the PKA/CREB-Sox9 and PP2A pathways in chicken micromass cultures. Cell Signal. 26, 468-82.

Kablar, B., Krastel, K., Tajbakhsh, S., Rudnicki, M. A., 2003. Myf5 and MyoD activation define independent myogenic compartments during embryonic development. Dev Biol. 258, 307-18.

Kahn, J., Shwartz, Y., Blitz, E., Krief, S., Sharir, A., Breitel, D. A., Rattenbach, R., Relaix, F., Maire, P., Rountree, R. B., Kingsley, D. M., Zelzer, E., 2009. Muscle contraction is necessary to maintain joint progenitor cell fate. Dev Cell. 16, 734-43.

Kan, A., Ikeda, T., Fukai, A., Nakagawa, T., Nakamura, K., Chung, U. I., Kawaguchi, H., Tabin, C. J., 2013. SOX11 contributes to the regulation of GDF5 in joint maintenance. BMC Dev Biol. 13, 4.

Kardon, G., 1998. Muscle and tendon morphogenesis in the avian hind limb. Development. 125, 4019-32.

Karp, S. J., Schipani, E., St-Jacques, B., Hunzelman, J., Kronenberg, H., McMahon, A. P., 2000. Indian hedgehog coordinates endochondral bone growth and morphogenesis via parathyroid hormone related-protein-dependent and -independent pathways. Development. 127, 543-8.

Karsenty, G., Kronenberg, H. M., Settembre, C., 2009. Genetic control of bone formation. Annu Rev Cell Dev Biol. 25, 629-48.

Kassar-Duchossoy, L., Gayraud-Morel, B., Gomes, D., Rocancourt, D., Buckingham, M., Shinin, V., Tajbakhsh, S., 2004. Mrf4 determines skeletal muscle identity in Myf5:Myod double-mutant mice. Nature. 431, 466-71.

Katoh, M., 2012. Function and cancer genomics of FAT family genes (review). Int J Oncol. 41, 1913-8.

Kavanagh, E., Church, V. L., Osborne, A. C., Lamb, K. J., Archer, C. W., Francis-West, P. H., Pitsillides, A. A., 2006. Differential regulation of GDF-5 and FGF-2/4 by immobilisation in ovo exposes distinct roles in joint formation. Dev Dyn. 235, 826-34.

Kawakami, Y., Uchiyama, Y., Rodriguez Esteban, C., Inenaga, T., Koyano-Nakagawa, N., Kawakami, H., Marti, M., Kmita, M., Monaghan-Nichols, P., Nishinakamura, R., Izpisua Belmonte, J. C., 2009. Sall genes regulate region-specific morphogenesis in the mouse limb by modulating Hox activities. Development. 136, 585-94.

Kawakami, Y., Wada, N., Nishimatsu, S., Nohno, T., 2000. Involvement of frizzled-10 in Wnt-7a signaling during chick limb development. Dev Growth Differ. 42, 561-9.

Kawakami, Y., Wada, N., Nishimatsu, S. I., Ishikawa, T., Noji, S., Nohno, T., 1999. Involvement of Wnt-5a in chondrogenic pattern formation in the chick limb bud. Dev Growth Differ. 41, 29-40.

Kawano, Y., Kypta, R., 2003. Secreted antagonists of the Wnt signalling pathway. J Cell Sci. 116, 2627-34.

Kearney, E. M., Farrell, E., Prendergast, P. J., Campbell, V. A., 2010. Tensile strain as a regulator of mesenchymal stem cell osteogenesis. Ann Biomed Eng. 38, 1767-79.

Keller-Peck, C. R., Mullen, R. J., 1997. Altered cell proliferation in the spinal cord of mouse neural tube mutants curly tail and Pax3 splotch-delayed. Brain Res Dev Brain Res. 102, 177-88.

Kelly, D. J., Jacobs, C. R., 2010. The role of mechanical signals in regulating chondrogenesis and osteogenesis of mesenchymal stem cells. Birth Defects Research Part C: Embryo Today: Reviews. 90, 75-85.

Khan, W. S., Tew, S. R., Adesida, A. B., Hardingham, T. E., 2008. Human infrapatellar fat pad-derived stem cells express the pericyte marker 3G5 and show enhanced chondrogenesis after expansion in fibroblast growth factor-2. Arthritis Res Ther. 10, R74.

Khayyeri, H., Checa, S., Tagil, M., Prendergast, P. J., 2009. Corroboration of mechanobiological simulations of tissue differentiation in an in vivo bone chamber using a lattice-modeling approach. J Orthop Res. 27, 1659-66.

Kim, Y. S., Nakanishi, G., Lewandoski, M., Jetten, A. M., 2003. GLIS3, a novel member of the GLIS subfamily of Kruppel-like zinc finger proteins with repressor and activation functions. Nucleic Acids Res. 31, 5513-25.

Kin, T., Ono, Y., 2007. Idiographica: a general-purpose web application to build idiograms on-demand for human, mouse and rat. Bioinformatics. 23, 2945-6.

King, E. D., Munger, B. L., 1990. Myotome and early neurogenesis in chick embryos. Anat Rec. 228, 191-210.

Kioussi, C., Briata, P., Baek, S. H., Rose, D. W., Hamblet, N. S., Herman, T., Ohgi, K. A., Lin, C., Gleiberman, A., Wang, J., Brault, V., Ruiz-Lozano, P., Nguyen, H. D., Kemler, R., Glass, C. K., Wynshaw-Boris, A., Rosenfeld, M. G., 2002. Identification of a Wnt/Dvl/beta-Catenin --> Pitx2 pathway mediating cell-type-specific proliferation during development. Cell. 111, 673-85.

Knight, M. M., Toyoda, T., Lee, D. A., Bader, D. L., 2006. Mechanical compression and hydrostatic pressure induce reversible changes in actin cytoskeletal organisation in chondrocytes in agarose. J Biomech. 39, 1547-51.

Knudson, W., Aguiar, D. J., Hua, Q., Knudson, C. B., 1996. CD44-anchored hyaluronan-rich pericellular matrices: an ultrastructural and biochemical analysis. Exp Cell Res. 228, 216-28.

Knudson, W., Loeser, R. F., 2002. CD44 and integrin matrix receptors participate in cartilage homeostasis. Cell Mol Life Sci. 59, 36-44.

Ko, J. Y., Im, G. I., 2014. Chondrogenic and Osteogenic Induction from iPS Cells. Methods Mol Biol.

Ko, J. Y., Kim, K. I., Park, S., Im, G. I., 2014. In vitro chondrogenesis and in vivo repair of osteochondral defect with human induced pluripotent stem cells. Biomaterials. 35, 3571-81.

Kobayashi, T., Lyons, K. M., McMahon, A. P., Kronenberg, H. M., 2005. BMP signaling stimulates cellular differentiation at multiple steps during cartilage development. Proc Natl Acad Sci U S A. 102, 18023-7.

Kontulainen, S., Sievanen, H., Kannus, P., Pasanen, M., Vuori, I., 2003. Effect of long-term impact-loading on mass, size, and estimated strength of humerus and radius of female racquet-sports players: a peripheral quantitative computed tomography study between young and old starters and controls. J Bone Miner Res. 18, 352-9.

Koyama, E., Shibukawa, Y., Nagayama, M., Sugito, H., Young, B., Yuasa, T., Okabe, T., Ochiai, T., Kamiya, N., Rountree, R. B., Kingsley, D. M., Iwamoto, M., Enomoto-Iwamoto, M., Pacifici, M., 2008. A distinct cohort of progenitor cells participates in synovial joint and articular cartilage formation during mouse limb skeletogenesis. Dev Biol. 316, 62-73.

Kratochwil, K., Galceran, J., Tontsch, S., Roth, W., Grosschedl, R., 2002. FGF4, a direct target of LEF1 and Wnt signaling, can rescue the arrest of tooth organogenesis in Lef1(-/-) mice. Genes Dev. 16, 3173-85.

Kronenberg, H. M., 2003. Developmental regulation of the growth plate. Nature. 423, 332-336.

Krull, C. E., 2004. A primer on using in ovo electroporation to analyze gene function. Dev Dyn. 229, 433-9.

Kumar, B. M., Yoo, J. G., Ock, S. A., Kim, J. G., Song, H. J., Kang, E. J., Cho, S. K., Lee, S. L., Cho, J. H., Balasubramanian, S., Rho, G. J., 2007. In vitro differentiation of mesenchymal progenitor cells derived from porcine umbilical cord blood. Mol Cells. 24, 343-50.

Kume, T., Jiang, H., Topczewska, J. M., Hogan, B. L., 2001. The murine winged helix transcription factors, Foxc1 and Foxc2, are both required for cardiovascular development and somitogenesis. Genes Dev. 15, 2470-82.

Kwon, A. T., Arenillas, D. J., Worsley Hunt, R., Wasserman, W. W., 2012. oPOSSUM-3: advanced analysis of regulatory motif over-representation across genes or ChIP-Seq datasets. G3 (Bethesda). 2, 987-1002.

Lahiry, P., Lee, L. J., Frey, B. J., Rupar, C. A., Siu, V. M., Blencowe, B. J., Hegele, R. A., 2011. Transcriptional profiling of endocrine cerebro-osteodysplasia using microarray and next-generation sequencing. PLoS One. 6, e25400.

Lamb, K. J., Lewthwaite, J. C., Bastow, E. R., Pitsillides, A. A., 2003. Defining boundaries during joint cavity formation: going out on a limb. Int J Exp Pathol. 84, 55-67.

Lau, K. H., Kapur, S., Kesavan, C., Baylink, D. J., 2006. Up-regulation of the Wnt, estrogen receptor, insulin-like growth factor-I, and bone morphogenetic protein pathways in C57BL/6J osteoblasts as opposed to C3H/HeJ osteoblasts in part contributes to the differential anabolic response to fluid shear. J Biol Chem. 281, 9576-88.

Leclerc, N., Luppen, C. A., Ho, V. V., Nagpal, S., Hacia, J. G., Smith, E., Frenkel, B., 2004. Gene expression profiling of glucocorticoid-inhibited osteoblasts. J Mol Endocrinol. 33, 175-93.

Lefebvre, V., Bhattaram, P., 2010. Vertebrate skeletogenesis. Curr Top Dev Biol. 90, 291-317.

Lefebvre, V., Smits, P., 2005. Transcriptional control of chondrocyte fate and differentiation. Birth Defects Res C Embryo Today. 75, 200-12.

Lelkes, G., 1958. Experiments in vitro on the role of movement in the development of joints. J Embryol Exp Morphol. 6, 183-6.

Lescher, B., Haenig, B., Kispert, A., 1998. sFRP-2 is a target of the Wnt-4 signaling pathway in the developing metanephric kidney. Dev Dyn. 213, 440-51.

Levi, G., Topilko, P., Schneider-Maunoury, S., Lasagna, M., Mantero, S., Cancedda, R., Charnay, P., 1996. Defective bone formation in Krox-20 mutant mice. Development. 122, 113-20.

Li, B., Ruotti, V., Stewart, R. M., Thomson, J. A., Dewey, C. N., 2010a. RNA-Seq gene expression estimation with read mapping uncertainty. Bioinformatics. 26, 493-500.

Li, J., Zhao, Z., Yang, J., Liu, J., Wang, J., Li, X., Liu, Y., 2009. p38 MAPK mediated in compressive stress-induced chondrogenesis of rat bone marrow MSCs in 3D alginate scaffolds. J Cell Physiol. 221, 609-17.

Li, X., Liu, P., Liu, W., Maye, P., Zhang, J., Zhang, Y., Hurley, M., Guo, C., Boskey, A., Sun, L., Harris, S. E., Rowe, D. W., Ke, H. Z., Wu, D., 2005. Dkk2 has a role in terminal osteoblast differentiation and mineralized matrix formation. Nat Genet. 37, 945-52.

Li, Y., Dudley, A. T., 2009. Noncanonical frizzled signaling regulates cell polarity of growth plate chondrocytes. Development. 136, 1083-92.

Li, Z., Kupcsik, L., Yao, S. J., Alini, M., Stoddart, M. J., 2010b. Mechanical load modulates chondrogenesis of human mesenchymal stem cells through the TGF-beta pathway. J Cell Mol Med. 14, 1338-46.

Liu, A., 2010. Laser capture microdissection in the tissue biorepository. J Biomol Tech. 21, 120-5.

Livak, K. J., Schmittgen, T. D., 2001. Analysis of relative gene expression data using real-time quantitative PCR and the 2(-Delta Delta C(T)) Method. Methods. 25, 402-8.

Loboa, E. G., Beaupre, G. S., Carter, D. R., 2001. Mechanobiology of initial pseudarthrosis formation with oblique fractures. J Orthop Res. 19, 1067-72.

Logan, M., Martin, J. F., Nagy, A., Lobe, C., Olson, E. N., Tabin, C. J., 2002. Expression of Cre Recombinase in the developing mouse limb bud driven by a Prxl enhancer. Genesis. 33, 77-80.

Logan, M., Tabin, C. J., 1999. Role of Pitx1 upstream of Tbx4 in specification of hindlimb identity. Science. 283, 1736-9.

Loganathan, P. G., Nimmagadda, S., Huang, R., Scaal, M., Christ, B., 2005. Comparative analysis of the expression patterns of Wnts during chick limb development. Histochem Cell Biol. 123, 195-201.

Long, F., Chung, U. I., Ohba, S., McMahon, J., Kronenberg, H. M., McMahon, A. P., 2004. Ihh signaling is directly required for the osteoblast lineage in the endochondral skeleton. Development. 131, 1309-18.

Longobardi, L., Li, T., Myers, T. J., O'Rear, L., Ozkan, H., Li, Y., Contaldo, C., Spagnoli, A., 2012. TGF-beta type II receptor/MCP-5 axis: at the crossroad between joint and growth plate development. Dev Cell. 23, 71-81.

Lu, C., Wan, Y., Cao, J., Zhu, X., Yu, J., Zhou, R., Yao, Y., Zhang, L., Zhao, H., Li, H., Zhao, J., He, L., Ma, G., Yang, X., Yao, Z., Guo, X., 2013. Wnt-mediated reciprocal regulation between cartilage and bone development during endochondral ossification. Bone. 53, 566-74.

Luo, J., Redies, C., 2005. Ex ovo electroporation for gene transfer into older chicken embryos. Dev Dyn. 233, 1470-7.

Luo, J., Yan, X., Lin, J., Rolfs, A., 2012. Gene transfer into older chicken embryos by ex ovo electroporation. J Vis Exp.

Macsai, C. E., Foster, B. K., Xian, C. J., 2008. Roles of Wnt signalling in bone growth, remodelling, skeletal disorders and fracture repair. J Cell Physiol. 215, 578-87.

Maeda, T., Sakabe, T., Sunaga, A., Sakai, K., Rivera, A. L., Keene, D. R., Sasaki, T., Stavnezer, E., Iannotti, J., Schweitzer, R., Ilic, D., Baskaran, H., Sakai, T., 2011. Conversion of mechanical force into TGF-beta-mediated biochemical signals. Curr Biol. 21, 933-41.

Mahmoudi, T., Li, V. S., Ng, S. S., Taouatas, N., Vries, R. G., Mohammed, S., Heck, A. J., Clevers, H., 2009. The kinase TNIK is an essential activator of Wnt target genes. EMBO J. 28, 3329-40.

Makino, A., Prossnitz, E. R., Bunemann, M., Wang, J. M., Yao, W., Schmid-Schonbein, G. W., 2006. G protein-coupled receptors serve as mechanosensors for fluid shear stress in neutrophils. Am J Physiol Cell Physiol. 290, C1633-9.

Malone, J. H., Oliver, B., 2011. Microarrays, deep sequencing and the true measure of the transcriptome. BMC Biol. 9, 34.

Mammoto, A., Connor, K. M., Mammoto, T., Yung, C. W., Huh, D., Aderman, C. M., Mostoslavsky, G., Smith, L. E., Ingber, D. E., 2009. A mechanosensitive transcriptional mechanism that controls angiogenesis. Nature. 457, 1103-8.

Mammoto, A., Mammoto, T., Ingber, D. E., 2012. Mechanosensitive mechanisms in transcriptional regulation. J Cell Sci.

Mammoto, T., Mammoto, A., Torisawa, Y. S., Tat, T., Gibbs, A., Derda, R., Mannix, R., de Bruijn, M., Yung, C. W., Huh, D., Ingber, D. E., 2011. Mechanochemical control of

mesenchymal condensation and embryonic tooth organ formation. Dev Cell. 21, 758-69.

Mao, B., Wu, W., Davidson, G., Marhold, J., Li, M., Mechler, B. M., Delius, H., Hoppe, D., Stannek, P., Walter, C., Glinka, A., Niehrs, C., 2002. Kremen proteins are Dickkopf receptors that regulate Wnt/beta-catenin signalling. Nature. 417, 664-7.

Mao, Y., Mulvaney, J., Zakaria, S., Yu, T., Morgan, K. M., Allen, S., Basson, M. A., Francis-West, P., Irvine, K. D., 2011. Characterization of a Dchs1 mutant mouse reveals requirements for Dchs1-Fat4 signaling during mammalian development. Development. 138, 947-57.

Marioni, J. C., Mason, C. E., Mane, S. M., Stephens, M., Gilad, Y., 2008. RNA-seq: an assessment of technical reproducibility and comparison with gene expression arrays. Genome Res. 18, 1509-17.

Marsano, A., Millward-Sadler, S. J., Salter, D. M., Adesida, A., Hardingham, T., Tognana, E., Kon, E., Chiari-Grisar, C., Nehrer, S., Jakob, M., Martin, I., 2007. Differential cartilaginous tissue formation by human synovial membrane, fat pad, meniscus cells and articular chondrocytes. Osteoarthritis Cartilage. 15, 48-58.

Martin, D. C., Atmuri, V., Hemming, R. J., Farley, J., Mort, J. S., Byers, S., Hombach-Klonisch, S., Csoka, A. B., Stern, R., Triggs-Raine, B. L., 2008. A mouse model of human mucopolysaccharidosis IX exhibits osteoarthritis. Hum Mol Genet. 17, 1904-15.

Martin, J. A., Buckwalter, J. A., 2002. Aging, articular cartilage chondrocyte senescence and osteoarthritis. Biogerontology. 3, 257-64.

Martinelli, D. C., Fan, C. M., 2007. Gas1 extends the range of Hedgehog action by facilitating its signaling. Genes Dev. 21, 1231-43.

Maruyama, T., Jiang, M., Hsu, W., 2013. Gpr177, a novel locus for bone mineral density and osteoporosis, regulates osteogenesis and chondrogenesis in skeletal development. J Bone Miner Res. 28, 1150-9.

Matsukura, Y., Muneta, T., Tsuji, K., Miyatake, K., Yamada, J., Abula, K., Koga, H., Tomita, M., Sekiya, I., 2014. Mouse synovial mesenchymal stem cells increase in yield with knee inflammation. J Orthop Res.

Matsumoto, K., Li, Y., Jakuba, C., Sugiyama, Y., Sayo, T., Okuno, M., Dealy, C. N., Toole, B. P., Takeda, J., Yamaguchi, Y., Kosher, R. A., 2009. Conditional inactivation of Has2 reveals a crucial role for hyaluronan in skeletal growth, patterning, chondrocyte maturation and joint formation in the developing limb. Development. 136, 2825-35.

McGinley, J. N., Zhu, Z., Jiang, W., Thompson, H. J., 2010. Collection of epithelial cells from rodent mammary gland via laser capture microdissection yielding high-quality RNA suitable for microarray analysis. Biol Proced Online. 12, 9026.

McGrew, L. L., Takemaru, K., Bates, R., Moon, R. T., 1999. Direct regulation of the Xenopus engrailed-2 promoter by the Wnt signaling pathway, and a molecular screen for Wnt-responsive genes, confirm a role for Wnt signaling during neural patterning in Xenopus. Mech Dev. 87, 21-32.

McMahon, L. A., Campbell, V. A., Prendergast, P. J., 2008a. Involvement of stretch-activated ion channels in strain-regulated glycosaminoglycan synthesis in mesenchymal stem cell-seeded 3D scaffolds. Journal of Biomechanics. 41, 2055-2059.

McMahon, L. A., Reid, A. J., Campbell, V. A., Prendergast, P. J., 2008b. Regulatory effects of mechanical strain on the chondrogenic differentiation of MSCs in a collagen-GAG scaffold: experimental and computational analysis. Ann Biomed Eng. 36, 185-94.

Meyer, E. G., Buckley, C. T., Steward, A. J., Kelly, D. J., 2011. The effect of cyclic hydrostatic pressure on the functional development of cartilaginous tissues engineered using bone marrow derived mesenchymal stem cells. J Mech Behav Biomed Mater. 4, 1257-65.

Michikami, I., Fukushi, T., Tanaka, M., Egusa, H., Maeda, Y., Ooshima, T., Wakisaka, S., Abe, M., 2012. Kruppel-like factor 4 regulates membranous and endochondral ossification. Exp Cell Res. 318, 311-25.

Mikic, B., Johnson, T. L., Chhabra, A. B., Schalet, B. J., Wong, M., Hunziker, E. B., 2000. Differential effects of embryonic immobilization on the development of fibrocartilaginous skeletal elements. J Rehabil Res Dev. 37, 127-33.

Miller-Delaney, S. F., Lieberam, I., Murphy, P., Mitchell, K. J., 2011. Plxdc2 is a mitogen for neural progenitors. PLoS One. 6, e14565.

Minina, E., Kreschel, C., Naski, M. C., Ornitz, D. M., Vortkamp, A., 2002. Interaction of FGF, Ihh/Pthlh, and BMP signaling integrates chondrocyte proliferation and hypertrophic differentiation. Dev Cell. 3, 439-49.

Minina, E., Schneider, S., Rosowski, M., Lauster, R., Vortkamp, A., 2005. Expression of Fgf and Tgfbeta signaling related genes during embryonic endochondral ossification. Gene Expr Patterns. 6, 102-9.

Minina, E., Wenzel, H. M., Kreschel, C., Karp, S., Gaffield, W., McMahon, A. P., Vortkamp, A., 2001. BMP and Ihh/PTHrP signaling interact to coordinate chondrocyte proliferation and differentiation. Development. 128, 4523-34.

Misra, M., Sours, E., Lance-Jones, C., 2012. Hox transcription factors influence motoneuron identity through the integrated actions of both homeodomain and non-homeodomain regions. Dev Dyn. 241, 718-31.

Miwa, N., Furuse, M., Tsukita, S., Niikawa, N., Nakamura, Y., Furukawa, Y., 2001. Involvement of claudin-1 in the beta-catenin/Tcf signaling pathway and its frequent upregulation in human colorectal cancers. Oncol Res. 12, 469-76.

Miyanishi, K., Trindade, M. C., Lindsey, D. P., Beaupre, G. S., Carter, D. R., Goodman, S. B., Schurman, D. J., Smith, R. L., 2006a. Dose- and time-dependent effects of cyclic hydrostatic pressure on transforming growth factor-beta3-induced chondrogenesis by adult human mesenchymal stem cells in vitro. Tissue Eng. 12, 2253-62.

Miyanishi, K., Trindade, M. C., Lindsey, D. P., Beaupre, G. S., Carter, D. R., Goodman, S. B., Schurman, D. J., Smith, R. L., 2006b. Effects of hydrostatic pressure and transforming growth factor-beta 3 on adult human mesenchymal stem cell chondrogenesis in vitro. Tissue Eng. 12, 1419-28.

Mizoguchi, F., Mizuno, A., Hayata, T., Nakashima, K., Heller, S., Ushida, T., Sokabe, M., Miyasaka, N., Suzuki, M., Ezura, Y., Noda, M., 2008. Transient receptor potential vanilloid 4 deficiency suppresses unloading-induced bone loss. J Cell Physiol. 216, 47-53.

Mochizuki, T., Muneta, T., Sakaguchi, Y., Nimura, A., Yokoyama, A., Koga, H., Sekiya, I., 2006. Higher chondrogenic potential of fibrous synovium- and adipose synovium-derived cells compared with subcutaneous fat-derived cells: distinguishing properties of mesenchymal stem cells in humans. Arthritis Rheum. 54, 843-53.

Moessinger, A. C., 1983. Fetal akinesia deformation sequence: an animal model. Pediatrics. 72, 857-63.

Momose, T., Tonegawa, A., Takeuchi, J., Ogawa, H., Umesono, K., Yasuda, K., 1999. Efficient targeting of gene expression in chick embryos by microelectroporation. Dev Growth Differ. 41, 335-44.

Mortazavi, A., Williams, B. A., McCue, K., Schaeffer, L., Wold, B., 2008. Mapping and quantifying mammalian transcriptomes by RNA-Seq. Nat Methods. 5, 621-8.

Mouw, J. K., Connelly, J. T., Wilson, C. G., Michael, K. E., Levenston, M. E., 2007. Dynamic compression regulates the expression and synthesis of chondrocyte-specific matrix molecules in bone marrow stromal cells. Stem Cells. 25, 655-63.

Muramatsu, T., Mizutani, Y., Ohmori, Y., Okumura, J., 1997. Comparison of three nonviral transfection methods for foreign gene expression in early chicken embryos in ovo. Biochem Biophys Res Commun. 230, 376-80.

Muramatsu T., M. Y., Okumura J., 1996. Live Detection of the firefly Luciferase Gene Expression by Bioluminescence in Incubating Chicken Embryos. Anim. Sci. Technol (Jpn). 67, 906-909.

Murray, P. D., Drachman, D. B., 1969. The role of movement in the development of joints and related structures: the head and neck in the chick embryo. J Embryol Exp Morphol. 22, 349-71.

Nakamura, H., Katahira, T., Sato, T., Watanabe, Y., Funahashi, J., 2004. Gain- and loss-of-function in chick embryos by electroporation. Mech Dev. 121, 1137-43.

Nam, J. S., Park, E., Turcotte, T. J., Palencia, S., Zhan, X., Lee, J., Yun, K., Funk, W. D., Yoon, J. K., 2007. Mouse R-spondin2 is required for apical ectodermal ridge maintenance in the hindlimb. Dev Biol. 311, 124-35.

Nam, J. S., Turcotte, T. J., Smith, P. F., Choi, S., Yoon, J. K., 2006. Mouse cristin/R-spondin family proteins are novel ligands for the Frizzled 8 and LRP6 receptors and activate beta-catenin-dependent gene expression. J Biol Chem. 281, 13247-57.

Naski, M. C., Wang, Q., Xu, J., Ornitz, D. M., 1996. Graded activation of fibroblast growth factor receptor 3 by mutations causing achondroplasia and thanatophoric dysplasia. Nat Genet. 13, 233-7.

Ni, C. W., Qiu, H., Rezvan, A., Kwon, K., Nam, D., Son, D. J., Visvader, J. E., Jo, H., 2010. Discovery of novel mechanosensitive genes in vivo using mouse carotid artery endothelium exposed to disturbed flow. Blood. 116, e66-73.

Niedermaier, M., Schwabe, G. C., Fees, S., Helmrich, A., Brieske, N., Seemann, P., Hecht, J., Seitz, V., Stricker, S., Leschik, G., Schrock, E., Selby, P. B., Mundlos, S., 2005. An inversion involving the mouse Shh locus results in brachydactyly through dysregulation of Shh expression. J Clin Invest. 115, 900-9.

Noor, A., Whibley, A., Marshall, C. R., Gianakopoulos, P. J., Piton, A., Carson, A. R., Orlic-Milacic, M., Lionel, A. C., Sato, D., Pinto, D., Drmic, I., Noakes, C., Senman, L., Zhang, X., Mo, R., Gauthier, J., Crosbie, J., Pagnamenta, A. T., Munson, J., Estes, A. M., Fiebig, A., Franke, A., Schreiber, S., Stewart, A. F., Roberts, R., McPherson, R., Guter, S. J., Cook, E. H., Jr., Dawson, G., Schellenberg, G. D., Battaglia, A., Maestrini, E., Jeng, L., Hutchison, T., Rajcan-Separovic, E., Chudley, A. E., Lewis, S. M., Liu, X., Holden, J. J., Fernandez, B., Zwaigenbaum, L., Bryson, S. E., Roberts, W., Szatmari, P., Gallagher, L., Stratton, M. R., Gecz, J., Brady, A. F., Schwartz, C. E., Schachar, R. J., Monaco, A. P., Rouleau, G. A., Hui, C. C., Lucy Raymond, F., Scherer, S. W., Vincent, J. B., 2010. Disruption at the PTCHD1 Locus on Xp22.11 in Autism spectrum disorder and intellectual disability. Sci Transl Med. 2, 49ra68.

Nowlan, N. C., Bourdon, C., Dumas, G., Tajbakhsh, S., Prendergast, P. J., Murphy, P., 2010a. Developing bones are differentially affected by compromised skeletal muscle formation. Bone. 46, 1275-85.

Nowlan, N. C., Dumas, G., Tajbakhsh, S., Prendergast, P. J., Murphy, P., 2012. Biophysical stimuli induced by passive movements compensate for lack of skeletal muscle during embryonic skeletogenesis. Biomech Model Mechanobiol. 11, 207-19.

Nowlan, N. C., Murphy, P., Prendergast, P. J., 2007. Mechanobiology of embryonic limb development. Ann N Y Acad Sci. 1101, 389-411.

Nowlan, N. C., Murphy, P., Prendergast, P. J., 2008a. A dynamic pattern of mechanical stimulation promotes ossification in avian embryonic long bones. J Biomech. 41, 249-58.

Nowlan, N. C., Prendergast, P. J., Murphy, P., 2008b. Identification of mechanosensitive genes during embryonic bone formation. PLoS Comput Biol. 4, e1000250.

Nowlan, N. C., Sharpe, J., Roddy, K. A., Prendergast, P. J., Murphy, P., 2010b. Mechanobiology of embryonic skeletal development: Insights from animal models. Birth Defects Res C Embryo Today. 90, 203-13.

O'Rahilly, R., Bossy, J., Muller, F., 1981. [Introduction to the study of embryonic stages in man]. Bull Assoc Anat (Nancy). 65, 141-236.

Oguchi, T., Ishiguro, N., 2004. Differential stimulation of three forms of hyaluronan synthase by TGF-beta, IL-1beta, and TNF-alpha. Connect Tissue Res. 45, 197-205.

Ohbayashi, N., Shibayama, M., Kurotaki, Y., Imanishi, M., Fujimori, T., Itoh, N., Takada, S., 2002. FGF18 is required for normal cell proliferation and differentiation during osteogenesis and chondrogenesis. Genes Dev. 16, 870-9.

Okita, K., Yamanaka, S., 2010. Induction of pluripotency by defined factors. Exp Cell Res. 316, 2565-70.

Olguin, P., Glavic, A., Mlodzik, M., 2011. Intertissue mechanical stress affects Frizzled-mediated planar cell polarity in the Drosophila notum epidermis. Curr Biol. 21, 236-42.

Olsen, B. R., 1996. Role of cartilage collagens in formation of the skeleton. Ann N Y Acad Sci. 785, 124-30.

Ornitz, D. M., Marie, P. J., 2002. FGF signaling pathways in endochondral and intramembranous bone development and human genetic disease. Genes Dev. 16, 1446-65.

Osborne, A. C., Lamb, K. J., Lewthwaite, J. C., Dowthwaite, G. P., Pitsillides, A. A., 2002. Short-term rigid and flaccid paralyses diminish growth of embryonic chick limbs and abrogate joint cavity formation but differentially preserve pre-cavitated joints. J Musculoskelet Neuronal Interact. 2, 448-56.

Ozpolat, B. D., Zapata, M., Daniel Fruge, J., Coote, J., Lee, J., Muneoka, K., Anderson, R., 2012. Regeneration of the elbow joint in the developing chick embryo recapitulates development. Dev Biol. 372, 229-38.

Pacifici, M., Koyama, E., Iwamoto, M., 2005. Mechanisms of synovial joint and articular cartilage formation: recent advances, but many lingering mysteries. Birth Defects Res C Embryo Today. 75, 237-48.

Pai, A. C., 1965. DEVELOPMENTAL GENETICS OF A LETHAL MUTATION, MUSCULAR DYSGENESIS (MDG), IN THE MOUSE. II. DEVELOPMENTAL ANALYSIS. Dev Biol. 11, 93-109.

Papaioannou, G., Mirzamohammadi, F., Kobayashi, T., 2014. MicroRNAs involved in bone formation. Cell Mol Life Sci. 71, 4747-61.

Pardo, S. J., Patel, M. J., Sykes, M. C., Platt, M. O., Boyd, N. L., Sorescu, G. P., Xu, M., van Loon, J. J., Wang, M. D., Jo, H., 2005. Simulated microgravity using the Random Positioning Machine inhibits differentiation and alters gene expression profiles of 2T3 preosteoblasts. Am J Physiol Cell Physiol. 288, C1211-21.

Parkkinen, J. J., Lammi, M. J., Inkinen, R., Jortikka, M., Tammi, M., Virtanen, I., Helminen, H. J., 1995. Influence of short-term hydrostatic pressure on organization of stress fibers in cultured chondrocytes. J Orthop Res. 13, 495-502.

Patel, M. J., Liu, W., Sykes, M. C., Ward, N. E., Risin, S. A., Risin, D., Jo, H., 2007. Identification of mechanosensitive genes in osteoblasts by comparative microarray studies using the rotating wall vessel and the random positioning machine. J Cell Biochem. 101, 587-99.

Pazin, D. E., Gamer, L. W., Capelo, L. P., Cox, K. A., Rosen, V., 2014. Gene signature of the embryonic meniscus. J Orthop Res. 32, 46-53.

Pei, M., He, F., Kish, V. L., Vunjak-Novakovic, G., 2008. Engineering of functional cartilage tissue using stem cells from synovial lining: a preliminary study. Clin Orthop Relat Res. 466, 1880-9.

Pelttari, K., Winter, A., Steck, E., Goetzke, K., Hennig, T., Ochs, B. G., Aigner, T., Richter, W., 2006. Premature induction of hypertrophy during in vitro chondrogenesis of human mesenchymal stem cells correlates with calcification and vascular invasion after ectopic transplantation in SCID mice. Arthritis Rheum. 54, 3254-66.

Persson, M., 1983. The role of movements in the development of sutural and diarthrodial joints tested by long-term paralysis of chick embryos. J Anat. 137 (Pt 3), 591-9.

Peters, K. G., Werner, S., Chen, G., Williams, L. T., 1992. Two FGF receptor genes are differentially expressed in epithelial and mesenchymal tissues during limb formation and organogenesis in the mouse. Development. 114, 233-43.

Peterson, R. S., Andhare, R. A., Rousche, K. T., Knudson, W., Wang, W., Grossfield, J. B., Thomas, R. O., Hollingsworth, R. E., Knudson, C. B., 2004. CD44 modulates Smad1 activation in the BMP-7 signaling pathway. J Cell Biol. 166, 1081-91.

Phinney, D. G., 2012. Functional heterogeneity of mesenchymal stem cells: implications for cell therapy. J Cell Biochem. 113, 2806-12.

Pienimaki, J. P., Rilla, K., Fulop, C., Sironen, R. K., Karvinen, S., Pasonen, S., Lammi, M. J., Tammi, R., Hascall, V. C., Tammi, M. I., 2001. Epidermal growth factor activates hyaluronan synthase 2 in epidermal keratinocytes and increases pericellular and intracellular hyaluronan. J Biol Chem. 276, 20428-35.

Pitsillides, A. A., Ashhurst, D. E., 2008. A critical evaluation of specific aspects of joint development. Dev Dyn. 237, 2284-94.

Pittenger, M. F., Mackay, A. M., Beck, S. C., Jaiswal, R. K., Douglas, R., Mosca, J. D., Moorman, M. A., Simonetti, D. W., Craig, S., Marshak, D. R., 1999. Multilineage potential of adult human mesenchymal stem cells. Science. 284, 143-7.

Potter, H., Weir, L., Leder, P., 1984. Enhancer-dependent expression of human kappa immunoglobulin genes introduced into mouse pre-B lymphocytes by electroporation. Proc Natl Acad Sci U S A. 81, 7161-5.

Provot, S., Schipani, E., 2005. Molecular mechanisms of endochondral bone development. Biochem Biophys Res Commun. 328, 658-65.

Raab-Cullen, D. M., Thiede, M. A., Petersen, D. N., Kimmel, D. B., Recker, R. R., 1994. Mechanical loading stimulates rapid changes in periosteal gene expression. Calcif Tissue Int. 55, 473-8.

Responte, D. J., Lee, J. K., Hu, J. C., Athanasiou, K. A., 2012. Biomechanics-driven chondrogenesis: from embryo to adult. FASEB J. 26, 3614-24.

Richter, W., 2009. Mesenchymal stem cells and cartilage in situ regeneration. J Intern Med. 266, 390-405.

Riddle, R. C., Taylor, A. F., Genetos, D. C., Donahue, H. J., 2006. MAP kinase and calcium signaling mediate fluid flow-induced human mesenchymal stem cell proliferation. Am J Physiol Cell Physiol. 290, C776-84.

Robinson, J. A., Chatterjee-Kishore, M., Yaworsky, P. J., Cullen, D. M., Zhao, W., Li, C., Kharode, Y., Sauter, L., Babij, P., Brown, E. L., Hill, A. A., Akhter, M. P., Johnson, M. L., Recker, R. R., Komm, B. S., Bex, F. J., 2006. Wnt/beta-catenin signaling is a normal physiological response to mechanical loading in bone. J Biol Chem. 281, 31720-8.

Robling, A. G., 2012. The interaction of biological factors with mechanical signals in bone adaptation: recent developments. Curr Osteoporos Rep. 10, 126-31.

Robling, A. G., Niziolek, P. J., Baldridge, L. A., Condon, K. W., Allen, M. R., Alam, I., Mantila, S. M., Gluhak-Heinrich, J., Bellido, T. M., Harris, S. E., Turner, C. H., 2008. Mechanical stimulation of bone in vivo reduces osteocyte expression of Sost/sclerostin. J Biol Chem. 283, 5866-75.

Roddy, K. A., Kelly, G. M., van Es, M. H., Murphy, P., Prendergast, P. J., 2011a. Dynamic patterns of mechanical stimulation co-localise with growth and cell proliferation during morphogenesis in the avian embryonic knee joint. J Biomech.

Roddy, K. A., Nowlan, N. C., Prendergast, P. J., Murphy, P., 2009. 3D representation of the developing chick knee joint: a novel approach integrating multiple components. J Anat. 214, 374-87.

Roddy, K. A., Prendergast, P. J., Murphy, P., 2011b. Mechanical influences on morphogenesis of the knee joint revealed through morphological, molecular and computational analysis of immobilised embryos. PLoS One. 6, e17526.

Rodriguez, J. I., Garcia-Alix, A., Palacios, J., Paniagua, R., 1988a. Changes in the long bones due to fetal immobility caused by neuromuscular disease. A radiographic and histological study. J Bone Joint Surg Am. 70, 1052-60.

Rodriguez, J. I., Palacios, J., Garcia-Alix, A., Pastor, I., Paniagua, R., 1988b. Effects of immobilization on fetal bone development. A morphometric study in newborns with congenital neuromuscular diseases with intrauterine onset. Calcif Tissue Int. 43, 335-9.

Rolfe, R., Roddy, K., Murphy, P., 2013a. Mechanical regulation of skeletal development. Curr Osteoporos Rep. 11, 107-16.

Rolfe, R., Roddy, K., Murphy, P., 2013b. Mechanical Regulation of Skeletal Development. Curr Osteoporos Rep.

Rot-Nikcevic, I., Reddy, T., Downing, K. J., Belliveau, A. C., HallgrÃ-msson, B., Hall, B. K., Kablar, B., 2006. Myf5^{-/-}:MyoD^{-/-} amyogenic fetuses reveal the importance of early contraction and static loading by striated muscle in mouse skeletogenesis. Development Genes and Evolution. 216, 1-9.

Rot, I., Kablar, B., 2013. Role of skeletal muscle in palate development. Histol Histopathol. 28, 1-13.

Ruano-Gil, D., Nardi-Vilardaga, J., Tejedo-Mateu, A., 1978. Influence of extrinsic factors on the development of the articular system. Acta Anat (Basel). 101, 36-44.

Rubin, J., Rubin, C., Jacobs, C. R., 2006. Molecular pathways mediating mechanical signaling in bone. Gene. 367, 1-16.

Rudnicki, J. A., Brown, A. M., 1997. Inhibition of chondrogenesis by Wnt gene expression in vivo and in vitro. Dev Biol. 185, 104-18.

Rudnicki, M. A., Schnegelsberg, P. N., Stead, R. H., Braun, T., Arnold, H. H., Jaenisch, R., 1993. MyoD or Myf-5 is required for the formation of skeletal muscle. Cell. 75, 1351-9.

Sabherwal, N., Bangs, F., Roth, R., Weiss, B., Jantz, K., Tiecke, E., Hinkel, G. K., Spaich, C., Hauffa, B. P., van der Kamp, H., Kapeller, J., Tickle, C., Rappold, G., 2007. Long-range conserved non-coding SHOX sequences regulate expression in developing chicken limb and are associated with short stature phenotypes in human patients. Hum Mol Genet. 16, 210-22.

Sakao, K., Takahashi, K. A., Arai, Y., Inoue, A., Tonomura, H., Saito, M., Yamamoto, T., Kanamura, N., Imanishi, J., Mazda, O., Kubo, T., 2008. Induction of chondrogenic phenotype in synovium-derived progenitor cells by intermittent hydrostatic pressure. Osteoarthritis and Cartilage. 16, 805-814.

Salvat, C., Pigenet, A., Humbert, L., Berenbaum, F., Thirion, S., 2005. Immature murine articular chondrocytes in primary culture: a new tool for investigating cartilage. Osteoarthritis Cartilage. 13, 243-9.

Sandelin, A., Alkema, W., Engstrom, P., Wasserman, W. W., Lenhard, B., 2004. JASPAR: an open-access database for eukaryotic transcription factor binding profiles. Nucleic Acids Res. 32, D91-4.

Sauka-Spengler, T., Barembaum, M., 2008. Gain- and loss-of-function approaches in the chick embryo. Methods Cell Biol. 87, 237-56.

Sawamura, C., Takahashi, M., McCarthy, K. J., Shen, Z., Fukai, N., Rodriguez, E. K., Snyder, B. D., 2006. Effect of in ovo immobilization on development of chick hind-limb articular cartilage: an evaluation using micro-MRI measurement of delayed gadolinium uptake. Magn Reson Med. 56, 1235-41.

Scaal, M., Gros, J., Lesbros, C., Marcelle, C., 2004. In ovo electroporation of avian somites. Dev Dyn. 229, 643-50.

Schmidtmer, J., Engelkamp, D., 2004. Isolation and expression pattern of three mouse homologues of chick Rgm. Gene Expr Patterns. 4, 105-10.

Schomann, T., Qunneis, F., Widera, D., Kaltschmidt, C., Kaltschmidt, B., 2013. Improved method for ex ovo-cultivation of developing chicken embryos for human stem cell xenografts. Stem Cells Int. 2013, 960958.

Scott, I. C., Blitz, I. L., Pappano, W. N., Imamura, Y., Clark, T. G., Steiglitz, B. M., Thomas, C. L., Maas, S. A., Takahara, K., Cho, K. W., Greenspan, D. S., 1999. Mammalian BMP-1/Tolloid-related metalloproteinases, including novel family member mammalian Tolloid-like 2, have differential enzymatic activities and distributions of expression relevant to patterning and skeletogenesis. Dev Biol. 213, 283-300.

Searls, R. L., Janners, M. Y., 1971. The initiation of limb bud outgrowth in the embryonic chick. Dev Biol. 24, 198-213.

Sen, B., Xie, Z., Case, N., Ma, M., Rubin, C., Rubin, J., 2008. Mechanical strain inhibits adipogenesis in mesenchymal stem cells by stimulating a durable beta-catenin signal. Endocrinology. 149, 6065-75.

Shakibaei, M., Mobasheri, A., 2003. Beta1-integrins co-localize with Na, K-ATPase, epithelial sodium channels (ENaC) and voltage activated calcium channels (VACC) in mechanoreceptor complexes of mouse limb-bud chondrocytes. Histol Histopathol. 18, 343-51.

Sharir, A., Stern, T., Rot, C., Shahar, R., Zelzer, E., 2011. Muscle force regulates bone shaping for optimal load-bearing capacity during embryogenesis. Development. 138, 3247-59.

Sharp, A. A., Fromherz, S., 2011. Optogenetic regulation of leg movement in midstage chick embryos through peripheral nerve stimulation. J Neurophysiol. 106, 2776-82.

Sharp, L. A., Lee, Y. W., Goldstein, A. S., 2009. Effect of low-frequency pulsatile flow on expression of osteoblastic genes by bone marrow stromal cells. Ann Biomed Eng. 37, 445-53.

Shen, J., Tsai, Y. T., Dimarco, N. M., Long, M. A., Sun, X., Tang, L., 2011. Transplantation of mesenchymal stem cells from young donors delays aging in mice. Sci Rep. 1, 67.

Shimabukuro, Y., Terashima, H., Takedachi, M., Maeda, K., Nakamura, T., Sawada, K., Kobashi, M., Awata, T., Oohara, H., Kawahara, T., Iwayama, T., Hashikawa, T., Yanagita, M., Yamada, S., Murakami, S., 2011. Fibroblast growth factor-2 stimulates directed migration of periodontal ligament cells via PI3K/AKT signaling and CD44/hyaluronan interaction. J Cell Physiol. 226, 809-21.

Shimizu, K., Chiba, S., Hosoya, N., Kumano, K., Saito, T., Kurokawa, M., Kanda, Y., Hamada, Y., Hirai, H., 2000. Binding of Delta1, Jagged1, and Jagged2 to Notch2 rapidly induces cleavage, nuclear translocation, and hyperphosphorylation of Notch2. Mol Cell Biol. 20, 6913-22.

Shtutman, M., Zhurinsky, J., Simcha, I., Albanese, C., D'Amico, M., Pestell, R., Ben-Ze'ev, A., 1999. The cyclin D1 gene is a target of the beta-catenin/LEF-1 pathway. Proc Natl Acad Sci U S A. 96, 5522-7.

Shum, L., Coleman, C. M., Hatakeyama, Y., Tuan, R. S., 2003. Morphogenesis and dysmorphogenesis of the appendicular skeleton. Birth Defects Res C Embryo Today. 69, 102-22.

Shwartz, Y., Farkas, Z., Stern, T., Aszodi, A., Zelzer, E., 2012. Muscle contraction controls skeletal morphogenesis through regulation of chondrocyte convergent extension. Dev Biol. 370, 154-63.

Sironen, R. K., Karjalainen, H. M., Elo, M. A., Kaarniranta, K., Torronen, K., Takigawa, M., Helminen, H. J., Lammi, M. J., 2002. cDNA array reveals mechanosensitive genes in chondrocytic cells under hydrostatic pressure. Biochim Biophys Acta. 1591, 45-54.

Sohn, P., Cox, M., Chen, D., Serra, R., 2010. Molecular profiling of the developing mouse axial skeleton: a role for Tgfbr2 in the development of the intervertebral disc. BMC Dev Biol. 10, 29.

Soleimani, M., Nadri, S., 2009. A protocol for isolation and culture of mesenchymal stem cells from mouse bone marrow. Nat Protoc. 4, 102-6.

Soshnikova, N., Zechner, D., Huelsken, J., Mishina, Y., Behringer, R. R., Taketo, M. M., Crenshaw, E. B., 3rd, Birchmeier, W., 2003. Genetic interaction between Wnt/beta-catenin and BMP receptor signaling during formation of the AER and the dorsal-ventral axis in the limb. Genes Dev. 17, 1963-8.

Spagnoli, A., O'Rear, L., Chandler, R. L., Granero-Molto, F., Mortlock, D. P., Gorska, A. E., Weis, J. A., Longobardi, L., Chytil, A., Shimer, K., Moses, H. L., 2007. TGF-beta signaling is essential for joint morphogenesis. J Cell Biol. 177, 1105-17.

Spater, D., Hill, T. P., O'Sullivan R, J., Gruber, M., Conner, D. A., Hartmann, C., 2006. Wnt9a signaling is required for joint integrity and regulation of Ihh during chondrogenesis. Development. 133, 3039-49.

St-Jacques, B., Hammerschmidt, M., McMahon, A. P., 1999. Indian hedgehog signaling regulates proliferation and differentiation of chondrocytes and is essential for bone formation. Genes Dev. 13, 2072-86.

Stern, C. D., 2005. The chick; a great model system becomes even greater. Dev Cell. 8, 9-17.

Steward, A. J., Kelly, D. J., Wagner, D. R., 2014. The role of calcium signalling in the chondrogenic response of mesenchymal stem cells to hydrostatic pressure. Eur Cell Mater. 28, 358-71.

Steward, A. J., Thorpe, S. D., Vinardell, T., Buckley, C. T., Wagner, D. R., Kelly, D. J., 2012. Cell-matrix interactions regulate mesenchymal stem cell response to hydrostatic pressure. Acta Biomater. 8, 2153-9.

Steward, A. J., Wagner, D. R., Kelly, D. J., 2013. The pericellular environment regulates cytoskeletal development and the differentiation of mesenchymal stem cells and determines their response to hydrostatic pressure. Eur Cell Mater. 25, 167-78.

Storm, E. E., Huynh, T. V., Copeland, N. G., Jenkins, N. A., Kingsley, D. M., Lee, S. J., 1994. Limb alterations in brachypodism mice due to mutations in a new member of the TGF beta-superfamily. Nature. 368, 639-43.

Storm, E. E., Kingsley, D. M., 1996. Joint patterning defects caused by single and double mutations in members of the bone morphogenetic protein (BMP) family. Development. 122, 3969-79.

Storm, E. E., Kingsley, D. M., 1999. GDF5 coordinates bone and joint formation during digit development. Dev Biol. 209, 11-27.

Sugars, R. V., Karner, E., Petersson, U., Ganss, B., Wendel, M., 2006. Transcriptome analysis of fetal metatarsal long bones by microarray, as a model for endochondral bone formation. Biochim Biophys Acta. 1763, 1031-9.

Summerhurst, K., Stark, M., Sharpe, J., Davidson, D., Murphy, P., 2008. 3D representation of Wnt and Frizzled gene expression patterns in the mouse embryo at embryonic day 11.5 (Ts19). Gene Expr Patterns. 8, 331-48.

Sundaramurthy, S., Mao, J. J., 2006. Modulation of endochondral development of the distal femoral condyle by mechanical loading. J Orthop Res. 24, 229-41.

Suzue, T., 1996. Movements of mouse fetuses in early stages of neural development studied in vitro. Neurosci Lett. 218, 131-4.

Taher, L., Collette, N. M., Murugesh, D., Maxwell, E., Ovcharenko, I., Loots, G. G., 2011. Global gene expression analysis of murine limb development. PLoS One. 6, e28358.

Taipaleenmaki, H., Harkness, L., Chen, L., Larsen, K. H., Saamanen, A. M., Kassem, M., Abdallah, B. M., 2012. The crosstalk between transforming growth factor-beta1 and delta like-1 mediates early chondrogenesis during embryonic endochondral ossification. Stem Cells. 30, 304-13.

Tajbakhsh, S., Rocancourt, D., Cossu, G., Buckingham, M., 1997. Redefining the genetic hierarchies controlling skeletal myogenesis: Pax-3 and Myf-5 act upstream of MyoD. Cell. 89, 127-38.

Takahashi, I., Nuckolls, G. H., Takahashi, K., Tanaka, O., Semba, I., Dashner, R., Shum, L., Slavkin, H. C., 1998. Compressive force promotes sox9, type II collagen and aggrecan and inhibits IL-1beta expression resulting in chondrogenesis in mouse embryonic limb bud mesenchymal cells. J Cell Sci. 111 (Pt 14), 2067-76.

Takahashi, K., Yamanaka, S., 2006. Induction of pluripotent stem cells from mouse embryonic and adult fibroblast cultures by defined factors. Cell. 126, 663-76.

Takata, S., Yasui, N., 2001. Disuse osteoporosis. J Med Invest. 48, 147-56.

Takeuchi, J. K., Koshiba-Takeuchi, K., Matsumoto, K., Vogel-Hopker, A., Naitoh-Matsuo, M., Ogura, K., Takahashi, N., Yasuda, K., Ogura, T., 1999. Tbx5 and Tbx4 genes determine the wing/leg identity of limb buds. Nature. 398, 810-4.

Tallheden, T., Karlsson, C., Brunner, A., Van Der Lee, J., Hagg, R., Tommasini, R., Lindahl, A., 2004. Gene expression during redifferentiation of human articular chondrocytes. Osteoarthritis Cartilage. 12, 525-35.

Tanda, N., Ohuchi, H., Yoshioka, H., Noji, S., Nohno, T., 1995. A chicken Wnt gene, Wnt-11, is involved in dermal development. Biochem Biophys Res Commun. 211, 123-9.

ten Berge, D., Koole, W., Fuerer, C., Fish, M., Eroglu, E., Nusse, R., 2008. Wnt signaling mediates self-organization and axis formation in embryoid bodies. Cell Stem Cell. 3, 508-18.

Theiler. K, 1972. The House Mouse. Springer, Berlin, Heidelberg, New York.

Thomas, J. T., Kilpatrick, M. W., Lin, K., Erlacher, L., Lembessis, P., Costa, T., Tsipouras, P., Luyten, F. P., 1997. Disruption of human limb morphogenesis by a dominant negative mutation in CDMP1. Nat Genet. 17, 58-64.

Thomas, J. T., Lin, K., Nandedkar, M., Camargo, M., Cervenka, J., Luyten, F. P., 1996. A human chondrodysplasia due to a mutation in a TGF-beta superfamily member. Nat Genet. 12, 315-7.

Thorpe, S. D., Buckley, C. T., Vinardell, T., O'Brien, F. J., Campbell, V. A., Kelly, D. J., 2008. Dynamic compression can inhibit chondrogenesis of mesenchymal stem cells. Biochem Biophys Res Commun. 377, 458-62.

Tice, D. A., Szeto, W., Soloviev, I., Rubinfeld, B., Fong, S. E., Dugger, D. L., Winer, J., Williams, P. M., Wieand, D., Smith, V., Schwall, R. H., Pennica, D., Polakis, P., 2002. Synergistic induction of tumor antigens by Wnt-1 signaling and retinoic acid revealed by gene expression profiling. J Biol Chem. 277, 14329-35.

Toma, C. D., Ashkar, S., Gray, M. L., Schaffer, J. L., Gerstenfeld, L. C., 1997. Signal transduction of mechanical stimuli is dependent on microfilament integrity: identification of osteopontin as a mechanically induced gene in osteoblasts. J Bone Miner Res. 12, 1626-36.

Tsumaki, N., Nakase, T., Miyaji, T., Kakiuchi, M., Kimura, T., Ochi, T., Yoshikawa, H., 2002. Bone morphogenetic protein signals are required for cartilage formation and differently regulate joint development during skeletogenesis. J Bone Miner Res. 17, 898-906.

Tsumaki, N., Okada, M., Yamashita, A., 2015. iPS cell technologies and cartilage regeneration. Bone. 70, 48-54.

Turley, E. A., Noble, P. W., Bourguignon, L. Y., 2002. Signaling properties of hyaluronan receptors. J Biol Chem. 277, 4589-92.

Valhmu, W. B., Raia, F. J., 2002. myo-Inositol 1,4,5-trisphosphate and Ca(2+)/calmodulin-dependent factors mediate transduction of compression-induced signals in bovine articular chondrocytes. Biochem J. 361, 689-96.

van Amerongen, R., Nusse, R., 2009. Towards an integrated view of Wnt signaling in development. Development. 136, 3205-14.

Van Gelder, R. N., von Zastrow, M. E., Yool, A., Dement, W. C., Barchas, J. D., Eberwine, J. H., 1990. Amplified RNA synthesized from limited quantities of heterogeneous cDNA. Proc Natl Acad Sci U S A. 87, 1663-7.

Varelas, X., Miller, B. W., Sopko, R., Song, S., Gregorieff, A., Fellouse, F. A., Sakuma, R., Pawson, T., Hunziker, W., McNeill, H., Wrana, J. L., Attisano, L., 2010. The Hippo pathway regulates Wnt/beta-catenin signaling. Dev Cell. 18, 579-91.

Vidal, M. A., Robinson, S. O., Lopez, M. J., Paulsen, D. B., Borkhsenious, O., Johnson, J. R., Moore, R. M., Gimble, J. M., 2008. Comparison of chondrogenic potential in equine mesenchymal stromal cells derived from adipose tissue and bone marrow. Vet Surg. 37, 713-24.

Visel, A., Thaller, C., Eichele, G., 2004. GenePaint.org: an atlas of gene expression patterns in the mouse embryo. Nucleic Acids Res. 32, D552-6.

Vogan, K. J., Epstein, D. J., Trasler, D. G., Gros, P., 1993. The splotch-delayed (Spd) mouse mutant carries a point mutation within the paired box of the Pax-3 gene. Genomics. 17, 364-9.

Vortkamp, A., Lee, K., Lanske, B., Segre, G. V., Kronenberg, H. M., Tabin, C. J., 1996. Regulation of rate of cartilage differentiation by Indian hedgehog and PTH-related protein. Science. 273, 613-22.

Wada, K., Itoga, K., Okano, T., Yonemura, S., Sasaki, H., 2011. Hippo pathway regulation by cell morphology and stress fibers. Development. 138, 3907-14.

Wada, N., Kawakami, Y., Ladher, R., Francis-West, P. H., Nohno, T., 1999. Involvement of Frzb-1 in mesenchymal condensation and cartilage differentiation in the chick limb bud. Int J Dev Biol. 43, 495-500.

Wagner, D. R., Lindsey, D. P., Li, K. W., Tummala, P., Chandran, S. E., Smith, R. L., Longaker, M. T., Carter, D. R., Beaupre, G. S., 2008. Hydrostatic pressure enhances chondrogenic differentiation of human bone marrow stromal cells in osteochondrogenic medium. Ann Biomed Eng. 36, 813-20.

Wagner, T., Wirth, J., Meyer, J., Zabel, B., Held, M., Zimmer, J., Pasantes, J., Bricarelli, F. D., Keutel, J., Hustert, E., Wolf, U., Tommerup, N., Schempp, W., Scherer, G., 1994. Autosomal sex reversal and campomelic dysplasia are caused by mutations in and around the SRY-related gene SOX9. Cell. 79, 1111-20.

Wang, J., Zhao, Y. C., Lu, Y. D., Ma, C. P., 2014. Integrated bioinformatics analyses identify dysregulated miRNAs in lung cancer. Eur Rev Med Pharmacol Sci. 18, 2270-4.

Wang, K. C., Garmire, L. X., Young, A., Nguyen, P., Trinh, A., Subramaniam, S., Wang, N., Shyy, J. Y., Li, Y. S., Chien, S., 2010. Role of microRNA-23b in flow-regulation of Rb phosphorylation and endothelial cell growth. Proc Natl Acad Sci U S A. 107, 3234-9.

Wang, L., Shao, Y. Y., Ballock, R. T., 2009. Carboxypeptidase Z (CPZ) links thyroid hormone and Wnt signaling pathways in growth plate chondrocytes. J Bone Miner Res. 24, 265-73.

Wang, N., Butler, J. P., Ingber, D. E., 1993. Mechanotransduction across the cell surface and through the cytoskeleton. Science. 260, 1124-7.

Wasserman, W. W., Sandelin, A., 2004. Applied bioinformatics for the identification of regulatory elements. Nat Rev Genet. 5, 276-87.

Watanabe, N., Tezuka, Y., Matsuno, K., Miyatani, S., Morimura, N., Yasuda, M., Fujimaki, R., Kuroda, K., Hiraki, Y., Hozumi, N., Tezuka, K., 2003. Suppression of differentiation and proliferation of early chondrogenic cells by Notch. J Bone Miner Metab. 21, 344-52.

Weigel, P. H., Hascall, V. C., Tammi, M., 1997. Hyaluronan synthases. J Biol Chem. 272, 13997-4000.

Wezeman, F. H., 1998. Morphological foundations of precartilage development in mesenchyme. Microsc Res Tech. 43, 91-101.

Wickham, M. Q., Erickson, G. R., Gimble, J. M., Vail, T. P., Guilak, F., 2003. Multipotent stromal cells derived from the infrapatellar fat pad of the knee. Clin Orthop Relat Res. 196-212.

Wielenga, V. J., Smits, R., Korinek, V., Smit, L., Kielman, M., Fodde, R., Clevers, H., Pals, S. T., 1999. Expression of CD44 in Apc and Tcf mutant mice implies regulation by the WNT pathway. Am J Pathol. 154, 515-23.

Wilhelm, B. T., Landry, J. R., 2009. RNA-Seq-quantitative measurement of expression through massively parallel RNA-sequencing. Methods. 48, 249-57.

Winning, R. S., Krull, C. E., 2011. Knockdown of ephrin-A5 expression by 40% does not affect motor axon growth or migration into the chick hindlimb. Int J Mol Sci. 12, 8362-71.

Winter, A., Breit, S., Parsch, D., Benz, K., Steck, E., Hauner, H., Weber, R. M., Ewerbeck, V., Richter, W., 2003. Cartilage-like gene expression in differentiated human stem cell spheroids: a comparison of bone marrow-derived and adipose tissue-derived stromal cells. Arthritis Rheum. 48, 418-29.

Wisniewska, M. B., Misztal, K., Michowski, W., Szczot, M., Purta, E., Lesniak, W., Klejman, M. E., Dabrowski, M., Filipkowski, R. K., Nagalski, A., Mozrzymas, J. W., Kuznicki, J., 2010. LEF1/beta-catenin complex regulates transcription of the Cav3.1 calcium channel gene (Cacna1g) in thalamic neurons of the adult brain. J Neurosci. 30, 4957-69.

Witte, F., Dokas, J., Neuendorf, F., Mundlos, S., Stricker, S., 2009. Comprehensive expression analysis of all Wnt genes and their major secreted antagonists during mouse limb development and cartilage differentiation. Gene Expr Patterns. 9, 215-23.

Wong, M., Siegrist, M., Goodwin, K., 2003. Cyclic tensile strain and cyclic hydrostatic pressure differentially regulate expression of hypertrophic markers in primary chondrocytes. Bone. 33, 685-93.

Woods, V. L., Jr., Schreck, P. J., Gesink, D. S., Pacheco, H. O., Amiel, D., Akeson, W. H., Lotz, M., 1994. Integrin expression by human articular chondrocytes. Arthritis Rheum. 37, 537-44.

Wright, E., Hargrave, M. R., Christiansen, J., Cooper, L., Kun, J., Evans, T., Gangadharan, U., Greenfield, A., Koopman, P., 1995. The Sry-related gene Sox9 is expressed during chondrogenesis in mouse embryos. Nat Genet. 9, 15-20.

Wu, X. B., Li, Y., Schneider, A., Yu, W., Rajendren, G., Iqbal, J., Yamamoto, M., Alam, M., Brunet, L. J., Blair, H. C., Zaidi, M., Abe, E., 2003. Impaired osteoblastic differentiation, reduced bone formation, and severe osteoporosis in noggin-overexpressing mice. J Clin Invest. 112, 924-34.

Yakar, S., Courtland, H. W., Clemmons, D., 2010. IGF-1 and bone: New discoveries from mouse models. J Bone Miner Res. 25, 2543-52.

Yalcin, H. C., Shekhar, A., Rane, A. A., Butcher, J. T., 2010. An ex-ovo chicken embryo culture system suitable for imaging and microsurgery applications. J Vis Exp.

Yamaji, N., Celeste, A. J., Thies, R. S., Song, J. J., Bernier, S. M., Goltzman, D., Lyons, K. M., Nove, J., Rosen, V., Wozney, J. M., 1994. A mammalian serine/threonine kinase receptor specifically binds BMP-2 and BMP-4. Biochem Biophys Res Commun. 205, 1944-51.

Yamamoto, M., Kuroiwa, A., 2003. Hoxa-11 and Hoxa-13 are involved in repression of MyoD during limb muscle development. Dev Growth Differ. 45, 485-98.

Yang, Y., Topol, L., Lee, H., Wu, J., 2003. Wnt5a and Wnt5b exhibit distinct activities in coordinating chondrocyte proliferation and differentiation. Development. 130, 1003-15.

Yuksel-Apak, M., Bogershausen, N., Pawlik, B., Li, Y., Apak, S., Uyguner, O., Milz, E., Nurnberg, G., Karaman, B., Gulgoren, A., Grzeschik, K. H., Nurnberg, P., Kayserili,

H., Wollnik, B., 2012. A large duplication involving the IHH locus mimics acrocallosal syndrome. Eur J Hum Genet. 20, 639-44.

Zeiter, S., Lezuo, P., Ito, K., 2009. Effect of TGF beta1, BMP-2 and hydraulic pressure on chondrogenic differentiation of bovine bone marrow mesenchymal stromal cells. Biorheology. 46, 45-55.

Zhang, K., Wong, P., Zhang, L., Jacobs, B., Borden, E. C., Aster, J. C., Bedogni, B., 2012. A Notch1-neuregulin1 autocrine signaling loop contributes to melanoma growth. Oncogene. 31, 4609-18.

Zhao, B., Li, L., Wang, L., Wang, C. Y., Yu, J., Guan, K. L., 2012. Cell detachment activates the Hippo pathway via cytoskeleton reorganization to induce anoikis. Genes Dev. 26, 54-68.

Zhao, Q., Eberspaecher, H., Lefebvre, V., De Crombrugghe, B., 1997. Parallel expression of Sox9 and Col2a1 in cells undergoing chondrogenesis. Dev Dyn. 209, 377-86.

Zhong, Z., Zylstra-Diegel, C. R., Schumacher, C. A., Baker, J. J., Carpenter, A. C., Rao, S., Yao, W., Guan, M., Helms, J. A., Lane, N. E., Lang, R. A., Williams, B. O., 2012. Wntless functions in mature osteoblasts to regulate bone mass. Proc Natl Acad Sci U S A. 109, E2197-204.

Zhou, M., Ma, J., Chen, S., Chen, X., Yu, X., 2014. MicroRNA-17-92 cluster regulates osteoblast proliferation and differentiation. Endocrine. 45, 302-10.

Zuniga, E., Rippen, M., Alexander, C., Schilling, T. F., Crump, J. G., 2011. Gremlin 2 regulates distinct roles of BMP and Endothelin 1 signaling in dorsoventral patterning of the facial skeleton. Development. 138, 5147-56.

Appendix A

Appendix Table A.1: Five uncharacterised proteins/unknown genes identified using Microarray technology.

ProbeName	Genebank Accession	Description	Fold Change	P-Value
Up-regulated				
A_66_P132861	AK082832	predicted gene 9918 Gene [MGI:3646315] [ENSMUST00000066324]	3.8783	0.00089
A_51_P471273	AK013700	RIKEN cDNA 2900055J20 Gene [MGI:1920251] [ENSMUST00000096572]	3.5631	4.94E-04
A_66_P111224	XM_001476372	PREDICTED: Mus musculus similar to crooked legs CG14938-PB (LOC100041430), mRNA [XM_001476372]	2.7239	0.00037
Down-regulated				
A_55_P2037772	AK132634	Putative uncharacterized protein [Source:UniProtKB/TrEMBL;Acc:Q3V179] [ENSMUST00000099100]	-24.735	0.00065
A_55_P1996216	AK050931	Putative uncharacterized protein [Source:UniProtKB/TrEMBL;Acc:Q8BQE4] [ENSMUST00000071059]	-5.166	6.58E-05

Omitted from further analysis, until characterisation could be sought.

Appendix Table A.2: Enrichment of muscle associated genes identified in the down-regulated gene category

Gene Ontology Term	**Gene count in study**	**Enrichment[1]**
Muscle Development/ Structure/ Function	**[69]**	**1.77×10^{-25} to 2.42×10^{-8}**
GO:0007517: muscle organ development	43	1.77×10^{-25}
GO:0060537: muscle tissue development	35	1.58×10^{-21}
GO:0014706: striated muscle tissue development	34	1.69×10^{-21}
GO:0055002: striated muscle cell development	23	1.63×10^{-19}
GO:0051146: striated muscle cell differentiation	27	1.36×10^{-18}
GO:0003012: muscle system process	24	2.32×10^{-18}
GO:0006936: muscle contraction	23	2.47×10^{-18}
GO:0055001: muscle cell development	23	3.74×10^{-18}
GO:0042692: muscle cell differentiation	29	2.11×10^{-17}
GO:0007519: skeletal muscle tissue development	22	3.22×10^{-15}
GO:0060538: skeletal muscle organ development	22	5.97×10^{-15}
GO:0006941: striated muscle contraction	10	2.42×10^{-8}

1. P-value of enrichment of GO terms using DAVID analysis software; similar results were found with GOstat

Appendix Table A.3: List of all DE down-regulated genes and fold change estimated by Microarray and RNA-seq, and evidence of any mesenchyme enrichment (≥3fold).

Gene id	Mesenchyme enriched ≥3 fold	RNA sequencing Down-regulated		Microarray Down-regulated	
		Fold Change	p-value	Fold Change	p-value
Fgf4		#[4]	0.000638844	41.054	0.00008
Tmem184a		#[1]	5.25E-06	13.264	0.04677
Mep1a		#[1]	0.010348707	10.561	0.00645
Dysfip1		#[1]	1.33E-07	6.812	0.01802
Fgf6	*	#[1]	1.11E-11	3.175	0.04425
2310050B05Rik		#[1]	4.13E-06		
2900079G21Rik		#[1]	4.76E-07		
Acpt		#[1]	0.045689548		
Cym		#[1]	0.041456515		
Foxd4		#[1]	1.15E-05		
Havcr1	*	#[1]	5.89E-06		
Lmod2	*	#[1]	2.49E-06		
Mir23b		#[1]	0.021403052		
Pnmt		#[1]	0.012794292		
Prame		##[1]	1.04E-05		
Ros1		#[1]	0.023630339		
Scn10a	*	#[1]	0.008723248		
Snai3		#[1]	0.000979848		
Stoml3		#[1]	0.036230472		
Tekt5		#[1]	0.026716473		
Tmsb15a		#[1]	0.030048338		
Ucp3	*	#[1]	0.031453558		
Yipf7		#	0.000163307		
A930003A15Rik		231.055	0.000287109	18.655	0.00782
Dbx1		179.594	5.29E-38	40.147	0.02491
Arx	*	158.132	0.00153276		
Mybph		148.831	4.60E-07	124.692	0.02395
Hspb3		146.551	4.60E-06		
Myf6	*	146.233	6.78E-06		
Gjd4		141.023	1.48E-05	39.542	0.00901
Myf5		131.785	7.62E-20		
Adprhl1		128.451	1.68E-06	6.578	0.01050
Sgcg		125.637	3.95E-06	4.691	0.00645
Sln		115.450	2.65E-05		
Chrnd		113.472	1.39E-10		
Myh7		108.322	4.98E-11		
Tnnc1		107.742	7.70E-07	87.484	0.02563
Lbx1		106.407	7.20E-12	11.171	0.01639
Tmem8c		103.616	1.46E-07	17.556	0.00371
Tceal7	*	100.473	2.35E-05		
1110059M19Rik		99.975	3.20E-05		
Myoz2		99.334	3.09E-06		
Trim55	*	99.055	8.55E-08		
Vgll2		98.294	1.39E-13	49.049	0.01175
Ankrd1		97.739	1.02E-06	75.139	0.00302
Cox8b		97.681	0.001255014		
Csrp3		96.892	1.21E-06		
Actn2		96.575	2.69E-07		
Chrng		96.232	9.54E-07	12.159	0.00627
Popdc3		94.586	0.000172639	4.403	0.02212
Cacng1		90.866	4.19E-07	32.059	0.04062
Mstn	*	90.078	4.12E-19	50.047	0.00709
Hfe2		87.940	2.07E-06	50.875	0.01598
Smyd1	*	87.679	3.17E-09	13.318	0.02829

[4] Fold Change not determined as no expression in Mutant

Myh3		87.097	3.27E-10		
Myl1		85.959	2.39E-05		
Xirp1	*	84.349	3.06E-05	5.065	0.00901
Mylpf		82.738	5.04E-05	26.582	0.01289
Actc1		81.479	3.62E-08		
Trim72		80.325	5.71E-11	44.156	0.02310
Tnnt1		80.285	1.40E-07	44.680	0.02166
Kbtbd5		77.398	5.15E-08	55.169	0.02044
Casq2	*	76.168	7.56E-05		
Lmod3		75.222	6.12E-06	32.640	0.02212
Tnnc2		74.725	1.91E-06		
Mb		73.707	7.16E-06	35.531	0.01765
Pax7		73.024	2.51E-74	23.660	0.00901
Ttn	*	72.937	1.86E-08	50.449	0.00834
Fitm1		72.173	1.34E-09	33.058	0.03818
Myod1		71.771	5.57E-17	45.123	0.00670
Tnnt2		69.284	3.10E-06		
Trdn		68.649	1.40E-07	54.363	0.03187
Atp1b4	*	67.690	1.68E-05		
Best3	*	67.237	6.34E-09	16.822	0.00371
Il17b		66.180	0.000185033		
Acta1		65.851	9.80E-05		
Mir133b		65.716	0.000606002		
Cox6a2		65.555	0.00048648		
Ankrd2	*	65.349	0.002450587		
Trim54		64.915	5.93E-05	33.576	0.04568
Krt33b		64.867	0.001294308	16.038	0.01225
Myl2		64.742	0.000253453	23.270	0.04191
Myom2		64.557	1.96E-09		
Lrrc30		63.825	9.24E-06		
Myh7b		63.715	2.77E-11	76.442	0.04129
3425401B19Rik		62.341	4.16E-06		
Myot	*	61.078	0.000103901		
Kbtbd10	*	60.151	1.71E-08	79.742	0.00371
Itgb1bp2		58.265	1.86E-05		
Neb	*	57.041	1.22E-08	35.800	0.01163
Myl4		56.963	6.14E-05	34.577	0.03079
Arpp21		56.688	4.24E-11	56.372	0.00958
Cacna1s		56.678	3.78E-07	58.404	0.03587
Chrna1		55.033	1.37E-09	76.917	0.00901
Tigd4		54.824	0.000385919		
Myog		53.537	2.55E-16	51.220	0.02105
Atp2a1		51.426	1.36E-06	9.285	0.00709
Tcap		48.488	0.00016188	61.371	0.01317
Ldb3	*	48.169	3.41E-05	7.006	0.03013
C130080G10Rik	*	48.033	0.008148424		
Mybpc1	*	47.960	5.21E-06		
Alpk3		47.897	2.10E-07	42.743	0.01598
Myo18b		47.329	1.16E-09	36.350	0.02675
Ampd1	*	47.163	9.24E-05		
Ripply1		46.845	0.020822695		
Klhl31	*	46.120	7.67E-06	19.278	0.02491
2310002L09Rik	*	46.103	1.07E-07	40.300	0.02491
Tnni1		44.819	2.11E-05		
Trpv1		44.032	0.00103819		
Atp13a5		43.397	4.89E-06	3.964	0.03171
Ablim3		43.325	1.57E-08	21.901	0.01126
Pitx3		42.860	9.67E-14	18.771	0.01175
Uts2r		42.751	9.28E-05		
Ache		42.710	4.67E-06	27.920	0.02629
Gm889		42.435	0.002373688		
Smpx		42.176	0.000413451	34.338	0.00399
Igfbp1		41.402	0.000458505	17.520	0.00901
Myh8	*	40.847	4.51E-09	19.589	0.02510
Tnnt3		40.508	0.00018347	17.435	0.03668
Rapsn		39.898	1.21E-08		
Gm7325		39.309	1.54E-08	48.412	0.00645
Cyp2ab1		38.930	0.002350375		
Hspb2		38.350	0.000109634	22.535	0.00627
Srpk3		37.989	0.000171147	38.197	0.00901

Kremen2		37.427	6.33E-07	17.221	0.00645
Mypn	*	36.927	4.18E-06	14.088	0.00327
Coro6		36.874	0.000398936		
Sh3bgr		35.425	5.65E-05	25.153	0.01735
Apobec2	*	35.312	0.00010877	58.828	0.03649
Obscn		35.116	4.00E-08	64.038	0.00789
Myl3		33.794	0.003700068	27.441	0.01610
Cdh15		32.652	1.57E-12	22.649	0.00575
Abra		31.900	0.005512519		
Cacng6		31.804	0.000299637		
Tmem182	*	31.716	0.004213734		
Synpo2l		31.489	1.69E-07		
F2		31.361	0.007704493	22.295	0.01017
Sypl2	*	31.244	0.00080006		
Rbm24		31.077	3.57E-10	22.326	0.00569
Scn3b	*	30.675	3.28E-06		
Cav3		30.120	0.000918982	22.934	0.00709
Mybpc3		29.921	0.000673869		
Ccnb3	*	29.525	1.28E-05		
Musk	*	29.129	1.84E-09	31.883	0.03444
Rgr		28.944	0.014988579		
Mylk4	*	28.587	9.03E-06	14.918	0.03171
Myom3		27.767	1.08E-07	14.330	0.03973
Ky		27.403	5.08E-07	9.045	0.02330
Dhrs7c		26.627	3.53E-05	22.417	0.02363
Mlc1		26.493	0.000342179	9.746	0.02166
Prkag3		26.251	0.000650341		
Tmprss2		25.890	2.74E-05		
Tmod1		25.608	3.13E-06	24.435	0.03973
Otog		25.430	8.59E-09		
Art1		25.144	7.18E-05	13.363	0.00371
Ckm		25.090	0.001359396		
Myoz1		24.844	0.000350615	18.794	0.02491
Mylk2		24.679	0.00136607	2.852	0.04700
Alpk2	*	24.629	7.57E-09	5.427	0.01050
Itgb6	*	24.278	3.85E-06	27.782	0.01388
Crhr2	*	24.268	0.004984818		
Jsrp1		22.778	0.000314804	10.029	0.02491
Tnni2		22.733	0.000708664	14.431	0.03055
Cblc		22.719	0.046710202		
Ptx4		21.644	2.31E-17		
Xirp2	*	20.984	3.73E-06		
Lrtm1	*	20.551	0.000894063		
Msc		20.402	3.53E-22	15.969	0.02491
Stac3		20.398	5.43E-06	9.553	0.04044
Btbd17		20.223	7.70E-11	18.216	0.00738
Sgca		19.899	6.32E-05	13.827	0.01633
Grip2		19.683	0.000641698		
Dok7		19.673	1.98E-10	15.493	0.01958
Klrb1c		19.361	0.034210789		
Fhad1		19.117	0.000146456	13.893	0.02110
Wdr16		18.658	0.020618305	35.858	0.02113
Barx2		18.601	5.29E-23		
Ckmt2		18.480	0.009086687		
Des		18.470	3.71E-05	14.972	0.00901
Mir133a-2		18.359	0.026213942		
Marveld2		18.354	8.73E-07	9.939	0.02491
Elovl3		18.044	4.46E-09		
Slc44a3	*	17.993	9.50E-07		
Murc	*	17.703	0.000725054	15.510	0.02212
Krt4	*	17.664	0.010105871		
Ryr1		17.564	6.05E-11	11.484	0.02110
Unc45b		17.298	4.20E-05	7.124	0.02110
Rtn2		16.606	3.50E-05	14.053	0.00627
Ccin	*	16.535	0.04105955		
1500017E21Rik		16.501	4.58E-07		
Zfp474		16.477	0.00741475		
Gm5105	*	16.465	2.29E-07		
Fam159a		15.637	0.000139788	6.503	0.02207
Frmpd1		15.590	3.25E-19	9.015	0.00627

Pgam2		15.539	0.00097618	19.873	0.01050
Asb2		15.411	0.00025413	9.920	0.00374
Duoxa1		15.409	0.001254674	4.989	0.03018
Casz1		15.171	1.55E-09	25.350	0.02291
Gja3	*	15.158	0.031671581		
Myom1		15.117	3.75E-05	12.371	0.02290
Myl6b		14.795	0.000124537	11.872	0.00503
Kcnc4		14.708	0.003835808		
Klhl38		14.705	6.02E-06		
Hhatl		14.547	0.001515536	4.586	0.03107
Popdc2		14.543	1.01E-07		
Colq	*	13.793	0.000636245	6.168	0.04554
Kcnk13	*	13.454	1.28E-06		
Tpm2		13.435	0.000344311	2.302	0.04191
Nrap		13.367	0.000125314		
Chrnb1		13.347	1.34E-05	7.600	0.01831
Myh6	*	13.294	0.000129867	8.711	0.01765
Slc25a18		13.092	0.000244044		
P2rx5		12.746	3.43E-05		
Capn3		12.740	0.000703589	8.047	0.01184
Gm572		12.481	0.030996655		
Rai2		12.397	0.000190941	8.946	0.00709
Rxrg		12.290	3.24E-05	7.048	0.00645
Scn4a		12.018	1.14E-11		
Fsd2	*	11.845	0.005482517		
Gal3st2		11.565	0.029992903		
Sag		11.513	4.76E-05		
Trim63		11.172	0.000444857		
Arhgap36	*	11.080	0.007757438		
Impg1		11.069	0.015160443		
Ect2l		10.884	0.030198614		
Cck		10.841	0.00024209	6.888	0.02336
Mustn1		10.824	7.41E-05	7.415	0.00682
Srl	*	10.785	0.000288666	12.709	0.02491
Tppp3		10.647	1.63E-10	9.028	0.01050
Stmn4		10.587	5.69E-17	8.410	0.03036
Thbs4		10.579	1.25E-57		
Gjd2		10.558	0.007216651		
Kbtbd12	*	10.438	0.013183456	16.975	0.02743
Sct		10.260	0.000351532	5.540	0.03042
1600029D21Rik		10.104	0.0078423	5.124	0.01578
Slc6a13		10.021	0.004168164		
Adam2		9.895	0.0211861		
Cilp		9.760	5.73E-25	9.731	0.00645
L3mbtl		9.449	0.032843435		
Pygm		9.409	0.001093758	4.666	0.01341
Hspb1		9.199	0.001579204	6.302	0.01307
Fbxl22		9.195	0.000212027	13.370	0.00740
Mir3072		9.024	0.003198372		
Akap6	*	8.846	0.000236632		
Pdlim3		8.838	0.002436503	5.509	0.01175
Odf3l1		8.787	0.001335064		
Snora43		8.705	0.046050196		
Myo5b	*	8.630	0.005148846	10.057	0.01194
Ntrk1		8.503	6.65E-05		
Ctnna3	*	8.473	0.000724585		
Folr4		8.420	0.000211253		
Traf3ip3		8.344	0.003080134	4.674	0.00881
Gnb3		8.324	0.039793053		
Cryab		8.192	0.000348192	5.632	0.00649
Txlnb	*	8.106	0.000781947	7.191	0.03042
Kcnc1	*	8.064	5.02E-06		
Slc28a2		7.901	2.56E-05	5.266	0.02310
Spink5		7.880	0.000118872	6.518	0.04425
Rbm20		7.791	4.89E-34		
Usp44		7.765	0.002121462		
Crym		7.748	1.05E-05	5.159	0.02207
Ablim2		7.636	0.005358528		
Frem2	*	7.520	2.27E-05	5.203	0.00901
Calb2		7.442	0.00381292		

Rrad		7.381	0.001844232	5.083	0.00371
Art5		7.313	0.001876818	6.279	0.02675
Mt3		7.302	0.00142808		
Hspb7		7.054	0.04163647		
Ppp1r3a	*	6.978	0.03150198		
Synpo2	*	6.952	7.65E-06		
Iqsec3		6.849	2.06E-08	13.668	0.03218
Etv4		6.796	4.50E-13		
Shc3		6.735	0.008690025		
Dusp13		6.642	0.03234326	18.884	0.00894
Tceal6		6.638	0.010139096		
Gatm	*	6.550	2.53E-05		
Ufsp1		6.540	0.000987288	3.081	0.02563
Amtn		6.450	6.37E-17		
Dusp27		6.311	0.001475933	3.935	0.01122
LOC100302688		6.256	0.006530937		
Klhl30		6.212	0.003567934	5.012	0.01694
Rbfox1		6.190	0.004453688		
Gpr83		6.152	3.21E-12		
Kcnj11		6.133	0.020393335		
Tecrl	*	6.093	1.22E-05	5.844	0.02675
Slc18a1		6.060	2.06E-05	4.951	0.03669
Acta2		6.045	0.00027772	4.818	0.04956
Enkur		5.975	0.000384266		
Ank1		5.965	6.86E-07	12.518	0.00371
Islr2		5.955	6.65E-11	5.198	0.00901
Mir25		5.944	0.041998686		
Atp1a2		5.864	0.001075117		
Htr2b	*	5.853	0.030107151	12.825	0.00901
Cpa5		5.778	5.29E-06		
Cecr2		5.750	6.03E-12		
LOC100499420		5.739	0.00032585		
Dnahc5		5.641	0.000310299		
Dner		5.639	5.36E-07		
Car3	*	5.611	0.000596286		
Ramp1		5.525	0.040157864		
Capn11		5.519	0.004820907		
Tslp		5.485	3.92E-06	3.504	0.02683
Serpina3n		5.472	0.002075378	6.027	0.03903
Nes		5.461	2.95E-10	5.573	0.00371
Ovgp1		5.449	0.006627217		
Sync		5.425	5.86E-10	5.719	0.03516
AF366264		5.396	0.042800741		
2310007A19Rik		5.350	0.003881734		
Slc2a5		5.271	5.39E-08		
Fgf8		5.254	0.015882792		
Tuba4a		5.238	0.004065209		
Smtnl2		5.180	9.01E-08	4.730	0.04271
Nol3		5.179	0.00243595	3.481	0.02908
Clcnka		5.177	0.007705476		
Adssl1		5.123	0.022447771	4.378	0.00901
F2rl1		5.106	3.92E-18	3.050	0.04447
ORF63		5.102	0.006766012		
Fgf5	*	5.098	4.04E-05		
Cdk5r1		5.062	3.26E-18	3.930	0.00901
Bex1		5.060	0.003064203	2.285	0.02491
Ostn		4.996	0.032133165		
Tspan33		4.983	8.36E-06	3.308	0.02310
Rimbp3		4.972	0.020203059		
Adora1		4.950	0.001180885		
Zmynd17		4.939	0.000574852		
Cap2	*	4.937	0.000200587	4.186	0.04786
Aifm3		4.912	0.000929811		
Pitx2		4.874	0.000814308		
Rasl10a		4.821	0.003305427	4.124	0.01373
Cd3g		4.749	0.041723914		
Hpcal4		4.745	0.026598756		
Casq1		4.735	0.033530375	3.068	0.01050
Tas1r1		4.695	0.043219376	6.324	0.01901
Gm11346		4.624	0.037549509		

Rprm		4.615	0.014824336		
Rit2		4.607	7.36E-06		
4933436C20Rik		4.591	0.000815015		
Snord99		4.571	0.001661383		
Fgfr4		4.545	6.99E-23	3.231	0.00933
Sh2b2		4.525	6.59E-05	2.988	0.04328
Spon2		4.490	1.29E-09	5.173	0.00627
Fam78a		4.482	0.001494111	3.724	0.00560
D930048N14Rik		4.426	0.009625517		
Snord83b		4.424	0.046506713		
Macrod1		4.419	0.002397058		
Tnfsf13b		4.412	0.045710756		
Ppp1r14c	*	4.402	0.004896588		
Ddc		4.399	0.000150515	2.720	0.03347
Tmem88b		4.362	4.89E-10		
Slc30a3		4.350	0.008431678		
Adcyap1r1		4.332	9.57E-17	3.919	0.02974
Kcne1l		4.331	2.28E-06		
4932438H23Rik	*	4.324	0.045421555		
Rgs16		4.318	4.08E-11		
5930412G12Rik	*	4.264	0.011044667		
Gpr120		4.171	0.035698806		
Jph2		4.160	0.000156224		
Tac1		4.139	2.18E-05		
Sept04		4.087	1.98E-06		
A430110N23Rik		4.081	2.89E-27		
Tex14		4.070	0.000570692	5.613	0.02023
Rragd		4.052	2.17E-08		
1700113I22Rik		4.024	0.000731808	2.601	0.00709
Htra4		4.015	7.54E-07		
Slc35f3		4.014	2.10E-08	3.144	0.03983
Megf10		4.009	1.37E-24	3.488	0.02491
Esrrb		3.990	0.000491894	3.647	0.01598
Zfp352		3.936	0.012205983		
Fndc5		3.925	0.00050277		
Gm1574		3.920	0.002391272	6.132	0.02675
Pabpc1l		3.898	0.001062351		
Insrr		3.891	0.000788901		
Dmpk		3.877	0.00326029	2.705	0.02212
Tead4	*	3.860	3.03E-13	4.381	0.03649
Myo16		3.848	3.94E-08		
Iffo1		3.837	0.000289585	2.640	0.01289
BY080835		3.826	0.016938161		
Cnr1		3.818	1.52E-13	2.590	0.00399
Tll2	*	3.805	0.000121063		
Mirg		3.791	0.016388196		
Sema6b		3.779	1.95E-07		
Camk2a		3.776	0.000910514		
Ppfia4		3.766	0.005944714		
Camk2b		3.762	0.000587067		
Pou3f1		3.761	7.85E-05		
Fabp3		3.748	0.046045376	2.962	0.04425
Vgll3	*	3.743	7.18E-20		
Trp63	*	3.724	0.024720208		
Col19a1	*	3.629	6.57E-05		
Snord65		3.628	0.049056944		
6230400D17Rik		3.615	0.023809995		
Dok5		3.607	0.021244085		
Tmem38a		3.593	0.018014843		
C4b		3.591	0.002928394	4.261	0.02829
Fzd10	*	3.577	0.021714725		
Gpr37		3.571	0.00851303	3.684	0.02983
Jakmip3		3.569	0.023481256		
6430562O15Rik		3.499	0.005665791		
Spnb1	*	3.493	0.00122522		
Lrrc39		3.473	0.018679961		
Erbb3		3.457	1.10E-16		
Cobl		3.448	0.010742417	20.443	0.03640
Coch		3.419	4.76E-07	3.814	0.03461
2900005J15Rik		3.402	0.029056216		

Bcam		3.389	0.00124051		
Prkcc		3.371	0.018418282		
Hrc		3.360	0.004990099	3.130	0.04550
Atp2b3	*	3.356	0.016922185		
Arg1		3.355	0.017844783		
Cdkn1a		3.317	0.000390277		
Tnfrsf12a		3.305	4.85E-05		
Ntn5		3.299	0.003150271		
Chodl		3.292	1.38E-05	3.152	0.04328
Zfp238		3.284	4.78E-08		
Gldc		3.263	0.000326193		
Tmem116		3.253	0.017991955		
Dpf3		3.251	0.032786354		
Spry1		3.243	2.75E-18		
Spry4		3.219	3.86E-18		
Gmpr		3.219	0.026099494	2.018	0.02337
Trim17		3.216	0.04712073		
Ccdc141	*	3.212	0.000148407		
Cnnm1		3.211	7.19E-06		
Myh1	*	3.185	0.013884554		
D17H6S56E-3		3.172	0.032055615		
Mip		3.168	0.013720797		
Dll1		3.162	1.73E-06	2.210	0.03516
Snap91		3.162	0.007990301		
Mir17hg		3.161	5.44E-05		
Meg3		3.155	0.030983905		
Jam2		3.148	0.036344194	3.594	0.03717
Unc5a		3.138	0.004421143		
Plch1		3.137	1.23E-05	4.047	0.00920
Tnmd		3.134	6.59E-13		
6330403A02Rik		3.126	0.000159805		
Gprc5a		3.117	8.03E-05		
Lhfpl1		3.116	4.10E-08		
Rbm38		3.116	0.012501553		
C1ql3		3.106	2.75E-08		
Cited1		3.103	0.000277615		
Hspb8		3.095	0.002956441		
Prg4		3.046	1.52E-07		
Snora34		3.038	0.049099265		
Snord52		3.010	0.011579628		
Nup210		3.006	1.07E-14	3.294	0.03042
Cenpv		2.996	8.48E-06		
Ambn		2.965	0.00160442		
Snora16a		2.962	0.047384799		
Dleu7		2.962	0.017802886		
Kirrel2		2.960	0.047889124		
Gpr20		2.955	8.98E-05		
Itga4	*	2.948	9.97E-11	3.381	0.03359
Pde1c		2.946	3.42E-08		
B3galt2	*	2.923	0.036346769		
Snhg7		2.919	0.006088416		
Palmd		2.902	0.023169218		
Spp1		2.901	0.043857363		
Doc2g		2.898	0.04842582		
Gcom1		2.896	0.005646488		
Itga7		2.849	0.000684807		
Pdlim1		2.848	1.45E-11		
1810041L15Rik	*	2.820	0.002356183	2.965	0.00901
Lrrn1	*	2.813	0.003220508	2.566	0.03397
Meox1		2.796	2.27E-11		
Kcnj10		2.792	0.02273419		
Mfsd2a		2.791	9.64E-06		
Tm6sf1		2.783	0.023438649	2.571	0.01333
Bin1		2.782	0.000548241	2.032	0.04754
Prox1	*	2.778	1.75E-05		
Pknox2		2.773	1.18E-08		
Spry2		2.755	6.11E-14		
Zic3		2.745	0.004207025		
Frmd3		2.745	2.09E-05		
Hbegf		2.741	0.000350767		

Ankrd23		2.736	0.021544801		
Shroom3		2.713	0.002091898		
Tmem100		2.707	5.15E-10		
Tubb6		2.693	0.001035104		
Slco5a1	*	2.691	0.004377646		
Eno3	*	2.687	0.034131718		
Hes6		2.686	0.001946887		
Col22a1		2.680	0.011807048		
Dynlt1a		2.675	0.036885253		
Nexn		2.652	0.014639095		
Gm14492		2.634	0.011746406		
Angptl7		2.632	0.012651786		
Ehbp1l1		2.631	0.00150257		
Sh2d5		2.616	0.044303872		
Arhgdig		2.616	0.000649376		
Rb1	*	2.614	0.000176926	2.391	0.00715
4933403O08Rik	*	2.604	0.016456786		
2010204K13Rik		2.599	1.45E-05		
Aknad1	*	2.590	0.003212914		
Asb10		2.578	0.006471367		
Il20rb		2.578	0.002114249		
2210403K04Rik		2.577	0.011615356		
Nptx1		2.577	0.000390855		
Dok3		2.569	0.049938133		
Lgi1		2.565	0.002611874		
Vamp1		2.557	0.038815305		
Glipr2	*	2.554	3.12E-13		
Sim1	*	2.553	0.033426892		
P2rx6		2.550	0.035400757	9.052	0.03973
Nnmt		2.549	0.005961276	2.407	0.04361
Dtx4		2.544	3.50E-12		
Camkv		2.540	0.003666581		
Tdrd1		2.534	1.58E-05		
Tnxb		2.528	1.10E-06		
Ppp1r14b		2.526	0.000513015		
Tchh		2.525	0.032617528		
Sall1		2.519	0.009263167		
Tbc1d8		2.515	1.81E-05		
Chrm3		2.512	0.000313547		
Prkcq		2.509	1.99E-06	2.254	0.01637
Plekhh1		2.500	3.68E-05	3.040	0.02140
Ank2		2.495	3.07E-13		
Mir3064		2.484	0.031260542		
Hsd11b1		2.483	0.009085944		
Cidea		2.475	0.016861321		
Tnik	*	2.470	3.19E-09		
E2f2		2.460	1.93E-10		
Atcay		2.457	0.018944588		
Aldh1a3		2.451	2.38E-08		
Pdlim4		2.449	0.000822125		
Scx		2.444	0.002779351		
Ngfr		2.444	2.43E-08		
Bves		2.436	0.018857391		
Col20a1		2.432	1.37E-06		
E330033B04Rik		2.427	0.039694776		
Ankrd33b		2.419	0.03187479		
Gamt		2.411	0.032919827		
Tmem150c		2.410	0.000118831		
Pip5k1b		2.406	0.003669955		
Ttyh2		2.403	2.55E-10	2.039	0.02337
Ak1		2.391	0.047782606		
Tppp		2.385	5.99E-05		
Tceal5		2.360	0.002343191		
Tubb2b		2.358	7.40E-08		
Ckb		2.354	8.98E-06		
Spg21		2.339	1.17E-10		
Gja5		2.332	0.007499588		
5330417C22Rik		2.332	0.041260172	9.153	0.02793
Dpep1		2.330	0.03652931		
Tcf15		2.324	0.000893465		

Adrb2		2.319	0.00525532		
Met		2.317	1.49E-08		
Hap1		2.305	0.00247612		
Mycl1		2.300	2.17E-07		
Dpysl5		2.298	7.19E-07		
Anxa8		2.298	0.013554134		
Stk32a		2.280	0.018216663		
Pla2g4c		2.279	0.023239176		
Csdc2		2.273	0.036761566		
Mir351		2.268	0.029594667		
C2cd4c		2.267	0.040396409		
En1		2.267	0.004580757		
Flnc		2.256	0.000125003	2.556	0.00645
Pdgfa		2.250	5.24E-08	2.044	0.03998
Shb		2.248	0.000601169		
Il1f9		2.247	0.004353474		
Nxph3		2.244	0.044254319		
Il33		2.234	1.77E-05		
Arc		2.221	0.027556014		
2700023E23Rik		2.211	0.00489536		
Atf3		2.211	7.60E-05		
Lamb3		2.210	0.001980772	3.323	0.03781
Padi2	*	2.210	0.018492502	2.303	0.02337
Creld1		2.208	0.009965288		
Kcnip4		2.204	0.000764541		
Rtl1		2.204	0.023526084		
Slc29a4		2.202	0.002415868		
Dusp6		2.197	4.43E-09		
Pls1		2.190	0.012618883		
Prdm8		2.186	0.016649886		
Cd44		2.183	1.40E-05	2.280	0.03042
Epcam	*	2.178	0.005086962		
Kera		2.173	0.000317803		
Cfl2		2.173	0.001038403		
Mical2		2.171	3.58E-07	4.486	0.01225
Rassf5		2.170	0.001317556		
Dusp14		2.166	0.000189953		
Egr2		2.165	0.000831611		
Pvrl1		2.165	3.22E-05		
Akap5		2.162	0.000550736		
Tbx1		2.160	0.046476272	2.509	0.04139
Rab40b		2.156	0.000857314		
Arhgap26		2.152	5.41E-07	2.049	0.04587
Magel2		2.148	0.000186304		
Pkia	*	2.142	0.001160308		
Snord47		2.140	0.008321211		
6530418L21Rik		2.123	3.70E-07	2.191	0.02113
Lfng		2.120	7.95E-06		
Dbndd1		2.119	0.011743153		
Adam1a		2.118	0.021037005		
Ccdc134		2.113	0.003468266		
1700094D03Rik		2.109	0.01745263		
Tmem108		2.096	0.044938087		
Sik1		2.093	0.004105596		
Jag2		2.087	0.002065917		
Htra3		2.077	6.80E-09		
Dnaic2		2.076	0.049783398		
Afap1l1		2.046	0.000727837		
Qprt		2.041	0.008007932		
Hn1		2.036	0.000326606		
Sod3		2.036	0.045428703		
Chrna4		2.035	5.32E-05		
Aoc2		2.034	0.014517152		
Chd7		2.029	5.11E-07		
Shisa2		2.029	3.39E-08		
Adamts20		2.028	8.50E-05		
Spink2		2.021	0.0189441		
Cdh4		2.014	1.27E-06	2.007	0.03107
Plat		2.013	7.79E-05		
Arid5a		2.009	0.002451172	2.060	0.03347

Zfp185		2.008	2.97E-08		
AW551984	*	2.003	0.047744733		
Rasef		2.003	0.027683519		
Gls2		2.000	0.010016291		
4930512H18Rik				65.074	0.02110
LOC100044755				38.678	0.04644
Myadml2	*			38.177	0.00645
1110002E22Rik				35.846	0.02491
2310015B20Rik				28.113	0.00627
Dmd	*			18.652	0.03538
Itgb1bp3	*			11.834	0.02928
Klk1b26				11.326	0.00627
Gm6880				9.406	0.01815
Gm2252				9.359	0.04924
Tpm3				8.967	0.01050
Zfp407				8.496	0.00957
Cdhr3				8.408	0.02932
LOC100048513				8.000	0.04677
Lrrc14b				7.035	0.04063
Dbh				6.355	0.03985
Pdlim5				6.314	0.01225
Slc25a18				6.291	0.02880
LOC100047320				6.147	0.03107
Gadl1				6.107	0.02675
Gckr				6.050	0.03042
LOC669787				5.825	0.00709
Smtnl1				5.458	0.01388
4933408N05Rik				5.111	0.03556
A2bp1				5.093	0.02044
Cldn3				5.040	0.01050
Myh4	*			4.639	0.02445
Asph				4.464	0.00709
Ms4a10				4.370	0.02212
Gm5091				4.180	0.02110
Cela3b				3.977	0.03055
Tpm1				3.850	0.00371
Serpina11				3.780	0.04081
Gm8617				3.770	0.04568
AA060545				3.592	0.04677
Erbb4				3.370	0.00371
Kcnj12				3.220	0.03387
Prss46				3.155	0.02675
Csn3				3.101	0.03075
Palm2				2.939	0.00399
Sept4				2.930	0.02751
4833419O12Rik				2.909	0.04676
4930429F24Rik				2.886	0.03856
4930511E03Rik				2.863	0.01289
Sirt7				2.862	0.03084
Fam169b				2.827	0.01050
6720420G18Rik				2.715	0.04890
1700125H20Rik				2.560	0.04677
Atp2a2				2.485	0.04550
4833415N18Rik				2.478	0.04328
LOC634496				2.397	0.04176
Has1				2.364	0.03442
Rhox5				2.361	0.02906
Speg				2.311	0.04918
Parm1				2.293	0.02212
C230098O21Rik				2.265	0.04554
AI314760				2.195	0.04843
Dusp8				2.145	0.02166
Dpysl3				2.139	0.04554
Celf1				2.127	0.02683
Ehd4				2.093	0.02629
Tmem100				2.089	0.01050
4922502B01Rik				2.057	0.00709
Abca8b				2.009	0.02974

Appendix Table A.4: List of all DE up-regulated genes and fold change estimated by Microarray and RNA-seq.

Gene id	RNA sequencing Up-regulated		Microarray Up-regulated	
	Fold Change	p-value	Fold Change	p-value
Cntnap5c	Inf[5]	0.00811168		
Htr4	Inf	0.015985671		
Phox2b	40.652	0.021683372		
Oprk1	33.523	0.009989198		
Th	14.885	0.019367024		
Olfm3	14.499	1.96471E-05		
Tinag	13.962	0.006855256		
Aqp5	11.241	0.03827926	2.976	0.02829061
Cntnap5b	10.734	0.007798118		
Lrp1b	10.356	2.67313E-10		
Stmn3	10.052	0.006003718		
Fstl5	9.993	0.031568933		
Pcp4	9.409	2.85327E-11		
Ces2g	9.142	0.000183355		
Bhlhe22	9.129	0.006008402		
Kcnip1	8.704	8.61502E-09	5.874	0.026830187
Ifi44	8.444	0.012913212		
Fam163a	8.348	5.13568E-05		
Galntl6	8.086	0.000220113		
3110047P20Rik	7.627	0.038093175		
Tmem28	7.574	0.000653005	3.785	0.03042167
Kcnj5	7.232	0.002870959	2.083	0.047536302
Tmem213	7.231	0.000548183		
Nefh	7.189	0.042118677		
Gm765	6.906	0.001092695		
Qrfpr	6.904	0.018242304		
9130404H23Rik	6.805	0.013520604		
Itgb2l	6.688	0.031025179		
Slc16a14	6.352	0.008701364		
6330407J23Rik	6.345	0.044510005		
Zpld1	6.175	0.010396425		
3110082D06Rik	6.083	3.90165E-06		
Grin2c	6.058	0.012818752		
Frem3	5.962	5.38805E-06		
Adh7	5.875	0.01468373		
Spock1	5.682	5.8183E-15		
Grm8	5.669	9.60601E-07		
Lingo2	5.580	3.48887E-11	4.696	0.009014199
Slfn10-ps	5.435	0.033647487		
Rmst	5.391	0.000311655		
Chrm2	5.227	0.001028715		
Kcnh3	5.208	0.000149503		
Lhcgr	5.169	0.006109941		
Zfp804a	5.100	6.23689E-06		
Nxph1	5.074	5.74355E-05		
Ina	5.034	0.018844215		
Kcnh5	4.935	9.19928E-05		
Cer1	4.931	0.004938087		
Trhde	4.916	3.38578E-13		
Lrrtm1	4.800	3.26074E-11	2.748	0.003270305

[5] Fold Change not determined as no expression in Control

Odz1	4.769	9.31145E-13		
Rasgrf2	4.726	6.94161E-09		
Hs3st5	4.725	0.018399541		
Gpr50	4.718	0.005342074		
Galnt13	4.712	2.28464E-05		
Irs4	4.699	8.89623E-05		
Gabrg3	4.615	0.014084194		
Pde11a	4.554	4.57853E-06		
Camp	4.524	5.80342E-05		
Cd96	4.494	2.02484E-05	6.327	0.007088687
Emr4	4.421	0.048807742		
Cdh8	4.394	2.04332E-11		
Darc	4.384	0.011011717	2.360	0.046771158
Kcnc2	4.369	0.002316834		
Grem2	4.358	6.87843E-18	4.909	0.0191443
Sstr4	4.334	0.000478644		
Kctd16	4.312	0.003200397		
Zfp804b	4.251	0.009898747		
Gpr88	4.242	2.11632E-09	3.497	0.020233307
Gabra5	4.198	3.91689E-05		
Cdh20	4.194	5.57411E-09		
Ltf	4.172	0.00010046		
Odz2	4.065	1.64435E-16		
Mdga2	4.019	3.19678E-10		
Rassf6	4.013	0.000941612		
Cldn11	4.012	5.82596E-19	4.339	0.026749311
Olfm4	3.995	0.000368956		
Pappa	3.983	2.52103E-18		
Cxcl5	3.977	0.007045612		
Nebl	3.977	3.43655E-09		
Wnt2	3.958	0.000104042		
Mx2	3.922	0.011710449		
Samd12	3.863	0.030721288		
Kcna2	3.848	0.000649711		
Dscam	3.841	0.000206703		
BC100530	3.818	0.035898844		
Sorcs3	3.813	7.88158E-09	3.265	0.024911175
Chd5	3.809	2.06004E-05	2.339	0.02829061
Dnahc2	3.805	1.6188E-10		
Cyp11a1	3.743	0.00526559		
Pcdh8	3.734	1.37966E-10	5.244	0.006449103
Pcdh11x	3.718	4.83242E-09		
Adora3	3.680	0.021555195		
St6gal2	3.627	0.000126933		
Nrxn3	3.625	0.001157601	2.646	0.046771158
Lamc3	3.587	0.003367514		
Lrrc7	3.584	0.000132273		
Syt2	3.563	0.014669478		
S100a9	3.546	2.28122E-09		
Wnt2b	3.497	9.69304E-09		
Sez6l	3.469	3.89725E-07		
Rtp4	3.467	1.40937E-05		
Wfikkn2	3.466	3.77228E-20	3.457	0.007088687
Apod	3.439	9.15031E-10	2.863	0.04700062
Ngp	3.393	1.11712E-06		
Rag1	3.383	0.000298643		
Grap2	3.366	0.027143322		
Negr1	3.354	2.19112E-11	2.904	0.008664596
Slitrk3	3.351	2.77517E-07		
Pnma2	3.348	0.000388047		
Bnc2	3.326	5.17221E-08		

Ankrd55	3.305	0.000166176		
Lrrn4	3.294	0.007133272		
Tmem90b	3.271	0.001382144		
Tulp2	3.263	0.007094287		
Plxna4	3.258	1.04676E-05	2.648	0.03042167
Nrg1	3.251	1.13062E-05	2.866	0.029743126
Glis3	3.250	8.99409E-05		
2010110P09Rik	3.230	0.034177208		
Lypd1	3.229	0.012599147		
Erc2	3.226	3.41887E-11	2.630	0.022361835
Lgals7	3.182	0.004911859		
Lrrn3	3.178	1.13647E-10	3.170	0.012865157
Figf	3.173	1.54196E-06	3.515	0.03106743
Cadm3	3.151	6.5051E-09		
Cd274	3.146	0.044689098		
Lama3	3.138	1.65109E-11		
Gprin3	3.130	0.013194692		
Lhfpl3	3.105	0.004501974		
Grin2a	3.105	0.001212279		
Il2rb	3.093	0.030047996		
Vstm2a	3.090	1.06252E-06	8.556	0.022071414
Grin3a	3.083	6.59045E-06		
Npy2r	3.076	0.043465598	4.083	0.016104808
Wnt16	3.065	0.000678927		
Aff2	3.061	7.0861E-07		
Bdh2	3.057	2.14413E-07	3.045	0.046683427
Chrm1	3.047	0.009294854	5.696	0.0432783
Chgb	2.987	0.015373266		
Cpa3	2.961	2.02486E-08		
Fat4	2.957	2.48032E-14		
Nhs	2.954	7.42082E-07		
Dsc3	2.944	7.23407E-07		
Prtn3	2.943	0.01258186		
Gm13154	2.930	0.029073583		
Lrfn2	2.926	1.53587E-06	2.999	0.04700292
Mme	2.916	4.60047E-10		
Stfa1	2.915	0.000355257		
Slc26a7	2.907	7.61292E-06		
Gsg1l	2.892	4.18696E-10		
C030030A07Rik	2.879	0.013809116		
Grpr	2.872	0.000323907		
Kcnd2	2.853	1.07959E-11		
Sned1	2.847	0.000172413		
Unc13c	2.835	0.000352109		
Rasgrf1	2.834	0.025886378		
Esr1	2.834	0.042051048		
Hgf	2.833	1.62534E-06		
Cacna2d3	2.822	3.46203E-08	2.877	0.03042167
Pcdhb2	2.811	0.004118991		
Trim30d	2.806	0.032401337		
Kctd8	2.802	0.014080311		
Zfp366	2.798	0.014737195		
D830031N03Rik	2.790	0.023177946		
Rasd2	2.786	0.007335242		
Slc22a3	2.780	0.00226207		
Pgr	2.773	0.017805759		
Aox3	2.764	0.017855151		
Cldn1	2.734	1.78588E-11		
Gprin2	2.732	0.014645987		
Mgat4c	2.727	0.003141679		
Csmd3	2.720	8.12645E-08		

Rassf9	2.718	0.001300208		
Ifltd1	2.707	0.021396163		
Pi15	2.702	2.92394E-07		
Aldh1a1	2.702	0.031247555		
Ptchd1	2.700	1.32068E-06		
Rims1	2.696	0.00361253		
Lmx1a	2.693	0.002502881		
Vnn1	2.685	0.001229868		
Tpsg1	2.683	0.013827512		
S100a8	2.682	0.001179789		
Aox4	2.680	0.005330953		
Gbp3	2.680	0.020948944		
Cadm2	2.669	5.97444E-05		
Thsd7b	2.669	3.65584E-08		
Stac2	2.664	1.06734E-05	2.518	0.021104623
Uprt	2.660	0.036481628		
Pcdhb6	2.657	0.000971057		
Syt5	2.657	0.014578781		
3110099E03Rik	2.652	0.028989904		
Clic5	2.644	0.000143118	2.598	0.015984364
Robo2	2.638	4.77656E-13		
Optc	2.636	0.006670803		
Bai3	2.634	9.03636E-07		
Gria2	2.630	0.003821262		
Hdc	2.627	0.00789997		
Edar	2.626	0.034376024		
A730069N07Rik	2.624	0.037926155		
Rtn4r	2.620	3.29944E-05		
Oprd1	2.615	0.015080163		
Mmp28	2.608	0.004942454		
Gpc5	2.607	0.001010127		
Dbc1	2.607	6.89248E-07		
Flrt1	2.604	4.38868E-06		
H60b	2.593	0.028096446		
Oprl1	2.566	0.006032349		
Fmn2	2.564	7.04459E-06		
Pgap1	2.548	9.99216E-05		
9130008F23Rik	2.537	0.016995569		
Hbb-bh1	2.533	0.000587881		
Grid2	2.533	0.004232619		
Pcdh10	2.529	9.72004E-12	2.565	0.017431902
Arhgap20	2.516	1.02353E-10		
Adamts12	2.514	6.89168E-05		
Grm4	2.514	0.000987148		
Siglec1	2.511	0.013051847		
Scg2	2.507	0.019336708		
Mmrn1	2.496	5.54907E-07		
Kcna1	2.487	6.31412E-09		
Scube2	2.486	1.19351E-08		
Lmx1b	2.479	3.20234E-05		
Lrrc4c	2.475	4.20325E-07		
Gm106	2.474	5.60136E-06		
Sorcs1	2.471	9.0741E-11		
Tcfcp2l1	2.467	0.00035783		
Thsd4	2.457	4.74163E-11		
Trpc5	2.450	0.044192008		
Dlg2	2.449	5.29662E-09		
Cntn4	2.441	0.00027323		
Klhl34	2.438	0.007011755		
Dkk2	2.436	1.28371E-08		
Fat2	2.433	0.000122468		

Rspo2	2.428	2.24518E-10	3.077	0.011657668
Sesn3	2.423	1.31833E-05		
Sorl1	2.422	3.60514E-07	2.193	0.03170701
H2-T24	2.407	0.011510566		
Vsnl1	2.407	0.001124722		
Tmem26	2.405	4.68593E-11		
Gabrb3	2.400	8.28704E-08		
Rgs9bp	2.394	0.000213765		
Crabp1	2.392	6.36088E-07	2.820	0.022896456
Fgf2	2.389	0.006861295		
Gpr21	2.388	0.049713237		
Ahr	2.385	1.25812E-08		
Lsamp	2.382	0.000115077		
Lcn2	2.380	0.00536202		
Zfp369	2.379	4.66917E-05		
Slit3	2.378	3.61817E-05		
Pcdhb10	2.375	0.014264068		
Tuba8	2.374	0.045281056		
Hcn1	2.374	0.000443861		
Accn1	2.371	0.030431602		
Maf	2.370	8.046E-11		
Gstt1	2.369	9.34437E-06	2.966	0.014203158
Epha4	2.367	1.09558E-06		
Cadps2	2.367	2.02583E-07		
Foxc2	2.362	3.77885E-09	2.091	0.022120591
Samd9l	2.359	4.06757E-05		
Pde3a	2.356	0.000252521		
Cnksr2	2.350	1.67466E-06	2.034	0.023361117
Olfml2a	2.348	0.004423579		
Rundc2a	2.339	0.000568975		
Prdm11	2.339	0.007433865		
Cxcl13	2.334	0.000815449		
2410066E13Rik	2.333	5.12866E-05		
Ptx3	2.327	4.83727E-10	2.724	0.009014199
Ptafr	2.325	0.012971943		
Mecom	2.324	9.89019E-10		
Pcdhga2	2.322	4.60663E-05		
Prrx1	2.321	9.53569E-11		
Foxd2	2.318	2.39873E-06		
Xpnpep2	2.318	1.89682E-05		
Adra1d	2.314	0.021633553		
Cbl	2.307	0.010130391		
Plb1	2.306	0.028733823		
Adra1b	2.304	0.003433491		
Enpep	2.299	2.53756E-06		
Ccdc158	2.295	0.045877342		
Ncam2	2.295	0.002124326		
Col8a1	2.295	1.09688E-09		
Myocd	2.292	0.040200711		
Ankrd45	2.288	0.047353982		
Slc40a1	2.286	1.12932E-09	2.326	0.006270704
Angptl4	2.282	0.004535418	2.277	0.030546911
Abca1	2.280	1.51947E-09		
Pdpr	2.277	0.007641978		
Cntn1	2.275	9.40642E-07	2.286	0.029743126
Slitrk6	2.274	3.4985E-08		
Zfp382	2.273	0.025343336		
Epha5	2.273	8.58459E-08		
Mgat5	2.272	0.027815516		
Hhip	2.265	5.90086E-05		
4930441O14Rik	2.265	0.034203402		

Sox5	2.263	0.018114271		
Kif13b	2.260	0.001190356		
Svep1	2.258	1.16294E-05		
Dnahc8	2.256	0.001986264		
Dlx6os1	2.255	0.000714783	2.995	0.022896456
Prdm6	2.255	1.31907E-06	2.316	0.020373477
Syt1	2.252	0.028025215		
Hyal1	2.249	0.000200445		
Dio3	2.249	0.003613222		
Shroom4	2.249	0.002278556		
Samd5	2.248	0.020010474		
Fam198a	2.247	9.27339E-09		
Sema5a	2.246	1.05617E-09		
Hbb-y	2.243	0.038467745		
Krt7	2.243	0.000961023		
Zbed6	2.241	0.019980525		
Xrn1	2.231	0.006731401		
Fam84a	2.228	2.96287E-07		
Rassf8	2.223	0.000601203		
Fam107a	2.223	0.004755457	2.136	0.022120591
Fgd3	2.223	0.030165821		
Prokr1	2.222	3.35816E-08		
Hmbox1	2.219	0.003467061		
Serpinb1a	2.218	0.000184334		
Ppp1r3b	2.212	1.4059E-08		
Ldb2	2.212	2.9089E-09		
Bace2	2.211	6.73151E-06	2.835	0.030364744
Elovl7	2.200	0.007187013		
Kcns3	2.199	2.78753E-06		
Stk32b	2.198	9.71846E-07		
Zkscan16	2.197	0.002988075		
Cntn5	2.196	0.013216323		
Gan	2.192	0.00130235		
Fmo1	2.191	0.001376719		
Krt15	2.190	0.024841916	5.601	0.036359612
Kcnb2	2.190	0.041471176	2.901	0.041941773
Foxo3	2.189	0.000246334		
L3mbtl3	2.189	6.73263E-09		
Lgr5	2.187	6.19424E-07		
Col8a2	2.187	8.85889E-10		
Rgs7bp	2.183	4.93168E-06		
Tox	2.182	4.55433E-08		
Thsd7a	2.179	7.40566E-06		
Pcdhga1	2.175	0.000730494		
BC005561	2.175	0.006359051		
Gfra2	2.173	3.02507E-08		
Cd83	2.173	1.31811E-05	2.157	0.0432783
Dpyd	2.171	3.1538E-06	2.310	0.02829061
Pappa2	2.170	0.000174666		
Alcam	2.165	9.22825E-10		
Scube3	2.161	0.000109247		
Cxcl14	2.161	2.3385E-06		
Ccbe1	2.159	4.98708E-07		
Rapgef5	2.159	2.88791E-05		
Masp1	2.158	0.006495732		
Cdkl5	2.155	0.026246787		
6430704M03Rik	2.150	0.003661461		
Kcnab1	2.146	3.71027E-05		
Nckap5	2.145	0.000387554		
Ace	2.144	0.003928341		
Spock2	2.144	1.40746E-07		

Ptch1	2.143	0.014230432		
Klf7	2.143	0.008730025		
N28178	2.142	0.03120798		
Trim30a	2.142	0.000562132		
Paqr6	2.142	0.010785309		
Opcml	2.140	1.0228E-05		
Sema3d	2.140	0.000504096		
Fgf10	2.139	8.88607E-08	2.478	0.03668818
Tns3	2.139	8.54283E-09		
Tlr7	2.137	0.003542479		
Gucy1a2	2.135	0.028616299		
Gbp6	2.131	0.000161545		
Apbb2	2.130	0.000665099		
Rnf182	2.128	0.000280459		
Igf1	2.124	5.59649E-09		
Cbln1	2.123	0.014485088		
Rassf4	2.118	7.75766E-08		
Hmcn1	2.117	1.17611E-05		
Pcdhga9	2.115	0.001917222		
Spn	2.109	0.038737032		
Elavl2	2.108	0.003871433		
C3	2.106	0.001376546		
Grm7	2.106	4.09248E-06		
Cpz	2.104	0.014086119		
Scn1a	2.102	0.01030945		
Lrfn5	2.100	0.007871477		
Epha3	2.097	5.43178E-07		
Sfrp2	2.092	8.71221E-09	2.618	0.013549614
Chrna7	2.091	0.00528383		
Enam	2.088	0.03526418		
Sarm1	2.086	0.003770446		
Evi2a	2.085	0.007561705		
Rnf180	2.079	0.008231714		
Ptplad2	2.077	0.002338624		
Krt18	2.075	1.68256E-05	2.290	0.024764035
Il1rl1	2.067	0.000501689		
Zfp618	2.064	0.000605746		
Hba-x	2.064	4.27266E-05		
Megf9	2.063	0.005656898		
Trim56	2.062	0.023901364		
Slc16a8	2.062	0.02993116		
Grp	2.059	0.016656605		
Ccdc30	2.057	0.015181653		
Slc4a11	2.048	0.016905863		
Hmgcs2	2.046	0.009096192		
Mpo	2.042	0.026482552		
Pdgfra	2.041	8.36077E-08		
Shank1	2.039	0.019115693		
Klf12	2.034	4.99436E-05		
Bmp3	2.030	3.60153E-06		
Wnt4	2.028	0.000376716		
Gm13152	2.027	0.002657245		
Rspo3	2.022	9.07763E-08		
Lonrf2	2.020	7.45703E-06		
Kitl	2.017	2.23348E-07		
1700003E16Rik	2.017	0.000337161		
Megf6	2.016	0.00033747	2.069	0.019919738
Zbtb7c	2.011	1.04392E-05		
Lphn3	2.011	6.2356E-05		
D130017N08Rik	2.009	0.012273568		
Ccdc60	2.007	0.001639865		

Rab17	2.006	0.030860461		
Slc5a3	2.004	4.00678E-07		
Syt16	2.001	0.000316039		
Kndc1			5.317	0.013908912
LOC100046616			4.014	0.04956006
Ccdc121			3.313	0.03042167
Gm5382			3.244	0.024911175
1700025F22Rik			3.023	0.015984364
Stat1			2.952	0.030546911
Slc5a7			2.908	0.021124505
Gpr4			2.836	0.04425495
AA387883			2.759	0.008290993
Gm3333			2.724	0.030546911
Nrip3			2.627	0.030546911
Nrxn1			2.587	0.03586748
Tmem178			2.561	0.006270704
Syn2			2.460	0.020233307
Penk			2.453	0.024911175
Krt13			2.427	0.04227364
E330013P04Rik			2.410	0.03668818
Fxyd7			2.325	0.024911175
Mgst1			2.283	0.035782292
LOC552880			2.278	0.034443438
Tmem145			2.270	0.012821585
5033411D12Rik			2.227	0.04737632
Rnd1			2.213	0.047857255
Me3			2.207	0.026873125
Stmn2			2.190	0.0417661
Fam196a			2.181	0.012889229
Fam181b			2.159	0.005028295
Gal3st4			2.119	0.029877413
Sfrs13b			2.106	0.010502099
Sult5a1			2.088	0.046443906
1500015O10Rik			2.050	0.027150191
BC068157			2.016	0.048310697
Ankrd29			2.005	0.033869874

Appendix B

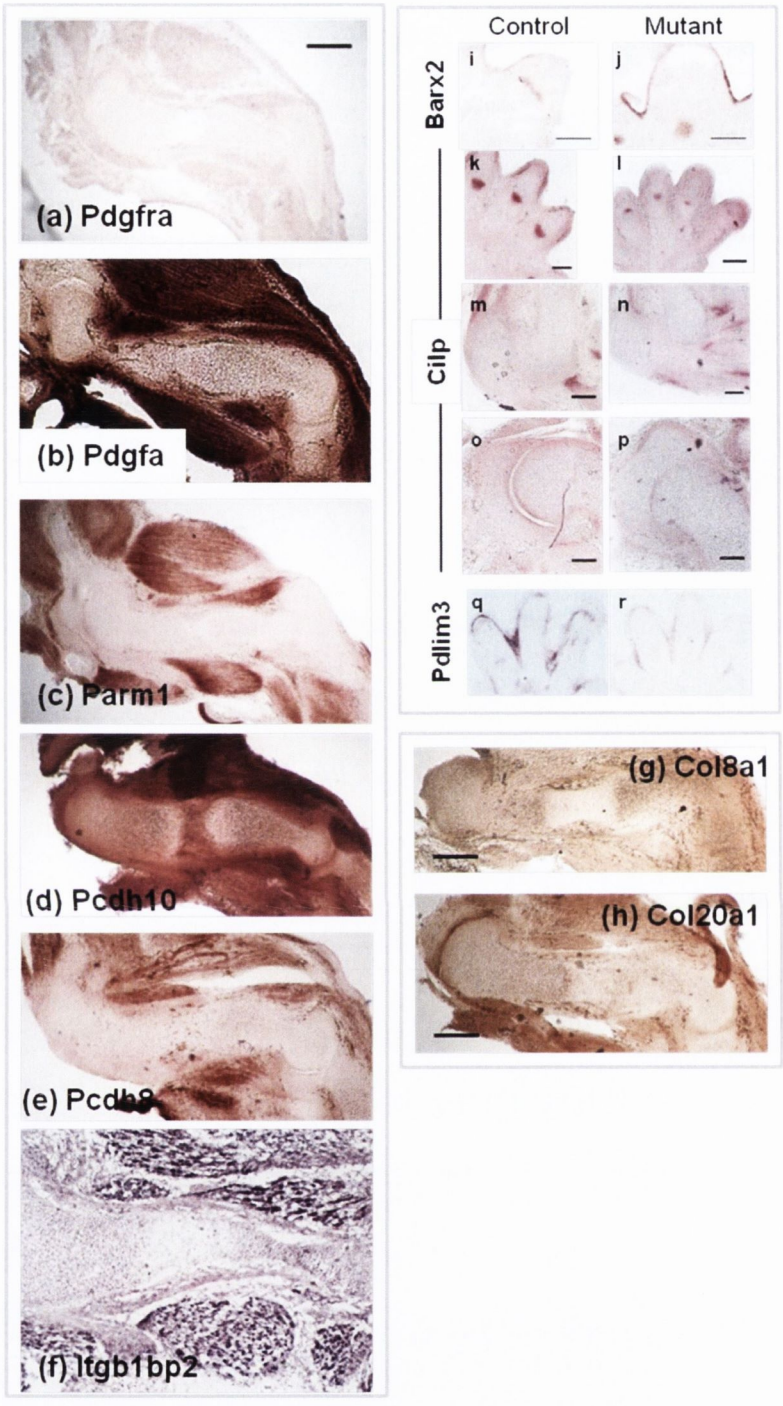

Appendix Figure B.1: *In situ* hybridisation Images of Genes identified to be differentially expressed, qualitative expression in TS23 control limbs. These genes are not associated with a specific cell signalling pathways but are potentially interesting because of their roles in growth (**a**. *Pdgfa*, **b**. *Pdgfra*), as cadherin receptors (**d**. *Pcdh10*,**e**. *Pcdh8*), integrin binding (f. *Itgb1bp2*), cartilage condensations (**i-j**, *Barx2*), cartilage expression (**k-p**, *Cilp*) the cytoskeleton (**q-r**, *Pdlim3*) and in the extracellular matrix (**g**. *Col8a1*,**h**. *Col20a1*). No differences were seen in the digit elbow or shoulder joints joints for *Barx2*, *Cilp* and *Pdlim3* expression, with only digits shown for *Barx2* and *Pdlim3*. All scale bars 100μm

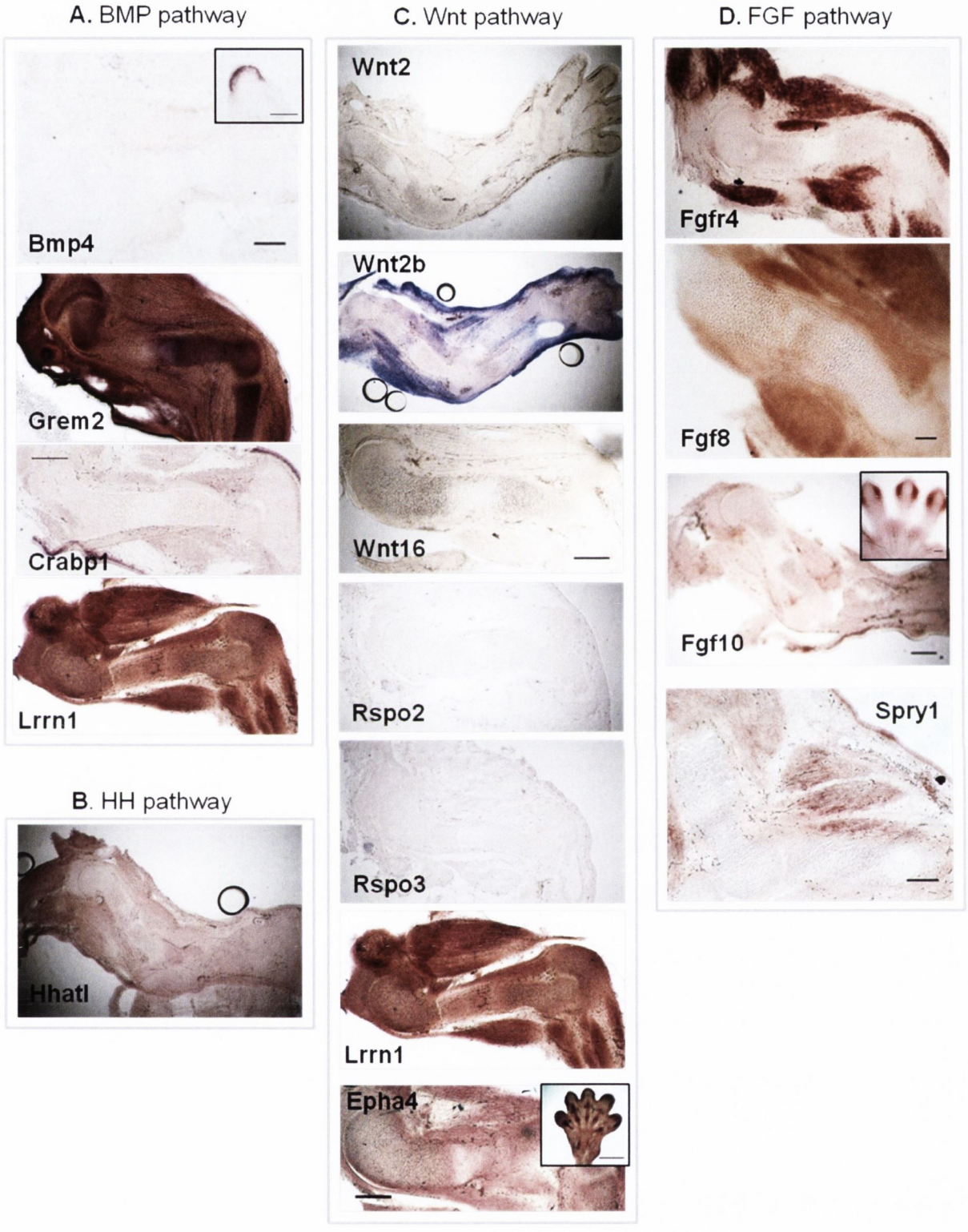

Appendix Figure B.2: *In situ* hybridisation Images of Genes identified to be differentially expressed associated with the BMP (A), Hedgehog (B), Wnt (C) and FGF (D) signalling pathways. Expression of all genes is shown on TS23 control forelimb tissue, with the boxed regions in three cases being in the hand plate. Genes shown are Bmp4, Grem2, Crabp1, Lrrn1 for BMP pathway in **A**. Hhatl for Hedgehog pathway in **B**. Wnt2, Wnt2b, Wnt16, Rspo2, Rspo3, Lrrn1 and Epha4, for the Wnt pathway in **C**. Fgfr4, Fgf8, Fgf10 and Spry1 were screened for the FGF pathway. All genes shown patterns were not followed up in the muscle-less mutant due to low levels of detection by ISH, or detection revealed expression only in the adjacent muscle. All scale bars 100μm.

Appendix C

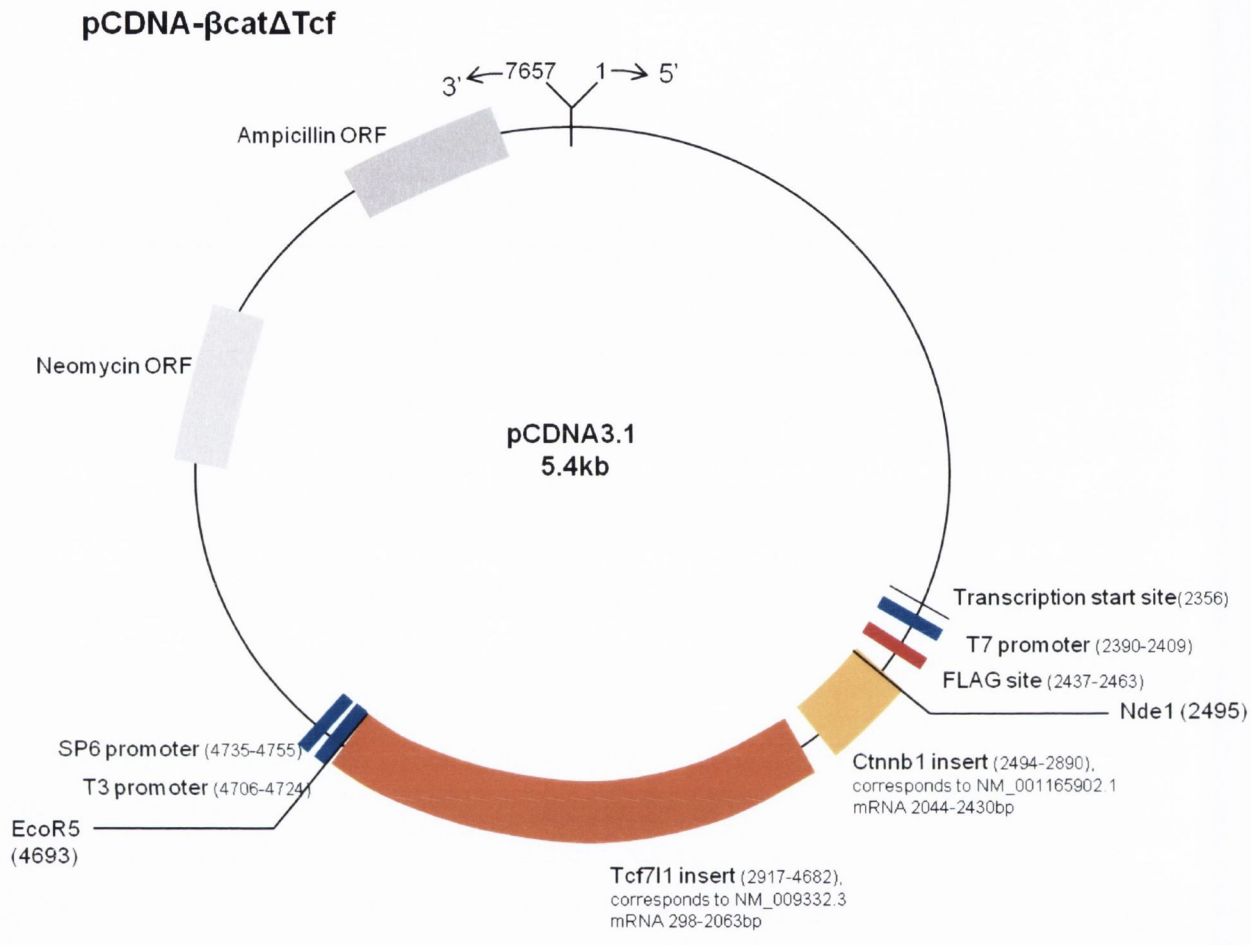

Appendix Figure C.1: Restriction map of pCDNA-βcatΔTcf, used for ectopic over-expression of β-catenin.Construct produced in collaboration with laboratory of Margaret Buckingham, Pasteur Insitute, by Frederic Relaix. The full sequence of the construct has been deposited in Genebank accession number KM189193.

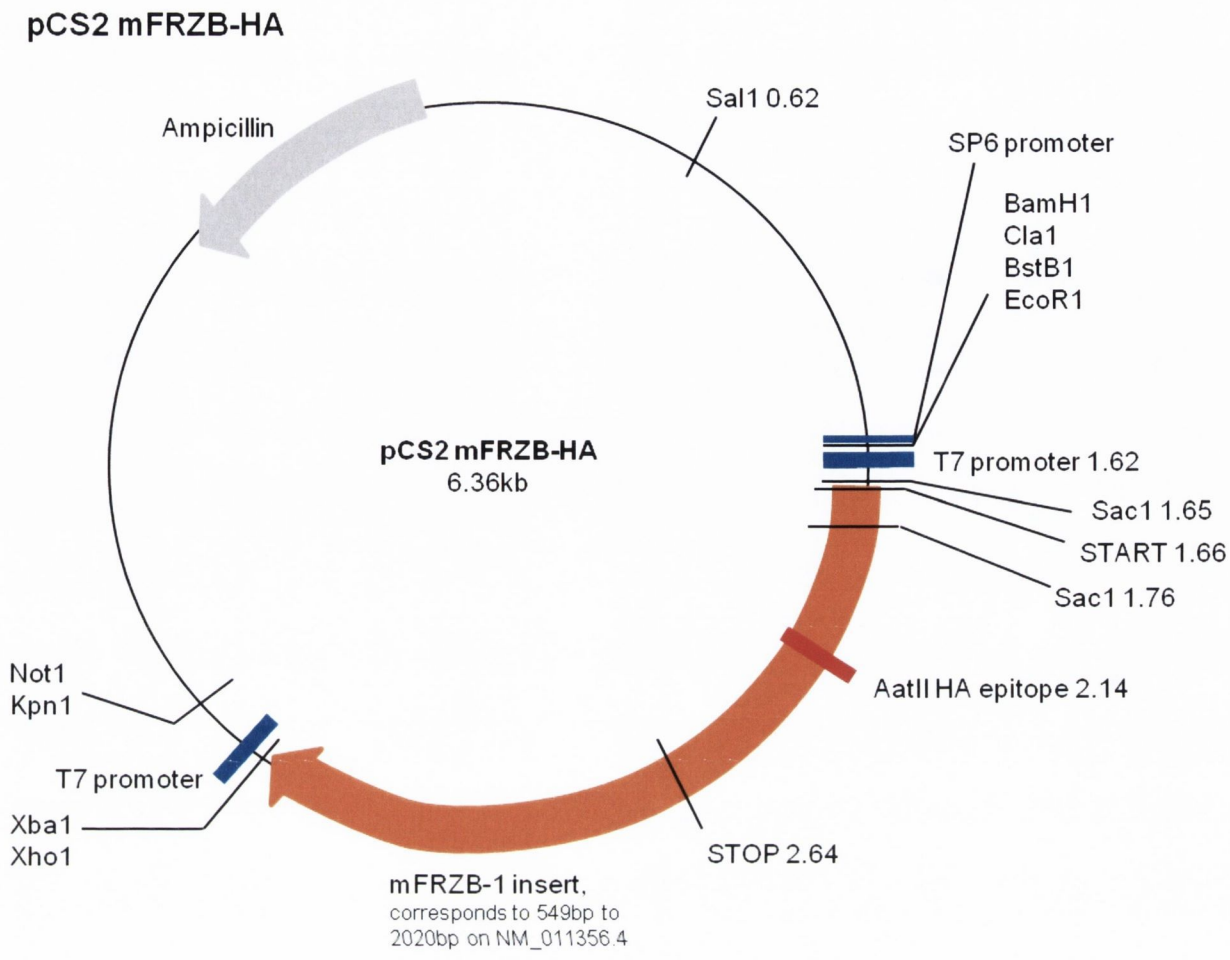

Appendix Figure C.2: Restriction map of pCS2mFRZB-HA, containing the HA epitope tag, used for ectopic over-expression of FRZB/Sfrp3.

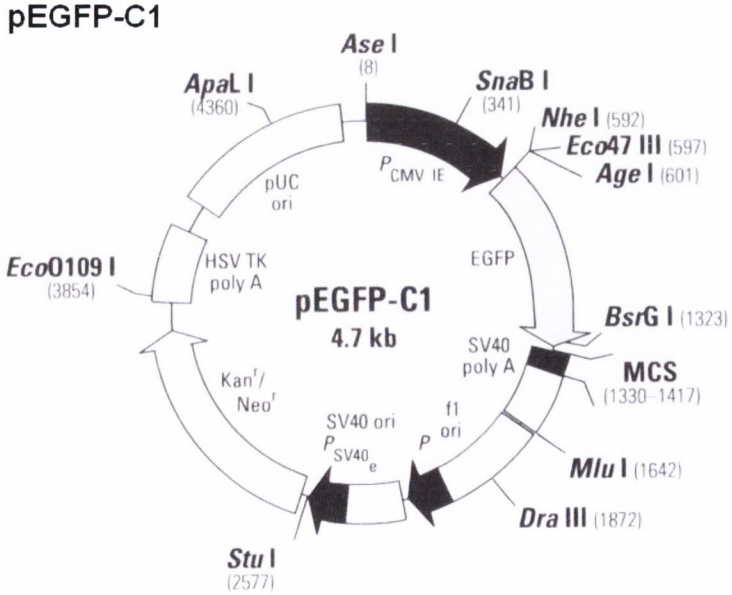

Appendix Figure C.3: Restriction map and multiple cloning site of pEGFP-C1.

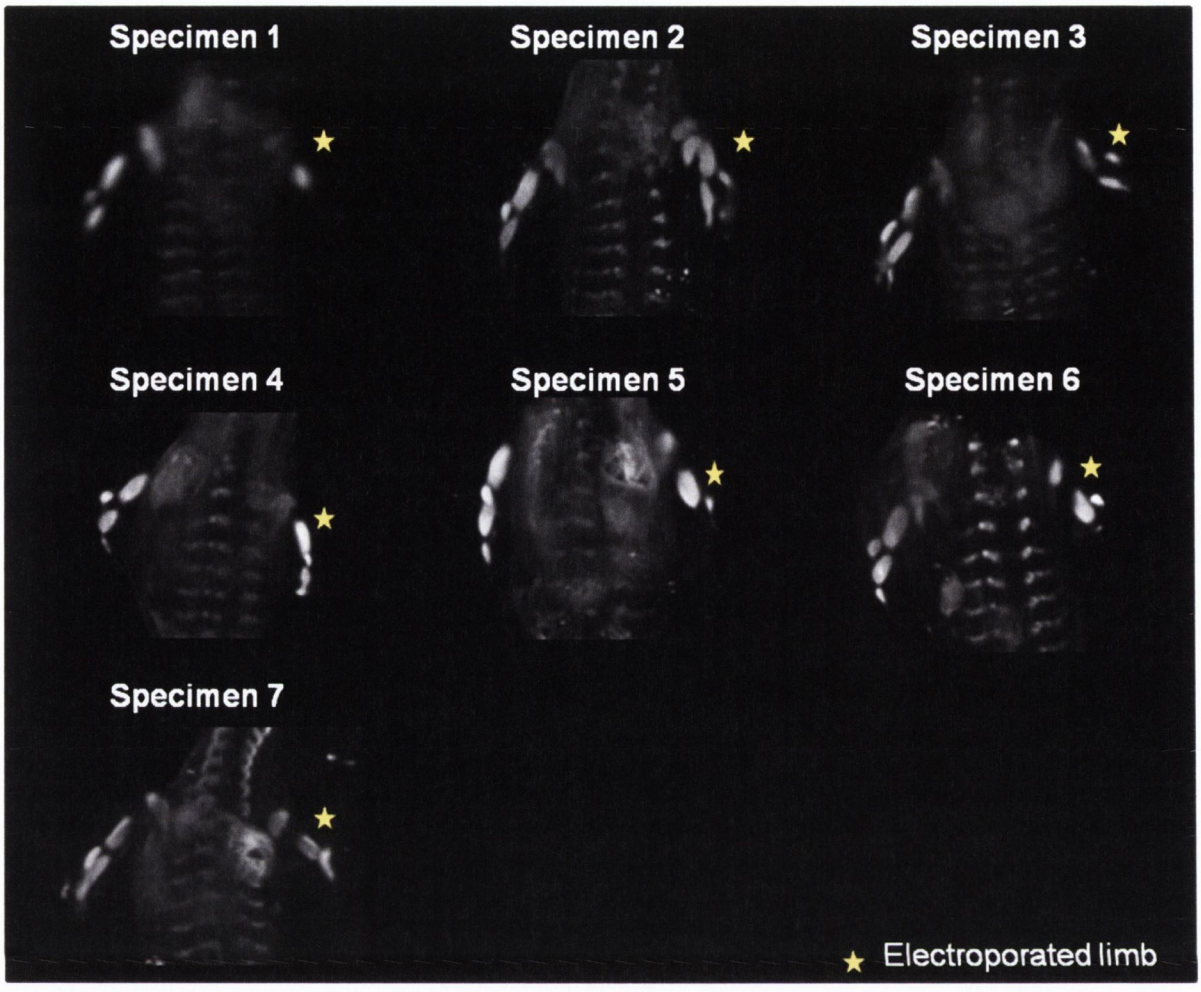

Appendix Figure C.4: Frontal views of upper torso from 3D volume representation of *Col2a1* expression for βcatenin electroporated specimen 1-7. Yellow star represents electroporated limb.

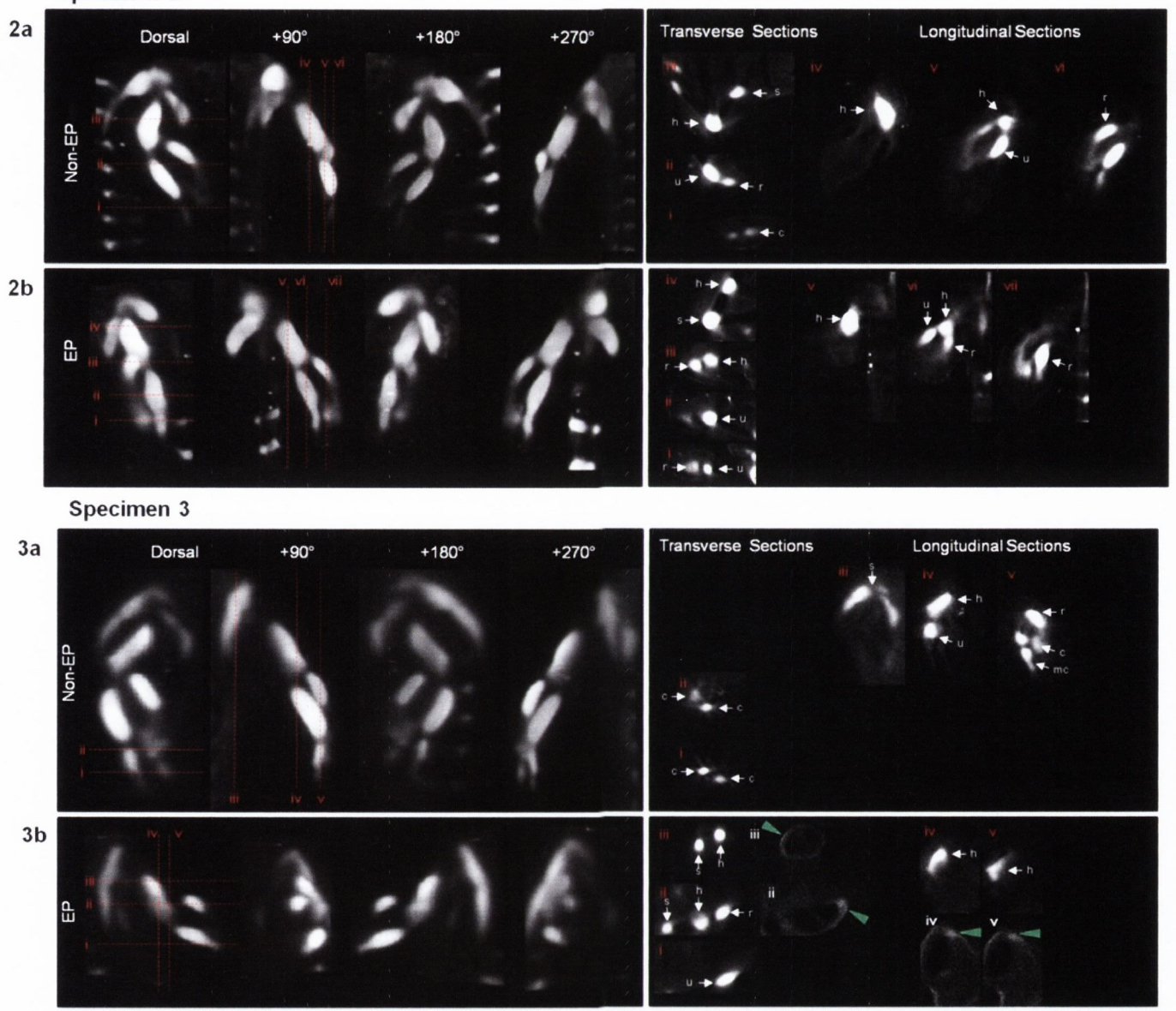
Specimen 2
2a
Dorsal
+90°
+180°
+270°
Transverse Sections
Longitudinal Sections
Non-EP
2b
EP
Specimen 3
3a
Dorsal
+90°
+180°
+270°
Transverse Sections
Longitudinal Sections
Non-EP
3b
EP

Specimen 5

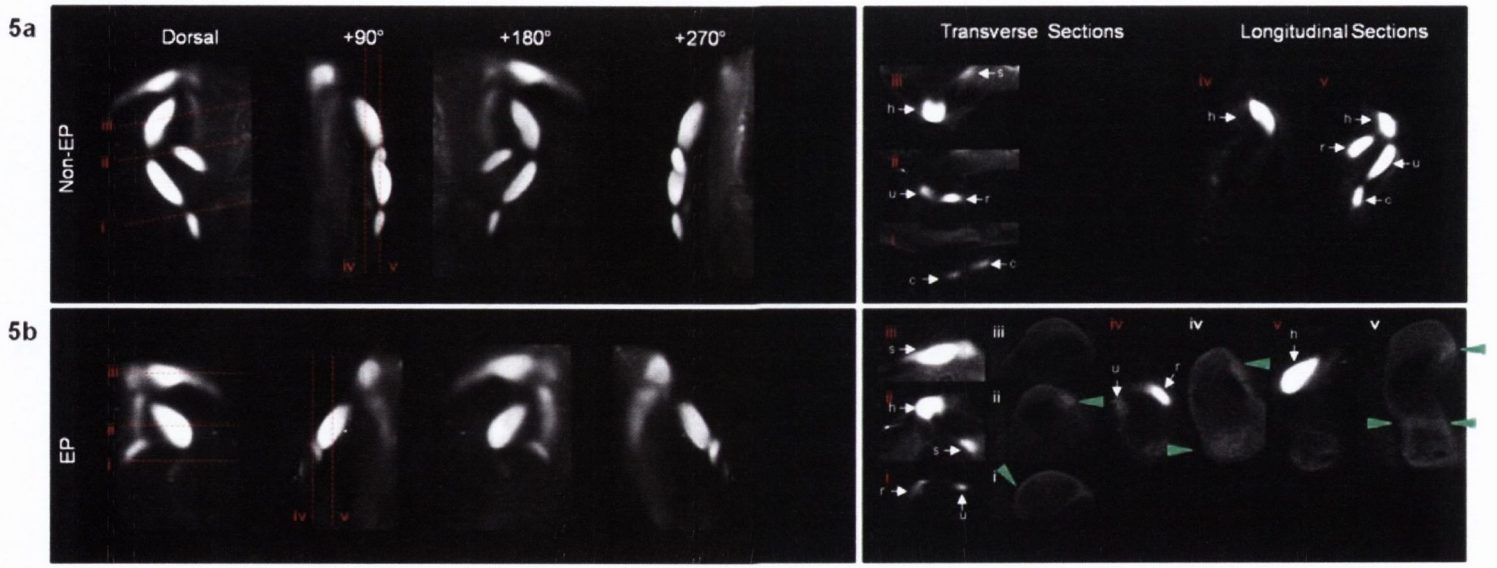

Specimen 6

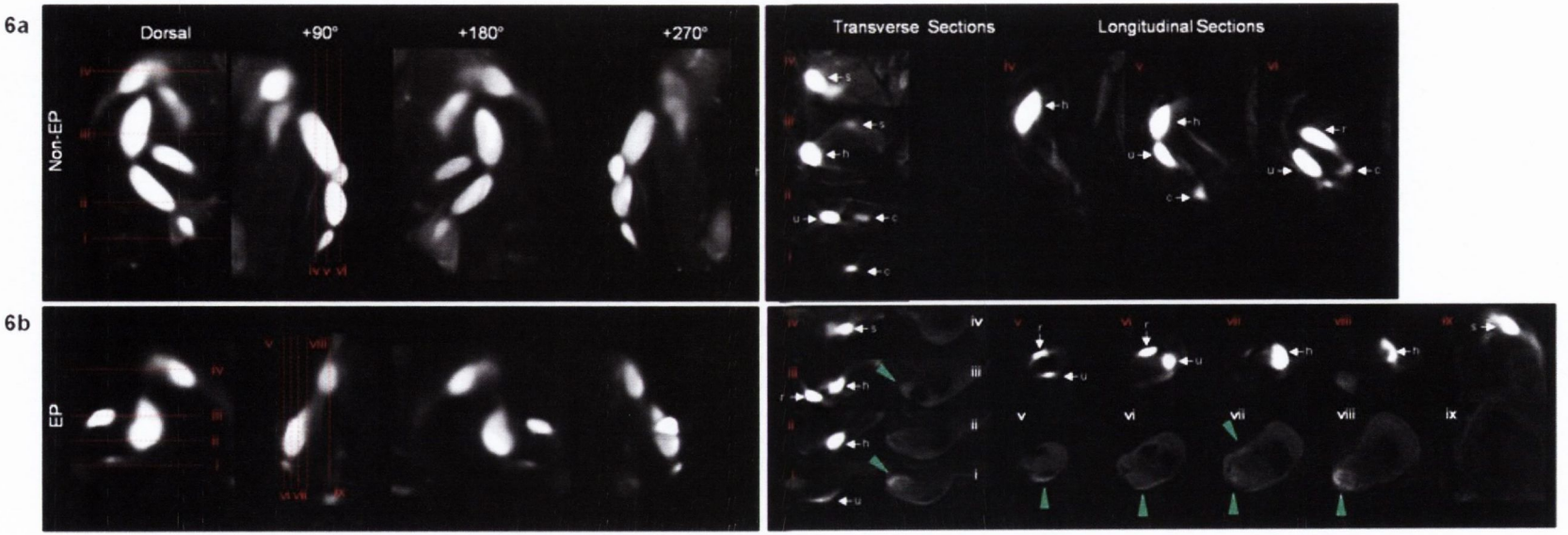

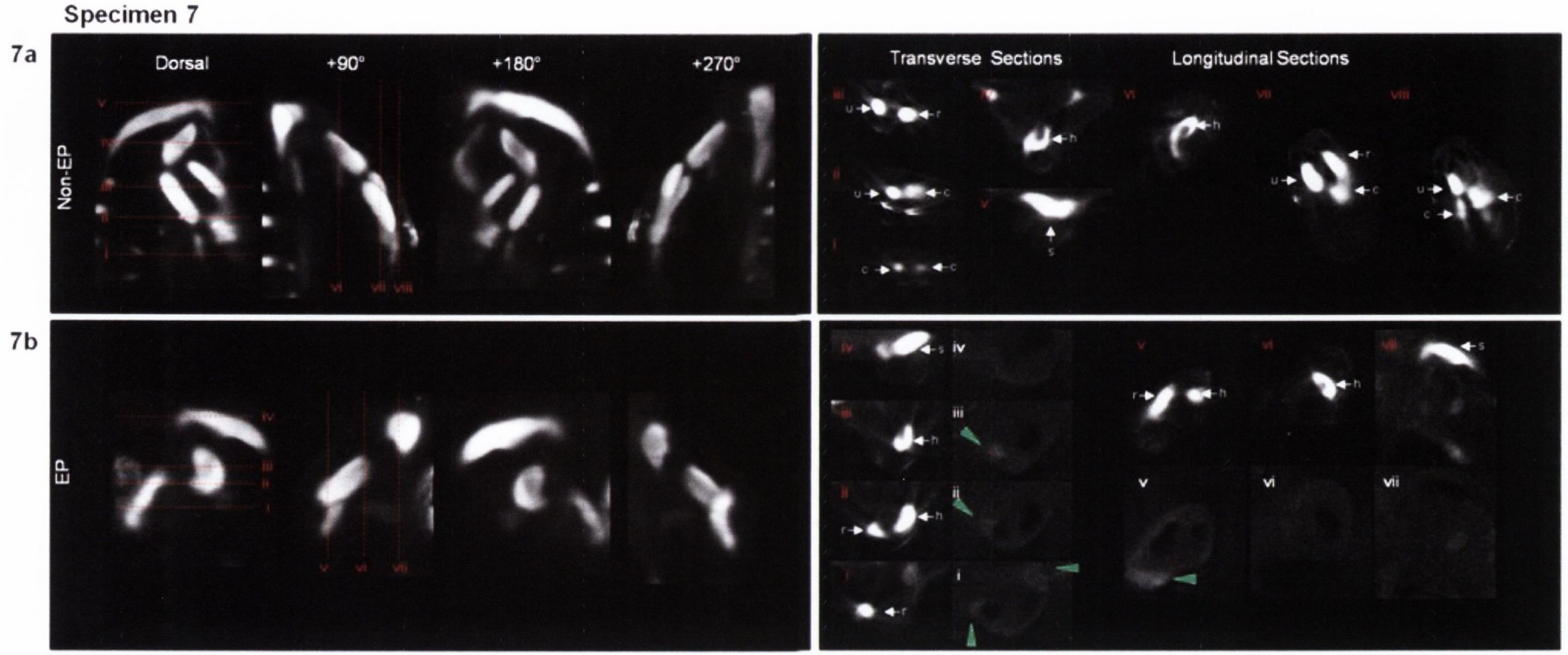

Appendix Figure C.5: Analysis of *Col2a1* and GFP expression in βcatenin electroporated Specimens 2-7. EP limb (**b**) compared to contra-lateral non-electroporated (non-EP) limb (**a**). External views of volume representation of the same limb following OPT scanning*Col2a1* expression is shown for each specimen, with rotations every 90°. Transverse and longitudinal sections were taken through the 3D reconstructions for *Col2a1* and *GFP* expression. Expressing tissue appears as white/light grey in the reconstructions. Specimen 2: **2a** (non-EP) (i-iii, transverse sections; iv-vi longitudinal sections) **2b** (EP) (i-iv, transverse sections; v-vii longitudinal sections). Specimen 3: **3a** (non-EP) (i-ii, transverse sections; iii-v longitudinal sections) **3b** (EP) (i-iii, transverse sections, iv-v longitudinal sections, Col2a1 and GFP shown). Specimen 5: **5a** (non-EP) (i-iii, transverse sections; iv-v longitudinal sections) **5b** (EP) (i-iii, transverse sections; iv-v longitudinal sections, Col2a1 and GFP shown). Specimen 6: **6a** (non-EP) (i-iv, transverse sections; iv-vi longitudinal sections) **6b** (EP) (i-iv, transverse sections; v-ix longitudinal sections, Col2a1 and GFP shown). Specimen 7: **7a** (non-EP)(i-v, transverse sections; vi-viii longitudinal sections) **7b** (EP) (i-iv, transverse sections; v-vii longitudinal sections, Col2a1 and GFP shown). Green arrows indicate GFP expression. s; scapula, h; humerus, u; ulna, r; radius, c; carpals.

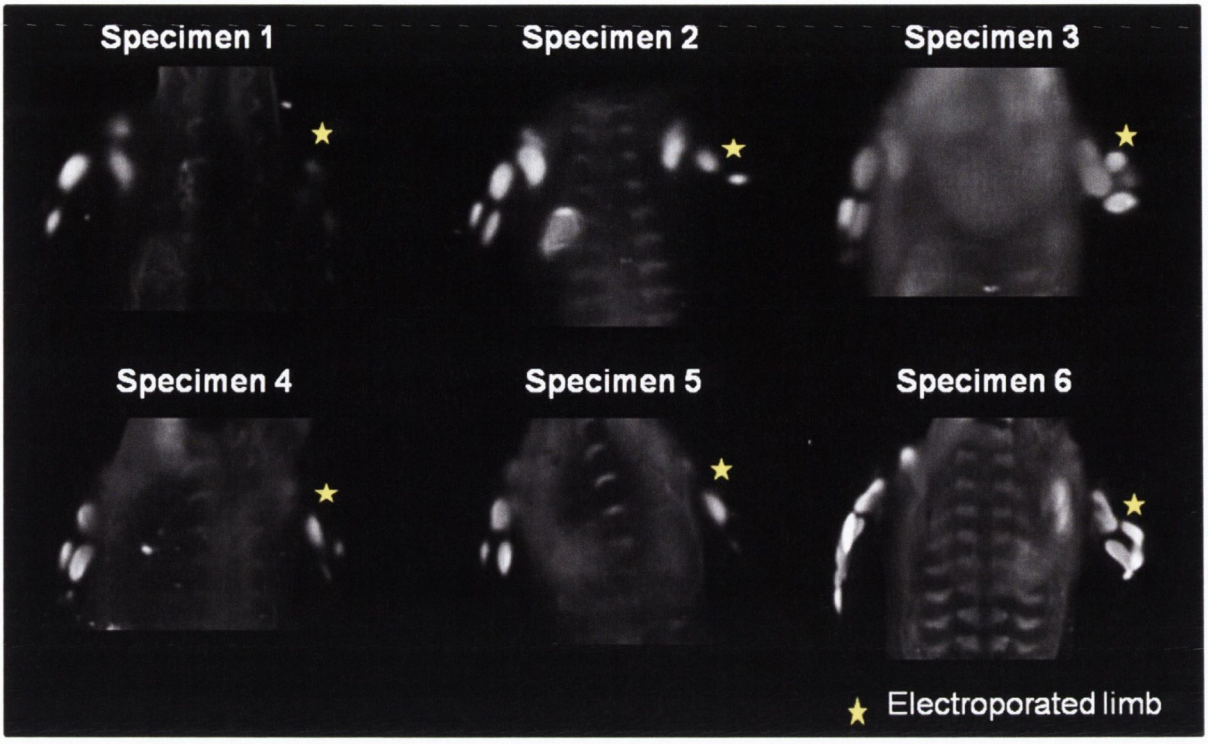

Appendix Figure C.6: Frontal views of upper torso from 3D volume representation of *Col2a1* expression sin Sfrp3 electroporated specimen 1-6. Yellow star represents electroporated limb.

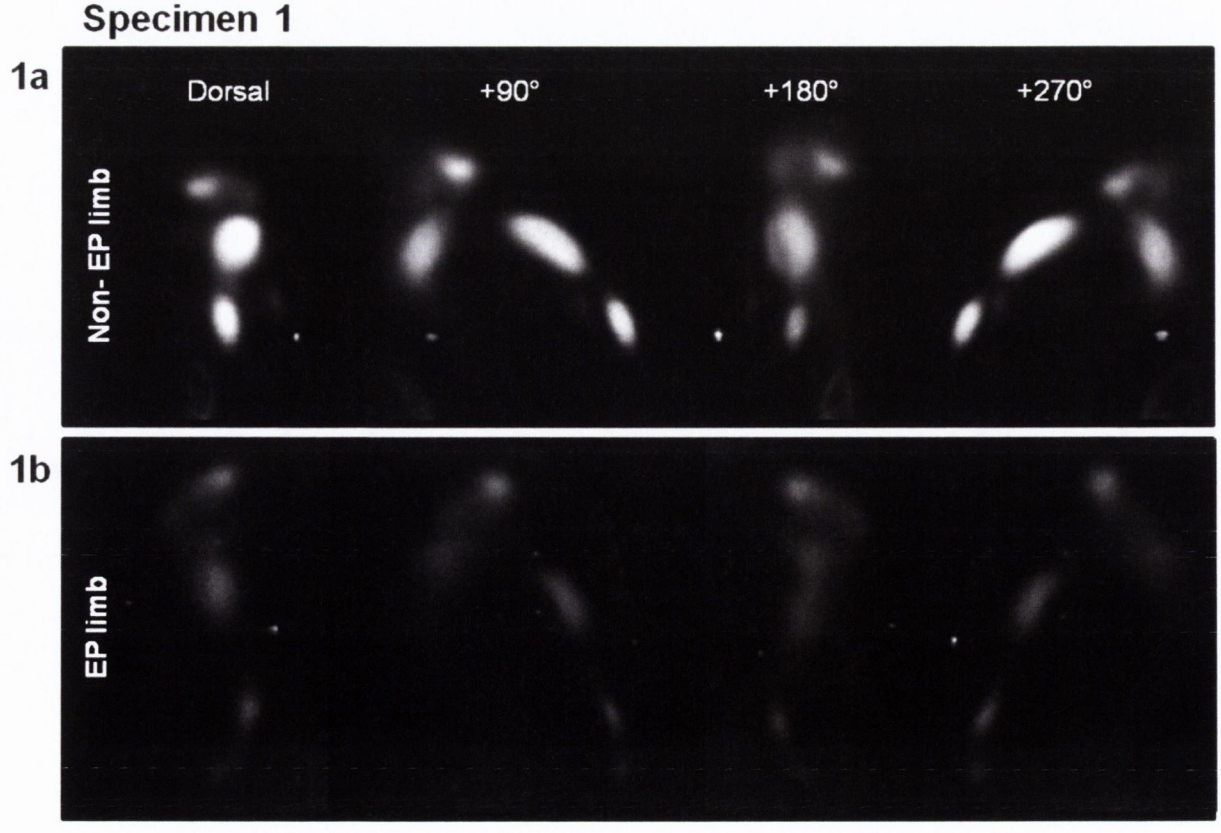

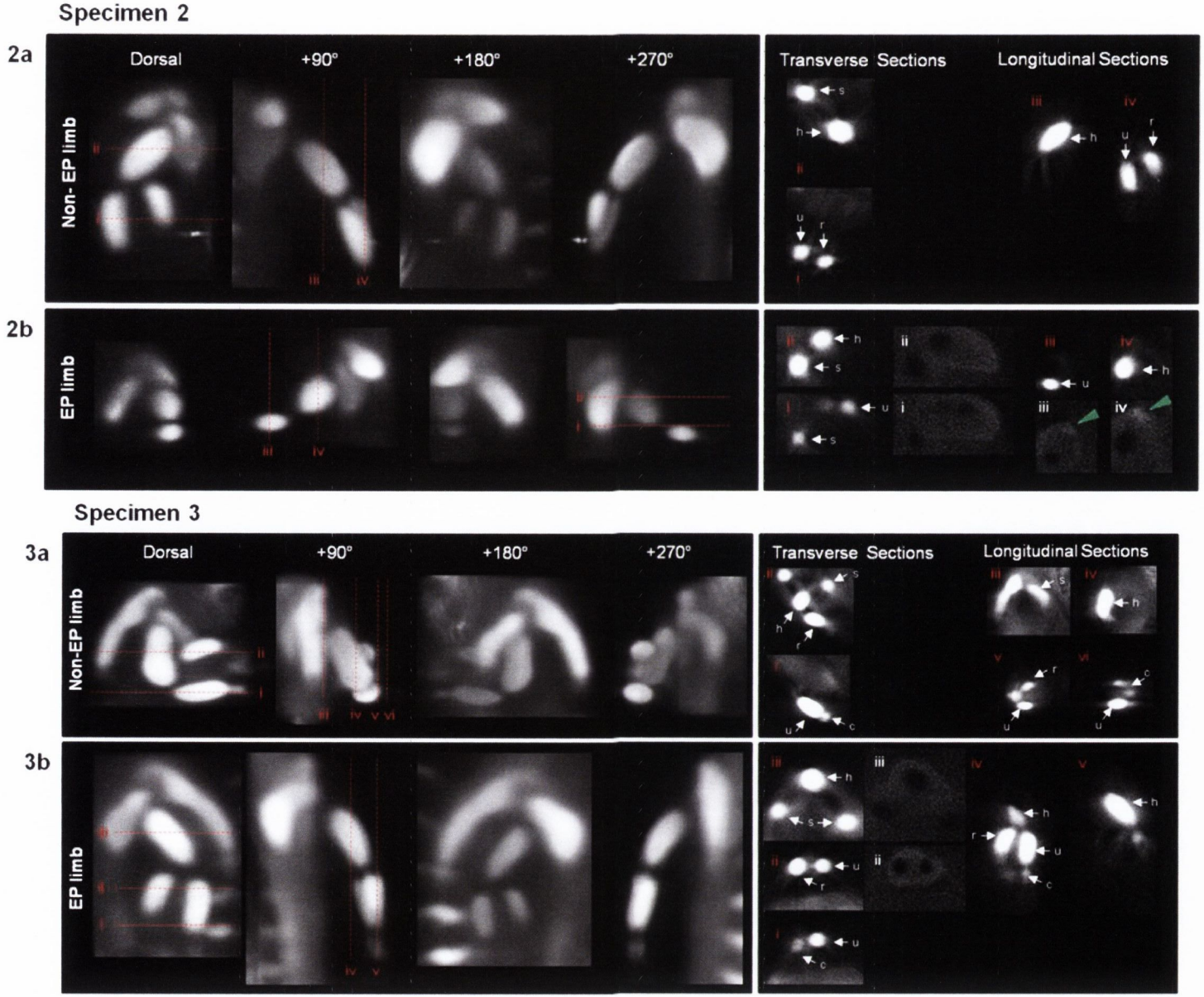
Specimen 2
2a
Dorsal
+90°
+180°
+270°
Transverse Sections
Longitudinal Sections
Non- EP limb
2b
EP limb
Specimen 3
3a
Dorsal
+90°
+180°
+270°
Transverse Sections
Longitudinal Sections
Non-EP limb
3b
EP limb

Specimen 4

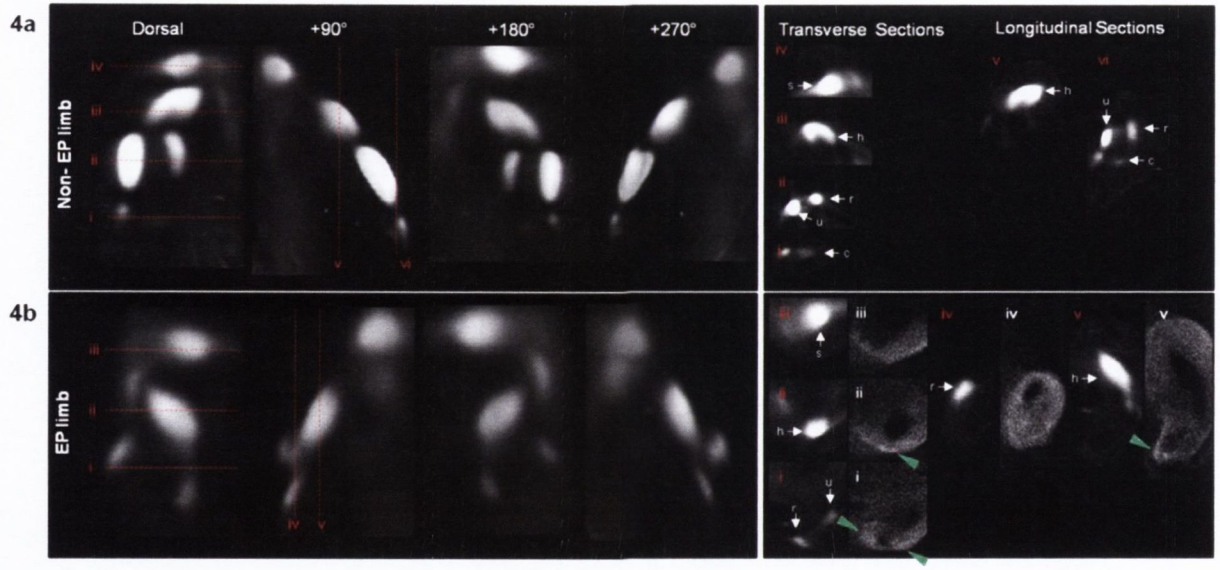

Specimen 5

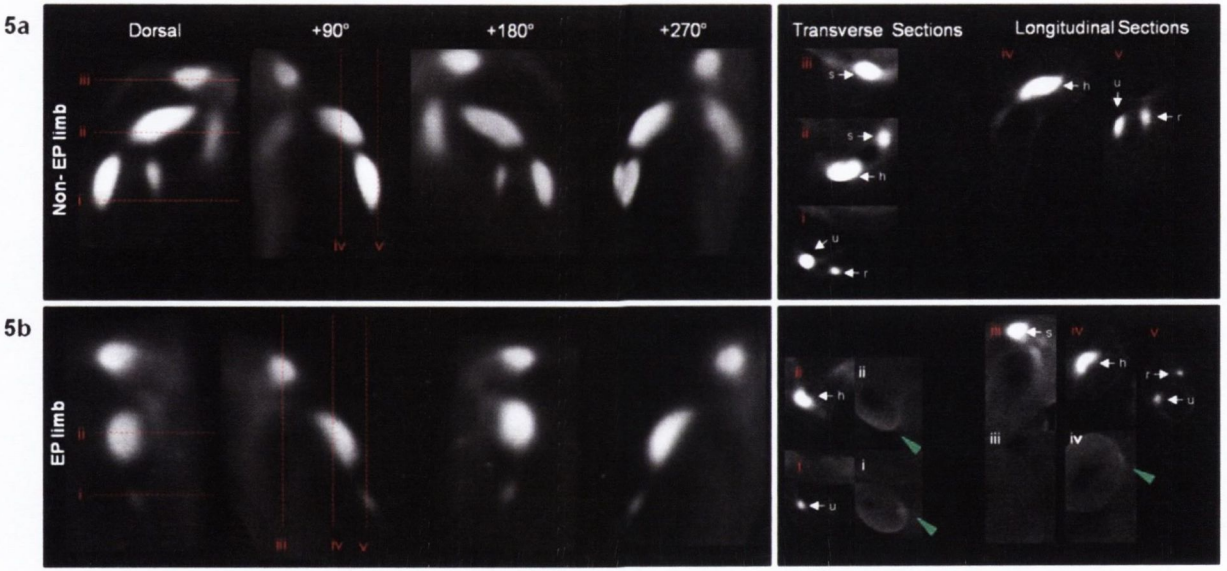

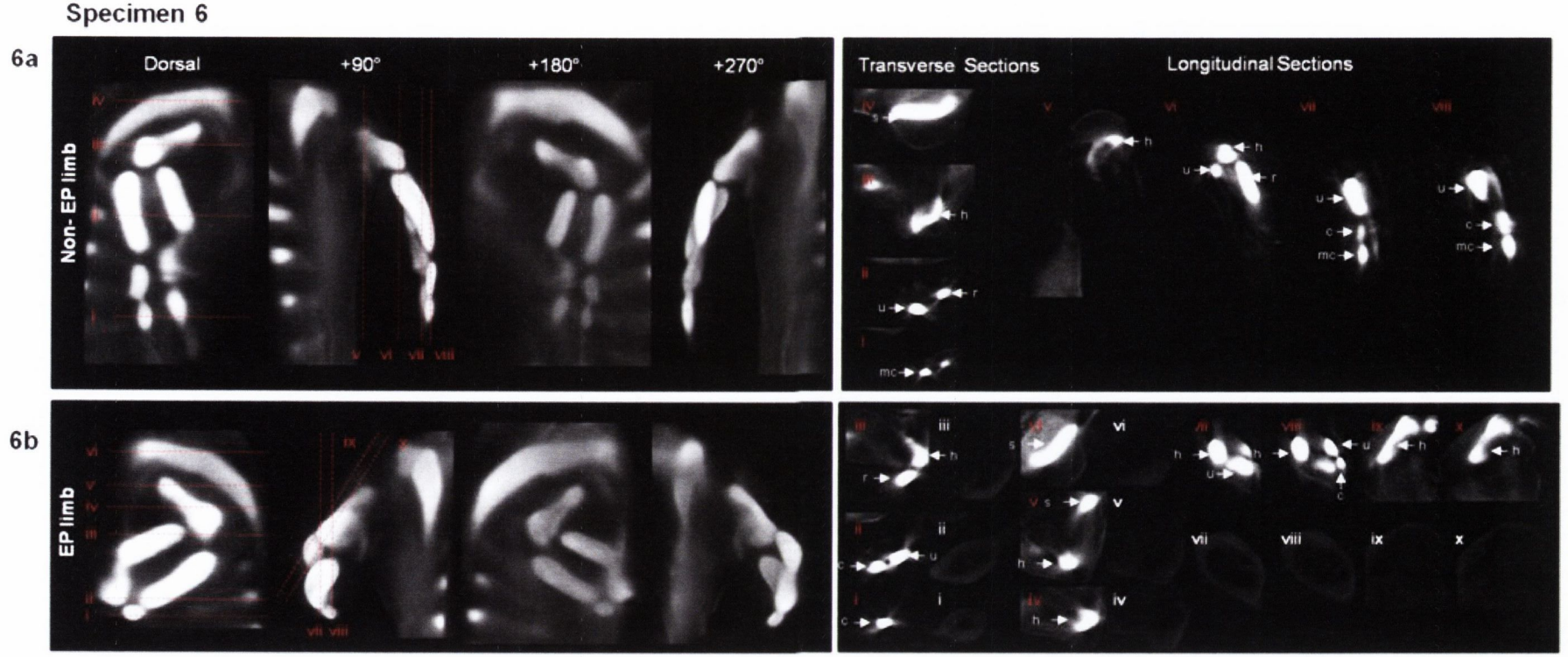

Appendix Figure C.7: Analysis of *Col2a1* and GFP expression in Sfrp3 electroporated Specimens 1-6. EP limb (**b**) compared to contra-lateral non-electroporated (non-EP) limb (**a**). External views of volume representation of the same limb following OPT scanning *Col2a1* expression is shown for each specimen, with rotations every 90°. Transverse and longitudinal sections were taken through the 3D reconstructions for *Col2a1* and *GFP* expression. Expressing tissue appears as white/light grey in the reconstructions. Specimen 1: **1a** (non-EP) **1b** (EP), Specimen 2: **2a** (non-EP) (i-ii, transverse sections; iii-iv longitudinal sections) **2b** (EP) (i-ii, transverse sections; iii-iv longitudinal sections, Col2a1 and GFP shown). Specimen 3: **3a** (non-EP) (i-ii, transverse sections; iii-vi longitudinal sections) **3b** (EP) (i-iii, transverse sections, iv-v longitudinal sections, Col2a1 and GFP shown). Specimen 4: **4a** (non-EP) (i-iv, transverse sections; v-vi longitudinal sections) **4b** (EP) (i-iii, transverse sections; iv-v longitudinal sections, Col2a1 and GFP shown). Specimen 5: **5a** (non-EP) (i-iii, transverse sections; iv-v longitudinal sections) **5b** (EP) (i-ii, transverse sections; iii-v longitudinal sections, Col2a1 and GFP shown). Specimen 6: **6a** (non-EP) (i-iv, transverse sections; v-viii longitudinal sections) **6b** (EP) (i-vi, transverse sections; vii-x longitudinal sections, Col2a1 and GFP shown). Green arrows indicate GFP expression. s; scapula, h; humerus, u; ulna, r; radius, c; carpals, mc; metacarpals.

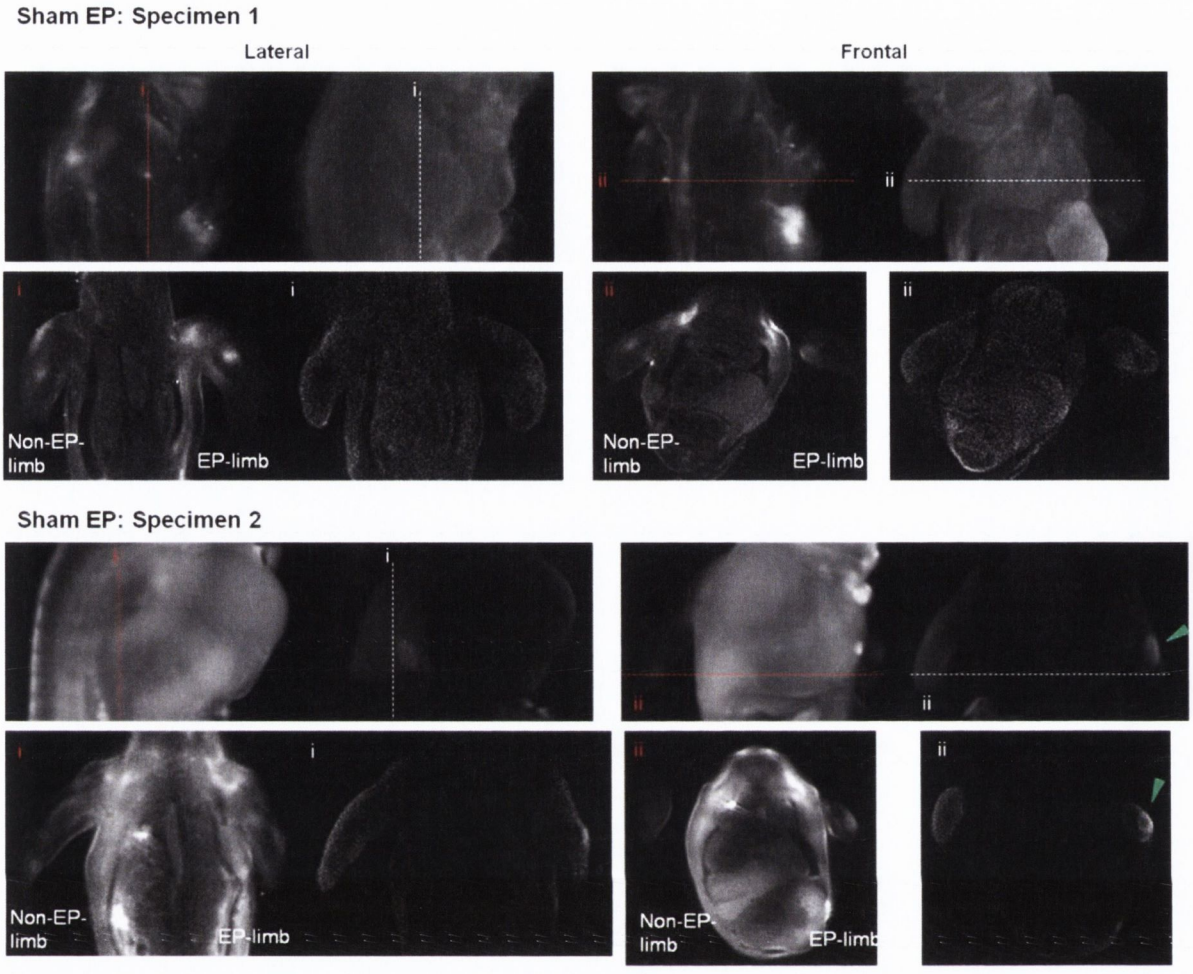

Appendix Figure C.8: Analysis of *Sfrp2* expression in Sham electroporated forelimbs. External views of volume representation of the same emrbyo following OPT scanning and reconstruction are shown (lateral) and rotated +180° (frontal). Red line indicated the plane of a virtual coronal (**i**) and transverse (ii) section for each limb; Sfrp2 expression shown in (**i**, **ii** red) alongside the GFP background surface channel (**i**, **ii** white). Expressing tissue appears as white/light grey in the reconstructions. Green arrow head shows GFP expression

Abstract:

The Mechanical Regulation of Skeletal Development: Identification and characterisation of mechanosensitive genes that contribute to tissue differentiation in bone and joint development.

Rebecca Rolfe

Mechanical stimulation has been implicated as an important regulator for the development of the skeleton. Decreased *in utero* foetal movement results in skeletal abnormalities including joint fusions and thin hypo-mineralised bones. Animal models that develop in the absence of mechanical stimulation show abnormal initiation and/or progression of ossification in long bones, loss of definition of tissue territories in the joint region and altered rudiment morphology. The skeletal system is a complex structure, and while we know much about the molecular mechanisms that guide the differentiation of progenitor cells into its individual elements; we know very little of the molecular mechanisms that sense and respond to mechanical stimulation to co-ordinate its correct development. The objective of this thesis was to uncover the molecular mechanisms underlying the response of developing skeletal cells to mechanical stimulation.

Using a mouse model (*Splotch-delayed*) that has altered mechanical stimulation due to the absence of limb musculature; the hypothesis that mechanical stimulation of the embryonic skeletal system impacts expression levels of genes implicated in developmentally important signalling pathways, was tested. A comparative transcriptome profiling approach was utilised. Differentially expressed genes were analysed based on gene ontology annotations and were shown to be involved in development and differentiation, cytoskeletal architecture and cell signalling. Analysis of cell signalling pathways that were altered revealed that the Wnt signalling pathway was the most strongly disturbed. Differentially expressed Wnt signalling components were identified to show spatially restricted patterns in the two most affected phenotypic sites in the muscle-less mutant. This led to the examination of the effect of altering Wnt signalling as a key point of integration for mechanical cues. *Ex ovo* electroporation targeting the developing limb allowed for the modulation of Wnt signalling, to assess whether manipulation of the pathway phenocopies what is seen following the removal of mechanical stimulation. Altering Wnt signalling was shown to have profound effects on chondrogenesis, however further refinement is required to target specific regions of the developing skeleton, to assess the localised response.

In parallel with the *in vivo* studies, chondrogenic differentiation was analysed in culture. Comparisons of adult stem cells and embryonic cell cultures exposed to hydrostatic pressure revealed that the application of mechanical stimulation showed similar responses in gene expression that are indicative of maintenance of a stable cartilage phenotype in both cell types, similar to that displayed in joint articular cartilage, preventing maturation and hypertrophy. This revealed that embryonic and adult cell types respond in a similar manner to mechanical stimulation, at least in this respect, and thus the information gained from the developing embryo can be applied to adult derived cells used for regenerative therapies.

This thesis demonstrates that embryonic movement generated by muscle contractions regulates the expression of key developmental regulatory genes and that such genes are involved in the transduction of biophysical stimuli to elicit a response in cellular differentiation in the embryonic skeleton. In particular it highlights the Wnt signalling pathway as a potential point of integration of mechanical and molecular signalling and the cytoskeletal components as mediators of the response. This work sheds light on the molecular mechanisms that interpret mechanical stimulation during skeletal development and provides a valuable resource for further investigation of the mechanistic basis of mechanoregulation of skeletal development.